

NEWCASTLE UNIVERSITY

**THE REACTIVITY AND ISOTOPIC
FRACTIONATION OF Fe-BEARING MINERALS
DURING SULFIDATION:
AN EXPERIMENTAL APPROACH**

BY

ALISON MCANENA

JANUARY, 2011

Submitted to Newcastle University in partial fulfilment of the requirements
for the degree of Doctor of Philosophy within the Faculty of Science,
Agriculture and Engineering

School of Civil Engineering and Geosciences
Newcastle University
Newcastle Upon Tyne
NE1 7RU
UK

DECLARATION

I hereby certify that the work presented in this thesis is my own, except where otherwise acknowledged, and has not been submitted previously for a degree at this, or any other
University

Alison McAnena

ACKNOWLEDGEMENTS

There are a number of people without whom the work within this thesis may not have been possible. First, and foremost, I am extremely grateful to my supervisor Dr Simon Poulton, whose teachings, sheer enthusiasm and determination, has allowed me to grow into an impassioned scientist who now sees the natural world in a different light...or at least in terms of endless biogeochemical cycles. I would also like to thank Simon for making my PhD experience the best that it could be and I am so lucky to have been his first PhD student.

I would also like to show my appreciation to a number of people, who without their time and experience I could not have completed this thesis: Dr Silke Severmann (Rutgers University) for both Umpqua River samples and all Fe isotope analysis reported in this study; Dr Bo Thamdrup (NORDSEE; University of Southern Denmark) and Dr Tanya Goldberg (Imperial College, London) for Aarhus Bay sediments and initial sediment sample characterisation; and finally Prof. James Farquhar and Dr Aubrey Zerkle for their invaluable advice and expertise in sections of this study. During my time at Newcastle, I would most definitely be lost without assistance from Rob, Ian, Bernie and especially Yvonne Hall.

Being able to get through this process in one piece was made a lot easier by my friends and colleagues at Newcastle, including the inhabitants of Room 3.04 (Lynsay, Rob, Jamie and Martin); and those who have helped me without question, and with great humour, in times of need (Sharon, Jen, Mark, Marie, Andy, Joe, Jill and, especially Phil Renforth), I am so happy you have all experienced this with me. I would also like to thank my family and best friend Pauline for their never ending motivation and enthusiasm throughout all my studies which has helped my work consistently over the last four years, I am so grateful for all of your support.

ABSTRACT

The presence of Fe bearing minerals at the sediment-water interface (within marine settings) promotes a variety of biological and abiological redox reactions during early diagenesis. The highly reactive nature of a portion of these Fe bearing minerals, with respect to organic and inorganic species, influences both porewater chemistry and the biogeochemical cycling of trace metals. Of particular importance is the reaction between 'reactive' Fe minerals and dissolved sulfide (which ultimately produces pyrite). This is a major process in the modern environment, but has also been prevalent throughout Earth's history and forms the basis for identifying different paleodepositional redox conditions in the ancient rock record. Initial experimental studies of the sulfidic reductive dissolution of pure synthetic Fe(III) oxides have provided detailed insight into the mechanism and rates at which different minerals release Fe(II)_{aq} into anoxic waters; whilst also describing the formation of reduced sulfide products including FeS and elemental sulfur. However, it remains unclear how realistic laboratory studies of the sulfidation of pure Fe minerals are in relation to natural sediment assemblages containing different minerals. Comparison of natural sediments with the reactivity of pure minerals studied under laboratory conditions thus forms the basis for the first part of this study.

Sediment cores were obtained from Aarhus Bay (Denmark) and the Umpqua River Shelf (North Pacific Basin, N. America), representing contrasting conditions in terms of the reactive Fe species present. Aarhus Bay sediment samples contain a high proportion of the most reactive Fe oxide minerals (e.g. ferrihydrite, lepidocrocite) at the surface, which decrease with depth throughout the core, leaving a near-constant concentration of slower reacting Fe oxide minerals (e.g. goethite, magnetite, hematite). These trends are reflected in decreased rates of reductive dissolution with depth in the core, as determined via sulfidation experiments of sediment sampled from different depth intervals. In contrast, the Fe oxide content of Umpqua River Shelf sediments is more homogeneously distributed, with the slower reacting Fe oxide species dominating the sediment assemblage. As such, rates of reaction with respect to dissolved sulfide do not differ vastly with depth. Based on the determination of rate constants during these experiments, this examination of the reactivity of Fe oxides suggests that the natural Fe

oxide assemblages react on a similar timescale (over the same order of magnitude) to that of synthetic minerals, suggesting that existing schemes for the reactivity of Fe oxide minerals towards dissolved sulfide provide a realistic framework for evaluating rates of reactivity in natural environments.

In a range of similar experiments, the rate and mechanism of the sulfide-mediated dissolution of synthetic Fe carbonate (siderite) has also been assessed, in addition to a sample of natural crystalline siderite from the 1.88 billion year-old Biwabik Iron Formation, North America. These experiments have been performed as a consequence of the prevalence of siderite in ancient sediments. Siderite is commonly assumed to be highly reactive towards dissolved sulfide. However, despite the common occurrence of siderite in ancient sediments, its reactivity has not previously been determined, a fact which impacts upon the use of Fe speciation in ancient sediments as a paleodepositional redox indicator. Although carbonates follow a different mechanism of dissolution than Fe oxides, probably via the direct formation of FeS at the mineral surface, the experiments performed here show that synthetic Fe carbonate dissolution in the presence of dissolved sulfide is faster than for most Fe oxide minerals (including ferrihydrite and lepidocrocite). Furthermore, although the reactivity of the ancient crystalline siderite sample was slower than for the synthetic siderite, this mineral was also relatively reactive, suggesting that all Fe carbonate minerals can be considered 'highly reactive' towards dissolved sulfide.

The final part of this thesis concerns an examination of Fe isotope fractionations during the sulfide-promoted reductive dissolution of a variety of synthetic Fe oxide minerals. The isotopic composition of Fe in natural rocks and sediments is commonly used to infer the processes responsible for Fe cycling during deposition and diagenesis. In particular, experiments with Fe reducing bacteria have demonstrated that isotopic fractionations of up to -1.3‰ may occur between the original oxide mineral and Fe(II) released to solution, and thus light Fe isotope values in ancient sediments have been used to reconstruct the antiquity or occurrence of bacterial Fe reduction. However, in all of these cases, the potential for an isotopic fractionation during the sulfide-promoted reductive dissolution of Fe oxides has been ignored. Thus it is important to quantify potential fractionations associated with this process in order to better evaluate Fe isotope compositions observed in the rock record. During both the reductive and dissolution steps of this abiotic reaction, a significant isotopic fractionation is observed,

the magnitude of which is dependent on the mineral phase under reaction, and the specific experimental parameters. This detailed study represents the first time that an isotopic fractionation has been demonstrated with regard to the reductive step, in addition to the subsequent dissolution step of the overall reaction. Isotopic fractionations in the dissolved phase are not as large as those sometimes found in association with bacterial Fe reduction, but are in the same range (up to $\sim -0.8\%$), suggesting that the influence of this reaction needs to be taken into careful consideration when evaluating Fe isotope compositions in modern and ancient sediments.

Overall, this study builds upon existing experiments which have assessed the reactivity of individual Fe(III) oxide minerals towards dissolved sulfide, to provide new insight with regard to (bio)geochemical Fe mineral cycling. In particular, this study provides kinetic and isotopic constraints that have the potential to greatly enhance reconstructions of syngenetic and diagenetic reactions occurring in modern and ancient environments.

TABLE OF CONTENTS

Declaration	2
Acknowledgements.....	3
Abstract.....	4
Table of Contents	7
List of Figures	11
List of Tables.....	16
CHAPTER 1: INTRODUCTION.....	19
1.1 THE ROLE OF IRON IN THE NATURAL ENVIROMENT	19
1.2 THESIS AIMS	22
1.3 THESIS OUTLINE.....	25
CHAPTER 2: LITERATURE REVIEW	27
2.1 IRON	27
2.1.1. The formation of iron minerals in nature: Sources	31
2.1.2. Depositional environments: Sinks	33
2.1.3. Early diagenesis and the redox cycling of Fe.....	36
2.1.4. The reactivity of iron bearing minerals	38
2.1.5. The reactivity of iron bearing minerals within natural environments	43
2.2 THE REACTIVITY OF IRON MINERALS UNDER SULFIDIC CONDITIONS	44
2.2.1. Iron and the sulfur cycle	44
2.2.2. Bacterial Sulfate Reduction	45
2.2.3. The formation of iron mono-sulfides and pyrite	47
2.2.4. The reductive dissolution of iron minerals within sulfidic environments	52
2.2.5. The classification of iron mineral reactivity	55
2.3 FE ISOTOPES	60

2.3.1. The role of Fe isotopes in examining early diagenetic sediment processes	60
2.3.2. Basic concepts	63
2.3.3. Dissimilatory iron reduction Vs. abiotic mineral dissolution: Fe isotope signatures	64
2.3.4. Fe isotopes in sedimentary systems: modern marine environments	65
CHAPTER 3: METHODS AND MATERIALS	69
3.1 INTRODUCTION	69
3.1.1. Fe-mineral synthesis	69
3.2 SEDIMENT CHARACTERISATION	71
3.2.1. Fe phase characterisation	72
3.2.2. Sulfur species extraction	77
3.3. SULFIDATION EXPERIMENTS	80
3.3.1. Closed system iron sulfidation	80
3.3.2. H ₂ S sediment incubation	82
3.4. CHEMICAL ANALYSIS	83
3.4.1. Determination of Fe(III)/Fe(II)	84
3.4.2. Non-reductive dissolution of Fe(III) oxides	87
3.4.3. Determination of sulfur products: Methylene Blue method	89
3.5 Fe ISOTOPE ANALYSIS	92
3.5.1. Isotope sampling	92
3.5.2. Multi Collector Inductively Coupled Plasma-Mass Spectrometry	93
CHAPTER 4: EXPERIMENTAL SULFIDATION OF Fe-RICH SEDIMENT CORES; UMPQUA RIVER, N.CALIFORNIA AND AARHUS BAY, DENMARK	94
4. 1. INTRODUCTION	94
4.1.1. The reductive dissolution of iron oxide minerals mediated by dissolved sulfide	94
4.1.2 Fe oxide minerals in a reactive continuum	99
4.2. RESEARCH AIMS	102

4.3 GEOGRAPHICAL SETTING	104
4.3.1. Aarhus Bay, Denmark	104
4.3.2. Umpqua River Shelf, Oregon, N. Pacific Basin	104
4.4 METHODS	105
4.4.1. Sediment characterization	105
4.4.2. Sulfidation experiments	107
4.5 RESULTS	109
4.5.1. Fe characterisation of sediment cores	109
4.5.2. Experimental sulfidation of iron oxide mineral assemblages	119
4.6 DISCUSSION	126
4.6.1. Pore-water and sedimentary analysis.....	126
4.6.2. FeS formation.....	127
4.6.3. Determination of Fe mineral reactivity	129
4.7 SUMMARY	150
CHAPTER 5: THE EXPERIMENTAL DISSOLUTION OF IRON CARBONATE MINERALS WITHIN SULFIDIC ENVIRONMENTS	152
5.1 INTRODUCTION	152
5.1.1. Fe(II) carbonate minerals	152
5.1.2. The formation of siderite in ancient environments	154
5.2 RESEARCH AIMS	158
5.3 METHODS	159
5.3.1. Materials	159
5.3.2. Natural crystalline siderite.....	160
5.3.3. Experimental parameters	161
5.3.4. Siderite blanks - the effect of varying pH	162
5.4 RESULTS	164
5.4.1. Chemical speciation.....	164
5.4.2. Dissolution of BIF stable siderite: Bilbawik Formation.....	168
5.5 DISCUSSION	170

5.5.1. Mechanism of siderite dissolution	170
5.5.2. Determination of the rate equation	171
5.5.3. Effect of pH.....	176
5.5.4. The reactivity of iron minerals	179
5.5.5. Application to natural environments: Rate of sulfide-mediated dissolution of siderite from the Bibwaik Iron Formation	181
5.6 SUMMARY	183
CHAPTER 6: IRON ISOTOPE FRACTIONATION DURING SULFIDE PROMOTED REDUCTIVE DISSOLUTION OF IRON (OXYHYDRO)OXIDE MINERALS	184
6.1 INTRODUCTION	184
6.6.1. Iron isotope fractionation during reductive dissolution.....	184
6.6.2. Hypothesised mechanism of isotopic fractionation	186
6.2 RESEARCH AIMS	188
6.3 METHODOLOGICAL CONSIDERATIONS	189
6.4 RESULTS	191
6.4.1. Chemical Speciation	191
6.4.2. Reaction Kinetics	196
6.4.3. FeS Formation	197
6.4.4 Fe Isotope data	198
6.5 DISCUSSION	201
6.5.1 Mechanistic controls on isotopic fractionation (I)	201
6.5.2 Dissolution and effect of adsorption.....	205
6.5.3 FeS formation	206
6.5.4 Mechanistic controls on isotopic fractionation (II).....	207
6.5.5 Applications to natural environments	212
6.6 SUMMARY	214
7. OVERALL CONCLUSIONS AND FUTURE WORK	215
8. REFERENCES	223

LIST OF FIGURES

CHAPTER 2

Figure 2.1: Major reactive iron sources and sinks where values in bold indicate influx of iron as Tg yr^{-1} (Raiswell, 2006).....	32
Figure 2.2: Metabolic mechanisms associated with early diagenesis (adapted from Froelich et al., 1979 and Canfield & Thamdrup, 2009), where the composition of OM is defined by Redfield (1958).....	37
Figure 2.3: The localised redox cycling of Fe(III)-Fe(II) within near surface sedimentary environment (adapted from Hering & Stumm, 1990).....	38
Figure 2.4: General mechanism of Fe(III) reductive dissolution within anoxic aqueous environments (adapted from Stumm & Sulzberger, 1992).....	42
Figure 2.5: The S cycle in near surface sediments (Jorgensen & Kasten, 2006).....	45
Figure 2.6: Additional pathways of pyrite formation.....	50
Figure 2.7: Reaction pathway of sulfide mediated reductive dissolution (Dos Santos Afonso & Stumm, 1992).....	53

CHAPTER 3

Figure 3.1: Examples of synthesised Fe(III) oxide minerals (pre-drying)	70
Figure 3.2: Figure 3.2: AAS calibration curve determined from known concentration standards of Fe(III).....	76
Figure 3.3: Sulfur species extraction line	79
Figure 3.4: Experimental iron sulfidation equipment	81
Figure 3.5: Sample chamber for de-oxygenating inject sample into reaction vessel...	83

Figure 3.6: The linear relationship observed between Fe(II) or Fe(III) concentration and absorbance plots, measuring dilute, known, concentrations of a stock standard Fe solution (1000 μ M).....	86
Figure 3.7: Comparison of non-reductive Fe(III) dissolution and H ₂ S catalysed dissolution of 0.1g ferrihydrite, initial sulfide = 1000 μ M	
Figure 3.8: Oxidation of sulfide in deoxygenated DIW, pH 7.5, Initial Sulfide = 494 μ M	92

CHAPTER 4

Figure 4.1: Sulfide mediated reductive dissolution of Fe(III) oxide minerals and the formation of elemental sulfur and iron mono-sulfides.....	96
Figure 4.2: Aarhus Bay sample site (Thamdrup <i>et al.</i> , 1996)	104
Figure 4.3: Umpqua River Shelf sample site.....	105
Figure 4.4: Pore water distribution of dissolved Fe ²⁺ _(aq) and HS ⁻ _(aq) in Aarhus Bay core sections.....	109
Figure 4.5(a +b): Concentration of Fe(III) oxide species (based on reactivity scheme classification) as a percentage of Fe within the total sediment sample	112
Figure 4.6(a +b): Solid phase sediment characterisation, normalized to concentration of highly reactive Fe species (FeHR)	112
Figure 4.7: Pore water distribution of dissolved Fe ²⁺ _(aq) and HS ⁻ _(aq) in Umpqua River Sediment sections	113
Figure 4.8: a) Comparison of Fe(III) species concentrations measured as a wt% of Fe in individual sediment samples and b) characterisation of Fe reactivity with respect to FeT describing overall mineralogy	115
Figure 4.9: a) Speciation of highly reactive Fe Oxide minerals, with respect to FeHR (Canfield <i>et al.</i> , 1992) b) Surface reduced Fe(II) present on mineral surfaces compared to pyrite formation within Umpqua River sediment (w.r.t. FeHR phases).....	116

Figure 4.10: Speciation plots of Fe(III) oxide minerals.....	121
Figure 4.11: Iron speciation and sulfide concentration profiles from iron sulfidation of Aarhus Bay sediments.....	123
Figure 4.12: Iron speciation and sulfide concentration iron sulfidation experiments of Umpqua River shelf sediments.....	125
Figure 4.13: FeS formation under experimental conditions: Synthetic minerals	127
Figure 4.14: Additional sulfide measured above initial sulfide concentration for sulfidation experiments with Umpqua River sediments	129
Figure 4.15: Determination of a fractional order (0.5) with respect to the initial sulfide concentration required for reductive dissolution	131
Figure 4.16: Profile of Fe a) reduction and b) dissolution of three ferrihydrite samples of different initial concentration	133
Figure 4.17: Profile of Fe(III) oxide a) reduction and b) dissolution of three Fe(III) oxide minerals varying in sulfide reactivity	134
Figure 4.18: Derivation of rate constant K and gamma distribution (Postma, 1993) for synthetic Fe(III) minerals under experimental sulfidation during a) reductive processes b) dissolution	138
Figure 4.19: Derivation of rate constant K and gamma distribution (Postma, 1993) for Aarhus Bay sediments under experimental sulfidation during a) reductive processes b) dissolution.....	143
Figure 4.20: Derivation of rate constant K and gamma distribution (Postma, 1993) for Umpqua River sediments under experimental sulfidation during a) reductive processes b) dissolution	144
Figure 4.21: Comparison of synthetic Fe(III) oxide reduction rates with the reactivity of natural sediments from a) Aarhus Bay b) Umpqua River.....	148
Figure 4.22: Comparison of synthetic Fe(III) oxide dissolution rates with the reactivity of natural sediments from a) Aarhus Bay b) Umpqua River	149

CHAPTER 5

Figure 5.1: Equations of siderite formation and reaction	155
Figure 5.2: Model of iron formation deposition within a stratified ocean.....	156
Figure 5.3: XRD pattern for (a) synthetic crystalline siderite, comparing peak positioning and abundance with (b) internal library minerals	159
Figure 5.4: Dissolution of 0.1g siderite over pH range 6.5-8.5 in deionised water	163
Figure 5.5: Dissolution of Fe(II) via iron sulfidation. Initial conditions a) 0.098g FeCO ₃ , 839 μM S ²⁻ , pH 7.44 b) 0.101g FeCO ₃ , 401 μM S ²⁻ , pH 7.35, c) 0.195g FeCO ₃ , 401 μM S ²⁻ , pH 7.4, d) 0.150g FeCO ₃ , 390 μM S ²⁻ , pH 7.4	165
Figure 5.6: Total Fe dissolution of siderite pH 7.5; for iron sulfidation experiments conducted at vary initial sulfide concentration (μM)(n.b. corrected for Fe carbonate dissolution under non-sulfidic conditions)	167
Figure 5.7: Total Fe(II) dissolution measured with varying initial FeCO ₃ concentrations	167
Figure 5.8: Speciation plot for the sulfidation of a natural siderite sample	168
Figure 5.9: Determination of a 0.5 reaction order from logarithmic plots of total dissolution rate and initial sulfide concentration.....	173
Figure 5.10: Logarithmic plot of total Fe(II) dissolution and surface area, observing a reaction order of 1 dependency on surface area	173
Figure 5.11: Fe(II) dissolution; 0.1g, 500μM S ²⁻ , values corrected for Fe(II) dissolution under non sulfidic conditions (see Figure 5.4)	177

CHAPTER 6

Figure 6.1: Chemical Speciation data for sulfidation experiment, pH 4. Data for surface-reduced Fe calculated from total Fe(II)mass balance	192
Figure 6.2: Chemical Speciation data for sulfidation experiments, circum-neutral to alkaline pH data for surface-reduced Fe calculated from total Fe(II)mass balance.....	193

Figure 6.3: Initial linear rates of Fe(II) dissolution for Fe (oxyhydr)oxide minerals (pH 4)	196
Figure 6.4: FeS formation via iron sulfidation experiments for Fe(III) oxide minerals, pH 4.....	198
Figure 6.5: Raw data for dissolved $\delta^{56}\text{Fe}$ and surface reduced $\delta^{56}\text{Fe}$ isotopic composition calculated from experimental iron sulfidation	199
Figure 6.6: Raw data for dissolved $\delta^{56}\text{Fe}$ and surface reduced $\delta^{56}\text{Fe}$ isotopic composition calculated from experimental iron sulfidation	200
Figure 6.7: Surface reduced $\delta^{56}\text{Fe}$ fractionation as a function of initial reduction rate	203
Figure 6.8: Rate of Fe(II) dissolution (pH 4).....	211
Figure 6.9: Linear relationship of dissolution- $\delta^{56}\text{Fe}$ isotopic fractionation as a function of Fe(II) dissolution rate (pH 4)	211

LIST OF TABLES

CHAPTER 2

Table 2.1: Common iron bearing minerals observed within natural environments (<i>adapted from Cornell & Schwertmann, 2003</i>).....	28
Table 2.2: Geological sinks for iron minerals (Cornell & Schwertmann, 2003)	34
Table 2.3: The reaction order of Fe bearing minerals, with respect to the rate of iron reductive dissolution (Canfield <i>et al.</i> , 1992)	57
Table 2.4: Rate constant and half-life of iron mineral reactivity associated with sulfide mediated reductive dissolution (Poulton <i>et al.</i> , 2004)	58
Table 2.5 Summary of Fe isotopic reactions (collated in Dausphas & Rouxel, 2006)	62

CHAPTER 3

Table 3.1: Calculated error per sequential extraction step.....	77
Table 3.2: Reactant concentrations for Diamine reagent strengths.....	91

CHAPTER 4

Table 4.1: Details of the rate equation for sulfide mediated reductive dissolution of Goethite, as determined by Pyzik & Sommer (1981)	95
Table 4.2: Kinetic determination of sulfide mediated reductive dissolution (Poulton, 2003; Poulton <i>et al.</i> , 2004).....	99
Table 4.3: Kinetic rate determination of ascorbic-mediated reductive dissolution.....	101
Table 4.4: Experimental parameters for iron sulfidation experiments.....	107

Table 4.5: Extractable Fe -speciation data for Aarhus Bay sediments	111
Table 4.6: Characterisation of Aarhus Bay sediment in terms of reactive Fe species .	111
Table 4.7: Extractable Fe -speciation data for Umpqua River sediments.....	117
Table 4.8: Characterisation of Umpqua river sediment in terms of reactive Fe species	118
Table 4.9: Parameters derived for reaction order determination (with respect to initial sulfide concentration).....	132
Table 4.10: Derivation of rate constant K for individual synthetic Fe(III) oxides.....	139
Table 4.11: Collation of statistical data for synthetic mineral experiments: Comparison of linearity correlation F Test Vs Levenes Test	139
Table 4.12: Derivation of rate constant K for natural Fe sediment assemblages: Aarhus Bay and Umpqua River Shelf sediments	145
Table 4.13: Collation of statistical data for natural sediment experiments: Comparison of linearity correlation F Test Vs Levenes Test	145

CHAPTER 5

Table 5.1: Initial conditions for iron sulfidation experiments	161
Table 5.2: Collation of statistical data representing the dissolution rates of FeCO ₃ during sulfidation: Experimental and Natural sediment studies.	169
Table 5.3: Values of logarithmic Fe(II) dissolution rate with varying initial dissolved sulfide and Fe(II) surface area (pH 7.3-7.5)	174
Table 5.4: Determination of rate constant k Fe diss for individual experiments, associated with initial reactant parameters and rate of Fe(II) dissolution	175
Table 5.5: Determination of rate constant k' for siderite dissolution experiments over pH range 6.5-8.5 (in terms of both surface area and Fe mineral concentration	178

Table 5.6: Collated statistical data of pH influencing Fe(II) dissolution experiments: F Test Vs Levenes Test	178
Table 5.7: Comparison of rate constant K_{Fediss} values: Iron Carbonates and Oxides ..	179
Table 5.8: Reactivity of iron bearing minerals catalysed by 1000 μM dissolved sulfide pH 7.5.....	181

CHAPTER 6

Table 6.1: Experimental conditions for iron mineral sulfidation	190
Table 6.2: Initial experimental results: Chemical and raw isotope data (pH 4)	194
Table 6.3: Initial experimental results: Chemical and raw isotope data (alkaline pH)	195
Table 6.4: Comparison for rate constant K_{Fe} for Fe(III) oxide mineral reactivity	197
Table 6.5: Corrected isotopic composition for reduction and dissolution during iron sulfidation	210
Table 6.6: Collated statistical data representing correlation of linearity of synthetic mineral experiments: F Test Vs Levenes Test.....	211
Table 6.7: Fe isotope fractionation associated with sulfide mediate reductive dissolution	213

CHAPTER 1: INTRODUCTION

1.1 THE ROLE OF IRON IN THE NATURAL ENVIRONMENT

The presence of iron bearing minerals within aquatic settings may provide a robust indication of the environment in which they were deposited (Raiswell *et al.*, 1988), from within both modern and ancient marine environments. The examination of iron minerals within natural sedimentary environments is extremely relevant to geochemical studies due to the varying reactivity of Fe carbonates, oxides and silicates in relation to a number of different solutes (Hering & Stumm, 1990), controlling diffusion into porewaters and the adjacent water column. Insoluble within oxic environments, abundant Fe(III) oxides are most commonly observed near the sediment surface in anoxic, organic-rich marine sediments (Berner, 1984). Here, subsequent changes in sediment oxygenation may take place during early diagenesis (including both biogenic and abiotic mechanisms; Froelich *et al.* 1979), allowing a series of redox reactions to occur below the sediment-water interface.

A series of redox processes (including dissolution, precipitation and adsorption reactions) occurs between the reactive iron mineral surface and dissolved solutes either within porefluids or in bottom waters adjacent to the sediment surface (Stone & Morgan, 1987; Appelo & Postma, 2005); utilising key nutrients, organic acids and trace metals available within the near-surface sedimentary system. Importantly, the presence of iron minerals are considered to regulate the concentration of dissolved sulfide within porewaters and also the anoxic water column (Canfield, 1989). Where dissolved sulfide (i.e. H_2S , HS^- and S^{2-}) is produced via the bacterial reduction of sulfate (BSR; Sweeney & Kaplan, 1980), it may act as a catalyst to reduce Fe(III) oxides to Fe(II), subsequently releasing Fe(II) into the surrounding environment. During this reaction, reduced phase

sulfide may be re-oxidised to form S species such as elemental sulfur (Yao & Millero, 1996) or (thio)sulfate; while sulfide remaining in solution will react with dissolved Fe(II) to precipitate a number of iron sulfide minerals (Rickard, 1995). The mechanism for the anoxic reductive dissolution of iron oxide minerals by sulfide is well characterised, as are the products of these reactants in the form of intermediate sulfur minerals (iron mono-sulfides, FeS(s)) and the subsequent formation of pyrite (FeS₂(s); Dos Santos Afonso & Stumm, 1992; Wilkin & Barnes, 1996).

Currently, a solid understanding of iron mineral reactivity within natural systems, concurrent with investigations of reaction kinetics under experimental laboratory conditions, has allowed a vast number of studies to detail the abiotic mechanisms of ongoing early diagenetic processes observed under different environmental settings (e.g. marine, sand aquifer, lake etc; Thamdrup *et al.*, 1994). Alongside early field studies of sulfide mediated reductive dissolution (Canfield, 1989; Canfield *et al.*, 1992), the examination of Fe(II) dissolution via microbial (dissimilatory) iron reduction (DIR; Lovely, 1991), the addition of organic acids (e.g. ascorbate; Postma, 1993) and the dissolution of Fe(II) mediated by siderophiles (Borer *et al.*, 2005) are all considered important regulators of the Fe(III)-Fe(II) cycle in sedimentary and soil systems, the mechanisms of which have been further investigated for sediments from a variety of different aquatic environments (lakes, shallow seas, continental shelves, deep ocean; Poulton & Raiswell, 2002; Raiswell, 2006).

Whilst the modern global marine system is predominantly oxic, there are notable exceptions in a very small number of continental basins which are characterised by Fe(II)-rich (ferruginous) waters (e.g. Lake Matano, Indonesia; Crowe *et al.*, 2011), or by the larger number of aquatic settings that are characterised by their euxinic (free water column sulfide) nature (e.g. the Black Sea; Canfield *et al.*, 1996; Lyons &

Severmann, 2006). Within euxinic settings, sulfide-promoted reductive dissolution is widespread, and an important precursor to pyrite formation (Raiswell & Anderson, 2005). This process also occurs close to the sediment water-interface in a great many environments, providing organic matter is abundant and bacterial sulfate reducers can flourish (Berner, 1985).

Alongside standard laboratory determinations of reaction mechanism and rate equations, isotope systematic studies have been widely used to identify both biological and abiotic reactions within natural sediments (e.g. Beukes *et al.*, 1990; Kaufmann *et al.*, 1990). Early studies of Fe rich environments utilised the cycling of carbon, oxygen and sulfur and associated isotopic fractionation signatures to trace changes in the redox state, bacterial activity and oxygen content within both modern sediment and soil systems and more importantly, the ancient rock record. More recently the advance of non-traditional isotope systems has proved useful in understanding transition metal cycling within redox sensitive sediments, and of particular relevance to this study, the isotopic fractionation of $\delta^{56}\text{Fe}$ isotopes to trace Fe(III) reduction and Fe(II) dissolution in both biological and abiological processes (reviewed extensively within Dauphas & Rouxel, 2006; Anbar & Rouxel, 2007 and Johnson *et al.*, 2008a).

What can be concluded from an extensive study of current literature (as examined in Chapter 2) is that there are still many unanswered questions regarding the mechanism and rates of iron mineral reductive dissolution (as determined through laboratory experiments), and the relevance of experiments with synthetic minerals to adequately evaluate the reductive dissolution of naturally occurring Fe minerals during sediment diagenesis. By bringing together a study of the experimental determination of reaction mechanisms and kinetics for synthetic Fe minerals and natural mineral assemblages, with the determination of isotope systematics during the process, a more thorough

understanding of the influence of chemical processes on the cycling of Fe in anoxic environments may be achieved.

1.2. THESIS AIMS

The collective aim of this thesis is to build upon previous knowledge obtained during laboratory investigations of sulfide mediated reductive dissolution of Fe(III) oxides (Dos Santos Afonso & Stumm, 1992; Peiffer *et al.*, 1992; Yao & Millero, 1996; Poulton, 2003; Poulton *et al.*, 2004a). By expanding on the experimental rationale developed in previous studies which examine the reactivity of a variety of Fe(III) oxide minerals during sulfidation, a new understanding of the links between pure mineral experiments within the laboratory and the reactivity of natural sediment assemblages within the sedimentary profile may be achieved. The objectives of this study are:

- *To detail the rate and mechanism of sulfide mediated reductive dissolution of Fe(III) oxides within a natural sedimentary assemblage.*

Previous investigations of naturally occurring Fe(III) oxide reductive dissolution have focused on reactions mediated by organic acids which are not specifically abundant within marine sediments (Postma, 1993; Larsen & Postma, 2001). However, the kinetics by which these processes occur are concurrent with the reactive continuum process described by Boudreau & Riddick (1991) in changing sediment mineralogy throughout a near surface sediment core, with a decrease of oxygen associated with bacterial processes during early diagenesis. The approach taken within these studies shall be applied to near surface, sediment assemblages undergoing natural sulfidation to assess the changing reactivity of Fe(III) oxide minerals with depth close to the sediment-water

boundary. Two sediment cores from geographically different settings, and of different Fe mineralogy will be compared to studies of individual, synthetic Fe(III) mineral sulfidation rates, to characterise firstly the contents of each sediment sample in comparison to the results described by an iron phase sequential extraction process; and secondly to provide a greater connection between Fe(III) oxides rates determined experimentally and those observed in field experiments.

- *A study of the reactivity of Fe carbonates in the presence of dissolved sulfide.*

Although formation of Fe carbonate minerals in modern environments tends to be somewhat limited, and generally restricted to specific settings in the modern environment, studies of the ancient rock record have recently increasingly shown that such minerals were a prevalent feature during the extensive occurrence of anoxic water column conditions in the past (e.g. Reinhard *et al.*, 2009; Poulton *et al.*, 2010). Due to the nature of modern Fe carbonate formation under low sulfide conditions, the reactivity of minerals such as siderite with respect to dissolved sulfide has never been experimentally determined. However, the presence of iron-carbonate minerals in terms of reconstructing past redox conditions, and it is commonly assumed that Fe carbonate is highly reactive towards dissolved sulfide. Thus a major aim of this thesis is the determination of the reactivity of Fe carbonate minerals and comparison to the reactivity scheme for Fe oxides reported by Poulton *et al.* (2004).

- *To evaluate Fe isotope fractionation during the sulfide promoted reductive dissolution of Fe(III) oxides.*

The Fe redox cycle through near surface sediments during early diagenesis has been widely studied with respect to isotopic tracing of biological iron reduction and oxidation processes in both modern marine sediments and within the ancient rock record (Johnson & Beard, 2005; 2006). The abiotic reductive dissolution of Fe(III) oxides in marine sediments by highly abundant dissolved sulfide occurs from a multistep surface process (Dos Santos Afonso & Stumm, 1992) which is hypothesised to favourably allow the fractionation of $\delta^{56}\text{Fe}$ isotopes during this reaction. A two step fractionation mechanism is proposed throughout this reaction, tracing the reduction of Fe(III)-Fe(II) via electron transfer between the formation of an adsorbed sulfide surface complex, and the highly reactive Fe(III) surface; and during the detachment of $\text{Fe(II)}_{\text{aq}}$ from the mineral surface during dissolution. The overall isotopic signature associated with the reaction of dissolved sulfide with a number of different reactive Fe(III) oxide minerals commonly observed within the modern sedimentary systems and those used as indicators of paleoenvironmental deposition, can therefore be compared with isotopic values associated with so called 'biosignatures' describing microbial respiration activity within similar environments.

1.3 THESIS OUTLINE

Following on from this brief introduction to the biogeochemical and isotopic cycling of Fe in natural environments, **Chapter 2** provides a literature review detailing Fe-mineral reduction and dissolution mechanism studies, and the rates at which these processes occur under both experimental and natural conditions. By focusing on the reaction between Fe minerals and dissolved sulfide during early diagenesis (primarily within marine sediments), studies which investigate the isotopic fractionation of such elements in nature are also discussed. The general experimental processes of both open and closed system iron sulfidation experiments used throughout this study are detailed in **Chapter 3** (Methodology), along with methods of sample analysis and natural sediment sample characterisation.

A comparison of the rates of sulfide mediated reductive dissolution between pure synthetic Fe oxide minerals and Fe oxide minerals found within natural sediment assemblages from *Aarhus Bay*, Denmark; and the *Umpqua River shelf*, N. Pacific, is investigated in **Chapter 4**. By investigating the iron sulfidation of Fe(III) rich sediment samples in comparison to pure synthetic minerals, a better understanding of the potential for studies of synthetic minerals to adequately reflect reaction kinetics in the environment is achieved.

A study detailing the mechanism and rate of Fe(II) carbonate (siderite) dissolution with dissolved sulfide is examined in **Chapter 5**. Through a series of sulfidation experiments, the reactivity of siderite with respect to dissolved sulfide is incorporated into a commonly used reactivity scheme for Fe(III) oxides of different crystalline structures, providing the first detailed insight into whether Fe carbonate minerals can be considered to be reactive towards dissolved sulfide on diagenetic timescales.

The final data chapter of this study (**Chapter 6**) details the isotopic fractionation of Fe oxides by the mechanisms explored in Chapter 4. By investigating the magnitude of fractionation between different product Fe species a greater understanding of Fe isotope fractionations observed in nature is observed, with major implications for the recognition of bacterial Fe reduction in modern and ancient sedimentary systems.

Finally, **Chapter 7** provides an overall summary of the research covered in this thesis, and includes suggestions for potential future activities related to this research.

CHAPTER 2: LITERATURE REVIEW

2.1. IRON

Iron, a first row transition metal, is the fourth most abundant element within the Earth's crust, and is found predominantly in the natural environment, incorporated into iron bearing minerals; most commonly as carbonates, oxides, silicates or sulfides (Haese, 2006). Upon weathering, oxidation and precipitation within an oxic hydrous environment, iron oxides (hydroxides and (oxyhydr)oxides) are readily formed and classified depending on the ratio of Fe to O/OH present within individual structures (Cornell & Schwertmann, 2003). These oxidised minerals (generally termed as iron (III) oxides throughout this study) vary greatly in colour, crystal structure, solubility and surface area depending on the electron configuration of precipitated structures.

Iron minerals are formed with either a divalent or trivalent (Fe^{2+} or Fe^{3+}) oxidation state (Haese, 2006) depending upon the conditions or environment under which minerals are precipitated, with greigite, magnetite and green rust minerals precipitate as mixtures of both Fe(II) and Fe(III) (Table 2.1; Cornell & Schwertmann, 2003). Under modern oxic conditions, iron (III) oxide minerals are of low solubility (and hence, mobility) in a majority of aqueous environments; whereas under anoxic conditions (created by oxygen-scavenging bacterial reactions in near surface sediments or open water columns, where there is an abundance of organic matter; Lovely, 1991) iron oxides are easily reduced, becoming unstable and increasing their solubility (Stone & Morgan, 1987). Freshly precipitated iron oxides are characteristically poor in crystallinity, and highly reactive due to their large surface areas, being abundant within surface and/or near surface sedimentary environments. These structures are metastable and readily

transform into more highly crystalline, thermodynamically stable iron oxides under conditions of oxidation and temperature increase.

Table 2.1 lists a number of the most commonly occurring iron oxide minerals which are characterised by their unique physical properties. The majority of compounds are octahedral ($\text{Fe}(\text{O})_6$ / $\text{FeO}_3(\text{OH})_3$) or tetrahedral ($\text{Fe}(\text{O})_4$) in structure with an account of individual Fe morphologies described below. By studying each minerals unique physical properties and structure (as collated by Cornell & Schwertmann, 2003; Pedersen, 2006), an understanding of the solubility and reactivity of differing minerals may be recognized.

Table 2.1: Common iron bearing minerals observed within natural environments
(adapted from Cornell & Schwertmann, 2003)

<i>Carbonates</i>	<i>Oxyhydroxides and hydroxides</i>	<i>Oxides</i>
Siderite $\text{Fe}^{\text{II}}\text{CO}_3$	Goethite $\alpha\text{-FeOOH}$ Lepidocrocite $\gamma\text{-FeOOH}$ Ferrihydrite $\text{Fe}_5\text{HO}_8.4\text{H}_2\text{O}$ Green Rust $\text{Fe}^{\text{III}}_x\text{Fe}^{\text{II}}_y(\text{OH})_{3x+2y-z}(\text{A}^-)_z$; $\text{A}^- = \text{Cl}^-; \frac{1}{2} \text{SO}_4^{2-}$	Hematite $\alpha\text{-Fe}_2\text{O}_3$ Magnetite Fe_3O_4 (as $\text{Fe}^{\text{II}}\text{Fe}^{\text{III}}_2\text{O}_4$)

Ferrihydrite (assumed formula $5\text{Fe}_2\text{O}_3.9\text{H}_2\text{O}$ or $\text{Fe}_5\text{HO}_8.4\text{H}_2\text{O}$)

Due to its poorly crystalline nature, there are many interpretations associated to the characterisation of ferrihydrite. Forming in solution as iron oxyhydroxides (water containing molecules), XRD analysis differentiates two specific orders of ferrihydrite (2-line or 6-line) which develop depending on precipitation, pH and temperature

conditions during formation, and may easily transform from one to the other (Kukkadapu *et al.*, 2003). Mineral synthesis of poorly structured ferrihydrite produces a red-brown precipitate, which is thermodynamically unstable, with a large surface area compared to more stable minerals ($< 400 \text{ m}^2\text{g}^{-1}$; BET surface analysis). Ferrihydrite is important in surface environments due to its common occurrence, highly reactive nature under anoxic conditions, and its ability as a precursor to readily transform into more stable crystalline oxide minerals.

Lepidocrocite ($\gamma\text{-FeOOH}$) / Goethite ($\alpha\text{-FeOOH}$)

Formed from the oxidation of $\text{Fe(II)}_{\text{aq}}$ from green rust in solution, lepidocrocite precipitates to form an orange powder which is highly crystalline, yet also reactive on a similar timescale to ferrihydrite, with a surface area $< 250 \text{ m}^2\text{g}^{-1}$. Lepidocrocite readily transforms to more stable oxide assemblage, and is least likely to be found within the unaltered sediment profiles (Schwertmann & Taylor, 1972). In comparison, as the end product of many iron oxide transformations, goethite is a highly stable, highly ordered iron oxide which reacts on a slower timescale than ferrihydrite or lepidocrocite. Yellow in colour, goethite has a surface area of $< 200 \text{ m}^2\text{g}^{-1}$.

Magnetite (Fe_3O_4)

The structure of magnetite represents a ferromagnetic mixture of $\text{Fe(II)}/\text{Fe(III)}$ species, which are octahedral/tetrahedral layered within the mineral structure. Oxidation processes will transform magnetite to green rust overtime, with green rust also a prominent precursor mineral to magnetite formation (Sumoondur *et al.*, 2088) With a low surface area ($< 100 \text{ m}^2\text{g}^{-1}$) magnetite is highly crystalline and slow to react.

Hematite (α -Fe₂O₃)

Hematite, an ageing product of ferrihydrite, is a major component of ancient Banded Iron Formations, giving these rocks a characteristic red colour. Also abundant in soils and sediments, hematite is particularly crystalline and relatively slow to react, with a smaller surface area than the previously mentioned iron oxide minerals ($<90 \text{ m}^2 \text{ g}^{-1}$).

Of note, the individual colour of each mineral is dependent on the bond length and angle between Fe-Fe central atoms within each tetrahedral or octahedral structure (Cornell & Schwertmann, 2003); with the electronic configuration of Fe oxide minerals denoted by Fe²⁺ states (1s², 2s², 2p⁶, 3s², 3p⁶, 3d⁶) and Fe³⁺ (1s², 2s², 2p⁶, 3s², 3p⁶, 3d⁵) defining the physical properties associated with mineral stability and reactivity. Crobsy *et al.* (1983) first identified the surface area reported above for many individual naturally occurring Fe oxide minerals, in comparison to synthetically pure Fe forms. This study utilised X ray Diffraction to monitor the effect aging has on freshly precipitated Fe minerals, and the changing crystalline morphologies which change with time; concluding that individual end products and associated surface areas are influenced by the initial morphology of Fe(II) or Fe(III) species (Haese, 2006). Therefore due to their stable nature, goethite and hematite are the most readily observed Fe minerals in modern soil and sedimentary environments.

Other mechanism of iron oxide formation include the hydrolysis of Fe(III) salts or transformation of unstable precursor oxides to thermodynamically stable goethite or hematite end members (Cornell & Schwertmann, 2003). This conversion of minerals includes changes in morphology, crystalline lattice order, surface area and porosity via dissolution and re-precipitation reactions; or solid phase structural transformations (Lui *et al.*, 2007) occurring during both low temperature geochemical cycling and within high temperature/pressure systems over time, termed *ageing*. In order to catalyse these

reactions, conversions are often mediated by the adsorption of $\text{Fe(II)}_{(\text{aq})}$ or $\text{H}_2\text{O}_{(\text{aq})}$ to an unstable iron oxyhydroxide mineral surface (i.e. ferrihydrite; Zhao *et al.*, 1994, Lui *et al.*, 2007), allowing an electron transfer between $\text{Fe(II)}_{\text{aq}}$ and the Fe(III) oxide surface to stabilise the mineral structure. This uptake allows the transformation and reorganisation of ferrihydrite mineral lattices to highly crystalline, stable lepidocrocite, goethite or hematite (Jeon *et al.*, 2003; Williams & Scherer, 2004; Pedersen *et al.*, 2005).

All of the properties listed above influence the Fe- bearing minerals ability to react under changing redox conditions, and with biogeochemical cycling at the water-sediment boundary in aquatic environments. Processes of reduction, dissolution, adsorption, oxidation, hydrolysis, precipitation and transformation of iron oxides are all commonly observed and highly investigated in natural aquatic systems (Stumm & Sulzberger, 1992), and it is important to constrain the conditions under which these reactions occur.

2.1.1. The formation of iron minerals in nature: Sources

Highly reactive iron minerals (FeHR; i.e. ferrihydrite, lepidocrocite) are a major constituent of modern soils and marine sediments (FeHR = ~ 45% of total iron abundance, where total Fe within sediments = 4-5% sediment weight; Poulton & Raiswell, 2002), and are also observed within the ancient rock record. Primarily formed as solid phase particulates during the oxidative weathering of terrestrial rocks (Krauskopf & Bird, 1995; Cornell & Schwertmann, 2003), Fe(III) minerals are readily transported to a variety of terrestrial and marine aqueous systems, via riverine, aeolian, glacial and coastal erosion systems (Figure 2.1; Haese, 2006, Poulton & Raiswell, 2002; 2005 Raiswell, 2006). The mobility of these detrital particles along with other trace

metals (either dissolved or particulate, Poulton & Raiswell, (2000)), abundant from the chemical weathering of sedimentary rocks and the podzolisation of soils (Schwertmann, 1991), create a flux of soluble Fe(III) particles to aqueous environments. Transport through fluvial riverine systems will deposited iron fractions into sinks such as freshwater or glacial originated lakes, shallow marine seas, continental shelves and deep ocean basins (Raiswell, 2006). On a much larger scale (alongside terrestrial fluxes of iron), other direct sources of Fe to marine systems (non-detrital) include iron associated with the weathering of crustal Fe-Mn nodules and deposits in the deep sea (Elderfield & Schultz, 1996; Cornell & Schwertmann, 2003); and hydrothermal fluids from vents emitting Fe(II), such as those along the Mid-Ocean Ridge to produce a wide variety of stable Fe oxides upon diffusion to the water column. These mechanisms are particularly important within the ancient rock record during times where the ancient ocean was recognised as anoxic or euxinic (Holland, 1984; Poulton *et al.*, 2004b; Lyons *et al.*, 2009), and hydrothermal activity was ongoing.

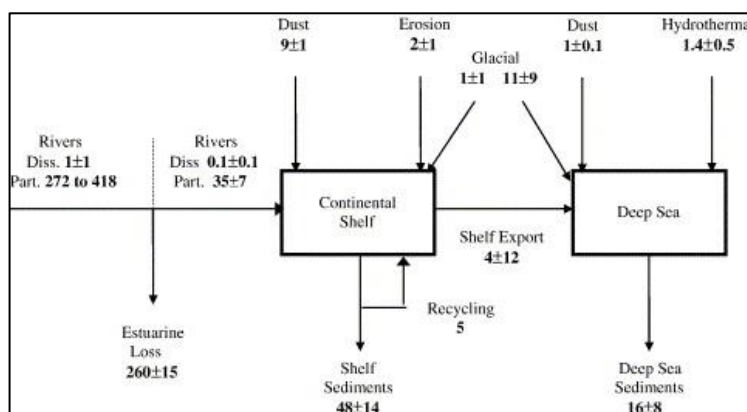


Figure 2.1: Major reactive iron sources and sinks (from Raiswell, 2006) where values in bold indicate influx of iron as Tg yr⁻¹.

Figure 2.1 identifies the major sources of highly reactive iron, whilst quantifying the global flux of iron species (both dissolved and particulate) between recognised sources and sinks, as described by Raiswell (2006) in order to constrain the widespread cycling of highly reactive iron species.

Once iron particulates are deposited at the sediment-water boundary, a number of diagenetic reactions (Froelich *et al.*, 1979; Berner, 1980, Van der Weijden, 1992), both biological and abiological in nature, occur within near surface sediments, determining the fate of iron redox species available for biogeochemical cycling. Under anoxic conditions, soluble Fe(III) particles will reduce and dissolve to produce aqueous Fe(II) in pore-waters (Stone & Morgan, 1987, Hering & Stumm, 1990); and upon diffusion back to an oxic water column, will readily re-oxidise Fe(II) to precipitate Fe(III) oxyhydroxides, to be re-deposited to the sediment-water boundary. Hence, although maybe not predominant, Fe(III) and Fe(II) formed diagenetically after sedimentary deposition are an important contributors to the global Fe cycle (Raiswell, 2006), with an *authigenic* flux contributing approximately 5 Tg/yr within marine and deep sea environments (Poulton & Raiswell, 2002; Elrod *et al.*, 2004).

2.1.2 Depositional Environments: Sinks

The environment in which Fe minerals are ultimately deposited determines the end member structure and redox state of Fe mineral assemblages in sediments, contributing to the availability of Fe(II) or Fe(III) for further reaction. The localities of these settings (Fe sinks: Cornell & Schwertmann, 2003; Raiswell, 2006) may be represented by a number of sedimentary deposits in the ancient rock record, within carbonate, sandstone or claystone formations. Cornell & Schwertmann (2003) (Table 2.2) describe a number

of these features and the class of iron mineral associated with each sink, which is reflected by factors such as bottom water oxygenation, stratification, and both detrital and authigenic Fe inputs. A variety of environmental and biological factors regulate the oxygen content of aquatic basins; either large scale marine, or localised and terrestrial (Demaison & Moore, 1980).

It is estimated that the Earths' atmosphere became increasingly oxygenated approximately 2.4 Gyr ago (Holland, 1984, 2006; Canfield, 2005), and has remained so since ~1.8 Ga. This had a major impact on the oxygen, sulfur and iron content of both ancient and modern oceans, which were, and are now, regulated by both the abundance of atmospheric oxygen saturating a given water mass; and subsequent bacterial photosynthetic processes (e.g. Croal *et al.*, 2004a; Kappler & Newman, 2004; Canfield *et al.*, 2006).

Table 2.2: Geological sinks for iron minerals (Cornell & Schwertmann, 2003)

Sink	Fe minerals and features
Lake	Freshwater, glacial meltwaters, stream input, Fe flux dominated by weathering of magmatic rocks and podzolised soil. Fully oxic or stratified. Anoxic or Euxinic bottom waters: Highly reactive species readily available.
Continental Shelf	Detrital and Authigenic input, coastal erosion.
Deep Sea	Continental Crust and basaltic nodes, Mn Oxides associated with Fe-Mn crusts
Hydrothermal	Fe(II) _{aq} rich plumes to oxic marine waters: lepidocrocite for transformation, Fe silicate rich.

Within modern aquatic environments, whether an entire water body is oxygenated is dependent upon the mixing of oxygen rich, eutrophic surface waters (which without influence, becomes anoxic with depth) and oxygenated, denser deep cold waters; via the physical mixing processes of upwelling and/or wind action (Tyson & Pearson, 1991). Within a sedimentary basin or silled continental margin, stratification may occur between periods of mixing (either seasonally, annually or only over geologic timescales) and controls the interface between oxic surface waters and denser anoxic water masses at depth. Open surface waters readily allow organic carbon in the form of deceased organic matter to fall through the water column, before being deposited on the sediment surface, fueling terminal electron acceptor processes (TEAPs; Lovely, 1991, Rullkotter, 2006) and microbial respiration in the upper sediment. Hence, without strong mixing of oxygenated waters, and without the production of oxygen at depth biologically, oxygen demand from aerobic microbial communities at the sediment-water interface may outstrip supply, allowing anoxic conditions to be developed in local marine systems (Calvert & Pedersen, 1993; Canfield *et al.*, 2006).

In comparison to modern oxic conditions, prior to the rise in atmospheric oxygen 2.4 Ga, ancient marine systems were predominantly anoxic and sulfide levels permanently low (with the later exceptions of sporadic continental euxinia (Reinhard *et al.*, 2009; Poulton *et al.*, 2010)). These conditions were supportive of the precipitation Fe carbonate minerals; and of Fe oxide formation to a higher extent than observed today, as documented within the widespread formation of banded iron formations in a number of localities (Klein, 2005). Periodically above the sediment-water boundary where organic material was vastly abundant, and where rates of sulfate reduction were sufficiently higher than that of iron reduction, euxinic (sulfidic) conditions persisted within low oxygen water columns (Raiswell & Berner, 1985; Lyons & Berner, 1992; Canfield *et*

al., 1996). These environments were synonymous with the formation of pyrite with an $\text{H}_2\text{S}_{(\text{aq})}$ rich water column reacting with detrital Fe oxide minerals (Lyons & Severmann, 2006), and where found today, are an important analogue (i.e. Black Sea; Canfield *et al.*, 1996) of the ancient euxinic systems observed continually throughout the ancient rock record.

2.1.3. Early Diagenesis and the redox cycling of Fe

As modern marine systems are generally oxygenated throughout the water column, a high abundance of reactive Fe(III) oxides at the sediment-water interface (Raiswell & Canfield, 1998) are observed. Near surface sediments may only become anoxic after a few centimetres depth, as oxygen from bottom waters is consumed by aerobic bacterial respiration reactions (Froelich *et al.*, 1979).

The orders of which these processes take place are significant in determining the oxygenation state of sediments at depth (Berner, 1980, Figure 2.3); and the primary TEAP reactions which take place during this progression of early sediment diagenesis are well characterised (Froelich *et al.*, 1979; Sorensen *et al.*, 1979). Summarised by Schulz (2006), the influencing factor which mediates anaerobic conditions is primarily the availability of organic matter (OM) produced in oxic surface waters, before falling through the water column to the sediment surface.

OXYGENATED BOTTOM WATERS + OM					
S E D I M E N T D E P T H (m)	OXIC SEDIMENT SURFACE				
	Electron Acceptor	Microbial Process	Mechanism	Product O ₂ /CO ₂	Zonation
	O ₂	Aerobic Respiration	(CH ₂ O) ₁₀₆ (NH ₃) ₁₆ (H ₃ PO ₄) + 138 O ₂ → 106 CO ₂ + 16 HNO ₃ + H ₃ PO ₄ + 122 H ₂ O	(+ HNO ₃ + H ₃ PO ₄)	OXIC
	NO ₂ ⁻ / NO ₃ ⁻	Nitrate Reducing	(CH ₂ O) ₁₀₆ (NH ₃) ₁₆ (H ₃ PO ₄) + 94.4 HNO ₃ → 55.2 N ₂ + 106 CO ₂ + H ₃ PO ₄	NO ₂ ⁻ NO ₃ ⁻	NITROGENOUS
	MnO ₂	Manganese Reducing	(CH ₂ O) ₁₀₆ (NH ₃) ₁₆ (H ₃ PO ₄) + 236 MnO ₂ → 236 Mn ²⁺ + 106 CO ₂	Mn ²⁺	MANGANOUS
	Fe ₂ O ₃ FeOOH	Iron Reducing	(CH ₂ O) ₁₀₆ (NH ₃) ₁₆ (H ₃ PO ₄) + 212 Fe ₂ O ₃ / 424 FeOOH → 424 Fe ²⁺ + 106 CO ₂ + H ₃ PO ₄ + 16 NH ₃ + 530/742 H ₂ O	Fe ²⁺	FERRUGINOUS
	SO ₄ ²⁻	Sulfate Reducing	(CH ₂ O) ₁₀₆ (NH ₃) ₁₆ (H ₃ PO ₄) + 53 SO ₄ ²⁻ → 53 S ²⁻ + 106 CO ₂ + H ₃ PO ₄ + 16 NH ₃ + 106 H ₂ O	H ₂ S	SULFIDIC
	CO ₂	Methanogenesis	(CH ₂ O) ₁₀₆ (NH ₃) ₁₆ (H ₃ PO ₄) → 53 CO ₂ + 53 CH ₄ + H ₃ PO ₄ + 16 NH ₃	CH ₄	METHANIC

Figure 2.2: Metabolic mechanisms and terminal electron acceptor processes associated with early diagenesis (adapted from Froelich et al., 1979 and Canfield & Thamdrup, 2009), where the composition of OM is defined by Redfield (1958).

Deposited OM will be oxidised whilst undergoing a series of biological reactions which exploit oxygen consuming electron acceptors along the way (reducing O₂, N, Mn, Fe(III), SO₄²⁻, CO₂ to O₂/CO₂, NO₃⁻, Mn²⁺, Fe²⁺, H₂S and CH₄ respectively). Figure 2.2 shows that only within the very surface of the sediment column (where organic matter is abundant) will oxygen be recycled; via bacterial consumption and further respiration of dissolved O₂. Below this oxic zone, oxygen is completely consumed and organic matter (along with an electron acceptor) is required for further oxidation (Herring & Stumm, 1990) allowing the continuation of the anaerobic microbial reactions outlined in Figure 2.2. In addition, the products of these reduction processes are available for further reaction. Iron which is biologically reduced to Fe²⁺ in porewaters, is easily reoxidised to FeOOH or magnetite in reaction with even low concentrations of oxygen (which has escaped consumption where both reactants diffuse through sediment; Lovely, 1993).

Therefore reactions at the boundary between both iron and sulfate reduction (via both biological and abiological means; Canfield & Thamdrup, 2009) may also overlap, and it is the premise of these reactions which are of great interest to this study.

2.1.4. The reactivity of iron bearing minerals

Within these diagenetically defined zones of reactivity, localised redox cycling of transition metals is primarily controlled by changes in O_2 concentration (and hence oxidation state; Figure 2.3; Hering & Stumm, 1990). Under oxic conditions Fe(III) oxides are considered thermodynamically stable (Stone & Morgan, 1987), but when reduced to a divalent state in an oxygen depleted environment, there is a significant increase in Fe mineral solubility and speciation. As the concentration of available Fe(III) as an electron acceptor for organic matter degradation often overwhelms the concentrations of other substrates (Lovely & Phillips, 1987), it is important to also carefully consider the effect of biologically reduced Fe alongside abiotic processes of reductive dissolution.

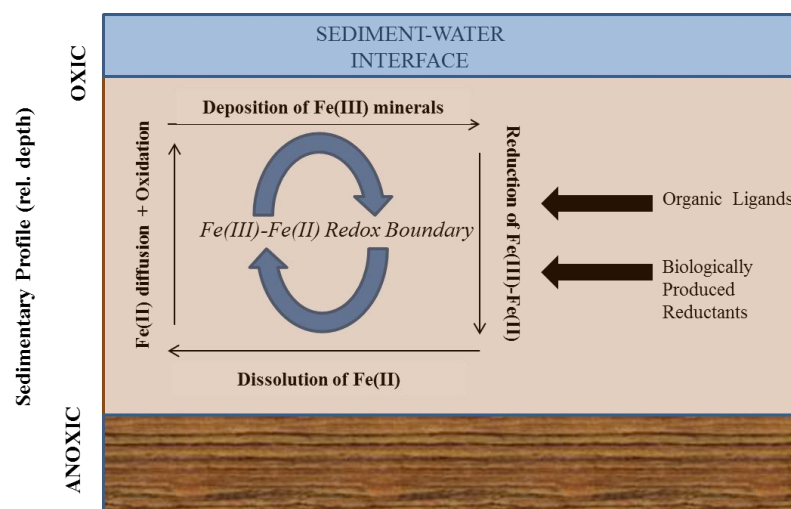
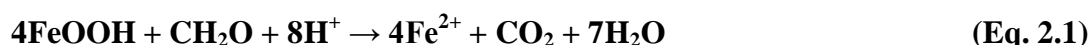


Figure 2.3: The localised redox cycling of Fe(III)-Fe(II) within near surface sedimentary environment (adapted from Hering & Stumm, 1990).

2.1.4.1. Biological Iron reduction

During the deposition of organic matter and particulate iron minerals, the microbially mediated iron reduction process outlined in Section 2.1.3 supports the biogeochemical cycles of carbon, oxygen and iron in near surface sediments (Lovely & Phillips, 1986). Dissimilatory iron reduction (DIR; Lovely, 1991) uses Fe(III) oxide minerals within anoxic sedimentary environments as terminal electron acceptors, reducing Fe(III) to Fe(II) and allowing subsequent dissolution of Fe(II) into anoxic systems. Many studies of this biological reaction have been performed (e.g. as reviewed in Lovely, 1991) with Fe(III) acting as a terminal electron acceptor for many dissimilatory reactions involving anaerobic bacterial strains, for example *Shewanella Alga* (Roden & Zachara, 1996) or *Shewanella Putrefaciens* (Roden, 2003; Bonneville *et al.*, 2006). An example of biological iron reduction (also in Figure 2.2) will oxidise organic carbon via acetate to carbon dioxide in the reaction described in Equation 2.1. The rate at which biological iron reduction and Fe(II) dissolution occurs, is a function of the accumulation of biogenically produced Fe(II) upon the residual Fe(III) oxide surface (Roden, 2004).



2.1.4.2 Iron Dissolution: Reductive and non-reductive processes

In contrast to the reductive dissolution processes Fe(III) oxides are subjected to in biological systems, the abiotic (or chemical) dissolution of Fe(III) oxides may occur in a variety of ways. It is well recognised that minerals undergoing a reductive process from Fe(III) to Fe(II) will dissolve more readily than solid phase Fe(III) to Fe(III)_{aq}, as Fe(III) is thermodynamically stable in most natural systems (Stone & Morgan, 1987; Wehrli *et*

al., 1989). This, in turn, demonstrates the ability of Fe minerals in reduced environments to dissolve more readily than those in oxic aqueous conditions.

Only when considering the weathering of Fe(III) minerals and their presence in oxygenated surface waters, may particulate Fe(III) species be readily dissolved by either photochemical reductive dissolution (Sulzberger & Laubscher, 1995; Borer *et al.*, 2005) or the action of soluble organic siderophores, described as organic ligands (i.e. desferrioxamine, DFO; Kraemer, 2004) produced biologically to scavenge and bind to Fe in Fe-limited environments (Hersman *et al.*, 1999). Zinder *et al.* (1986) outline the mechanism by which Fe(III) may also dissolve without undergoing a reductive reaction (i.e. in the presence of oxalate under acidic conditions) compared to proton catalysed reductive dissolution (which quickly weakens the Fe-O bond, before electron transfer and detachment of the central Fe atom) which although not important for the reaction of Fe(III) oxides under sulfidic conditions, may be a prominent catalyst of Fe(II) dissolution in other anoxic aqueous environments.

The dissolution of Fe(III) oxide species in anoxic environments occurs as a multistep, surface controlled reaction (Zinder *et al.*, 1986; Hering & Stumm, 1990). The hydroxylated nature of an oxide mineral surface (FeOH^- or FeOH_2^+) may be either protonated or deprotonated in solution, depending on the nature of the solute reacting at the solid oxide surface. The reactivity of functional groups on the oxide surface (OH/H₂O) defines the rate and mechanism by which dissolution occurs. The zero point of charge (ZPC) for FeOOH minerals (Schindler & Stumm, 1987) indicates that the surface mineral charge when neutral is zero. When in reaction with an acidic solution, protons attracted to the mineral surface create a positive charge (H^+). Below the PZC, (or in reaction with hydroxide ions, OH^-) a negative charge is observed. Of interest to this study, the *reductive* dissolution of Fe(III) oxides promoted by ligands (either acids

or anions) begins with the formation of adsorbed surface complexes on the active outer electron shell of the oxide mineral. Hydrated surface sites (or functional groups) will be displaced by solutes within aqueous environments which may contain organic acids (including chelators or binding ligands) such as EDTA or ascorbate (Banwart *et al.*, 1989; Dos Santos Afonso *et al.*, 1990), biologically produced reductants which adsorb onto the oxide surface (e.g. H₂S; Pyzik & Sommer, 1981), or metal ion species in solution (e.g. Fe²⁺_{aq}; Zinder *et al.*, 1986; Wehrli *et al.*, 1989; Suter *et al.*, 1991).

These species will adsorb (or *bind*) onto the central Fe-metal atom to create a precursory, inner sphere surface complex (Morgan & Stumm, 1987; Schindler & Stumm, 1987) which mediates an electron transfer between the bound surface complex and bulk oxide mineral to reduce Fe(III) to Fe(II). Of note, reaction processes are further catalysed in the presence of both a surface complex solute and reducer, with previous studies concentrating on the proton promoted reductive dissolution of a variety of Fe(III) minerals with organic acids such as ascorbate with oxalate or citrate (Banwart *et al.*, 1989; Suter *et al.*, 1991; and more recently Hyacinthe *et al.*, 2006). During this process of electron transfer, reductants adsorb to form a surface bridging complex, and will oxidise before releasing from the mineral surface. Weakening of the Fe-O bond will also occur during this process, allowing the energetically favourable detachment of Fe into solution as Fe(II)_{aq}.

Weiland *et al.*, (1988) describe a correlation between the rate of Fe(II) dissolution and surface interactions occurring between the reactive oxide mineral and a given solute (containing H⁺, OH⁻, weak acids or anions) in reaction, specifically that the dissolution rate associated with Fe(II)_{aq} moving into solution is a function of the concentration of surface species adsorbed from solution. With continual Fe(II) dissolution, changes in the surface charge are reflected in the rate at which Fe(II) is removed from the mineral

surface, which in general rate equations is assumed to have a homogeneous distribution of surface functional groups for reaction (Stone & Morgan, 1987). The mechanistic step which controls these rates of reaction may vary however, with a rate limiting step occurring at the slowest point of reaction (Stumm & Sulzberger, 1992), during either the adsorption of the reductant solute (generally a fast reaction), the inner sphere electron transfer or the detachment of Fe(II) from the mineral surface. This typically is the slowest reaction of the mechanism due to the dependence of reaction conditions under which reactions are set (i.e. under acidic or circum-neutral conditions, allowing the protonation or hydrolysis of a labile Fe(II) complex). Figure 2.4 refers to a simplified mechanism of ligand promoted reductive dissolution (also see Zinder *et al.*, 1986), which indicates the rate at which each step proceeds.

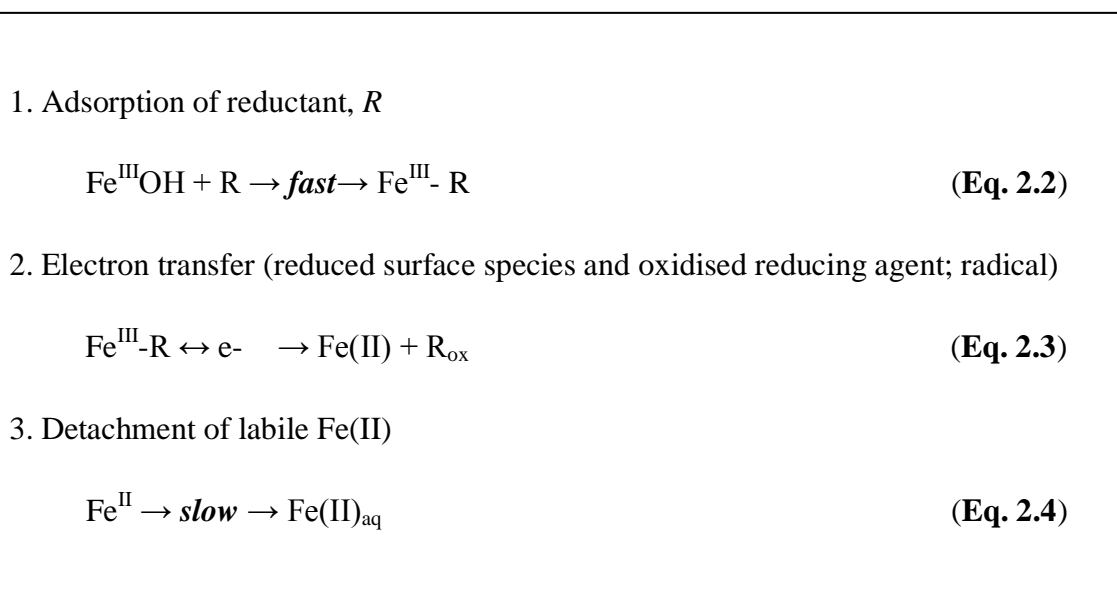


Figure 2.4: General mechanism of Fe(III) reductive dissolution within anoxic aqueous environments (adapted from Stumm & Sulzberger, 1992).

2.1.5 The reactivity of iron bearing minerals within natural environments

Of the many experimental papers which describe the rates and mechanisms of Fe(III) oxide reactivity during reductive dissolution, there are few which have linked laboratory studies which define reactivity of pure Fe-minerals, to studies of the reactivity of a mixture of different Fe oxides observed within natural sediment assemblages. Previous studies which aim to evaluate the rates and mechanism of Fe(III) oxide reductive dissolution, do so under laboratory conditions examining the reaction between synthetic, individual Fe(III) mineral and a naturally occurring reducing agent, e.g. ascorbate (Banwart *et al.*, 1989; Dos Santos Afonso *et al.*, 1990; Suter *et al.*, 1991; Deng, 1997), a reducing organic acid associated with the degradation of humic and fulvic acids (but is not found prominently in marine systems). Whilst following the mechanism of ligand promoted reductive dissolution, examinations of ascorbic acid induced Fe(II) dissolution agree that in addition to a reducing agent, a surface complexing agent (e.g. oxalate; Banwart *et al.*, 1989) is required to further catalyse Fe(II) dissolution in natural environments, especially under conditions of low pH (< 3). Whilst the rates and reactive mechanisms of individual Fe(III) minerals are widely agreed upon as dependent on a number of physical aspects of Fe(III) structural organisation (e.g. mineralogy, crystallinity, surface area), the rate at which these reactions occurs also relies on the concentration of the reducing agent in reaction.

Postma (1993) provides the first detailed study of iron reactivity measured within a suite of natural sediment samples. Analogous to a reactive continuum process (Boudreau & Ruddick, 1991) which describes the continuous oxidation of organic matter during early diagenesis (mediated by the abundance of heterogeneously mixed minerals with differing reactive properties), the reaction of a sediment assemblage with ascorbic acid traces the concentration of dissolved Fe(II) as a fraction of the bulk unreacted mineral.

Comparable rates of reaction were observed for sediments of characterised Fe morphologies with models of pure synthetic Fe(III) minerals (Postma, 1993; Larsen & Postma, 2001; Larsen *et al.*, 2006), allowing for the first time an abiotic model of iron reactivity throughout a sediment core which contains a heterogeneous mix of highly, poorly and unreactive Fe(III) minerals. What has never been reported, however, is a model which represents the reactivity of Fe mineral assemblages under analogous conditions to those in marine environments (i.e under anoxic or sulfidic systems).

2.2 THE REACTIVITY OF IRON MINERALS UNDER SULFIDIC CONDITIONS

2.2.1 Iron and the Sulfur cycle

The biogeochemical cycling of Fe within sedimentary systems is closely linked to redox cycles of other highly reactive elements, such as manganese and sulfur (Canfield *et al.*, 1993; Thamdrup *et al.*, 1994; Van Cappellen & Wang, 1996). As a predominant source, approximately 1.3×10^9 Tg yr⁻¹ (Jorgensen & Kasten, 2006) of sulfate is introduced into seawater from the chemical and oxidative weathering of continental rocks (Berner, 1985; 1991), with minor sources originating from volcanic emissions of sulfur dioxide into the atmosphere and hydrothermal inputs (see Canfield & Farquhar, 2009).

Sulfur species within modern oxygenated marine environments are dominated by seawater sulfate (SO₄²⁻; Joergensen & Kasten, 2006), undergoing a +6 to -2 change in oxidation state in reduced environments. Marine sediments represent a significant sink for both organic matter and seawater sulfate deposition (Berner, 1964), incorporated into near surface sediments during early diagenesis, and initiating a series of biological and abiotic reactions representing the sedimentary sulfur cycle (e.g. Jorgensen, 1977;

Figure 2.5). These reactions represent 1) the biological reduction of sulfate to produce hydrogen sulfide in anoxic sediments 2) the oxidation of hydrogen sulfide (to elemental S, polysulfide or (thio)-sulfate species) 3) precipitation of metal sulfide species and 4) bacterially disproportionation of elemental S to hydrogen sulfide and sulfate (Jorgensen & Kasten, 2006).

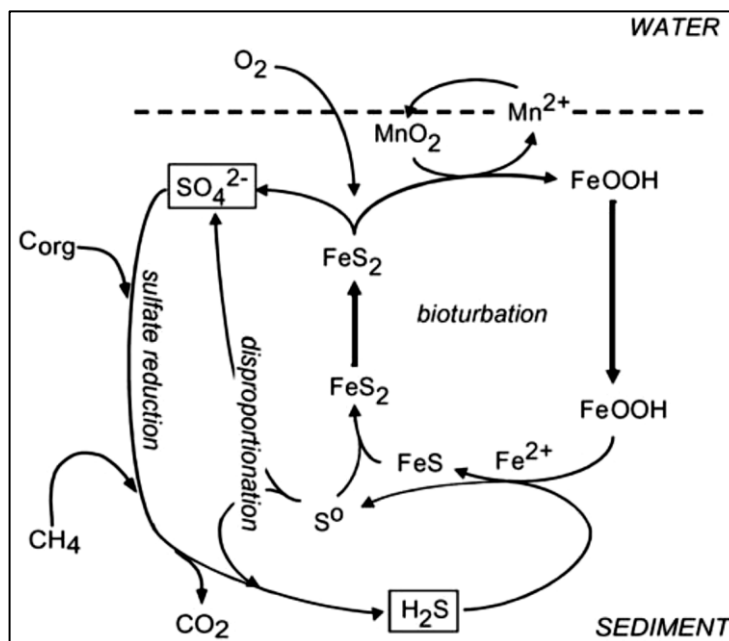


Figure 2.5: The S cycle in near surface sediments (Jorgensen & Kasten, 2006).

2.2.2 Bacterial Sulfate Reduction

Oxygen consuming chemical and biological processes associated with early diagenesis have been discussed in Section 2.1.3. Bacterial sulfate reduction (BSR) within near surface sediments (<10 cm) takes place at depth where all O₂ has been consumed or diffused by migration to surface environments (Berner, 1985). Bacteria (e.g. *Desulfovibrio*; Joergensen, 1977) utilise sulfate as a terminal electron acceptor during the anaerobic respiration of organic matter, producing hydrogen sulfide as a by-product (Equation 2.6):



Dissolved hydrogen sulfide may then either migrate to the sediment surface where it will be oxidised to form re-cycled sulfate within at the sediment- water interface; or will react with adjacent iron minerals or dissolved Fe(II), where it will either be oxidised (in the case of reaction with iron minerals) or will precipitate as solid iron mono-sulfide, and eventually pyrite (Berner, 1969; 1985).

2.2.2.1 Sulfur oxidation

After the bacterial reduction of sulfate to sulfide, H₂S in pore waters continues to react; either in the presence of iron bearing minerals to form FeS and pyrite, or to produce oxidised sulfur species such as elemental S or (thio)sulfate (Dos Santos Afonso & Stumm, 1992; Yao & Millero, 1996; Poulton, 2003).

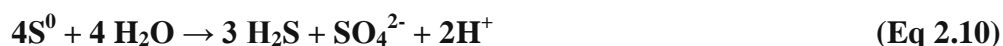
As BSR takes place within anoxic sediments, the oxidation of dissolved sulfide in solution does not necessarily take place utilising O₂ (as observed in Millero *et al.*, 1987) and the presence of other oxidants within the near surface, such as Fe(III) or Mn oxides, become important for biogeochemical S cycling (Aller & Rude, 1988; Yao & Millero, 1996; Schippers, 2004; Jorgensen & Kasten, 2006). An example of the formation of oxidised S species is reported in Equation 2.7 and 2.8. Experimental studies of oxidation of hydrogen sulfide mediated by Fe(III) reduction (Yao & Millero, 1996) examine the importance of Fe(III)-Fe(II) reduction mediated by dissolved sulfide in the formation of elemental sulfur (Poulton, 2003; Equation 2.7 and 2.8):



Additional field investigations of marine sediments also measure the oxidised product of BSR produced sulfide as elemental S (Equation 2.8), suggesting that the oxidation of precipitated iron mono-sulfides (FeS) energetically favours the production of elemental S (shown experimentally in Poulton, 2003), compared to the oxidation of pyrite, which tends towards sulfate formation which only occurs in normal, oxic marine environments (Schippers & Jorgensen, 1994; 2001; Equation 2.9).



Finally, further to this reaction, bacteria may also utilise elemental S (or thiosulfate) during disproportionation (*Thiobacillus*; Thamdrup *et al.*, 1993) to produce both a reduced state sulfur species and an oxidised sulfate phase (Equation 2.10), completing the biogeochemical cycling of sulfur in sedimentary environments (Canfield & Thamdrup, 1996; Joergensen & Kasten, 2006).



2.2.3 *The formation of iron mono-sulfides and pyrite*

Precipitating as a black solid (Berner, 1964), the formation of iron mono-sulfide (FeS) species in both marine and limnic environments naturally occurs as a reaction between dissolved Fe(II) (in pore-water or a ferruginous water column) and BSR produced hydrogen sulfide. The mechanisms which support the secondary reaction to pyrite formation (Berner, 1970), have however been debated in a number of field and laboratory studies. The presence of both FeS and FeS₂ in marine sediments act as excellent indicators of the environmental conditions (including organic matter

abundance, oxygenation and sulfidation processes) encountered at the time of formation and deposition (Raiswell *et al.*, 1988).

The precipitation of solid phase FeS is a pH dependant reaction, influenced by both the concentration and speciation of dissolved sulfide in solution. Rickard (1995) proposed two mechanisms of formation, defined in Equation 2.11 and 2.12:



The form of hydrogen sulfide species is controlled by the pH range within which BSR reactions take place (generally under circumneutral conditions; Rickard, 1997; 2006), and is important in studies of iron reactivity in anoxic sedimentary environments (Equation 2.11). Experimental studies of synthetic FeS formation (Rickard, 1995) determine the effect of pH over both sulfide rich (bisulfide, 2HS^-) and sulfide poor (H_2S) pathways; where neutral-alkaline environments utilise hydrogen sulfide at a faster rate than in sediments $< \text{pH } 7$.

Structurally, FeS forms are differentiated by their crystalline properties, which propose different mechanisms of pyrite formation. Freshly precipitated FeS is unstable and poorly crystalline, compared to complexes such as greigite (Fe_3S_4) or mackinawite (Fe_{1+x}S), which are defined as metastable and tetragonal or framboidal in structure (Raiswell, 1982).

Solubility studies of iron mono-sulfide species have been performed in terms of pH dependence (pH 3 – 10; Rickard, 2006), producing dissolution of FeS which occurs

relatively easily as shown in Equations 2.13 and 2.14 respectively; where both equations indicate a return of hydrogen sulfide to the S cycle (as H₂S and HS⁻).



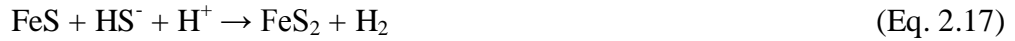
Rickard, 2006 also indicates that a pH *independent* reaction may occur due to the formation of dissolved, aqueous FeS (FeS_{aq}), observed specifically under neutral-alkaline anoxic environments. At pH >8, in highly sulfidic environments (1 x 10^{-5.7} M; Rickard, 2006), FeS_{aq} clusters dominate the total dissolved sulfide profile (Equation 2.15), instead of assumed products H₂S and HS⁻:



Sedimentary pyrite (FeS₂) observed in anoxic organic rich, sedimentary systems requires the super-saturation of precursor FeS with dissolved hydrogen sulfide to form; which acts as a stable end product of Fe and S reactivity (Wang & Morse, 1996; Raiswell, 1997). The formation of pyrite is represented generally in Equation 2.16, however metastable FeS may interact with a number of sulfide species under different conditions of oxygenation, which all ultimately form pyrite. However, in some cases an oxidising agent is required to catalyse pyrite formation (Figure 2.6; Wilkin & Barnes, 1996; Wang & Morse, 1996; Rickard, 1997; Rickard & Luther, 1997; Benning *et al.*, 2000):



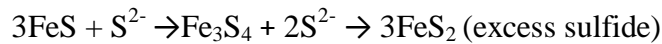
HS- pathway:



Polysulfide pathway:



Greigite Intermediate pathway:



Zero valent sulfur pathway:



Figure 2.6: Additional pathways of pyrite formation

Irrespective of reaction stoichiometry and reagents, there are two recognised mechanisms of pyrite crystallisation from an oxidised FeS: 1) The dissolution of FeS(s) to FeS(aq) and subsequent precipitation of FeS₂ nuclei upon the surface of solid phase FeS; or 2) The transformation of the FeS surface to form a transitional layer of pyrite nucleation between the FeS bulk solid and sulfide in solution (Wang & Morse, 1996). The morphology and structure of pyrite observed within marine sediments are defined by the mechanism and rate by which pyritisation occurs, and also by the structural properties of precursor FeS. Framboidal pyrite (Raiswell, 1982; Butler & Rickard, 2000; Hunger & Benning, 2007) is observed as the product of the fast dissolution and poly-nucleation of sulfidised FeS (i.e. either utilising mackinawite or greigite; Wilkin &

Barnes, 1997; Benning *et al.*, 2000) to form FeS₂; and is important as a marker of depositional environment (i.e. marsh or coastal sediments) due to its unique structure. In comparison, a crystalline euhedral pyrite is expected from the slow precipitation of pyrite nuclei on a FeS surface (Wilkin & Barnes, 1996). Although most studies referred to in this Thesis focus on the reactivity of FeS and FeS₂ in anoxic environments, studies of mackinwite in comparison (Benning *et al.*, 2000) will only form pyrite in an oxidised environment (via greigite). Hence in the absence of oxygen below the sediment – water boundary, the presence of oxidising agents are vital in determining a pyritic structure.

To classify the extent of pyrite formation from an environment rich in these reactive iron minerals, the *Degree of Pyritization* (DOP: derived within Raiswell & Berner, 1985; Canfield *et al.*, 1996; Raiswell & Canfield, 1998) is calculated to account for the concentration of FeS or pyrite associated Fe within a natural sediment. Equation 2.21 describes the concentration of Fe of HCl extractable Fe and Fe bound to sulfur in pyrite.

$$\text{Degree of Pyritization} = [\text{Fe}_{\text{pyrite}}] / [\text{Fe}_{\text{pyrite}} + \text{HCL soluble Fe}] \quad (\text{Eq. 2.21})$$

Canfield *et al.*, 1996 characterise DOP ratios between 0- 0.45 indicative of normal, oxygenated marine sediments, 0.45 - 0.75 representing a low oxygen/anoxic environment, and values between 0.75 - 1 (complete sulfidation of iron minerals) indicative of euxinic deposition environments.

2.2.4 The reductive dissolution of iron minerals within sulfidic environments

Via the study of FeS and FeS₂ formation, the rates and mechanisms which regulate Fe²⁺ and S²⁻ availability in sedimentary pore water systems can be evaluated. The reductive dissolution of Fe(III) oxide minerals by dissolved sulfide in solution has been thoroughly investigated in previous laboratory studies, describing a surface controlled reaction dependent upon the initial sulfide concentration and mineral surface area available for reaction (Pyzik & Sommer, 1981).

The recognised mechanism of sulfide promoted reductive dissolution (Dos Santos Afonso & Stumm, 1992) is described in Figure 2.7. As discussed in Section 2.1.4.2, the formation of surface complexes occurs via the adsorption of a reductant species in solution (i.e. dissolved sulfide) to hydroxyl groups on the reactive surface of an oxide mineral, creating an inner sphere complex. An electron transfer between the negatively charged sulfur species and central Fe atom of surface complex, reduces Fe(III)-Fe(II) before releasing adsorbed sulfur in an oxidised form (generally determined by electron mass balance as elemental S, Yao & Millero, (1996); however some studies report sulfate as an end product associated with the catalysis of Fe(III) reduction). The protonated reduced state Fe (II) complex on the mineral surface is then detached into solution, bearing a new reactive Fe(III) site for reaction. As a secondary reaction, dissolved Fe²⁺ in solution can then react with additional dissolved sulfide to form FeS (Rickard, 1974).

Surface complex formation on reactive mineral surface:



Electron Transfer between bulk and reactive Fe:



Oxidation of adsorbed reagent:



Fe(II)_{aq} dissolution (deprotonation of the mineral surface) and production of new surface site available for reaction



Formation of elemental S



Figure 2.7: Reaction pathway of sulfide mediated reductive dissolution (Dos Santos Afonso & Stumm, 1992) occurring on the reactive surface of Fe(III) oxide minerals

The rate at which dissolution of Fe(II) occurs follows first order kinetics in relation to the initial concentration of Fe(III) oxide species, determined experimentally by Pyzik & Sommer, (Goethite; 1981), Berner & Canfield (Magnetite; 1987), Dos Santos Afonso & Stumm (Hematite; 1992), Peiffer *et al.*, (Lepidocrocite; 1992) Yao & Millero (Hydrous Ferric Oxide; 1996) and Poulton (2-line Ferrihydrite, 2003). As the slowest step within the reaction mechanism (Hering & Stumm, 1990), the dissolution of Fe(II) is therefore the rate determining step, and highly influenced by the pH (and therefore protons available for reaction) at which the reaction occurs (Dos Santos Afonso & Stumm, 1992; Poulton, 2003; Peiffer & Gade, 2007); further catalysing the reaction under acidic conditions, but inhibiting dissolution to a much slower rate at pH >7.

Whilst it is widely agreed that the mineral surface area available for reactivity possesses a reaction order of 1 (i.e. first order rate law; Pyzik & Sommer, 1981; Poulton, 2003), the significance of dissolved sulfide concentrations is debated, with values ranging between 0.5 (Pyzik & Sommer, 1981) and 1.5 (Rickard, 1974). In order to verify these differences in dissolved sulfide influence, Poulton (2003) and Poulton *et al.*, (2004) analysed the sulfidation rates experimentally for a variety of Fe(III) oxide minerals including ferrihydrite, lepidocrocite, goethite, magnetite and hematite. The results obtained were shown to produce a fractional reaction order of 0.5 dependent upon the initial concentration of dissolved sulfide in solution for all Fe(III) minerals. These studies also directly compared for the first time the rate of S oxidation relative to Fe (II) dissolution, with the former being 15 times faster than that of Fe(II) dissolution at circumneutral pH, inferring reduced phase Fe(II) may require a further catalysis (from the next protonated complex site; Pyzik & Sommer, 1981; Zinder *et al.*, 1986, Poulton, 2003) in order to be released into solution, and for the reaction to continue. From the observations, an empirical rate equation can be derived; describing the rate of sulfide mediated reductive dissolution (defined by Poulton, 2003):

$$\mathbf{R_{Fe} = K_{Fe} (H_2S)_{t=0}^{0.5} A} \quad \mathbf{(Eq. 2.27)}$$

where R_{Fe} defines the rate of Fe(II) dissolution ($M \text{ min}^{-1}$), K_{Fe} represents the rate constant measured for individual reactions ($\text{mol}^{0.5} \text{ l}^{0.5} \text{ m}^{-2} \text{ min}^{-1}$), $(H_2S)_{t=0}$, the initial sulfide concentration in solution (M), and A is the Fe(III) mineral surface area ($\text{m}^2 \text{ g}^{-1}$).

2.2.5 *The classification of iron mineral reactivity*

The bacterial reduction of sulfate generally occurs rapidly within the top few cm of organic-rich sediments (Raiswell, 1993). However, according to field observations, pore water profiles within these sections are often dominated by dissolved Fe(II), and not the accumulation of dissolved sulfide as expected (Berner, 1984); leading early studies of pyrite formation to deduce that the presence of iron (III) oxides, and the formation of FeS acts as a buffer to regulate dissolved sulfide concentrations in sedimentary pore waters (Berner, 1969). This hypothesis was first derived after the examination of sulfur species in Gulf of California marine sediments (Berner, 1964; 1969) which report a general conclusion that a decrease in down-core sulfate concentrations will be reflected by increasing dissolved sulfide with depth.

In examining the influence of iron availability on pyrite formation, boundaries of iron presence within core sediments (*high, medium and low*) were defined as a ratio of iron concentration with respect to dissolved sulfide measured with a core section (Berner, 1969). These primary studies introduced the concept of 'reactive iron' (Berner, 1969; 1984; Rickard, 1974; Raiswell, 1982) defined as detrital iron particles deposited within an organic rich layer (e.g. iron oxyhydroxides) which react quickly with dissolved sulfide. It was concluded that only once these minerals had undergone reductive dissolution processes, and the formation of FeS had titrated dissolved Fe(II) from porewater, dissolved sulfide could then begin to accumulate in pore water. In order to quantify the fraction of reactive iron available for pyrite formation within sediment assemblages, the iron content of pyrite which was extractable with boiling hydrochloric acid (Berner, 1970) was used to characterise the reactive iron phase, potentially determining goethite, hematite, fine grained oxyhydroxide minerals and some species of Fe-silicates (Raiswell, 1982; 1993) as a mixture within sediments. Fe-species which

were not extractable after this time were classed as unreactive towards dissolved sulfide (e.g. bulk silicate minerals; Raiswell & Canfield, 1998).

Subsequent studies of Fe and S cycling during diagenetic reactions, and in the formation of pyrite specify that both iron abundance and reactivity will limit pyrite formation in near surface sedimentary systems (Berner, 1984; Canfield, 1989), with fine grained iron oxyhydroxide minerals such as hydrous ferric oxide (HFO) or ferrihydrite, reacting fastest with dissolved sulfide (Canfield *et al.*, 1992). In order to constrain the rates of reactivity between individual Fe(III) minerals, kinetic experiments reflecting the rate of sulfidation of reactive iron minerals which are generally observed within marine sediments were devised (Canfield, 1989), measuring the concentration of dissolved sulfide in solution in reaction with iron oxide minerals including ferrihydrite, lepidocrocite, goethite and hematite over a set time period. These experiments were used to differentiate easily extractable, highly reactive, poorly crystalline iron minerals such as ferrihydrite and lepidocrocite, from stable, crystalline minerals including goethite and hematite which reacted at a slower rate with dissolved sulfide. Canfield *et al.*, (1992) collates all published data relevant to the rates of sulfidation, and hence reactivity, of Fe-bearing minerals reported at that time (Table 2.3), defining these minerals using the calculated rate constant K , associated with Fe(II) dissolution. Once this highest reactive iron oxide phase has been consumed, slower reacting minerals will continue to react with dissolved sulfide to release Fe(II)_{aq}, and hence throughout a near surface sediment profile, the sacrifice of easily extractable iron oxyhydroxide minerals contributes to the rapid formation of FeS and FeS₂ from ferruginously dominated pore waters (Canfield, 1989; Raiswell, 1993).

Table 2.3: The reaction order of Fe bearing minerals, with respect to the rate of iron reductive dissolution (Canfield *et al.*, 1992)

Iron mineral	Rate constant K, (yr⁻¹)	Reference
Ferrihydrite	2200	Pyzik & Sommer, 1981 Canfield, 1989
Lepidocrocite	>85	Canfield, 1989
Goethite	22	Pyzik & Sommer, 1981
Hematite	12	Canfield <i>et al.</i> , 1992
Magnetite (uncoated/coated)	$6.6 \times 10^{-3} / 1.3 \times 10^{-3}$	Berner & Canfield, 1987
Reactive Silicates	3×10^{-3}	Canfield <i>et al.</i> , 1992
Sheet Silicates	8.2×10^{-6}	Canfield <i>et al.</i> , 1992

Most recently, Poulton (2003) and Poulton *et al.*, (2004) produced a set of data examining the rates of iron sulfidation for similar key Fe minerals referred to within the classical reactivity schemes represented by Canfield 1989 and Canfield *et al.*, 1992. The importance of this study represents a set of experimental data used in determining the reactivity of Fe bearing minerals in terms of mineral half-life under one set of kinetic calculations, relative to data compiled from a variety of studies (Table 2.3). Poulton *et al.*, 2004 observed a similar order of Fe-mineral reactivity to previous schemes, but with a range of sulfidation rates (Table 2.4) between 5 minutes (freshly precipitated HYO) to 182 days (hematite), reflecting the change in structural morphology and energetic stability of these minerals whilst undergoing sulfidation processes. As the rate equations derived to measure the concentration of Fe(II)_{aq} in solution over time differ between the studies of Canfield vs. Poulton, a comparison of half-life, or rate constant measurements cannot be made directly, however all studies which have contributed to the formation of these reactivity schemes agree on the order

of iron mineral reactivity, and the general order of magnitude over which they react, be it over a period of hours, days or years.

Table 2.4 Rate constant and half-life of iron mineral reactivity associated with sulfide mediated reductive dissolution (Poulton *et al.*, 2004)

Iron Mineral	K (mol^{-0.5} l^{0.5} m⁻² min⁻¹)	Half Life ($\tau_{1/2}$)
Freshly precipitated HFO	4.3-8.6 x 10 ⁻⁶	5.0 mins
2-line Ferrihydrite	1.1 x 10 ⁻⁶	12.3 hours
Lepidocrocite	6.1 x 10 ⁻⁶	10.9 hours
Goethite	7.3 x 10 ⁻⁸	63 days
Magnetite	1.0 x 10 ⁻⁶	72 days
Hematite	4.2 x 10 ⁻⁷	182 days

In addition to determining the rate of individual synthetic minerals in reaction with dissolved sulfide, the studies of Pyzik & Sommer (1981), Canfield (1989) and Canfield *et al.*, (1992) also measured the rate of sulfide mediated reductive dissolution in a variety of anoxic and oxygenated near surface sediments, in order to determine the half life of iron mineral reactivity within a natural setting. However, as it is difficult to extract individual mineral structures from a heterogeneous sediment assemblage, an improvisation to the original boiling HCl-extraction of *reactive* iron (Berner, 1970) has been developed which initiates a multi-step sequential extraction procedure in order to extract individual Fe-minerals phases, reflecting the order of reactivity with dissolved sulfide in natural systems. The extraction sequence devised by Poulton & Canfield (2005) defines:

1. *Fe carbonates (siderite, Fe_{-carb});*
2. *Easily extractable, highly reactive minerals (ferrihydrite, lepidocrocite; FeO_{x1});*
3. *Reducible crystalline Fe minerals (goethite, hematite; (FeO_{x2});*
- 4 *Magnetite (Fe_{mag});*
5. *Poorly reactive (some reactive Fe-silicates; Fe-_{PRS}); and*
6. *Unreactive Fe (unreactive silicates FeU).*

Whilst methods of extraction for iron-sulfide species are well constrained (HCl extraction: Berner, 1970; Chromium reduction: Canfield *et al.*, 1986), tests of iron speciation from natural sediment assemblages using the extraction method of Poulton & Canfield, (2005) infer that the extraction of highly reactive (*FeHR*) phases (Fe_{carb}, FeO_{x1}, FeO_{x2}, Fe_{mag} and Fe_{pyrite}) are distinguishable from each other within a sediment core, allowing a greater correlation to studies which determine the reactivity of individual Fe minerals. Overall Fe(III) morphology defines the reactivity of minerals within these environments termed highly reactive (including ferrihydrite, lepidocrocite, goethite, hematite, magnetite, pyrite), poorly reactive (Fe silicates) or unreactive with respect to dissolved sulfide, as classed within Canfield *et al.*, (1992).

2.3 Fe ISOTOPES

Traditionally, stable isotope systems have been used to trace the biogeochemical cycling of carbon, nitrogen, oxygen and sulfur in a variety of biological and abiotic reactions within modern marine systems and the ancient rock record. The pathways by which some of these isotopes fractionate with regards to iron mineral reactivity and FeS formation (as reviewed in Johnson *et al.*, 2004), have been useful in determining the reaction pathway of biological iron reduction and Fe(II) dissolution, the systematics of oxidised sulfur, and formation of iron monosulfide products in near surface sediment systems.

Recently, the emergence of techniques to measure the isotopic fractionation associated with redox transition metal reactivity (Fe, Mo, Cr; Anbar & Rouxel, 2007), has allowed a significant amount of data to be gathered with regards to answering important questions of early earth and seawater oxygenation; and widespread iron formation deposition and cessation between approximately 2.4 and 1.8 Ga (Rouxel *et al.*, 2005; Johnson *et al.*, 2008a); and hence are of interest to geochemical and paleo-oceanography studies.

2.3.1. The role of Fe isotopes in examining early diagenetic sediment processes

The first experimental investigations of Fe isotope fractionation were conducted in order to obtain a *biosignature* value for dissimilatory iron reduction within sedimentary systems (Beard *et al.*, 1999), important in order to constrain evidence of early microbial respiration within the ancient rock record (Johnson *et al.*, 2003; Beard & Johnson, 2004; Johnson & Beard, 2006). However, these investigations were quickly countered with arguments of smaller, but significant isotope fractionations associated with non-

biological mineral reactivity within similar environments (Anbar *et al.*, 2000; Bullen *et al.*, 2001; Roe *et al.*, 2003), questioning whether signatures observed in sediment samples are solely of a biological nature. Alongside studies of naturally occurring Fe carbonates (Wiesli *et al.*, 2004; Johnson *et al.*, 2005) and sulfides (Butler *et al.*, 2005; Severmann *et al.*, 2006), an array of experimental and theoretical investigations (Polyakov & Mineev, 2000; Schauble *et al.*, 2001) have been instigated to trace the mechanism of Fe isotope fractionation of Fe(III) oxides under different conditions, constraining individual Fe isotope signatures representing redox reactions of Fe(III)-Fe(II) cycling at the sediment-water interface. Beard *et al.*, (2003) measured the Earth's bulk crust as homogenous (with a $\delta^{56}\text{Fe}$ composition of 0‰), which is comparable to the composition of igneous rocks and also of oxygenic weathering products (Fantle & DePaolo, 2004), due to low solubility within modern oxygenated marine systems. Therefore, when Fe isotope fractionations are observed in natural systems, they tend to be produced by a change in redox state (whether biological or chemical, oxidative or reductive) of Fe(III)-Fe(II); or a change in bonding environment (Roe *et al.*, 2003; Johnson *et al.*, 2004). A summary of these fractionations and associated reactions are listed in Table 2.5. These pathways of isotopic fractionation are all common in the biogeochemical cycling of iron in near surface, marine sediments; and are primarily controlled by the availability of oxygen or anaerobic bacteria within pore waters or an adjacent water column (Bullen *et al.*, 2001; Croal *et al.*, 2004a). Both biologically and chemically mediated redox processes associated with transition metal cycling produce larger isotope fractionation signatures than those which are mediated by speciation alone (Hill & Schauble, 2008).

Table 2.5 Summary of Fe isotopic reactions (collated in Dauphas & Rouxel, 2006)

Reaction		$\delta^{56}\text{Fe}$	References
$\text{Fe(II)}_{\text{aq}}\text{-Fe(III) oxides}$	DIR	-1.3	Beard <i>et al.</i> , 1999
$\text{Fe(II)}_{\text{aq}}\text{-Fe(III) oxides}$	Abiotic precipitation	-0.9	Bullen <i>et al.</i> , 2001
$\text{Fe(II)}_{\text{aq}}\text{-Fe}_2\text{O}_3$	Abiotic precipitation	0.1	Skulan <i>et al.</i> , 2002
$\text{Fe(II)}_{\text{aq}}\text{-Fe(III)}_{\text{aq}}$	Abiotic Oxidation	-2.9	Welch <i>et al.</i> , 2003
$\text{Fe(II)}_{\text{aq}}\text{-Fe(II)}>\text{Fe(III) oxides}$	Abiotic Adsorption	-2.1	Icopini <i>et al.</i> , 2004
$\text{Fe(II)}_{\text{aq}}\text{-Fe(III) oxides}$	Photosynthetic Fe oxidation	-1.5	Croal <i>et al.</i> , 2004
$\text{Fe(II)}_{\text{aq}}\text{-Fe(II)}>\text{Fe(III) oxides}$	Experimental Adsorption in DIR	-0.9	Crosby <i>et al.</i> , 2005
$\text{Fe(II)}_{\text{aq}}\text{-Fe}_3\text{O}_4$	DIR	-1.3	Johnson <i>et al.</i> , 2005

In oxygenated modern marine environments, the formation of insoluble hydrous Fe oxyhydroxide minerals from weathered Fe(III) particulates, undergo bacterially mediated reduction to produce dissolved Fe(II) in near surface environments; after which oxidation (via O₂ diffusion or bacterially mediated), precipitation and adsorption processes (Icopini *et al.*, 2004) can all potentially be identified by unique isotopic signatures. Until now, isotopic fractionations have never been measured on abiotic reductive dissolution processes involving sulfide mediators. This is surprising due to the well characterised redox reactions occurring during this process (as described by Dos Santos Afonso & Stumm, 1992); and hence further investigations (involving experimental and field studies) are required in order to determine the influence such fractionations would have in associated with those well defined for biological processes of iron reduction.

2.3.2 Basic concepts

An advance in analytical methods and instrumentation in the past decade has presented novel ways in which transition metal isotopes are measured, via the development of Multi-Collector Inductively Coupled Plasma Mass Spectrometry (MCICP-MS)

(Albarede & Beard, 2004; Arnold *et al.*, 2004). Iron is the fourth most abundant element on Earth, with four stable isotopes - ^{54}Fe (5.84%); ^{56}Fe (91.76%); ^{57}Fe (2.12 %) and ^{58}Fe (0.28%), which are reported as isotopic ratios of delta notation (δ), per mil (as $^{56}\text{Fe}/^{54}\text{Fe}$ are the most abundant isotopes, this ratio is commonly reported, ‰), derived from raw data as shown in Equation 2.28. Values are presented relative to the internationally recognised IRMM-14 standard or a calibrated igneous rock sample (with an isotopic value of approximately 0‰). The fractionation factor between 2 isotopic species (A and B) is described in Equation 2.29, and generally maintains a value close to 1.

$$\delta^{56}\text{Fe} = ((^{56}\text{Fe}/^{54}\text{Fe}_{\text{sample}}) / (^{56}\text{Fe}/^{54}\text{Fe}_{\text{standard}}) - 1) \times 10^3 \quad (\text{Eq. 2.28})$$

$$\text{Fractionation factor } \alpha_{\text{A-B}} = (\delta^{56}\text{Fe}_\text{A} + 1000) / (\delta^{56}\text{Fe}_\text{B} + 1000) \quad (\text{Eq. 2.29})$$

$$\text{Enrichment Factor } \epsilon_{\text{A-B}} = (\alpha_{\text{A-B}} - 1) \times 10^3 \quad (\text{Eq. 2.30})$$

Equation 2.30 describes the enrichment factor associated with unidirectional isotopic processes which increase the concentration of an isotope value in reaction. Values of isotopic fractionation analysed by MC-ICP-MS are measured to a precision of $0.05\text{‰} \pm 0.15\text{‰}$ based on multi-laboratory studies of replicate measurements, with a number of known internal and bracketing standards (Albarede & Beard, 2004). The isotopic difference of $\delta^{56}\text{Fe}$ isotopes between two constituents is described by a Δ (Equation 2.31), with a maximum isotopic range of approximately 4-5‰ (Beard *et al.*, 2003) dependent upon biological or abiotic reactions occurring within low temperature, sedimentary or aqueous environments (Anbar & Rouxel, 2007).

$$\Delta_{\text{A-B}} = \delta^{56}\text{Fe}_\text{A} - \delta^{56}\text{Fe}_\text{B} \quad (\text{Eq. 2.31})$$

2.3.3 Dissimilatory iron reduction (DIR) Vs Abiotic mineral dissolution: Fe isotope signatures

In order to fully assess the influence of both biological and abiotic redox reactions within natural systems, with regards to Fe isotope fractionation, detailed experimental studies are required to understand the often multistep mechanisms which promote fractionation of Fe species within sediments, (Butler *et al.*, 2005; Severmann *et al.*, 2006; Staubwasser *et al.*, 2006).

Beard *et al.*, (1999) is recognised as the first experimental paper showing that reductive dissolution of ferrihydrite by *Shewanella Algae* produces $\delta^{56}\text{Fe(II)}_{\text{aq}}$ species approximately 1.3‰ lighter than the ferrihydrite substrate it originated from. Subsequent laboratory studies (Icopini *et al.*, 2004; Crosby *et al.*, 2004; 2007) have argued that bacterial reduction of Fe(III) oxides require an isotopic equilibrium effect caused by electron exchange between naturally sorbed Fe(II) onto the reactive Fe(III) oxide surface, playing an important role in determining the magnitude of the isotopically light Fe(II)_{aq} signature observed in solution. As sorption occurs naturally to Fe(III) reactive oxide surfaces (Williams & Scherer, 2004), this process effects the isotopic variability of dissimilatory iron reduction (DIR) produced Fe(II)_{aq}, and reflects an abiotic influence over the use of *biosignatures*, creating uncertainty over the robust nature of biological isotope tracers.

In contrast, abiotic methods of reduction and dissolution associated with Fe(III) oxides and the production of Fe(II)_{aq}, have utilised anion exchange chromatography in order to investigate the importance of equilibrium effects which occur during the formation of Fe-ligand species in solution during Fe(II) dissolution (Anbar *et al.*, 2000; Bullen *et al.*, 2001; Roe *et al.*, 2003). The differences in bonding environment promote an isotopic fractionation, which although smaller in magnitude than corresponding biological redox

reactions (Rouxel *et al.*, 2005), still contribute to the $\delta^{56}\text{Fe}$ record in modern sedimentary systems. Experimental studies of iron isotope fractionation during abiotic dissolution processes (Brantley *et al.*, 2001; 2004; Skulan *et al.*, 2002; Weiderhold *et al.*, 2006) have focused on a number of well characterised mechanisms are significant to $\text{Fe}^{2+}_{(\text{aq})}$ production. Proton promoted methods of dissolution (Pyzik & Sommer, 1981) give no fractionation (or a slightly heavy isotopic signature) when pure Fe(III) minerals are dissolved in HCl (Skulan *et al.*, 2002; Brantley *et al.*, 2004; Weiderhold *et al.*, 2006). However, in comparison, processes including the use of siderophores and organic ligand reducing agents (oxalate; Borer *et al.*, 2005) produce isotopically light $\text{Fe}^{2+}_{(\text{aq})}$ signatures of between $\delta^{57}\text{Fe} = -0.5$ to -2.6% . Features which constrain the variability of these isotopic fractionations are associated with the mineral surface, which if reflected as homogeneous, will not produce an isotopic fractionation between mineral surface and pore fluid (Skulan *et al.*, 2002), with the reacting ligands affinity towards Fe on the mineral surface (allowing either kinetic or equilibrium effects to occur) also exerting an importance influence on fractionations (Brantley *et al.*, 2001; 2004).

2.3.4 Fe isotopes in sedimentary systems: modern marine environments

Redox cycling of Fe(III) and Fe(II) between oxic and anoxic environments at the sediment-water boundary supports the fractionation of $\delta^{56}\text{Fe}$ isotopes, via a number of biological and abiological diagenetic reactions. Within marine sediments, separate processes of dissimilatory iron reduction and the dissolution of Fe(II) mediated by bacterial sulfate reduction both produce isotopically light $\delta^{56}\text{Fe}$ values of $\text{Fe}^{2+}_{(\text{aq})}$, partially distinguishable depending upon the environments under which they were formed. Severmann *et al.*, (2006) and Staubwasser *et al.*, (2006) both describe the isotopic fractionation of $\delta^{56}\text{Fe}$ isotopes within near surface, anoxic sediments and

porewaters which are conducive to either promoting dissimilatory iron reduction (Lovely, 1991), and hence an abundance of $\text{Fe}^{2+}_{(\text{aq})}$; or bacterial sulfate reduction which provides a supply of dissolved sulfide in porewater for further reaction (Canfield, 1989) to iron mono-sulfides and eventually pyrite.

In continental margin sediments which support the dissimilatory iron reduction of reactive Fe(III) minerals (Berquist & Boyle, 2006; Severmann *et al.*, 2006), the abundance of freely available, isotopically light $\text{Fe}^{2+}_{(\text{aq})}$ ($\delta^{56}\text{Fe} < -3 \text{ ‰}$; Beard *et al.*, 1999) may readily diffuse back into near surface oxic pore waters (or oxygenated bottom waters at the sediment surface) and precipitate into an iron oxyhydroxide mineral which carries the isotopically light signature from which it was formed (Beard *et al.*, 2003; Beard & Johnson, 2004). This recycling of reactive Fe(III) instigates an important isotopic signature which maybe imparted further into Fe(III) minerals which are transported into deep waters or basin floors, from shelf settings. Severmann *et al.*, (2008) traced recycled isotopically light Fe(III) minerals from an oxic shelf within the Black Sea as it was transported to the euxinic basin floor. The sediments analysed, which contained abundant concentrations of highly reactive Fe minerals and pyrite were consistently isotopically light, as scavenged from the settling recycled Fe(III) mineral flux, in comparison to the bulk sediment measured on the oxic Black Sea shelf.

The influence of dissimilatory iron reduction is not only observed within marine sediments, but within both natural and artificial lake systems (Teutsch *et al.*, 2009; Song *et al.*, 2011). Interestingly, although few studies have characterised the redox cycling of $\delta^{56}\text{Fe}$ isotopes at the oxic - anoxic boundary in lake environments. These systems are driven by dissimilatory iron reduction, also producing isotopically light signatures ($\delta^{56}\text{Fe}^{2+} = < -1.88 \text{ ‰}$ Lake Nyos, Teutsch *et al.*, 2009); but becoming increasingly

heavier ($\delta^{56}\text{Fe} = +0.83 \text{ ‰}$) with depth, corresponding to isotopically heavy bottom waters below the redox interface.

In contrast to these low sulfide systems, marine environments which permit extensive bacterial sulfate reduction will also produce isotopically light $\delta^{56}\text{Fe}^{2+}_{(\text{aq})}$. However, due to the presence of dissolved sulfide in pore water, very little Fe^{2+} will be diffused back to the oxygenated sediment surface, and instead will contribute to the formation of solid iron mono-sulfide species in sediments (Severmann *et al.*, 2006; Staubwasser *et al.*, 2006). Butler *et al.*, (2005) report an isotopic fractionation of between -0.3 to -0.85 ‰ during the experimental precipitation of FeS from isotopically light $\delta^{56}\text{Fe}^{2+}$. However, although the composition of FeS reflects the reduced porewater Fe^{2+} from which it came, it is understood that the isotopic signature associated with FeS formation is not that which subsequently influences pyrite formation, even though FeS is the dominant precursor for sedimentary pyrite (Severmann *et al.*, 2008). Further investigation is required into the isotope fractionations associated with experimental FeS formation in natural sediments, and subsequent pyrite formation, due to the importance with which both species presence in modern sediments and the ancient rock record is regarded. Aside, whilst pyrite formation measured within modern sediments (Beard *et al.*, 2003; Severmann *et al.*, 2006; reviewed in Dauphas & Rouxel, 2006) produces relatively small fractionations (between $\delta^{56}\text{Fe} = 0$ and - 1‰); pyrite samples from the ancient rock record (Johnson *et al.*, 2003; Rouxel *et al.*, 2005; Yamaguchi *et al.*, 2005; Johnson & Beard, 2006; <2.4Ga) is associated with much larger fractionations, between 1 and - 3.5‰ (See Dauphas & Rouxel, 2006; Figure 14). Studies by Rouxel *et al.*, 2005 hypothesise the vast difference to these $\delta^{56}\text{Fe}$ values to be associated with the increase in atmospheric oxygen at this time (Barley *et al.*, 2005), increasing the production of bacterially produced sulfate and hydrogen sulfide in ancient oceans, and altering the

abundance of reactive iron observed (via the precipitation of FeS and FeS₂), regulating the iron redox cycle at this time.

In modern oceans, in comparison to continental shelf sediment studies (Berquist & Boyle, 2006; Severmann *et al*, 2006; Staubwasser *et al.*, 2006) which undergo extensive Fe(III)-Fe(II) reduction during dissimilatory iron reduction, and subsequent re-oxidation at the sediment surface to produce a benthic Fe(II) flux of light $\delta^{56}\text{Fe}$ isotopes, Homoky *et al.*, (2009) provide the first data of possible Fe isotope fractionation within deep sea environments (Crozet Plateau, 4000m). No fractionation is associated with pore waters from these deep sea sediments, which was thought to reflect the low reactivity and organic matter contents, compared to the highly reactive nature of Fe(III) minerals observed within continental shelf sediments (also Homoky *et al.*, 2009).

From the extensive investigation of iron isotope fractionations which occur during experimental and natural sediment studies of Fe(III) mineral biogeochemical cycling, it is surprising that possible isotopic fractionation during sulfide mediated reductive dissolution of Fe(III) oxides has not yet been evaluated. An examination of mechanisms which may mediate fractionation would be highly beneficial to isotopic studies of modern and ancient sediments, in comparison to well characterised signatures associated with both biological activity and the precipitation of FeS provoking isotopic fractionations.

CHAPTER 3: METHODS AND MATERIALS

3.1 INTRODUCTION

All materials within this study were prepared from Analytical Grade chemical reagents using de-ionised water (DIW; 18M Ω H₂O; trace metal content parts per billion). Glassware was washed in a 10% (v/v) nitric acid bath for 24 hours; and repeated rinsing with laboratory tap water, followed by DIW in triplicate. Glassware in contact with iron, sulfur or sediment samples was cleaned with concentrated aqua regia (3 parts 12N hydrochloric acid: 1 part concentrated nitric acid). Experiments requiring anoxic aqueous conditions were subjected to a de-oxygenation by passing ultra-pure nitrogen gas (UPN_{2(g)}; 99.999% N_{2(g)}) through an Agilent Technology oxygen trap and indicator for at least one hour after induction of UPN_{2(g)} to the reaction vessel.

3.1.1 Fe-mineral synthesis

Iron-bearing minerals (including 2-line ferrihydrite, goethite, magnetite, hematite and siderite; Figure 3.1) were synthesised via the methods described by Cornell & Schwertmann (2003). Poorly crystalline 2-line ferrihydrite (formula unknown, reported as Fe₅HO₈.4H₂O or 5Fe₂O₃.9H₂O) was synthesised by adjusting the pH of 500 mL 0.1 M Fe(NO₃)₃.9H₂O solution to pH 7.5 via the slow addition of approximately 330 mL of 1 M KOH. The sample was then washed thoroughly with DIW to remove nitrate contaminants, and dried at room temperature. Goethite (α -FeOOH) was synthesised from a solution containing 50 mL 1 M Fe(NO₃)₃ and 90 mL 5 M KOH, which was heated at 70°C for 60 hours to produce a yellow precipitate. Hematite (Fe₂O₃) was produced by heating a solution of 0.02 M Fe (NO₃)₃.9H₂O (dissolved in preheated 0.002 M HCl) for 7 days at 98°C to give an orange-red precipitate.

Samples of synthetic lepidocrocite and magnetite were provided by Dr S. Poulton, and prepared using the methods described in Schwertmann & Cornell (1991). Lepidocrocite (γ -FeOOH) was prepared by adjusting the pH of a 0.06 M FeCl₂ solution to pH 7 with NaOH, while slowly oxidising Fe(II) via the addition of O_{2(g)}. To obtain magnetite (Fe₃O₄), an anoxic solution of 3.33 M KOH and 0.27 M KNO₃ (240 mL) was slowly added to a preheated 0.3 M Fe(II)SO₄·7H₂O solution (560 mL) at 90 °C to allow precipitation of synthetic magnetite under a constant flow of N_{2(g)}. After constant stirring for one hour, the black powdered mineral was washed thoroughly with DIW and dried.

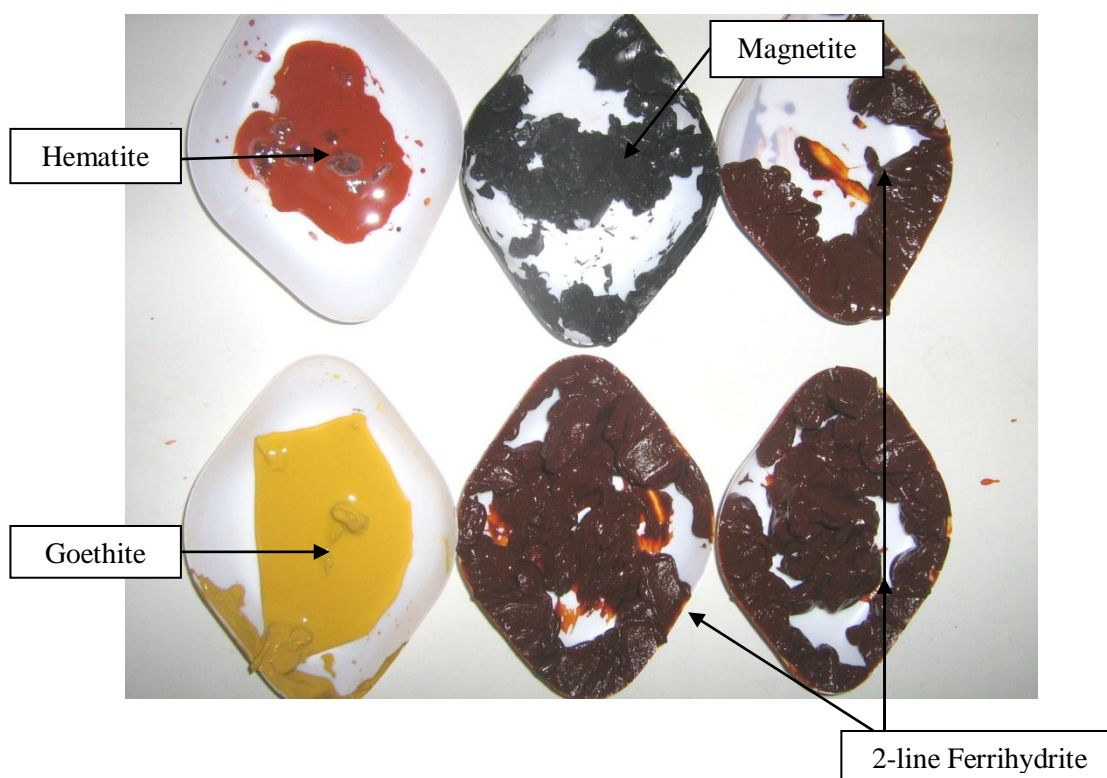


Figure 3.1: Examples of synthesised Fe(III) oxide minerals (pre-drying)

Siderite (Fe^{II}CO₃) was prepared under completely anoxic conditions within an anaerobic chamber according to the synthetic procedure of Poulton & Canfield (2005). A deoxygenated solution of 0.5 M Na₂HCO₃ was added drop-wise into a solution of 0.5 M

FeCl₂·4H₂O under constant flow of N₂(g) to precipitate a light green mineral (Jensen *et al.*, 2002), which was transferred to sealed tubes and centrifuged for 3 minutes at 3000 rpm. After repeated washing with deoxygenated DIW, the solution was vacuum filtered to dry and stored frozen at -80°C to avoid significant sample oxidation.

Before characterisation, all Fe-minerals were ground using an agate mortar and pestle to a fine, homogeneously sized powder (< 63 µm). Iron mineralogy was determined using X-ray diffraction (XRD) with the intention of recognising impurities within the synthesised samples. Powders were analysed using a PANalytical X'Pert ProDiffractometer with Cu Kα radiation (λ = 1.54 Å), with all minerals giving characteristic peaks compared to XRD-internal library traces. The surface area of each mineral was determined using multi-point BET (Brunauer, Emmett & Teller) Surface Area analysis (Gemini 2375 V4.02) by Dr Karen Wicks at AFESS, University of Reading, producing measurements of 183.60 m²/g, 128.30 m²/g, 35.23 m²/g, 2.47 m²/g and 11.6 m²/g for ferrihydrite, lepidocrocite, goethite, hematite and siderite respectively.

3.2 SEDIMENT CHARACTERISATION

Two sediment cores from a) Aarhus Bay, Denmark (*courtesy of Dr Bo Thamdrup, NORDCEE, University of Southern Denmark*); and b) Umpqua River shelf, N. Pacific Basin (*courtesy of Dr Silke Severmann, Rutgers University, NJ*) were obtained for experimental study between September 2007- January 2009. Upon sampling, cores were immediately stored under a N_{2(g)} saturated atmosphere and frozen to avoid oxidation of reactive Fe mineral phases. An air-tight glove-box was deoxygenated with UPN_{2(g)} for 2 hours prior to use, and kept under positive pressure throughout the sectioning process.

Cores were introduced into the glove box via an airtight septum and winch. Samples were sectioned at intervals of a) 2cm from core surface (*Aarhus Bay sediment*) and b) 1 cm between the core surface and 10 cm depth, after which samples were taken every 2 cm between 10 cm – 36 cm (*Umpqua River shelf sediments*). Samples were stored in individual 50 mL centrifuge tubes, sealed then defrosted under a substantial flow of N_{2(g)}. After which, sample tubes were centrifuged at 3000rpm for 3 minutes to separate sediment from pore-water fluid samples, with 1 mL aliquots removed for individual pore-water analysis (see later Methodology Section 3.4). Centrifuge tubes were immediately re-sealed and stored frozen under N_{2(g)} atmosphere to avoid sample oxidation before use.

3.2.1 Fe phase characterisation

3.2.1.1 The reactivity of iron bearing minerals

To characterise Fe mineral phases associated with natural sediment assemblages, an operationally defined sequential extraction procedure (Raiswell *et al.*, 1994; Poulton & Canfield, 2005) was applied to define the range of reactive Fe species and the total Fe content throughout individual core sections. This speciation method characterises highly reactive Fe mineral phases and poorly reactive Fe-bearing silicates within sediments (Poulton & Raiswell, 2002; Raiswell *et al.*, 2006), based on early studies of iron mineral reactivity with respect to dissolved sulfide (Canfield 1989; Canfield *et al.*, 1992; Raiswell & Canfield, 1996; Poulton *et al.*, 2004). Fe bearing minerals are classified according to distinguished differences in highly reactive iron minerals such as ferrihydrite, goethite, hematite and magnetite (which react with sulfide over a matter of minutes/hours/days) with those which react poorly, over a much longer timescale (Fe-silicates, 10⁵ – 10⁶ years). These phases are defined as:

$$\text{Reactive Fe (Fe}_{\text{HR}}) = \text{Fe}_{\text{carb}} + \text{FeOx}_1 + \text{FeOx}_2 + \text{Fe}_{\text{mag}} + \text{Fe}_{\text{AVS}} + \text{Fe}_{\text{py}} \quad (\text{Eq. 3.1})$$

$$\text{Poorly reactive Fe (Fe}_{\text{PR}}) = \text{Fe}_{\text{prs}} \quad (\text{Eq. 3.2})$$

$$\text{Unreactive Fe (Fe}_{\text{U}}) = \text{FeT} - (\text{Fe}_{\text{HR}} + \text{Fe}_{\text{PR}}) \quad (\text{Eq. 3.3})$$

Poulton *et al.*, (2004) and Poulton & Canfield, 2005 define highly reactive iron phases as iron carbonate minerals (e.g. siderite; Fe_{carb}), Fe(III) oxides which react quickly with dissolved sulfide such as ferrihydrite or lepidocrocite (FeOx_1), and those which react slightly slower (goethite, hematite; FeOx_2). The Fe_{HR} phase also includes magnetite (Fe_{mag}) and Fe in reaction with sulfur species, for example acid volatile extractant iron mono-sulfides and pyrite (FeS and FeS_2), due to the significant abundance of iron-sulfur end members within the natural environment. Poorly reactive iron species (Fe_{PRS}) includes Fe associated with sheet clay silicate minerals, with Fe_{U} phases being residual minerals completely unreactive towards dissolved sulfide and non-extractable during the sequential extraction procedure (non-reactive silicate minerals). The total Fe (FeT) within the sediment was also measured on a separate sample, and in turn used to calculate the fraction of unreactive Fe within each section.

3.2.1.2 Fe sequential extraction procedure

Extractions were performed in 10 mL Sarstedt screw top vials, with all extractions taking place at room temperature and initial sediment sample sizes between 100-200 mg. In order to assess the error associated with the extraction procedure, one sediment sample was chosen to be analysed in replicate (Umpqua River sediment, 9-10cm depth; $n = 7$). In order to reduce any error produced by over-extraction or by leaching of one

phase into another, the minimum amount of sequential steps were performed, with extraction times chosen to reflect the speciation of high reactive Fe phases from the modern sediment core analysed in this study.

Step 1. Easily reducible Fe oxides (FeOx₁)

In order to extract highly reactive, easily reducible Fe(III) oxides, a hydroxylamine HCl extraction was carried out. 34.75g hydroxylamine-hydrochloride (NH₂OH.HCl) was washed into a 500 mL volumetric flask with 125 mL of acetic acid (CH₃COOH 25% v/v dilution), and then made to the volumetric mark of 500 mL with DIW. 10 mL of hydroxylamine reagent was added to each sediment sample vial and continually shaken at room temperature for 48 hours before being washed via centrifugation for three minutes at 4000 rpm. A 20x dilution was then prepared for FeOx₁ analysis by atomic absorption spectrometry (AAS).

Step 2. Reducible Fe oxides (FeOx₂)

A sodium dithionite reagent was prepared to extract stable, crystalline Fe oxides (goethite, hematite). As this solution naturally oxidises over a short period of time, and reagent was prepared immediately prior to use. A 500 mL solution containing 58.82 g tri-sodium citrate (C₆H₅Na₅O₇·2H₂O) and 50 g sodium dithionite (Na₂S₂O₄) were buffered to pH 4.8 by addition of 20 mL acetic acid. 10 mL of dithionite solution was added to each sample and placed on a shaker for 2 hours, after which a 20x dilution was prepared for analysis by AAS.

Step 3. Magnetite extraction (Fe_{mag})

An ammonium oxalate reagent was prepared specifically for the extraction of magnetite. 0.2M ammonium oxalate ($(NH_4)_2C_2O_4 \cdot H_2O$) was added to 0.17M oxalic acid ($(COOH)_2 \cdot 2H_2O$), with 10mL of oxalate solution added to individual samples, then shaken for 6 hours. After extraction of Fe_{mag} , the remaining solid sediment sample was decanted into a glass test tube and oven dried before Step 4.

Step 4. Poorly reactive silicate Fe (Fe_{prs})

A boiling 12N HCl extraction (Raiswell *et al.*, 1994) was used to extract poorly reactive silicate Fe from sediment samples. From the oven dried samples, 5 mL of cold 12N HCl was added to each sample and brought to the boil over 1 minute. The tube was held in the flame to vigorously boil for a further one minute, then immediately quenched with DIW to stop the reaction. The solution was poured into a 100 mL volumetric flask and made to mark with DIW. The solution was then diluted for AAS analysis as before.

Step 5. Total Fe extraction (Fe_T)

The procedure for determining total Fe concentration within a sediment assemblage was adapted from a $HNO_3/HF/HClO_4$ extraction procedure described by both Walsh (1980) and Poulton & Canfield (2005). 100 mg of homogenised sediment was furnace ashed overnight at 570 °C, before being transferred to a clean Teflon flask. To the sediment sample, 5 mL concentrated nitric acid followed by 5 mL 37% hydrofluoric acid (HF) was added, with 1 mL 60% perchloric acid ($HClO_4$) to oxidise residual organic matter. Samples were left to evaporate overnight at 130 °C until dry, leaving a light yellow-white coloured precipitate in the Teflon flask. 2.5 mL boric acid (50 g/L; H_3BO_3) was added to the solid and heated again at 130°C overnight, converting insoluble Al

hexafluorates to soluble Al-salts. Once cooled, the sample was re-dissolved in 50% (v/v) HCl acid with gentle heating, then washed into a 100 mL flask with D.I.W. The sample was then subsequently diluted for AAS analysis.

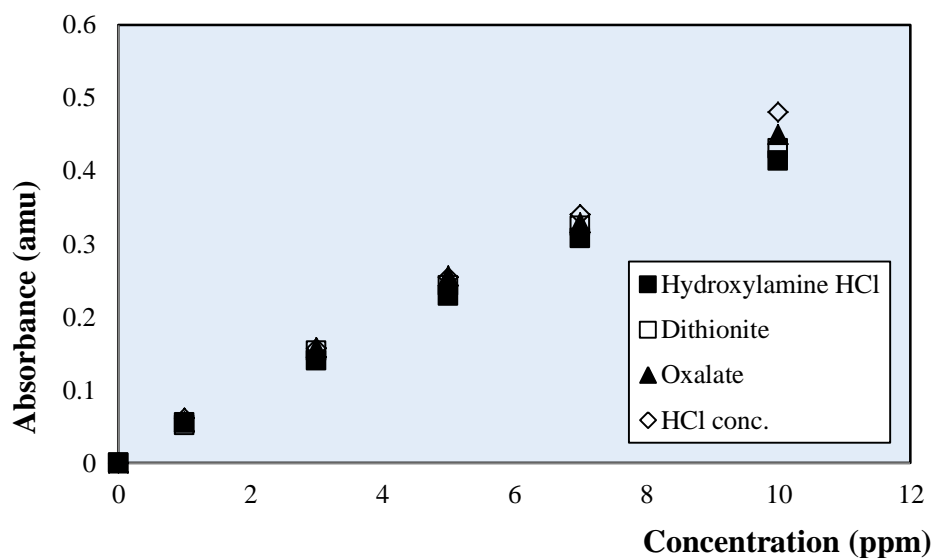


Figure 3.2: AAS calibration curve determined from known concentration standards of Fe(III)

Figure 3.2 represents the AAS calibration for the extractants of each step of the sequential extraction procedure with a known concentration of Fe stock standard (1,3,5,7,10 ppm). The error associated with each step was determined by analysing a number of replicates of one sediment sample, under the same conditions as the main batch of extractions. Table 3.1 indicates that there is little variance during the sequential extraction step, with an RSD (relative standard deviation around the mean) of less than 4% (n=8 samples).

Table 3.1: Calculated error per sequential extraction step

	Hydrox.HCl FeOx ₁	Na.Dith FeOx ₂	Am.Oxa Fe _{mag}	HCl Fe _{pr}	HCl FeT
Average (Wt %)	0.384	0.432	0.276	0.077	4.517
± Std. Dev	0.007	0.007	0.006	0.003	0.048
RSD (%)	1.72	1.71	2.13	3.75	1.06

In addition to the traditional sequential extraction procedure described for individual Fe mineral phases, samples chosen for use in Chapter 4 were subjected to an initial 0.5 M HCl extraction to determine the magnitude of surface bound iron which had been diagenetically reduced prior to sampling (Fe(II)_{surf}; Thamdrup *et al*, 1994). After samples were acid washed for approximately 12 hours in 6M HCl, samples were centrifuged and diluted for AAS analysis as described above, with a 1 mL aliquot of supernatant added to an Fe-specific UV-Spectrometry reagent (Ferrozine) for instant analysis. Further details on this method are described in Section 3.4.1. Taking into account the degree of reduced iron which has previously undergone reaction within sediment, the true fraction of highly reactive minerals characterised by FeOx₁ minerals may be determined.

3.2.2 Sulfur species extraction

A uniform experimental procedure was set-up for the extraction of acid volatile sulfides (AVS) and pyrite from both Aarhus Bay and Umpqua River shelf sediments (Section 4.1). During the reaction, samples were heated along with a reducing agent (either HCl or CrCl₂), trapping hydrogen sulfide gas with silver nitrate (AgNO₃) to form silver sulfide (Ag₂S) for further analysis (Figure 3.3). The reported recovery of FeS and pyrite from this extraction was determined by replicate measurements of pure mineral phases

as $95 \pm 2.6\%$ (Canfield *et al.*, 1986), validating this procedure as a highly effective method of sulfide determination. Replicate measurements of Umpqua River sediment samples at depth 9-10cm produces a sample mean of 0.155 ± 0.005 Wt (%), RSD = 3.2%.

3.2.2.1 Acid Soluble Sulfur

Boiling HCL extractions were used to separate acid soluble sulfur species (e.g. FeS) from sediments (according to the method of Berner, 1970). For the extraction of easily reducible sulfur species (e.g. AVS; Acid Volatile Sulfur as FeS), an individual freeze dried sediment sample (100-150mg) was placed into 3-arm round bottom flask, evacuated of oxygen using a constant flow of $N_2(g)$ (to avoid sulfide oxidation) and secured on a heating mantle. Flasks were connected to a cold water condenser, which in turn was attached to sulfide traps containing 250 μ l 1M $AgNO_3$ solution in DIW. The apparatus was deoxygenated for approximately 15 minutes, before 8 mL 50% v/v HCl was added to the flask, and the temperature increased to boiling point. If no sulfide was precipitated within the trap after 15 minutes, it was assumed no AVS was present in the sample and the next extraction step (Pyrite extraction via chromium chloride reduction) could commence. Otherwise, if sulfide was present precipitating into solution (as a brown solid), the extraction continued for 1 hour.

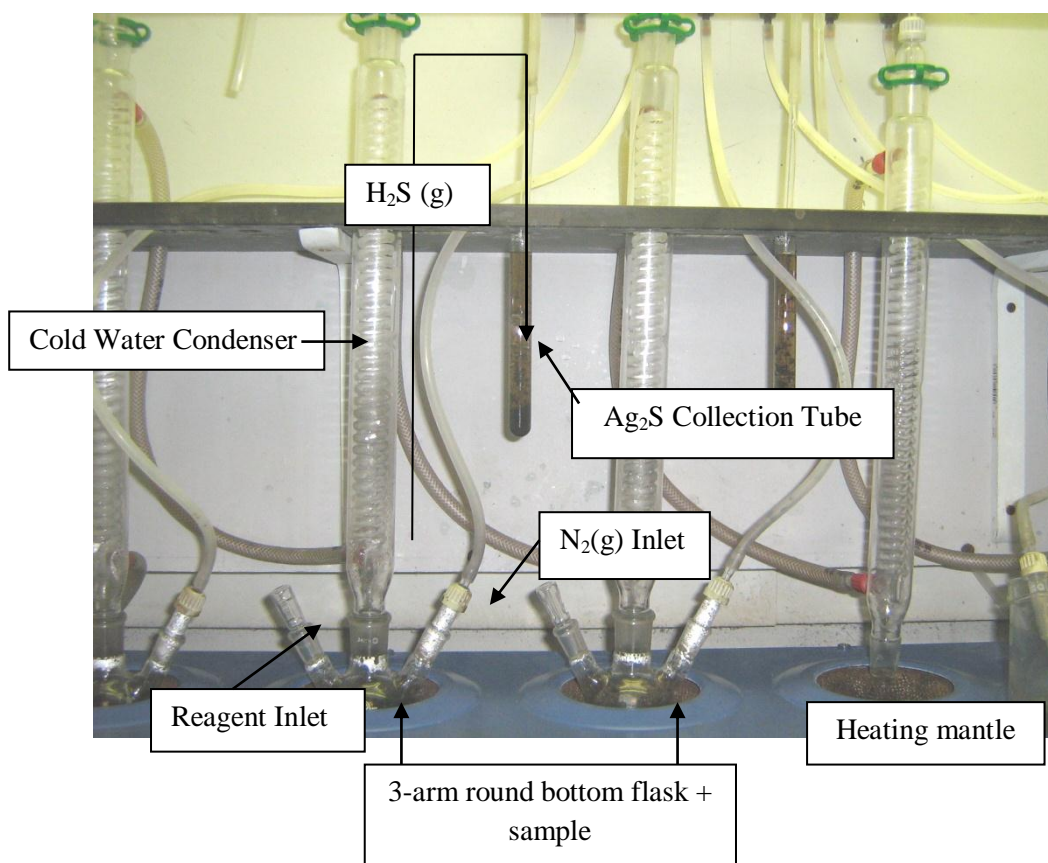


Figure 3.3: Sulfur species extraction line

3.2.2.2. Chromium Reduction

Chromium chloride solution (as 2 mol/L CrCl_2) was prepared by reacting 533 g/L $\text{CrCl}_3 \cdot 6\text{H}_2\text{O}$ dissolved in 1 L 10% v/v HCl acid under a constant flow of $\text{N}_2(\text{g})$ in the presence of an activated zinc catalyst for twelve hours (Canfield *et al.*, 1986; Fossing & Jørgensen, 1989). During this time, the reagent changed from dark green (oxidized Cr) to blue (reduced Cr). CrCl_2 was then stored in airtight 60 mL syringes ready for use. Where no AVS was present in the previous HCl extraction step, the same AgNO_3 trap used previously could be used to trap pyrite-S in the form of Ag_2S . However, a new trap was introduced if AVS was present in the first extraction. As the sample boiled under $\text{N}_2(\text{g})$, 16 mL CrCl_2 solution was injected quickly into the round bottom flask via

syringe and the system closed. The pyrite sample was extracted for 1 hour before the trap was removed, and the precipitate washed with DIW and dried on filter paper, before weighing to determine the final FeS and/or pyrite content.

3.3. SULFIDATION EXPERIMENTS

3.3.1. Closed system iron sulfidation

Experimental sulfidation apparatus (Figure 3.4) consisted of a 1 L Pyrex reaction vessel with five gas-tight inlet ports to accommodate a pH electrode, a sample inlet/outlet valve, a glass pipette for HCl addition, and a glass de-oxygenation tube. As the sulfidation reaction consumes protons (e.g. Dos Santos Afonso & Stumm, 1992), deoxygenated HCl (0.001-0.1 M) was added via a Titra-lab TIM856 Titration Manager to maintain the required pH. Reaction temperature was held at 25°C using a 10 L water bath.

A 100 mM sulfide stock solution was prepared by dissolving $\text{Na}_2\text{S}\cdot 9\text{H}_2\text{O}$ in DIW under $\text{N}_2(\text{g})$. Before addition, $\text{Na}_2\text{S}_{(\text{s})}$ crystals were washed quickly with DIW to remove any oxidised surfaces from the solid. Experiments were performed via addition of a known volume of stock sulfide solution to 1 L of deoxygenated 0.1 M NaCl, and the solution stirred rapidly. Prior to starting the reaction, the initial concentration of dissolved sulfide in the reaction vessel was measured in triplicate.

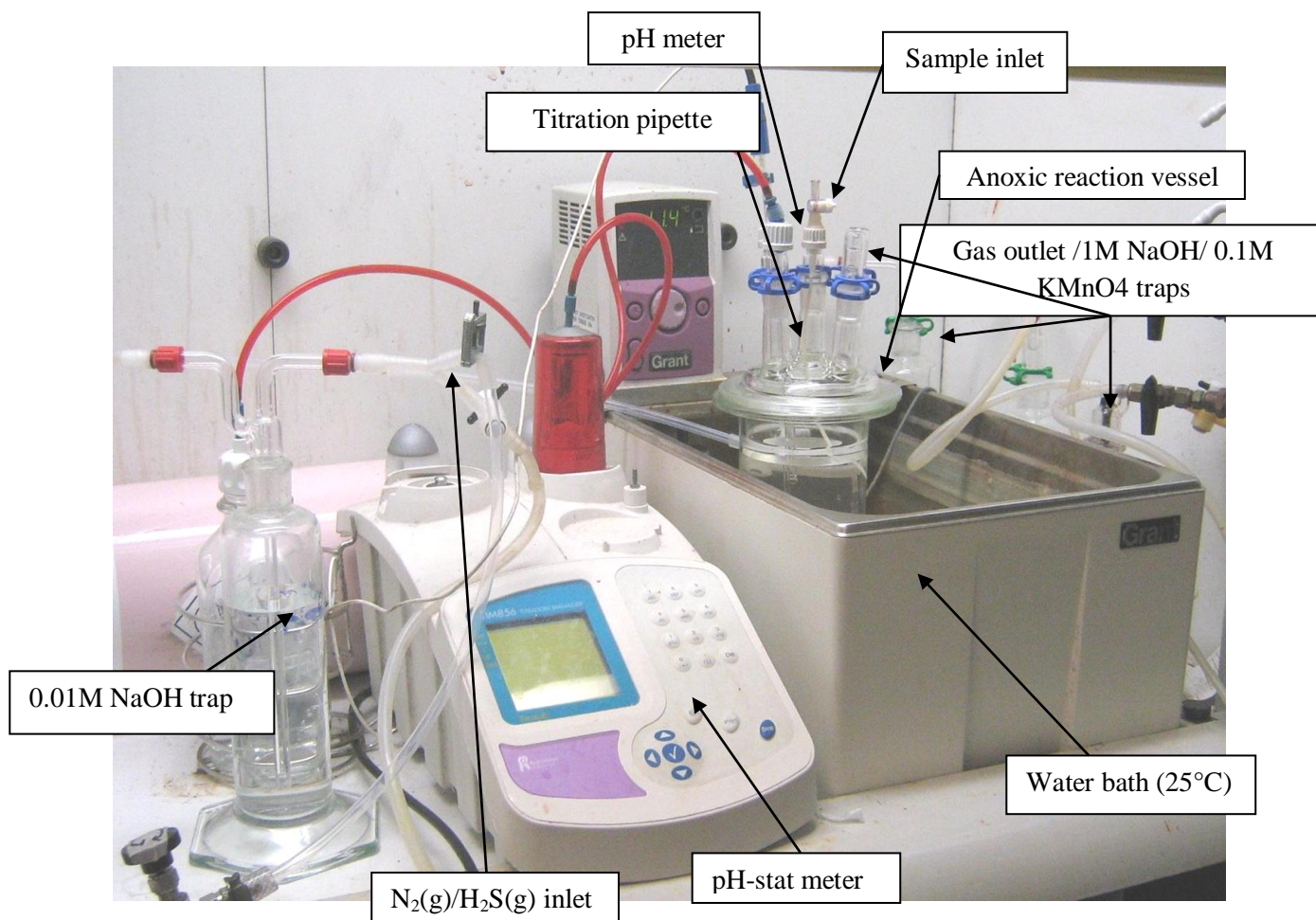


Figure 3.4: Experimental iron sulfidation equipment

A known weight of the Fe (oxyhydr)oxide mineral ($0.01 < 1$ g) was then de-oxygenated in a 5 mL solution containing DIW or buffer (Figure 3.4). The flow of $N_2(g)$ was then switched off and the input valve opened to force the de-oxygenated sample solution rapidly into the vessel. This process took less than 5 seconds and all ports remained closed, thus allowing the Fe (oxyhydr)oxide to be added to the reaction vessel under anoxic conditions (see Poulton, 2003; Poulton *et al.*, 2004).

3.3.2 *H₂S sediment incubation*

Both synthetic mineral and natural sediment experiments were also carried out using a continuous flow of H₂S gas (based on the studies of Wilkin & Barnes 1996; Benning *et al.*, 2000; 0.5% H₂S(g): 99.5% oxygen-free N₂(g); Scientific and Technical Gases) in order to conduct open system experiments on model sediments undergoing a reactive continuum process. Before entering into the 5-port reaction vessel containing 1 L DIW (deoxygenated for at least one hour prior use), H₂S gas was passed through a dilute (0.01 mol/L) sodium hydroxide (NaOH) trap, removing contaminants, and allowing saturation of deionised water with H₂S(g) to a known concentration. From the gas outlet, excess and headspace H₂S(g) passed from the reaction vessel through two 1M NaOH sulfide traps and then a 0.1 mol/L potassium permanganate (KMnO₄) indicating trap (turning from purple to brown with H₂S(g) saturation) in order to neutralise remaining toxic gases. An initially high flow rate of H₂S(g) allowed saturation of DIW for at least 1 hour, characterised by a decrease in pH which eventually became stable.

After this, the rate of flow of H₂S(g) was decreased to approximately 10 cm³/L (a 'few' bubbles per second) to maintain saturation. 1 mL samples were taken in triplicate to measure the concentration of the initial dissolved sulfide (Methylene Blue Method, Section 3.4.3). Experiments at high pH (7.5- 8) were buffered with sodium tetra-borate (0.1M Na₂B₄O₇·10H₂O) in both the dilute NaOH trap (5 mL) and reaction vessel (10 mL) to maintain solution pH throughout the reaction. In order to accommodate a larger volume of sediment, a larger induction syringe for the de-oxygenation and induction of sample was used (Figure 3.5).

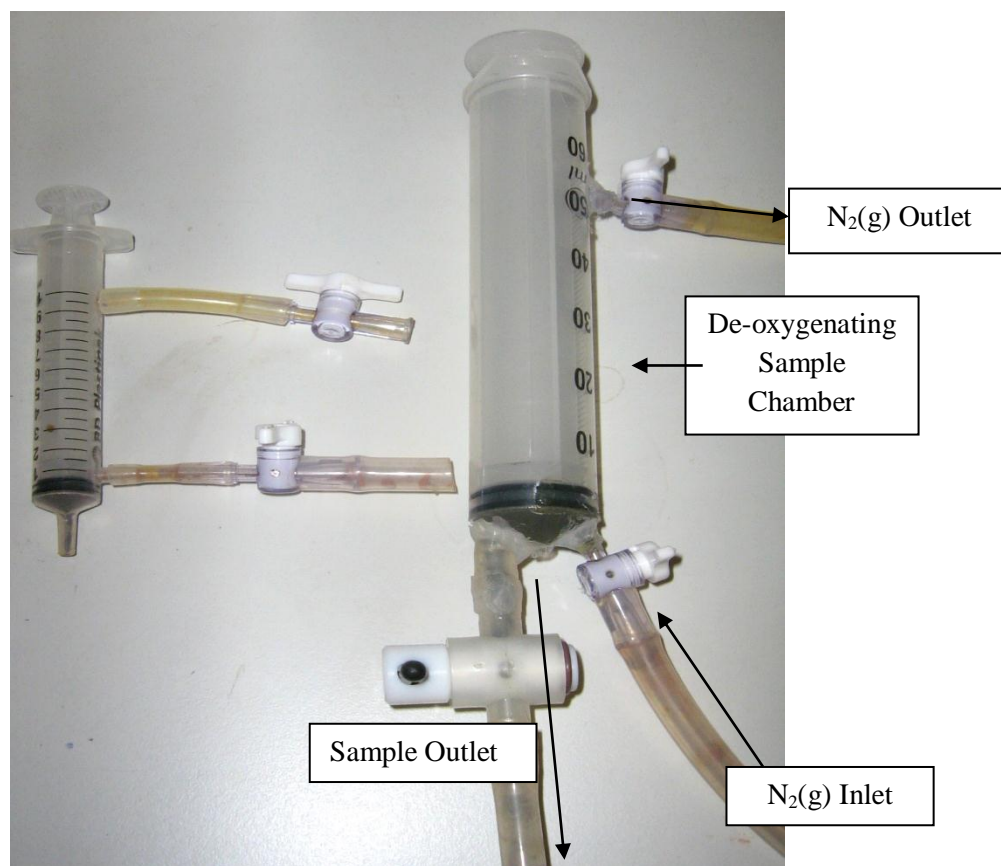


Figure 3.5: Laboratory sealed deoxygenating syringes for sample injection of a) pure synthetic minerals (small syringe) b) sediment slurries (large syringe).

3.4. CHEMICAL ANALYSIS

Samples for analysis of solid and dissolved phases were taken at timed intervals by an air tight 10 mL or 50 mL syringe, fixed with a colorimetric reagent and analysed immediately via UV-Visible spectrophotometry using a Thermo-Genesys 6 UV-spectrophotometer (UV-Spec) to avoid sample oxidation. UV-Spec was used to analyse Fe species in solution (compared to other analysis techniques such as Flame Atomic Absorption Spectrometry or Inductively Coupled Plasma Atomic Emission Spectrometry) due to the efficient and immediate sample run and analysis time,

accuracy and ease of sample preparation, vital in avoiding sample oxidation of reduced Fe and S species.

3.4.1 Determination of Fe(III)/Fe(II)

The Ferrozine method (Stookey, 1970) was used to measure solubilised iron species in natural waters, using a colorimetric reagent (a monosodium salt hydrate of 3-(2-pyridyl)-5,6-diphenyl-1,2,4-triazine-p-p'-disulfonic acid; 'Ferozine'). Voillier *et al.* (2000) proposed a revised method of this procedure in which both Fe(III) and Fe(II) species found in natural and pore waters could be distinguished with the use of a reducing agent and buffer. Ferrozine reagent (0.01mol/L) was prepared in 0.1 mol/L ammonium acetate ($\text{CH}_3\text{COONH}_4$). A reducing agent of 1.4 mol/L hydroxylamine hydrochloride ($\text{H}_2\text{NOH.HCl}$) was prepared in 2M HCl. A buffer of 10 mol/L $\text{CH}_3\text{COONH}_4$ was prepared with adjustment to pH 9.5 drop-wise with ammonium hydroxide solution ($\text{NH}_{3(\text{aq})}$).

Dissolved Fe

Dissolved Fe(II) in solution was measured via the addition of 500 μL Ferrozine to 1mL sample (filtered through 0.2 μm PTFE syringe filters) and shaken well. After ten minutes, the solution was analysed spectrophotometrically at 562nm. Dissolved Fe(III) species in the sample was measured by adding 188 μL hydroxylamine hydrochloride reducing agent to 1mL of the sample, and allowing to react for ten minutes. After this time, 63 μL of ammonium acetate buffer was added to the solution and shaken thoroughly before being analysed at 562nm.

Surface reduced Fe

To measure the concentration of reduced iron (Fe(II)) associated with the surface of the Fe(III) oxide, 1 mL unfiltered sample was digested in 1 mL 10% v/v 12N HCl under an atmosphere of N₂(g) to dispel H₂S(g) from the sample. 100 µL digested sample was then added to 2mL DIW with 400 µL Ferrozine reagent and 200 µL ammonium acetate buffer, shaken well, then analysed at 562nm after 10 minutes. The concentration of surface reduced Fe(II) also incorporates dissolved Fe(II), therefore in order to calculate true surface concentration, dissolved Fe(II) was subtracted from the total. To analyse for surface Fe(III) species, a separate 100 µL sample of digested iron was added to 4 mL DIW, with 500 µL hydroxylamine hydrochloride reducing agent and 400 µL Ferrozine reagent. After ten minutes, 400 µL of ammonium acetate buffer was added, and the sample analysed spectrophotometrically at 562nm.

Standardisation and calibration of Ferrozine for UV Spectrophotometry

Using known concentrations of Fe(II) and Fe(III) stock standards (i: 1, 5, 10, 25, 50, 100, 250 µM and ii: 10, 50, 100, 250, 500, 750, 1000 µM), calibration curves were produced for individual dissolved and surface bound Fe(II) and Fe(III) species (Figure 3.x), using the methods described in 3.4.1.

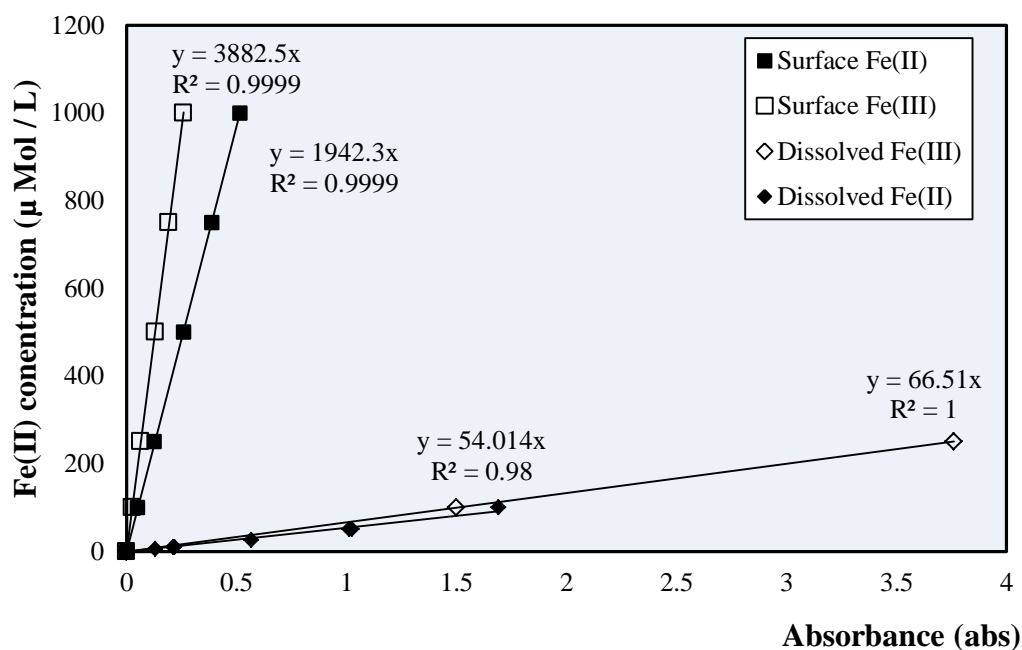


Figure 3.6: The linear relationship observed between Fe(II) or Fe(III) concentration and absorbance plots, measuring dilute, known, concentrations of a stock standard Fe solution (1000µM).

The values denoting the linear slopes in Figure 3.x (i.e. Dissolved Fe(II) : $y = 54.01x$; constant = 54.01) are representative of the constants used in the calculation of Fe concentration from absorbance measurements during UV Spectrophotometry.

Total Fe

In order to calculate the total amount of Fe(II) and Fe(III), 1 mL unfiltered samples were digested in 1 mL 50% v/v 12N HCl under a flow of N₂(g). 100µL of digested sample was added to 3mL DIW with 400µL Ferrozine solution, allowed to react for ten minutes before the addition of 400µL ammonium acetate buffer and spectrophotometric analysis. The total Fe(III) in solution was measured by analysing a fresh 100µL digested sample, added to 4 mL DIW, 500 µL hydroxylamine hydrochloride reducing solution

and 400 μL Ferrozine reagent. After 10 minutes, 400 μL ammonium acetate buffer was added and the sample shaken, and measured by UV-Spec 562nm.

Measurement of diagenetic Fe(II) associated with sediment assemblage surface

The measurement of solid phase Fe minerals within natural sediments must take into consideration any diagenetic reactions that have influenced the assemblage at the near sediment surface. This includes the previous reduction of Fe(III) oxide mineral phases to produce surface bound Fe(II) which has yet to detach into porewaters. After a 0.5N HCl extraction, 7 μL of supernatant was added to 1 mL of Ferrozine diluted with 18 μL DIW, and analysed as before after ten minutes. This value which constitutes surface bound Fe(II) in a natural sediment assemblage could then be subtracted from the total Fe(III) measurement to provide a measurement of unreacted FeOx minerals during solid phase sediment analysis.

3.4.2 Non-reductive dissolution of Fe(III) oxides

By measuring the dissolution of Fe(III) minerals in DIW only (i.e. non-reductive dissolution in the absence of sulfide), the rate at which Fe(III) dissolves can be taken into consideration when calculating the rate of dissolution mediated by sulfide. An example for ferrihydrite is given in Figure 3.7. This shows that at pH 7.5, dissolution of Fe(III) into solution is low and constant ($<5 \mu\text{M/L}$), whereas at pH 4, a gradual increase of $<100 \mu\text{M/L}$ Fe(III) was measured (possibly due to interaction with weak (0.01M) HCl required to lower solution pH). Whether this increase in concentration is related to continual dissolution of Fe(III) from the mineral surface, or is the result of Fe(III) concentrations in equilibrium in solution, it is important to consider how a

“background” concentration of Fe in solution effects the interpretation of iron concentrations measured during Fe mineral reductive dissolutions. Nevertheless, H₂S-mediated dissolution is shown to completely overwhelm that of non-reductive dissolution (Poulton, 2003); and only under more acidic conditions will the effects of Fe dissolution without sulfide reaction, be required to be considered (and subtracted) from total concentrations measured during sulfide mediated reductive dissolution of Fe minerals.

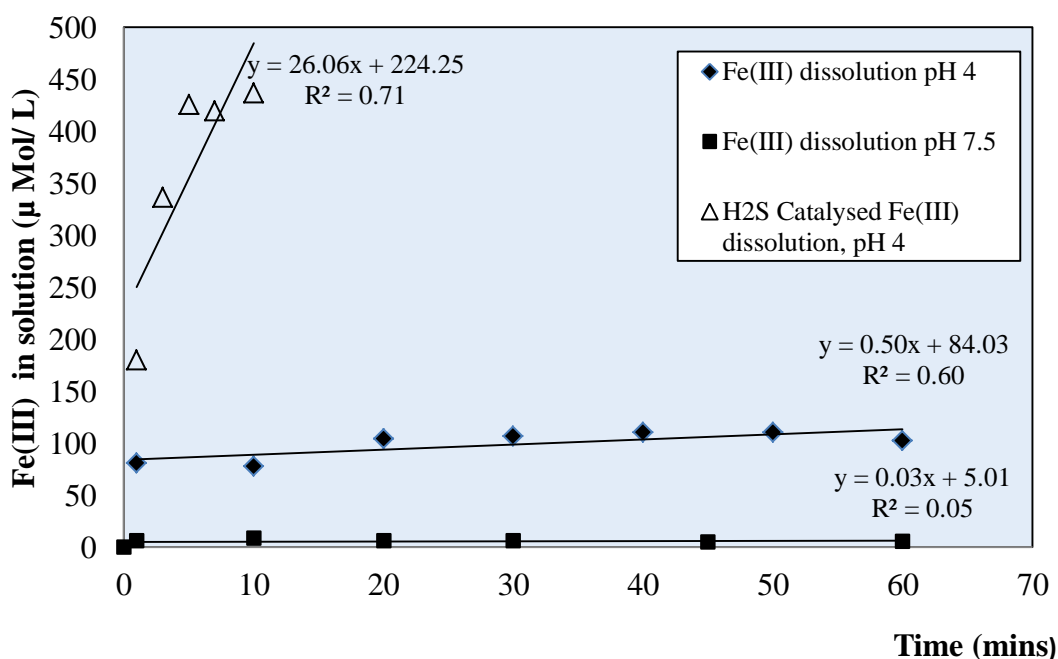


Figure 3.7: Comparison of non-reductive Fe(III) dissolution and H₂S catalysed dissolution of 0.1g ferrihydrite, initial sulfide = 1000μM.

3.4.3 Determination of sulfur products: Methylene Blue method

3.4.3.1 Standardisation of stock sulfide solution

Stock solutions of 0.1M potassium iodate, 0.1M sodium thiosulfate (Convol), 0.1M iodine and freshly dissolved starch solution were prepared for the iodometric determination of stock sulfide concentration:

Preparation of working solutions

- 1) 25mL potassium iodate, 1g of potassium iodine and 3mL of 1M sulphuric acid were added to a 250 mL conical flask. Sodium thiosulfate solution was titrated into the flask until a pale yellow colour was achieved, and 2-3mL starch could be added. The titration was continued slowly until the solution in the flask turn clear. (Working solution = 0.05N sodium thiosulfate)
- 2) 20 mL iodine was pipetted into 250 mL conical flasks and titrated with sodium thiosulfate until pale yellow. As before, 2-3 mL of starch solution was added to the flask and the titration continued until clear. (Working solution = 0.005N iodine).

Preparation of stock standard:

Immediately after the preparation of 1mM stock solution (See 3.3.1) a 200 mL volumetric flask was filled to level with DIW and deoxygenated with $UPN_2(g)$ for one hour. After the addition of ~1-5 mg of anhydrous sodium carbonate (to acts as a buffer), 250 μ L of stock sulfide was added to the flask, which was then filled with deoxygenated water.

Procedure:

Triplicate standards and blanks were prepared by adding 10 mL of DIW and 1-2 g potassium iodide to 150 mL conical flasks, alongside 20 mL 0.005N iodine solution and 2 drops of sulphuric acid. Into three flasks, 25 mL of stock sulfide standard was added; whilst 25 mL of DIW was added to the last three. Solutions were titrated with sodium thiosulfate until pale yellow, before starch indicator was added and the titration completed. The volumes of thiosulfate added to each vial was recorded and the concentration of stock sulfide calculated in $\mu\text{M/L}$.

3.4.3.2. Methylene Blue analysis

At the same time as stock sulfide iodometric titration, the calibration of UV spectrophotometer for Methylene Blue reagent could be obtained; and n=8 replicates aliquots set aside for analysis (containing 1000 μM of stock per sample).

To measure dissolved sulfide and FeS in solution, the Methylene Blue Method (Fogo & Popowsky, 1949; Cline, 1968) was used. Methylene Blue reagent ($\text{C}_{16}\text{H}_{18}\text{N}_5\text{SCl}$) was prepared from dilutions of N, N-dimethyl-p-phenylenediamine sulfate and ferric chloride ($\text{FeCl}_3 \cdot 6\text{H}_2\text{O}$) in 500mL cooled 50% (v/v) HCl (Table 3.2).

Dissolved sulfide samples were measured on 1 mL filtered (0.2 μm PTFE filters) aqueous samples, shaken with 100 μL Methyl-Blue solution and analysed spectrophotometrically at a wavelength of 670nm. Solid phase sulfide (as FeS) was also measured via this technique due to the dissolution of FeS in Methylene Blue (e.g. Poulton, 2003), on unfiltered 1mL samples, with the concentration of FeS determined after subtraction of dissolved sulfide.

Table 3.2: Reactant concentrations for Diamine reagent strengths

Sulfide Concentration ($\mu\text{M/L}$)	Diamine concentration (g /500 mL)	Ferric Concentration (g /500 mL)	Dilution Factor
Strong: 250-1000	20	30	1:50
Mild: 50-250	8	12	2:25
Weak: 5-50	2	3	1:1

Therefore, once the sulfide concentration is determined, and the absorbance of samples are measured using UV spectrophotometry, the F factor for individual Methylene Blue reagents can be calculated, which represents a constant measured in a known mixed diamine reagent.

Total oxidised sulfur was calculated as the difference between the initial sulfide concentration in each experiment and the total sulfide concentration as the reaction progresses (calculated as solid phase plus dissolved sulfide) due to difficulty in measuring elemental sulfur spectrophotometrically using acetone or cyanide fixing reagents. In order to measure the sulfur products associated with the sulfidation of Fe-bearing minerals, UV-Visible Spectrophotometry was used to measure species such as dissolved sulfide in solution and the formation of iron monosulfide (FeS). Figure 3.8 indicates the concentration of dissolved sulfide over a realistic experimental timescale in order to determine the likelihood of natural sulfide oxidation, without the aid of an iron

(III) catalyst. Results indicate that from the sulfide *blank*, an average concentration of $485\mu\text{M} \pm 7 \mu\text{M}$ (RSD = 1.4%) is measured, and hence approximately only $10\mu\text{M}$ of sulfide is naturally oxidised within this system, over an experimental period.

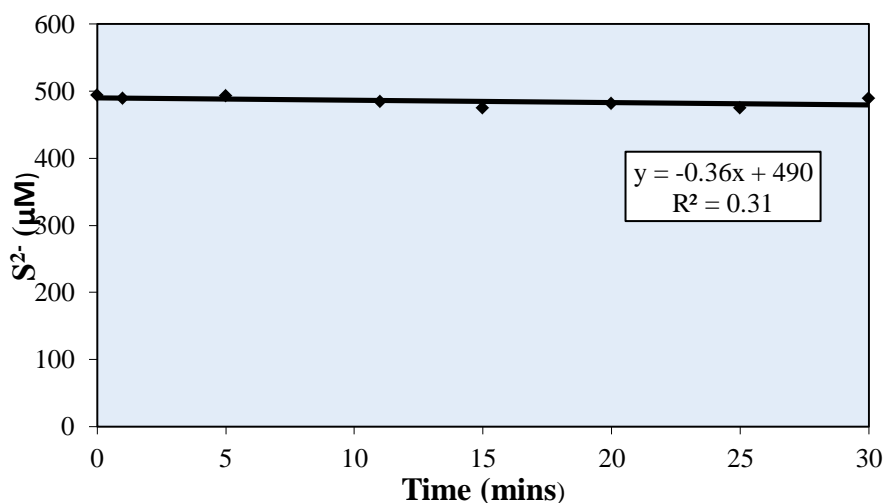


Figure 3.8: Oxidation of sulfide in deoxygenated DIW, pH 7.5, Initial Sulfide = $494 \mu\text{M}$.

3.5 Fe ISOTOPE ANALYSIS

3.5.1 Isotope Sampling

At specified time intervals, a 10 mL air-tight syringe was filled for the isotopic analysis of dissolved Fe(II), surface-reduced Fe(II) and un-reacted Fe(III) in solution. Dissolved Fe(II) was collected through a $0.2 \mu\text{m}$ PTFE syringe filter in an LPDE Nalgene bottle containing $100 \mu\text{L}$ 10% (v/v) HCl. The filter was then immediately washed with 2-3 drops of deoxygenated DIW and 10 mL 1% HCl passed through the filter into a second bottle to dissolve and collect surface-reduced Fe(II) and FeS. This rapid, weak acid procedure left remaining unreacted Fe(III) unaffected (see Poulton, 2003) and hence, the filter was washed with deoxygenated DIW and 10 mL concentrated HCl slowly

passed through into a third bottle to dissolve the remaining unreacted Fe(III) for bulk mineral analysis.

3.5.2 Multi Collector Inductively Coupled Plasma-Mass Spectrometry

Iron isotope analyses were performed on a suite of dissolved Fe(II)_{aq}, surface bound Fe(II) and unreacted Fe(III) oxide samples by Dr S. Severmann (Rutgers University; Severmann *et al.*, 2006) at the University of California, Santa Cruz and at the Woods Hole Oceanographic Institute. Samples were analysed by a Thermo-Finnigan High Resolution multi collector-inductively coupled mass spectrometer (Neptune), via the methods of Beard *et al.*, (2003) (for sample purification using anion exchange chromatography) and of Arnold *et al.*, (2004) (for a description of instrumental parameters). Standards including an international Fe isotope standard (IRMM-014), and a digest of the initial Fe(III) oxide phase were analysed. Isotope ratios of ^{57/54}Fe and ^{56/54}Fe, normalized to starting material were measured, with an instrumental error of ± 0.05‰ commonly reported within a suite of analytical and instrumental papers (including Albarede & Johnson, 2004; Arnold *et al.*, 2004).

CHAPTER 4: EXPERIMENTAL SULFIDATION OF Fe-RICH SEDIMENT CORES; Umpqua River, N. California and Aarhus Bay, Denmark

4. 1. INTRODUCTION

4.1.1. The reductive dissolution of iron oxide minerals mediated by dissolved sulfide

Where $\text{Fe(II)}_{\text{aq}}$ is released to anoxic bottom waters during the (bio)geochemical reduction of Fe oxides, its presence may place major constraints on pore-water sulfide concentrations, the formation of iron sulfide species and the release of (potentially toxic) trace metals adsorbed on the oxide surface (Canfield, 1989; Canfield *et al.*, 1992). Defining the rate of Fe(III) mineral reactivity during early diagenetic reductive dissolution has been the focus of a variety of studies involved in understanding the biogeochemical cycling of iron at the sediment-water interface (Berner, 1980; 1984; Raiswell *et al.*, 1996; Canfield, 1989; Canfield *et al.*, 1992), where the most commonly observed iron oxides include: highly reactive hydrous ferric oxides (such as ferrihydrite), lepidocrocite, goethite, magnetite and hematite (Raiswell & Canfield, 1998; Schwertmann & Cornell, 1991).

In order to understand the role of Fe redox cycling in near surface sediments, numerous experimental papers have investigated mechanisms, and reported rates, of reductive dissolution processes for different Fe(III) oxide minerals. Pyzik & Sommer (1981) report the first multi-step pathway of sulfide mediated reductive dissolution of goethite under experimental conditions. In order to reduce Fe(III), it was proposed that goethite must undergo surface protonation, sulfide adsorption to the oxide surface and electron transfer to reduce Fe(III) to Fe(II). The paper defines a rate equation (Equation 4.1) associated with the rate at which sulfidation of iron oxide minerals is influenced by

initial sulfide concentration, H^+ activity and surface area of the mineral. To determine the rate at which these reactions occur, initial rate theory was used to assess the rate of Fe(III) reduction for multiple iron oxide minerals. The rate of reaction was defined as:

$$d(\text{reduction Fe})/dt = kS_t^{0.5} (H^+)^{0.5} A^1_{FeOOH} \quad (\text{Eq. 4.1})$$

Where S_t is the total initial sulfide concentration (mol L^{-1}), H^+ represents the hydrogen ion activity (mol L^{-1}), A represents the initial surface area of the iron oxide in the reaction vessel ($\text{m}^2 \text{L}^{-1}$), and k defines the rate constant ($\text{m}^2 \text{L}^{-1}$). Table 4.1 indicates the parameters determined experimentally for this rate equation by Pyzik & Sommer (1981), implying that the total sulfide concentration exerts a fractional order (0.5) of reaction dependence, as does proton activity with a first order dependency on the mineral surface area.

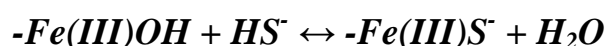
Table 4.1 Details of the rate equation for sulfide mediated reductive dissolution of Goethite, as determined by Pyzik & Sommer (1981).

Sample	Mineral	Reducing agent	Rate Equation, R	k'	Rate order coefficient
Goethite	Synthetic	Hydrogen Sulfide	$R = kS_t^a(H^+)^bA^c$	0.017	$a= 0.5 / b= 0.5 / c = 1.0$

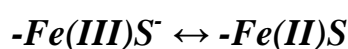
Dos Santos Afonso & Stumm (1992) built upon the study of Pyzik & Sommer (1981) and revised the mechanism for the reductive dissolution of hematite by sulfide (Figure 4.1), which has subsequently been widely applied in a number of experimental studies investigating the reactivity of different Fe(III) oxide minerals (Peiffer *et al.*, 1992; Yao & Millero, 1996; Poulton 2003, Poulton *et al.*, 2004). The model presented by Dos

Santos Afonso & Stumm (1992) is representative for all Fe(III) oxides studied within this thesis, as it has been shown to be consistent with studies of sulfidation of a number of Fe oxide minerals, including ferrihydrite (Poulton, 2003), lepidocrocite (Peiffer *et al.*, 1992; Poulton *et al.*, 2004), goethite (Poulton *et al.*, 2004), magnetite (Raiswell & Canfield, 1998; Poulton *et al.*, 2004) and hematite (Poulton *et al.*, 2004). The mechanism details an adsorbing reductant HS⁻ species which is the catalyst for forming an inner sphere surface sulfide complex on the reactive outer electron layer of the oxide surface.

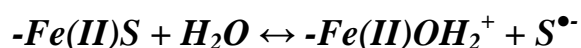
a) Surface complex formation



b) Electron transfer



c) Release of oxidised S



d) Detachment of Fe(II)



e) Formation of Elemental S



f) Formation of FeS

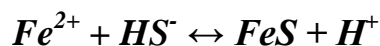


Figure 4.1: Sulfide mediated reductive dissolution of Fe(III) oxide minerals and the formation of elemental sulfur and iron mono-sulfides (Dos Santos Afonso & Stumm, 1992)

The substitution of the surface hydroxyl group after surface complex formation mediates an electron transfer from surface-associated Fe(III) to Fe(II), and the release of an oxidised sulfur radical from the reactive oxide surface. In solution, the hydroxylated reduced iron surface will undergo protonation, weakening the metal bond and allowing the detachment of Fe(II) into pore-waters, leaving behind a newly created reactive surface site, freely available for reaction.

This reaction is a multi-step, surface-controlled process, the rate of which is influenced by factors including pH, initial sulfide concentration and the initial quantity of iron oxide (and hence the available surface area) of mineral available for reaction. Where Fe(II) is released into anoxic aqueous environments, the aqueous ferrous species will continue to react with free HS⁻ to produce solid phase iron monosulfide (FeS(s)), which is a precursor to pyrite formation during diagenesis (Rickard, 1974; Berner 1984). The dominant S oxidation product observed in the reaction of hematite with dissolved sulfide by Dos Santos Afonso & Stumm (1992) was reported as dissolved sulfate, with a minor to negligible percentage of poly-sulfides and thio-sulfates measured in solution. However, in later experimental papers regarding many other Fe(III) oxide minerals, the formation of sulfate was determined to be a minor oxidation product, with elemental S identified as the major product of reductive dissolution (Pyzik & Sommer, 1981; Yao & Millero, 1996; Poulton, 2003; Poulton *et al.*, 2004).

The kinetics with which these reactions occur have commonly been based either on the rate of sulfide oxidation, the overall rate of Fe(III) reduction (assuming a 2:1 ratio of reduced Fe(II) to oxidised S product, in accordance with the mechanism of electron transfer described by Dos Santos Afonso & Stumm (1992)), and the rate of dissolution of Fe(II)_{aq} from the oxide surface. Previous experimental studies of sulfide mediated reductive dissolution reactions generally focus on one of these phases, with the

exception of Poulton (2003) and Poulton *et al.*, (2004) who compared the rates of all three iron and sulfur reactions in order to evaluate the differences in reactivity in terms of sulfide oxidation, Fe(III) reduction and an overall reductive-dissolution mechanism. The general rate equation derived by Poulton (2003) was defined for closed system, batch experiments using synthetic iron minerals, with a known starting concentration of dissolved sulfide at constant pH (7.5):

$$\mathbf{R_i = k_i (H_2S)_{t=0}^{0.5} A} \quad \mathbf{(Eq\ 4.2)}$$

Where R_i is either the rate of sulfide oxidation (R_s) or Fe dissolution (R_{Fe}) in $\text{mol L}^{-1} \text{min}^{-1}$, k_i is the calculated rate constant for sulfide oxidation (k_s) or Fe(II) dissolution (k_{Fe}) in $\text{mol}^{0.5} \text{L}^{0.5} \text{m}^{-1} \text{min}^{-1}$, $(H_2S)_{t=0}$ is the initial sulfide concentration (mol L^{-1}) dependent on a rate order of 0.5, and A represents the initial ferrihydrite surface area ($\text{m}^2 \text{L}^{-1}$), which is first order dependent. Using these rate equations, Poulton (2003) determined that sulfide oxidation occurs approximately 15 times faster than that of Fe(II) dissolution at circumneutral pH, due to the lack of protons available to promote release of Fe(II) to solution.

The results obtained using Equation 4.2 were also used to propose a scheme of reactivity (Poulton *et al.*, 2004) classifying different Fe minerals with regard to individual rates of reaction. Table 4.2 compares the rate constants of iron dissolution (calculated via a series of iron sulfidation experiments) for a number of reactive Fe(III) oxides derived from Poulton (2003) and Poulton *et al.*, (2004). For each experiment, a fractional rate order dependency (0.5) was observed for initial sulfide concentration, with the initial surface area of Fe mineral being first order. Due to the varying

crystalline morphology of these minerals, the differences in reactivity with respect to dissolved sulfide classifies a scheme of iron mineral reactivity, with the majority of iron oxide minerals ranging in reactivity from minutes to tens of days (Poulton *et al.*, 2004).

Table 4.2. Kinetic determination of the rate of sulfide mediated reductive dissolution of synthetic Fe oxide minerals (Poulton, 2003; Poulton *et al.*, 2004).

Sample	Mineral	Reducing agent	Rate Equation, R	k_{Fe}'	Rate order coefficient
Ferrihydrite	Synthetic	Sulfide	$R = k_{fe/s} (H_2S)_{t=0}^a A^b$	8.4×10^{-6}	$a = 0.5 / b = 1.0$
Hydrous Ferric Oxide	Synthetic	Sulfide	$R = k_{fe/s} (H_2S)_{t=0}^a A^b$	$6.0 \times 10^{-6(a)}$	$a = 0.5 / b = 1.0$
Lepidocrocite	Synthetic	Sulfide	$R = k_{fe/s} (H_2S)_{t=0}^a A^b$	6.1×10^{-6}	$a = 0.5 / b = 1.0$
Goethite	Synthetic	Sulfide	$R = k_{fe/s} (H_2S)_{t=0}^a A^b$	7.3×10^{-8}	$a = 0.5 / b = 1.0$
Magnetite	Synthetic	Sulfide	$R = k_{fe/s} (H_2S)_{t=0}^a A^b$	1.0×10^{-6}	$a = 0.5 / b = 1.0$
Hematite	Synthetic	Sulfide	$R = k_{fe/s} (H_2S)_{t=0}^a A^b$	4.2×10^{-7}	$a = 0.5 / b = 1.0$

(a) Represents the average value of k'_{Fe} for HFO sulfidation. Experiments conducted at pH 7.5

4.1.2. Fe oxide minerals in a reactive continuum

The aforementioned studies describe the reactivity of synthetic, pure Fe minerals under highly controlled conditions. However, in nature, mixtures of Fe oxide minerals within sediment assemblages occur, with changes in morphology and crystallinity with depth within a sediment core (Larsen & Postma, 2001). In experimental studies of reductive dissolution implied within natural settings (as opposed to the experiments described above using synthetic minerals), the first studies of Fe-rich natural sediment samples in reaction with an ascorbic acid reductant (Banwart, 1989; Dos Santos Afonso *et al.*, 1990; Suter *et al.*, 1991; Postma, 1993; Roden, 2003; 2004; Hyacinthe *et al.*, 2006) followed a rate equation which is more appropriate to consider gradual changes in

reactivity with depth in the sediment profile. The rate at which reductive dissolution occurred was defined for pure synthetic minerals as (Postma, 1993):

$$J/M_0 = k' (m/M_0)^\gamma \quad \text{(Eq. 4.3)}$$

Where J defines the overall rate of dissolution (moles s⁻¹), M₀ is the initial mass of Fe(III) oxide, m/M₀ is the fraction of Fe(II) in solution in relation to initial mass of the undissolved mineral, k' is the rate constant (s⁻¹) and γ is the rate order related to changes in the crystalline structure and mineralogy over time.

Reductive dissolution experiments carried out by Postma (1993) with synthetically derived Fe(III) oxides (ferrihydrite, goethite and hematite; pH 3) reveal a first order dependency with respect to m/M₀ whilst utilising ascorbic acid as a reductant, with the initial rate at which increasing amounts of Fe(II) measured in solution increasing sharply from t=0 mins, but slowing as M₀ decreased with progressive Fe(III) reduction. Postma (1993), Larsen & Postma (2001) and Larsen *et al.*, (2006) built upon the synthetic mineral studies to determine the rates of reductive dissolution for natural Fe(III) oxide assemblages, describing the changing mineral characteristics throughout Fe rich sediment cores in terms of a reactive continuum process (Boudreau & Riddick, 1991).

The results of these ascorbate mediated experiments highlight that changing mineralogy, Fe oxide crystallinity and surface area all influence the rate of abiotic reductive dissolution in natural Fe oxide assemblages. When comparing a suite of synthetic Fe(III) oxides (and then subsequently synthetic Fe-bearing minerals and Fe(III) oxide assemblages from natural sediments), the values of individual rate

constant (k_{Fe}) were calculated to cover a range of 2 orders of magnitude between different Fe oxide minerals (i.e. ferrihydrite and goethite $\sim 10^{-4}$ to 10^{-6}), a scale which is similarly reflected in the rate constant calculated from known changing mineralogy throughout sediment sample depths of the Rømø aquifer, albeit at a faster rate (10^{-3} to 10^{-5} , Larsen *et al.*, 2006). Table 4.3 also indicates that the rate order coefficients in natural sediments are higher than observed for synthetic minerals, highlighting a greater degree of mineral heterogeneity for natural samples.

Table 4.3. Kinetic rate determination of ascorbic-mediated reductive dissolution

Sample	Mineral	Reducing agent	Rate Equation	k'	γ	Ref.
Ferrihydrite	Synthetic	Ascorbic Acid	$J/m_0 = k'(m/m_0)^\gamma$	4.0×10^{-4}	1.1	Postma, 1993
Bight of Aarhus	Marine sediment	Ascorbic Acid	$J/m_0 = k'(m/m_0)^\gamma$	7.3×10^{-3}	4.7	
Rømø Sand	Oxidised Aquifer Sediment	Ascorbic Acid	$J/m_0 = k'(m/m_0)^\gamma$	5.3×10^{-5}	2.8	
2L-Ferrihydrite	Synthetic	Ascorbic Acid	$J/m_0 = k'(m/m_0)^\gamma$	7.6×10^{-4}	2.3	Larsen & Postma, 2001
6L-Ferrihydrite	Synthetic	Ascorbic Acid	$J/m_0 = k'(m/m_0)^\gamma$	7.4×10^{-4}	2.5	
Goethite	Synthetic	Ascorbic Acid	$J/m_0 = k'(m/m_0)^\gamma$	5.4×10^{-6}	1.0	
Lepidocrocite	Synthetic	Ascorbic Acid	$J/m_0 = k'(m/m_0)^\gamma$	3.9×10^{-5}	1.6	

4.2. RESEARCH AIMS

A comparison between the reactivity of synthetic Fe(III) oxides and Fe(III) oxide assemblages in natural sediments has never been reported for sulfide mediated reductive dissolution. However, the studies of Postma (1993), Larsen & Postma (2001) and Larsen *et al.* (2006) investigating the reduction of natural Fe oxides by ascorbate (which is generally not a significant reductant of Fe oxides during marine sediment diagenesis), suggest that this is required to evaluate whether studies of sulfidation rates of synthetic Fe minerals are valid for use in models of marine sediment diagenesis. The focus of this chapter is thus to investigate rates of Fe oxide reductive dissolution mediated by dissolved sulfide in natural sediment assemblages, utilizing a reactive continuum approach, initially derived in Postma (1993).

The reactivity of a number of synthetic Fe(III) oxides, including ferrihydrite, goethite and magnetite, which are commonly found within anoxic, near surface sediments will initially be evaluated. These oxides differ in individual rates of reactivity with respect to sulfide mediated reductive dissolution (i.e. minutes and hours to days), allowing determination of the rates of total Fe reduction and the rate coefficient for the specific rate equation derived within this chapter. Once rates of reductive dissolution for the pure Fe oxide minerals have been defined, the rates of iron sulfidation of natural iron oxide assemblages will be determined and compared. Two marine sediment cores have been chosen to exemplify changes in iron oxide morphology with depth, and by subjecting sediments from different depths to conditions of excess sulfide, the rate of reductive dissolution can be determined to evaluate how rates change during diagenesis due to the changing morphology and availability of iron oxides with depth.

The primary objectives of this chapter are:

- 1) Determine the rates of reductive dissolution of pure Fe (III) oxide minerals under constant concentrations of dissolved sulfide (which has never before been performed for most of the major Fe oxides).
- 2) Derive a rate equation for use in the measurement of the rates of reactivity of Fe oxides in natural sediments.
- 3) Compare the rates obtained via synthetic experiments with those for two different Fe rich sediment cores, which are characterised as having differing iron mineral morphologies.

4.3 GEOGRAPHICAL SETTING

4.3.1 Aarhus Bay, Denmark

Figure 4.2 illustrates the site of the Aarhus Bay sediment core, sampled at a water depth of 16 m, approximately 5 km from the Jutland coast, with the site lying transitionally between the Baltic and North Sea at 56°09'10"N, 10°19'20"E (Thamdrup *et al.*, 1994; Thamdrup *et al.*, 1996). Core samples were collected by Dr Bo Thamdrup (NORDCEE, University of Southern Denmark) in January 2009 using a box-corer, and immediately sub-cored (25 cm) in Plexiglas tubes and frozen until analysis.

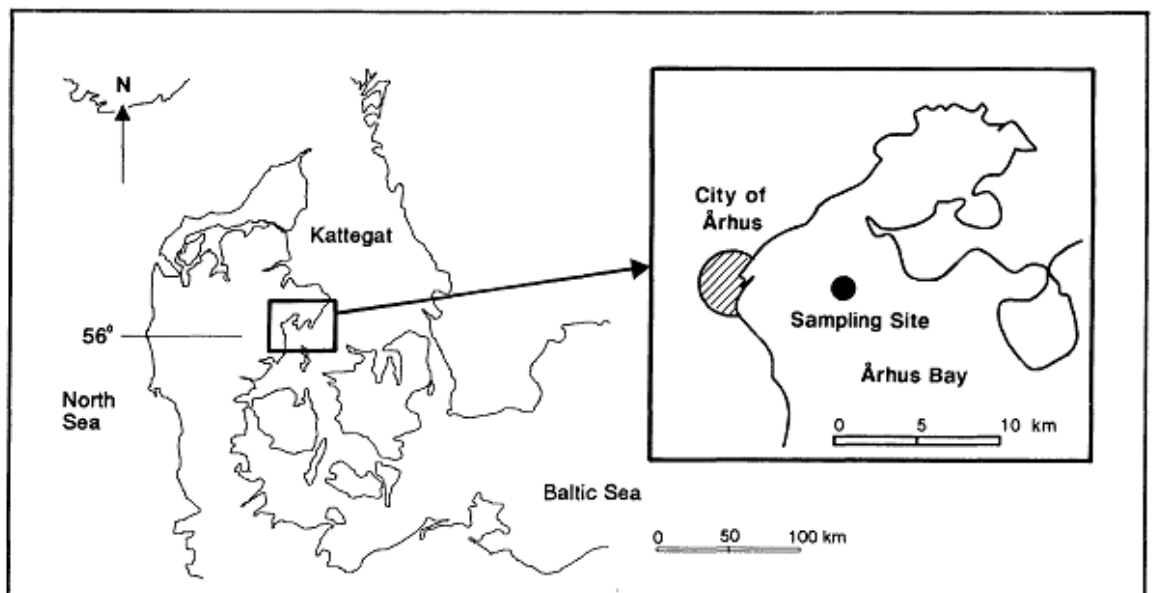


Figure 4.2: Aarhus Bay sample site (Thamdrup *et al.*, 1996)

4.3.2 Umpqua River Shelf, Oregon, N. Pacific Basin

A 50 cm sediment core was collected by Dr Silke Severmann during a scientific cruise on the RV *Wecoma*, (September 2007), near the North Western coast of the United States. The site lies at 42°N, 124°W at a water depth of 192 m on a continental shelf margin in the Northern Pacific Ocean, close to the border of southern Oregon and

northern California. The sediment was immediately frozen upon sampling to avoid oxidation of Fe sulfides, and the transformation of unstable highly reactive Fe oxyhydroxides to more stable crystalline, slower reacting species. The geographical setting of the sampling site is shown in Figure 4.3.

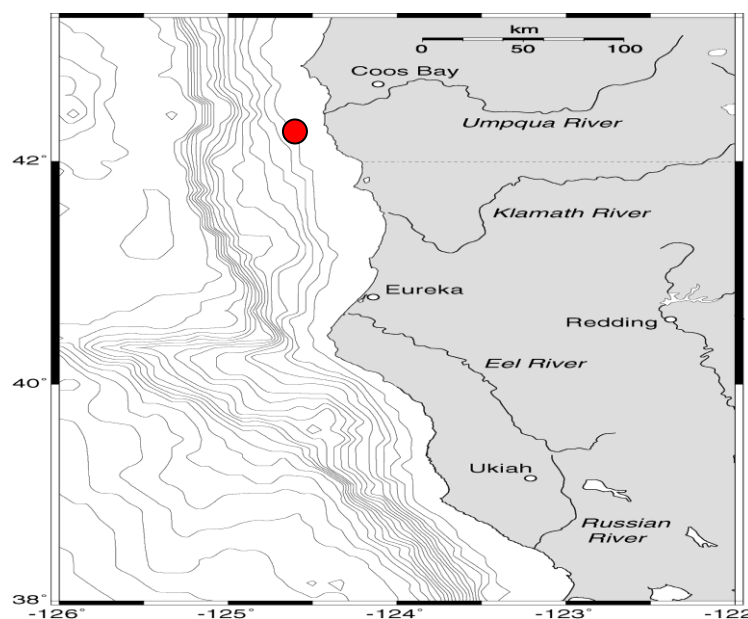


Figure 4.3: Umpqua River Shelf sample site (supplied by Dr Silke Severmann)

4.4 METHODS

4.4.1 Sediment characterization

4.4.1.1 Aarhus Bay

Marine sediment samples from Aarhus Bay, Denmark were characterised by the sequential extraction procedure of Poulton & Canfield (2005) by Dr Tanya Goldberg. Instead of traditional centrifuge methods of pore water extraction from each core section, a Rhizon syringe sampler was used to extract porewaters for analysis of

dissolved iron and sulfide. The use of Rhizon samplers in a N₂ filled glove bag allowed the sampling of pore waters to be performed anoxically.

As a method of determining the solid phase iron content of natural sediment assemblages, a refined version of the sequential iron extraction method of Poulton & Canfield (2005) was used. Carbonate-associated Fe (not considered to be significant in these low carbonate sediments) and FeOx₁ phases were initially extracted with 0.5 M HCl, a technique commonly used in modern sediment studies (Thamdrup *et al.*, 1994; Methodology Section 3.2.1.1 and 3.4.1). This allowed the determination of Fe(III) associated with poorly crystalline Fe oxides such as ferrihydrite to be measured, along with any unsulfidized solid phase Fe(II) which formed diagenetically by the reduction of original Fe(III) oxides. Therefore, in order to calculate the true concentration of unreacted FeOx₁ minerals within sediment assemblages, the value of surface reduced Fe(II) was subtracted from the total value of 0.5 M HCl extractable FeOx₁. The FeOx₂ pool was then extracted by dithionite, followed by an oxalate extraction to determine magnetite associated Fe (Section 3.2.1.1).

4.4.1.2 Umpqua River shelf sediments

Solid phase characterisation of Umpqua River shelf sediments was also undertaken by the iron sequential extraction scheme of Poulton & Canfield (2005). Immediately after sectioning of the core to 1-2 cm sections, samples were placed in centrifuge tubes under a continuous flow of nitrogen, and centrifuged to separate porewaters from sediment prior to analysis. A full method rationale of the sequential extraction procedure is presented in Section 3.2.1.1.

4.4.2 Sulfidation experiments

The initial conditions for each experiment are shown in Table 4.4. Batch experiments were performed (as described in Methodology Chapter Section 3.3.2; Benning *et al.*, 2000; Poulton (2003) and Poulton *et al.*, (2004)) within a 1L air-tight glass vessel with individual inlets for sampling, pH probe and gas induction/removal. The vessel contained 1L of continuously stirred deoxygenated, deionised water, and H₂S_(g) was continuously flushed through the vessel for 1 h to achieve saturation (observed after a constant pH was obtained).

Table 4.4: Experimental parameters for iron sulfidation experiments

Experiment	Mineral	pH	Initial sample wt (g)	Initial Fe_{HR} (μM)	Initial* H₂S (μM)
Synthetic 1	Ferrihydrite	6.9	0.13	1346	944
Synthetic 2	Ferrihydrite	6.7	0.45	4461	693
Synthetic 3	Ferrihydrite	6.5	0.70	7250	361
Synthetic 4	Goethite	6.8	0.30	3375	1054
Synthetic 5	Magnetite	6.7	1.00	12857	1054
Umpqua River	0-1cm	7.1	9.67	1715	1238
Umpqua River	3-4cm	7.3	18.07	3717	1189
Umpqua River	8-9cm	7.5	24.88	4932	1176
Umpqua River	10-12cm	7.4	25.00	4567	876
Umpqua River	14-16cm	7.3	25.00	4808	1011
Aarhus Bay	0-1cm	7.0	1.50	193	1156
Aarhus Bay	17-19cm	6.9	5.15	255	1098

*Cumulative standard deviation of all experiments (where t=0 sample is taken in triplicate) = ± 77μM, RSD = ± 6.9%.

To help maintain a constant pH during the reaction itself, a borate buffer (~ pH 6.5- 7.5) was added to the reaction solution. Synthesised Fe(III) oxide minerals and natural sediment samples were deoxygenated in DIW for at least 30 minutes and then injected

directly into the vessel. Samples were taken to measure total iron reduction, iron monosulfide formation and sulfide oxidation periodically from the first minute of reaction. During experiments of natural sediment sulfidation, some interference (probably from natural dissolved organic matter released by reaction with the acid in the reagents) occurred during measurement of FeS (which is performed on unfiltered samples with Methylene Blue). Thus it was not possible to determine solid phase FeS in the experiments with natural sediments.

4.5 RESULTS

4.5.1 Fe characterisation of sediment cores

4.5.1.1 Aarhus Bay, Denmark

Pore-water measurements from Aarhus Bay sediments (Figure 4.4) indicate that anoxic conditions are achieved close to the sediment-water interface, allowing 150-200 μM of $\text{Fe}^{2+}_{\text{aq}}$ to accumulate within the first 2 cm of the core, before decreasing with depth. As $\text{Fe}^{2+}_{\text{aq}}$ is removed (via pyrite formation, Figure 4.5b), and the more highly reactive Fe oxides are consumed (Figure 4.5a), $\text{HS}^{-}_{\text{(aq)}}$ begins to accumulate in pore waters below 5cm depth.

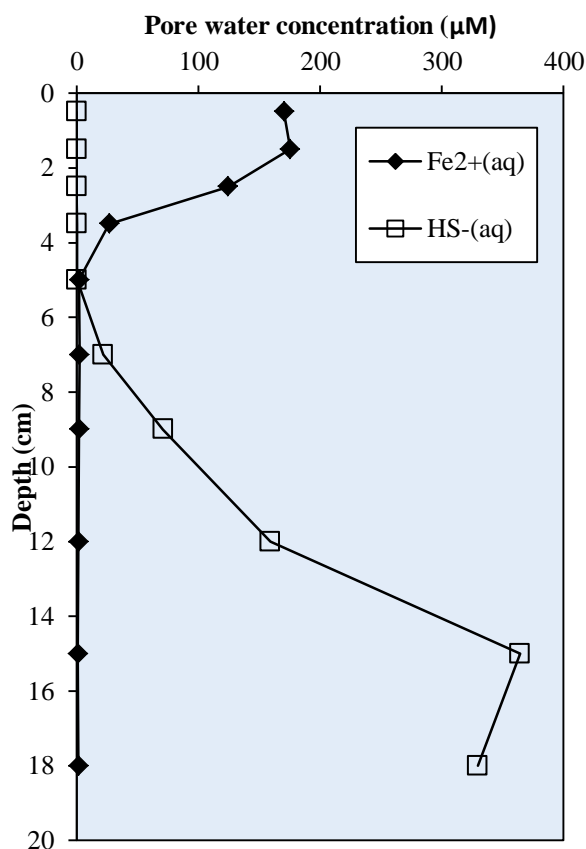


Figure 4.4: Pore water distribution of dissolved $\text{Fe}^{2+}_{\text{(aq)}}$ and $\text{HS}^{-}_{\text{(aq)}}$ in Aarhus Bay core sections.

Tables 4.5 and 4.6 report data collated from the sequential extraction of solid phase Fe minerals from Aarhus Bay sediments. Solid phase analyses used to characterise iron oxide phases within Aarhus Bay sediment (Figure 4.5a) show that between 0-9 cm depth, unreacted FeOx_1 (determined from the removal of 0.5M HCl derived surface bound Fe(II) from total 0.5M HCl Fe) dominates the iron oxide phases (~0.6 – 0.2 wt.%), with a lower concentration of FeOx_2 over this depth (0.2 – 0.11 wt.%). Both of these iron oxide pools decrease with depth as sulfide in pore waters reduces reactive iron oxide minerals (with an additional contribution from dissimilatory Fe reduction). FeOx_2 is shown to decrease at a slower rate in keeping with the slower rate of reaction of dissolved sulfide with regard to FeOx_2 oxides such as goethite and hematite. Figure 4.5b illustrates the fraction of surface bound Fe(II), which initially increases to a depth of ~5 cm, followed by a subsequent decrease as $\text{Fe}^{2+}_{(\text{aq})}$ is eventually released from the mineral surfaces. Below 2 cm depth, an increase in pyrite is observed as highly reactive Fe oxides are consumed and dissolved sulfide begins to accumulate in pore-waters, readily available for further reaction and to convert free $\text{Fe}^{2+}_{(\text{aq})}$ to pyrite.

Figure 4.6a and 4.6b normalises data with respect to total concentrations of FeHR minerals within the sediment assemblage, allowing a comparison of recognised, fast reacting mineral classes for sulfidation. Figure 4.6a shows that unreacted FeOx_1 (which has not undergone previous diagenetic processes, i.e. bacterial reduction) dominates the highly reactive phase between 0-5cm depths within the core (~ 40%). In comparison, FeOx_2 minerals contribute approximately 20% of highly reactive iron in the sediment. Below 5 cm, this value decreases following natural reduction processes, which are reflected in the increase of pyrite in Figure 4.6b. Throughout the core, very little surface reduced Fe(II) is observed, indicating a fast reaction of mineral dissolution. From the results of these solid phase iron analyses, two core sections were chosen to study

experimentally (0-1 cm, 17-19 cm). These sections show significant differences in iron oxide concentrations and morphologies, and therefore are expected to show major differences in the rates of reactivity of Fe(III) oxides towards dissolved sulfide.

Table 4.5: Extractable Fe speciation data for Aarhus Bay sediments (dry weight %)

Sample Depth (cm)	0.5N HCl-Fe(III)Ox ₁ Wt (%)	0.5N HCl Fe(II) Wt(%)	Na. Dith. FeOx ₂ Wt(%)	Am. Oxa. Fe _{mag} Wt(%)	Fe _{pyrite} Wt (%)	FeT Wt(%)
0-1	0.40	0.02	0.23	0.09	0.30	2.66
17-19	0.13	0.01	0.07	0.08	0.66	2.43

Table 4.6: Characterisation of Aarhus Bay sediment in terms of reactive Fe species

Depth (cm)	Fe HR	Fe(II) /FeHR	FeOx ₁ /FeHR	FeOx ₂ /FeHR	Fe _{mag} /FeHR	Py /FeHR	Fe(II) /FeT	FeOx ₁ /FeT	FeOx ₂ /FeT	Fe _{mag} /FeT	FeHR /FeT
0-1	1.04	0.02	0.38	0.22	0.09	0.29	0.01	0.15	0.09	0.11	0.40
17-19	0.95	0.01	0.14	0.07	0.08	0.70	0.004	0.05	0.03	0.03	0.40

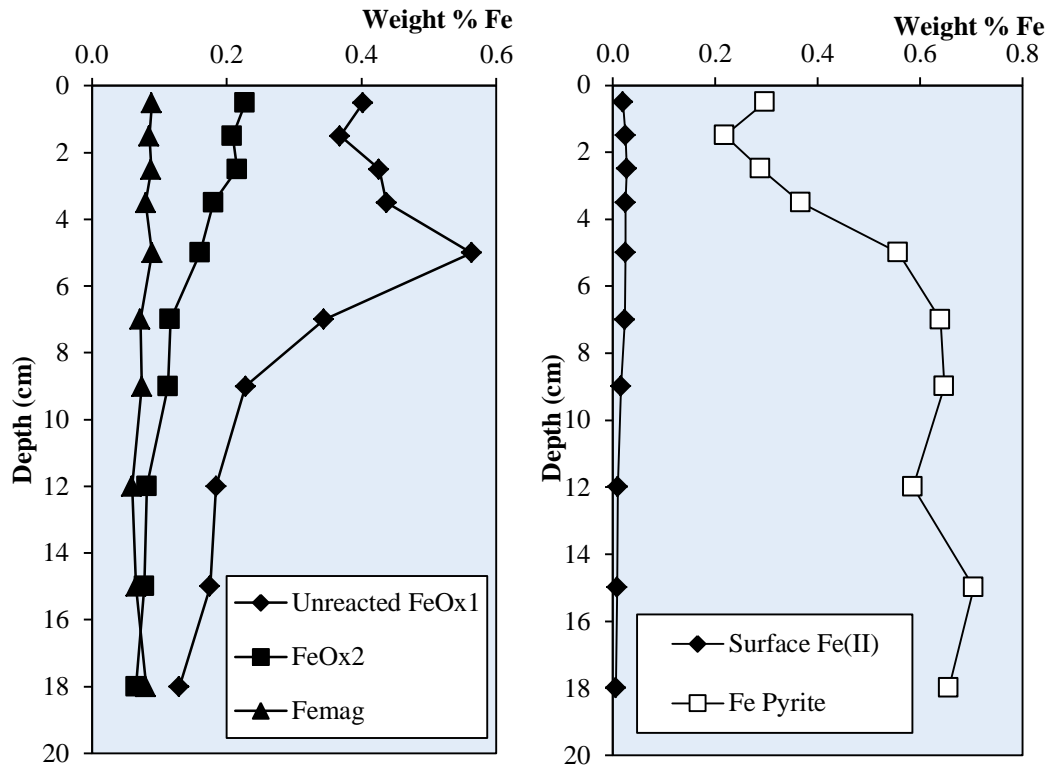


Figure 4.5(a +b): Concentration of Fe species (based on reactivity scheme classification) as a percentage of Fe within the total Aarhus Bay sediment sample.

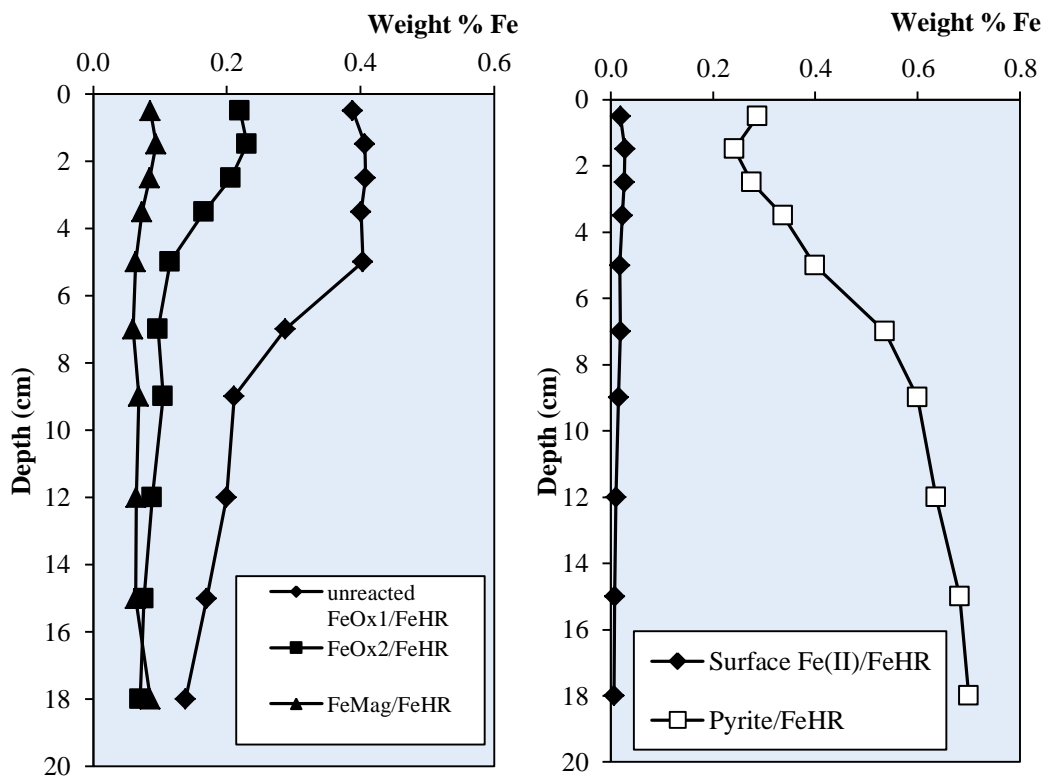


Figure 4.6(a +b): Aarhus Bay solid phase sediment characterisation, normalized to concentration of highly reactive Fe species (FeHR).

4.5.1.2 Umpqua River Shelf, N. Pacific Basin

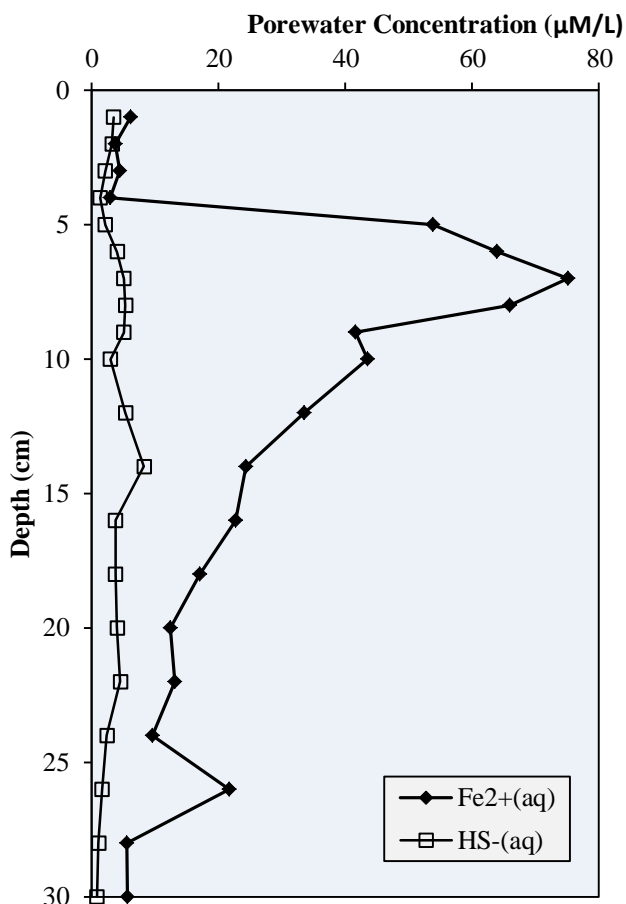


Figure 4.7: Pore water distribution of dissolved $\text{Fe}^{2+}(\text{aq})$ and $\text{HS}^-(\text{aq})$ in Umpqua River sediment sections.

The concentration of dissolved iron in pore waters extracted from the Umpqua River shelf sediment core, indicates that reductive dissolution of Fe minerals becomes a significant process at ~4 cm below the sediment-water interface, with only a low concentration of dissolved iron found in a reduced state in the upper section of the core (<5 μM , Figure 4.7). At this depth, a sharp increase in $\text{Fe}^{2+}(\text{aq})$ in pore waters is observed, demonstrating conditions for the dissolution of highly reactive Fe(III) oxide species to occur. Below this maximum, the concentration of $\text{Fe}^{2+}(\text{aq})$ decreases gradually throughout the core. In contrast to the Aarhus sediments, rates of $\text{Fe}^{2+}(\text{aq})$ generation are

sufficient to buffer dissolved sulfide to minimal levels throughout the core, although $\text{Fe}^{2+}_{(\text{aq})}$ concentrations decrease with depth as the most reactive Fe oxides are gradually consumed. In order to classify the raw data presented in Table 4.7 with regards to iron mineral reactivity (as defined in Raiswell *et al.*, 1998; Poulton and Raiswell, 2002), iron pools were categorized as highly reactive, poorly reactive or unreactive with respect to rates of reaction with dissolved sulfide (Table 4.8). Highlighted rows represent samples which were chosen for experimental purposes.

The concentrations of individual mineral phases are compared in Figure 4.8a and Figure 4.8b. Highly reactive mineral phase FeOx_1 (largely representing ferrihydrite) has been corrected for surface reduced Fe(II) within the sediment assemblage, resulting from previous diagenetic (i.e. organic) or biological reduction processes within the natural environment. This unreacted FeOx_1 is of a low concentration at depth, as a consequence of high quantities of surface reduced Fe(II) present on the mineral surface. Concentrations of FeOx_2 and Fe_{mag} are higher than unreacted FeOx_1 and appear relatively constant to 15 cm depth, implying that very little change in morphology, and hence reactive processes, have occurred with regard to these mineral pools over this depth interval (i.e. it is the FeOx_1 pool that has dominantly been reduced). Below 15 cm depth, a gradual decrease in FeOx_2 is observed as reduction of this less reactive pool starts to occur. Figure 4.8b represents an almost constant low concentration of surface reduced Fe(II) measured on the sediment surface (fluctuating ~ 0.2 wt %), compared to an more significant increase in pyrite formation with depth (0.05 – 0.25 wt %).

In Figure 4.9a, the total FeOx_1 pool is divided into unreacted FeOx_1 and total FeOx_1 , with the data plotted in terms of normalization to FeHR, to clearly show the relative proportions of the different Fe pools that together make up the FeHR fraction. FeOx_2

minerals dominate the highly reactive Fe fraction within the upper core section, but with a gradual decrease with depth after 8 cm. The percentage of magnetite which contributes to the total iron measurement is relatively constant (~20%), suggesting that this Fe pool is not reactive during early diagenesis at this site. The observed downcore increase in the proportion of FeHR which is present as pyrite (Figure 4.9b) matches the total reduction in the FeOx₁ (unreacted Fe(III) + surface-reduced Fe (II)) plus FeOx₂ pools with depth. The concentration of organic carbon varies from 1.5-1.8% wt., with the highest values tending to be at depth.

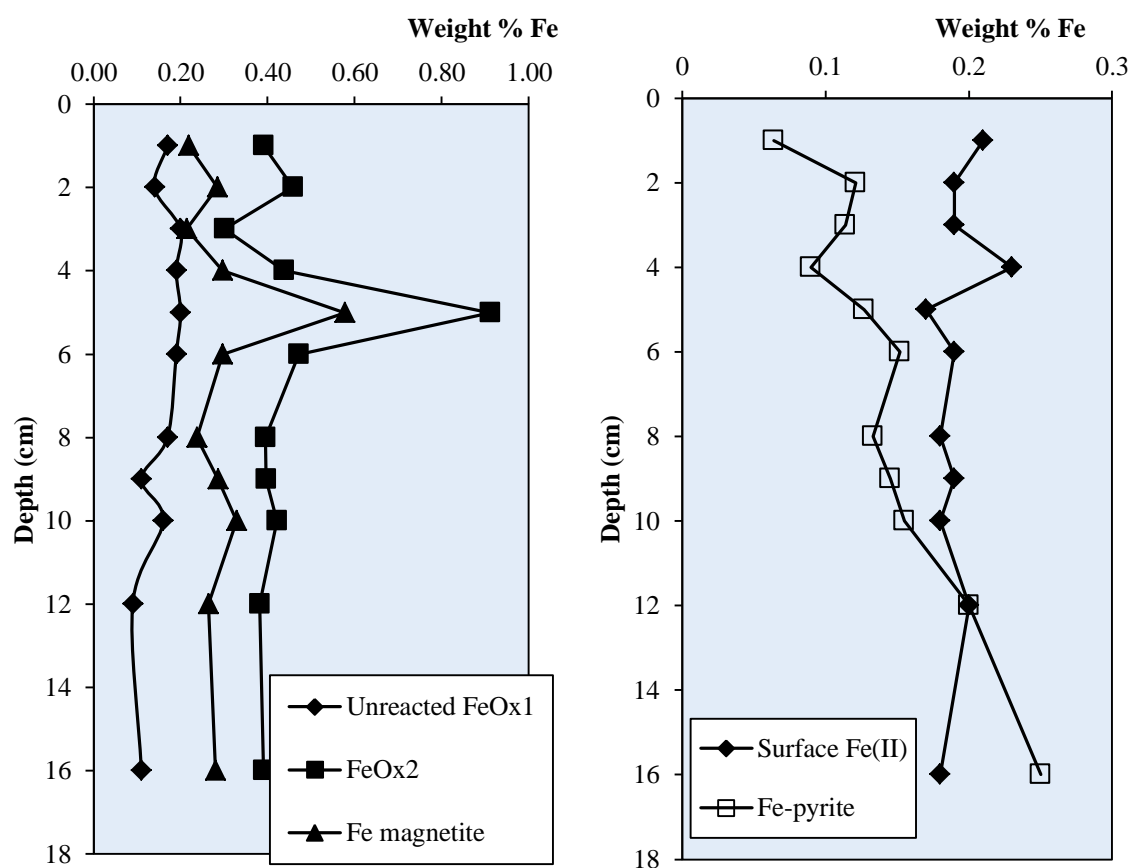


Figure 4.8: a) Comparison of Fe(III) species concentrations measured as a wt% of Fe in individual sediment samples and b) characterisation of Fe reactivity with respect to FeT describing overall mineralogy of Umpqua River sediments

Downcore decreases in unsulfidized reactive Fe minerals (III) are not as extreme at the Umpqua River site, relative to the Aarhus Bay site (c.f. Figures 4.6a and 4.9a). This allows an evaluation of potential differences in depth changes in sediment reactivity at the two contrasting sites. Samples were taken from depths of 0-1 cm, 3-4 cm, 8-9 cm, 10-12 cm and 14-16 cm to undergo sulfidation experiments, in order to represent the observed relatively minor mineralogical changes with depth at the Umpqua River site (Table 4.8).

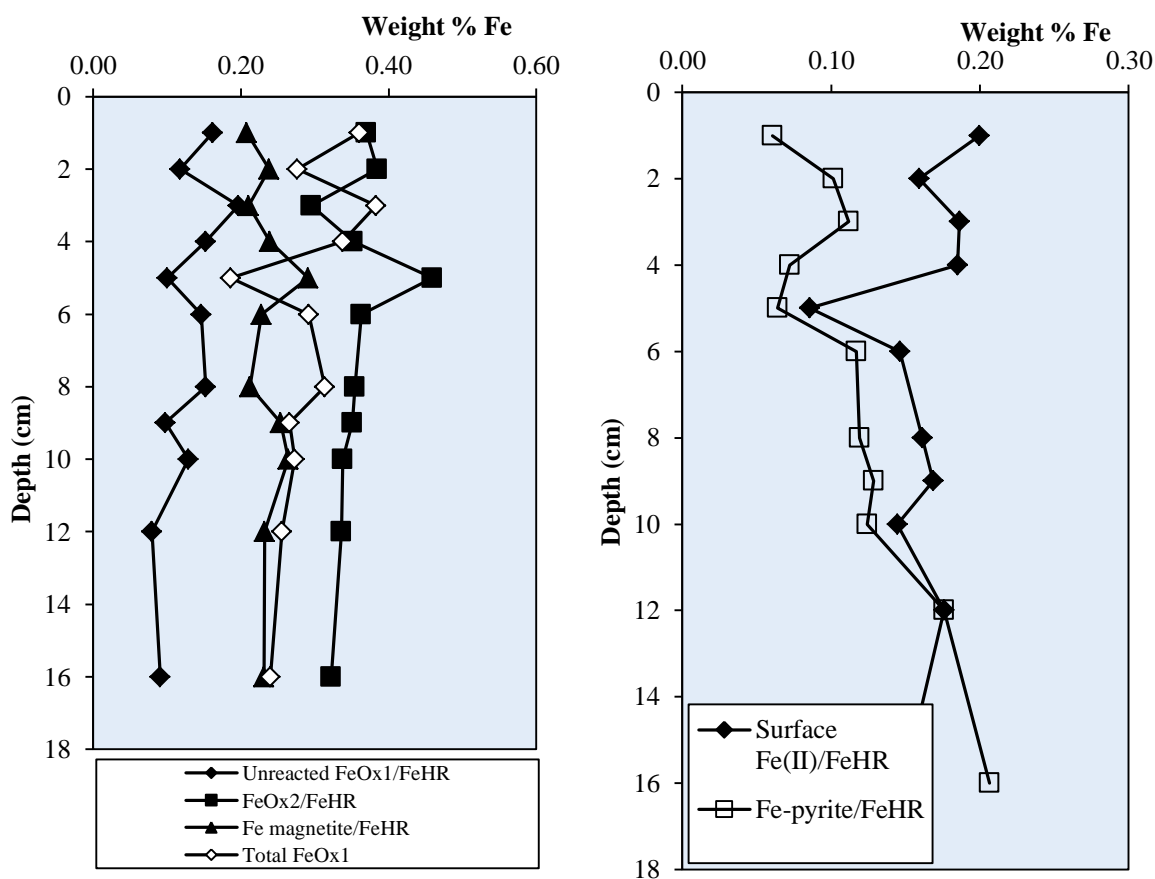


Figure 4.9: a) Speciation of highly reactive Fe Oxide minerals, with respect to FeHR (Canfield et al., 1992) b) Surface reduced Fe(II) present on mineral surfaces compared to pyrite formation within Umpqua River sediment (w.r.t. FeHR phases)

Table 4.7: Extractable Fe -speciation data for Umpqua River sediments

Sample Depth	0.5N HCl Fe(III)Ox₁ Wt (%)	0.5N HCl Fe(II) Wt(%)	Na.Dith FeOx₂ Wt(%)	Am.Oxa Fe_{mag} Wt(%)	Fe_{pyrite} Wt(%)	HCl Fe_{Prs} Wt(%)	FeT Wt(%)
0-1cm	0.17	0.21	0.39	0.22	0.06	0.05	4.68
1-2cm	0.14	0.19	0.46	0.28	0.12	0.05	4.50
2-3cm	0.20	0.19	0.30	0.21	0.11	0.04	4.54
3-4cm	0.19	0.23	0.44	0.30	0.09	0.05	4.45
4-5cm	0.20	0.17	0.91	0.58	0.13	0.10	4.60
5-6cm	0.19	0.19	0.47	0.30	0.15	0.06	4.59
7-8cm	0.17	0.18	0.40	0.24	0.13	0.04	4.54
8-9cm	0.11	0.19	0.40	0.29	0.15	0.04	4.51
9-10cm	0.16	0.18	0.42	0.33	0.16	0.05	4.59
10-12cm	0.09	0.2	0.38	0.26	0.20	0.05	4.59
14-16cm	0.11	0.18	0.39	0.28	0.25	0.06	4.45

Table 4.8: Characterisation of Umpqua river sediment in terms of reactive Fe species.

Sample Depth	Fe HR	Fe(II) /FeHR	FeOx₁ /FeHR	FeOx₂ /FeHR	Fe_{mag} /FeHR	Pyrite /FeHR	Fe(II) /FeT	FeOx₁ /FeT	FeOx₂ /FeT	Fe_{mag} /FeT	FeHR /FeT
0-1cm	1.05	0.20	0.16	0.37	0.21	0.06	0.04	0.04	0.08	0.05	0.22
1-2cm	1.19	0.16	0.12	0.38	0.24	0.10	0.04	0.03	0.10	0.06	0.27
2-3cm	1.02	0.19	0.20	0.30	0.21	0.11	0.04	0.04	0.07	0.05	0.22
3-4cm	1.24	0.18	0.15	0.35	0.24	0.07	0.05	0.04	0.10	0.07	0.28
4-5cm	1.99	0.09	0.10	0.46	0.29	0.06	0.04	0.04	0.20	0.13	0.43
5-6cm	1.30	0.15	0.15	0.36	0.23	0.12	0.04	0.04	0.10	0.06	0.28
7-8cm	1.12	0.16	0.15	0.35	0.21	0.12	0.04	0.04	0.09	0.05	0.25
8-9cm	1.13	0.17	0.10	0.35	0.25	0.13	0.04	0.02	0.09	0.06	0.25
9-10cm	1.25	0.14	0.13	0.34	0.26	0.12	0.04	0.03	0.09	0.07	0.27
10-12cm	1.14	0.18	0.08	0.34	0.23	0.18	0.04	0.02	0.08	0.06	0.25
14-16cm	1.21	0.15	0.09	0.32	0.23	0.21	0.04	0.02	0.09	0.06	0.27

4.5.2. Experimental sulfidation of iron oxide mineral assemblages

4.5.2.1 Synthetic Fe(III) oxide mineral

Speciation data for iron sulfidation experiments for a variety of synthetic iron oxide minerals are shown in Figure 4.10. During experiments with goethite, hematite, and for the experiment with the lowest concentration of ferrihydrite, dissolved sulfide was maintained at a near constant level throughout the course of each experiment. During the reductive dissolution of ferrihydrite at higher concentrations, the rapid nature of the initial reaction maintained dissolved sulfide at a low level, but sulfide subsequently began to slowly rise as the reaction progressed since H₂S gas was continuously purged through the reaction vessel as the reaction progressed (i.e. as the rate of sulfide removal decreased with time).

Thus, initial sulfide concentrations (Table 4.4) were estimated by regression analysis of the dissolved sulfide data for all experiments. A linear relationship was established between dissolved sulfide concentrations sampled over $t = 1-10$ mins, and the line extrapolated back to the y-axis ($t = 0$ mins), representing the true initial sulfide concentration prior to addition of synthetic iron or sediment sample. The relatively minor rise in dissolved sulfide observed for experiments performed at higher concentrations of ferrihydrite (Figure 4.10) does not appreciably affect any subsequent determination of reaction rates, since much of the reaction occurs rapidly, prior to a significant increase in dissolved sulfide. The plots in Figure 4.10 show similar patterns of Fe and S speciation to those reported in Poulton (2003) and Poulton *et al.*, (2004) at pH 6.5-6.8. As experiments were performed at near neutral pH, very little dissolved iron was released from the mineral surface, which is reflected in all plots of Figure 4.10, which instead show an increase in surface reduced Fe(II) instead. During the reductive

dissolution of all minerals examined, any $\text{Fe(II)}_{\text{aq}}$ that was released into solution, mostly reacted rapidly to form FeS .

During the sulfidation of natural marine sediments, it was not possible to determine solid phase FeS in natural samples due to an unknown interference (presumably by organic matter) when trying to measure total sulfide by spectrophotometer (i.e. dissolved plus FeS). However, it was possible to measure the total amount of Fe reduced during the experiments, since colour development during the Fe(II) spectrophotometric measurements was not affected. Thus, the concentrations of Fe(II) reduced were determined following a total Fe(II) measurement, as discussed in Section 3.2.1.1 and Section 3.4.1. Dissolved Fe(II) was then subtracted to give surface-reduced Fe(II) plus $\text{FeS}_{(\text{s})}$ (e.g. as observed in Figure 4.11 + Figure 4.12).

4.5.2.2 Sediment sulfidation experiments

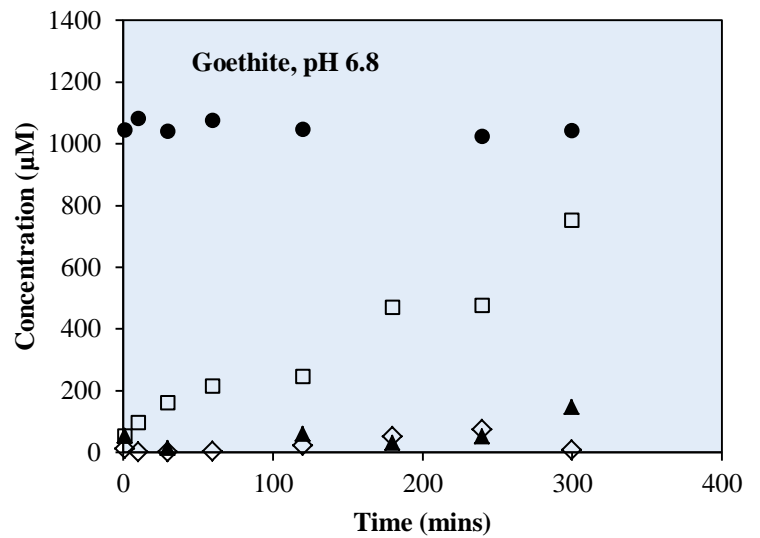
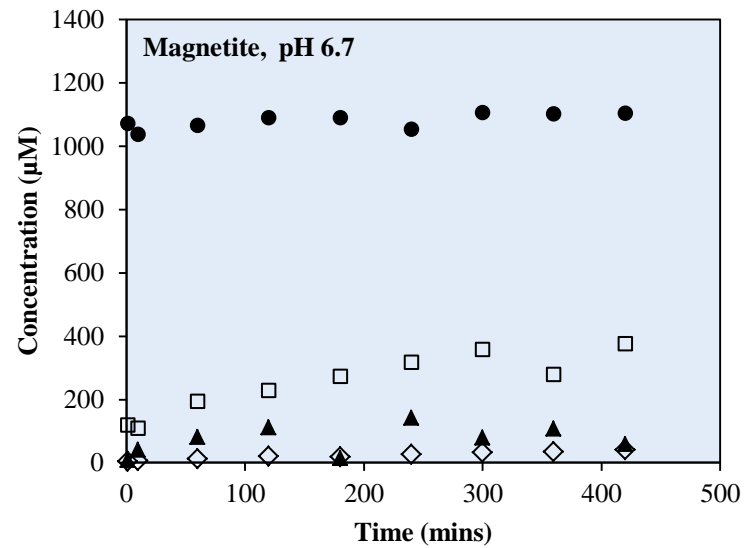
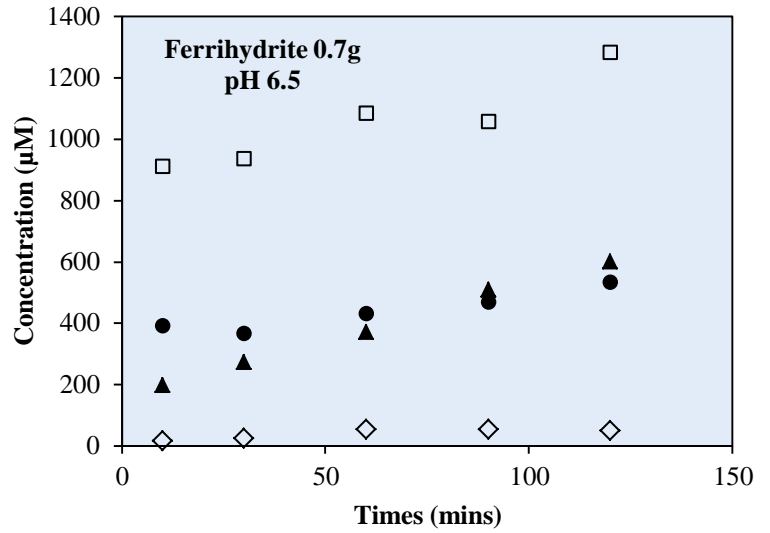
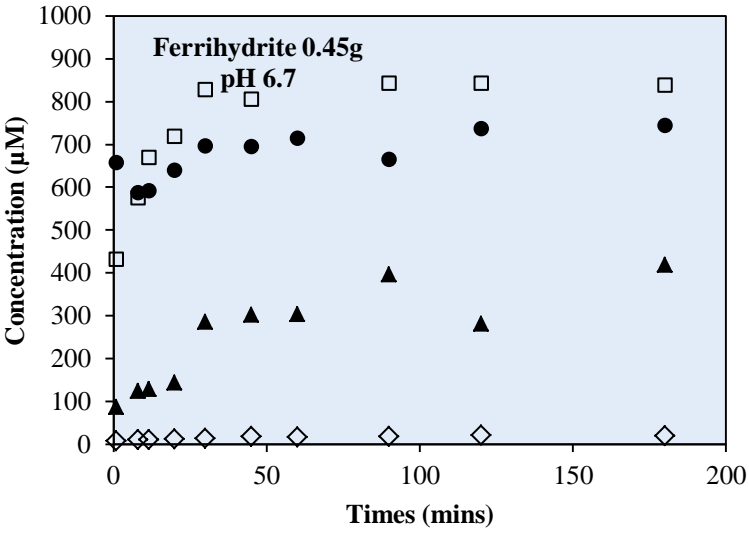
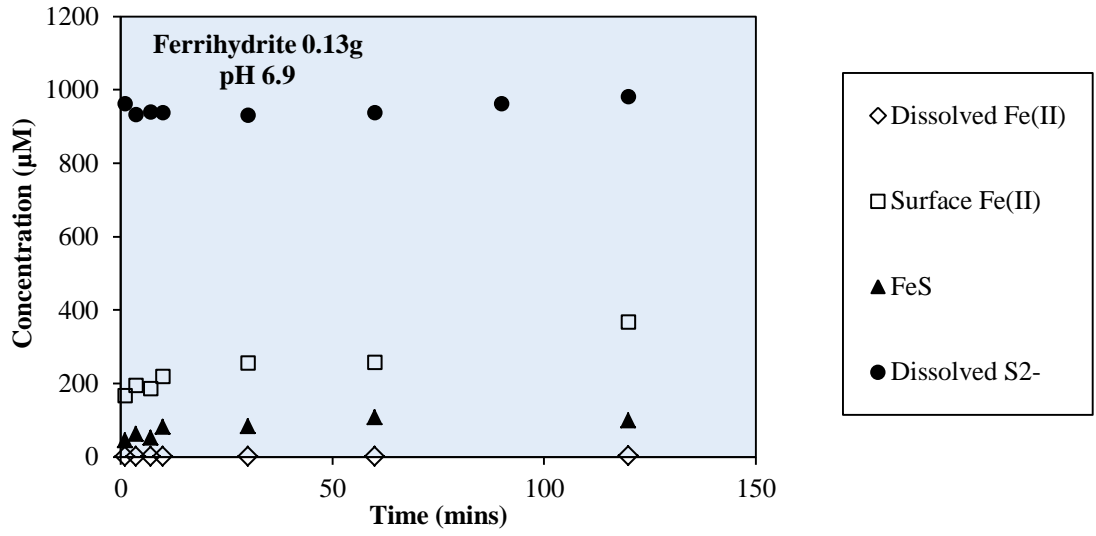
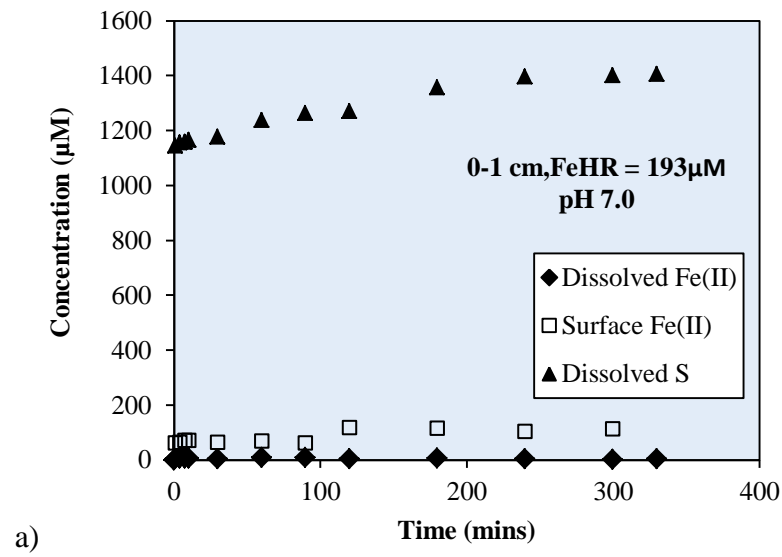


Figure 4.10: Speciation plots of Fe(III) oxide minerals.

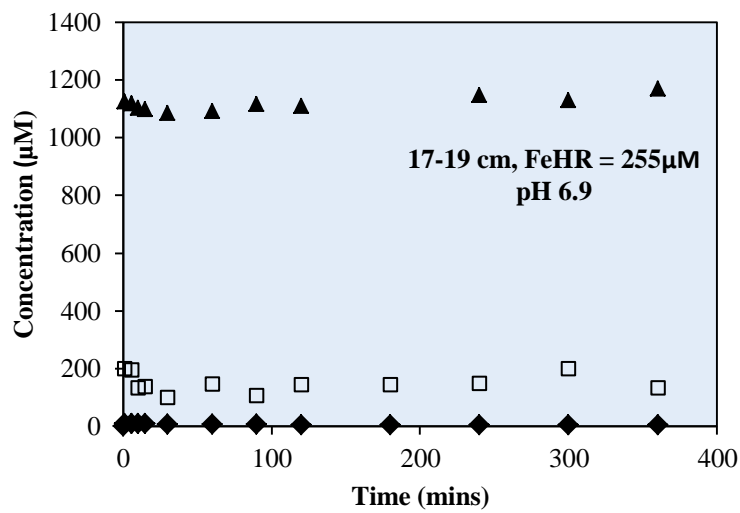
4.5.2.3 Aarhus Bay sediment core

Iron sulfidation experiments (Methodology Section 3.3.2) were performed on two core sections from Aarhus Bay, Denmark. The first sample from the upper core section (0-1 cm) contains high concentrations of unreduced FeOx_1 and an appreciable concentration of FeOx_2 , also present (Table 4.5). The second core sample (17-19 cm) has lower concentrations of Fe in both the pools of FeOx_1 and FeOx_2 (Table 4.5). In both cases, concentrations of surface reduced Fe(II) are low and similar in concentration (Figure 4.5b and also Figure 4.11) and thus possible release of this already reduced Fe to solution is unlikely to have a significant impact on the relative reactivities of each sample.

Resultant speciation profiles (Figure 4.11) indicate that the sample from 17-19 cm (Figure 4.11b) maintains a relatively constant dissolved sulfide concentration (average sulfide concentration = $1117 \pm 24 \mu\text{M}$, RSD = 2%) but with a minor increase over time. However, the more rapidly reacting sample at 0-1 cm (Figure 4.11a) shows a clear increase in dissolved sulfide (between 1000-1400 μM), which is above the sulfur concentration achieved during reaction preparation where the system was saturated with dissolved sulfide. As pH was consistently maintained throughout this experiment, this increase does not relate to an increased ability to accommodate more sulfide at lower pH. Instead, this increase likely relates to the formation of aqueous FeS complexes, which would be expected to be more significant as more $\text{Fe}^{2+}_{(\text{aq})}$ is released to solution (i.e. for the more reactive sediment split; see discussion below). In Figure 4.11 concentrations of dissolved $\text{Fe}^{2+}_{(\text{aq})}$ are minimal, consistent with the high concentrations of dissolved sulfide, which would maintain dissolved $\text{Fe}^{2+}_{(\text{aq})}$ at a low level via the formation of FeS. The concentration of surface-reduced Fe(II) is also relatively low, but shows a gradual increase over time.



a)



b)

Figure 4.11: Iron speciation and sulfide concentration profiles from iron sulfidation of Aarhus Bay sediments.

4.5.2.2 Umpqua River sediment core

Batch iron sulfidation experiments were performed under similar conditions (Table 4.4) to Aarhus Bay samples on individual sediment core sections, with samples taken for $\text{Fe(II)}_{\text{aq}}$, surface reduced Fe(II) plus $\text{FeS}_{(\text{s})}$ and dissolved S^{2-} . Figure 4.12 shows Fe and S

speciation profiles during the sulfidation of Umpqua River shelf sediments, for samples between 0-16 cm depth. These experiments indicate an increase in dissolved sulfide concentration, as with the most rapidly reacting Aarhus Bay sediment sample, the extent of which appears to be related to the initial concentration of FeHR. These profiles also measure a low concentration of $\text{Fe}^{2+}_{(\text{aq})}$ in solution, which is expected over the experimental pH range 7.4-7.6 (Table 4.4). Hence, the general speciation profile observed during the sulfidation of Fe(III) mineral assemblages compares well to those observed by Poulton (2003) and Poulton *et al.* (2004) for a variety of synthetic Fe oxide minerals under similar experimental conditions.

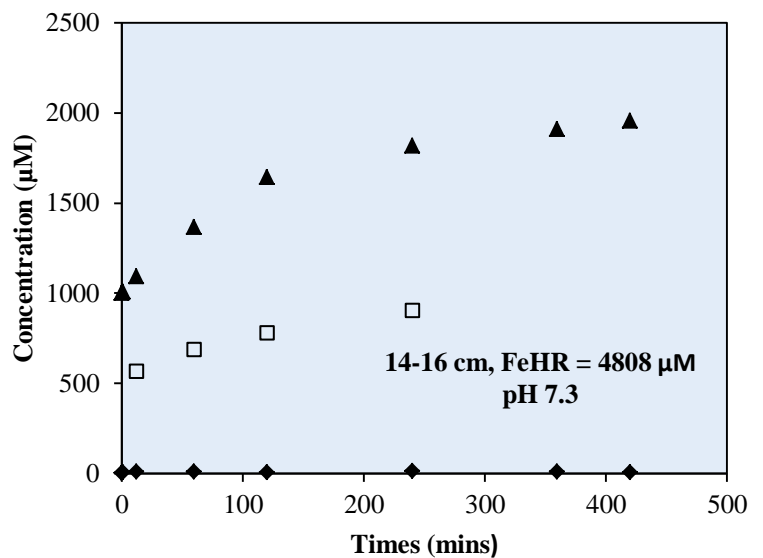
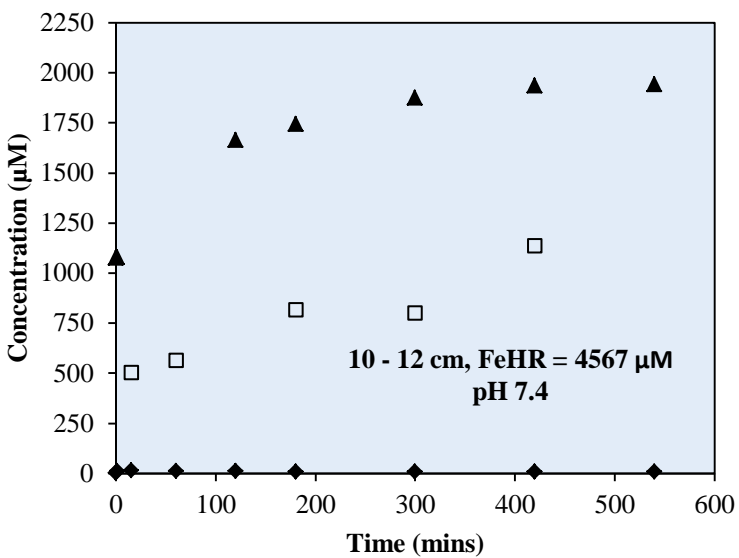
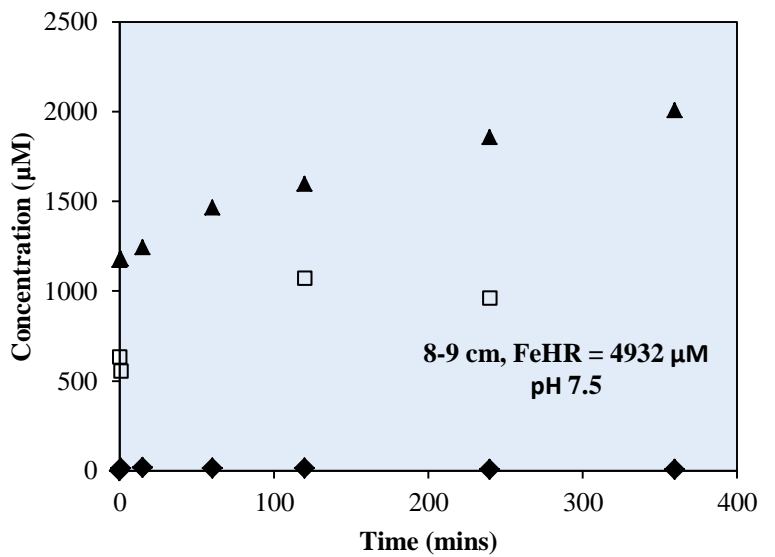
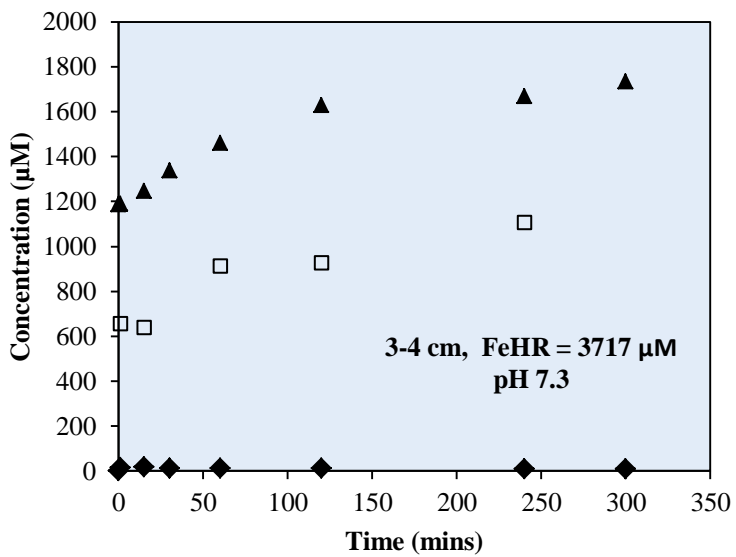
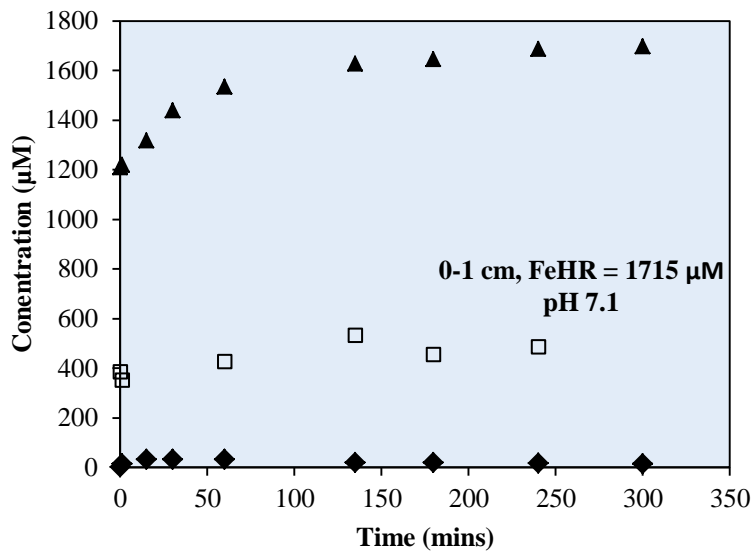


Figure 4.12: Iron speciation and sulfide concentration iron sulfidation experiments of Umpqua River shelf sediments.

4.6 DISCUSSION

4.6.1. Pore-water and sedimentary analysis

The gradual decrease in pore water $\text{Fe}^{2+}_{(\text{aq})}$ indicates that the rate of reductive dissolution slows throughout the both sediment core profiles, related to a change in Fe(III) oxide morphology from the most highly reactive, poorly crystalline ferrihydrite minerals found in near surface sediments (FeOx_1), to more crystalline, slower reacting Fe(III) species (Canfield *et al.*, 1992). Pyrite increases with depth in both cores (Figures 4.5 and 4.8) and is present in the shallowest samples, suggesting that sulfate reduction is occurring close to the sediment-water interface and throughout the deeper parts of the cores producing dissolved sulfide for reactions. For the Aarhus Bay core, concentrations of porewater $\text{Fe}^{2+}_{\text{aq}}$ buffers dissolved sulfide to very low levels over the upper 7 cm (Figure 4.4), and then dissolved sulfide increases with depth as a significant fraction of the most reactive Fe minerals (FeOx_1) have been reduced (Figure 4.5). In comparison to the Umpqua core dissolved sulfide concentrations which are buffered $< 10\mu\text{M HS}^-$ throughout (Figure 4.7), the zone of Fe-rich porewaters extracted from Aarhus bay sediments extends much deeper. Pyrite contents are also lower in the Umpqua core (c.f. Figures 4.5b and 4.8b), suggesting overall that reduction of Fe oxides by sulfide is a significant process within the Aarhus Bay core; whereas dissimilatory Fe oxide reduction, or reductive dissolution of Fe(III) oxides mediated by organic processes, may have been of greater significance for the Umpqua River core.

In terms of different reactive Fe pools, Figure 4.6 shows that the Aarhus Bay sediment changes significantly from being dominated by unreacted FeOx_1 type minerals (e.g. ferrihydrite; $< 40\%$) in the upper core section, to having similar concentrations of extractable FeOx_1 and FeOx_2 phases between 10 and 20 cm, which is reflected in the accumulation of dissolved sulfide in pore-waters over the same interval. The sediment

section from the Umpqua River shelf differs from Aarhus Bay as both the FeOx₁ and FeOx₂ pools show relatively constant profiles with depth (Figure 4.8 and Figure 4.9), with the FeOx₂ pool being significantly greater than the unreacted FeOx₁ pool. These differences in Fe oxide morphology between the two cores provide an ideal opportunity to compare the reactivity of the Fe oxides remaining in these two contrasting environments.

4.6.2. FeS formation

Figure 4.13 represents the rate of formation of FeS from differing initial Fe(III) starting concentrations for experiments with synthetic ferrihydrite. The trend observed is similar to that for total Fe(III) reduction, where the largest concentrations of Fe(III) (0.7g) produce solid FeS at a faster rate than 0.45 and 0.13g respectively, which is expected as FeS is a major component of the total Fe(III) reduction phase in synthetic mineral experiments (Figure 4.13).

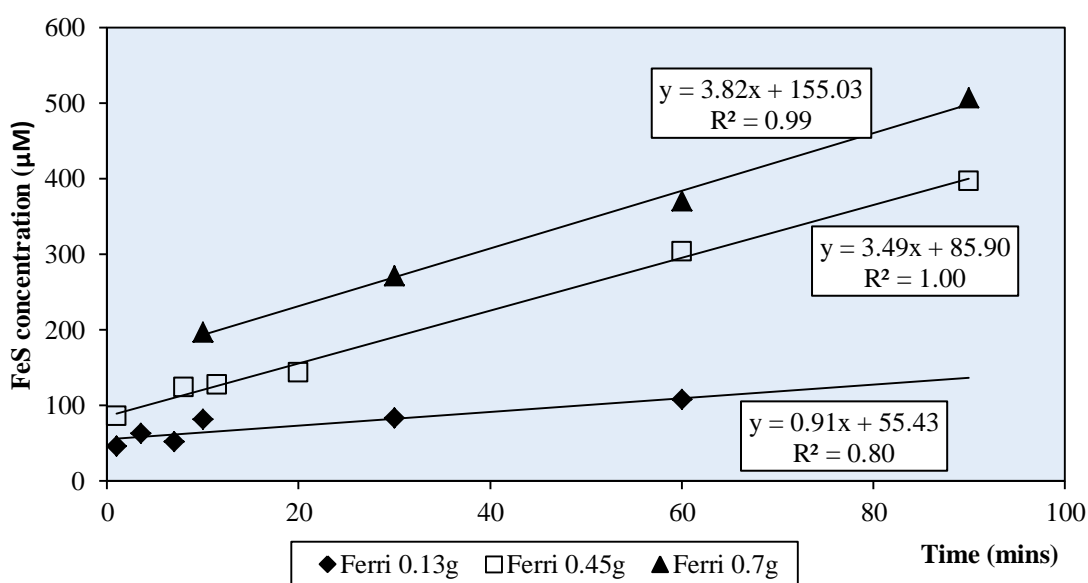


Figure 4.13: FeS formation under experimental conditions: Synthetic minerals

Poulton *et al.* (2004) suggest that solid phase FeS will be the overwhelming Fe sulfide species formed during experiments at circumneutral pH with synthetic Fe oxides, with aqueous FeS species (see Luther *et al.*, 1996) only being a very minor component due to extensive dissolution at experimental pH (Luther *et al.*, 1996). This is supported by high concentrations of solid FeS formed in the experiments with synthetic Fe oxides (Figure 4.13). However, these findings are in contrast to those obtained during sulfidation experiments performed with natural sediments. Here, it was not possible to measure solid phase FeS, and a marked increase in measured dissolved sulfide above the saturation point ($\sim 1000\mu\text{M}$) was measured as the experiments progressed (Figures 4.11 and 4.12). Figure 4.14 shows the increase in measured 'dissolved' sulfide above the initial concentration ($t = 0$ mins) during the course of the sulfidation experiments with Umpqua River sediment.

Additional sulfide is shown to increase with both increasing FeHR and depth within the Umpqua River core (Table 4.4), suggesting that the 'dissolved' sulfide is a product of the reductive dissolution reaction. A likely explanation for this increase in dissolved sulfide is that it represents the formation of aqueous FeS species. Hence, it appears that in contrast to experiments with pure Fe oxides, aqueous FeS species are a major product during sulfidation of natural sediments. It is speculated here that this may occur due to stabilization of the aqueous FeS, potentially as a result of the action of organic matter solubilised during the reaction, or the presence of organic sulfides reacting with OM (e.g. thiols; Vairavmurthy & Mopper, 1987) dissolved in porefluids, which may also be implicated in the fact that solid phase FeS was not measurable in the natural sediment experiments. The Fe present as the aqueous FeS was not detectable by the Ferrozine spectrophotometric technique used to determine dissolved $\text{Fe}^{2+}_{(\text{aq})}$, as indicated by the very low dissolved $\text{Fe}^{2+}_{(\text{aq})}$ measured in all experiments. However, the pH of the

reagents used to determine dissolved $\text{Fe}^{2+}_{(\text{aq})}$ was > 8 , and at this pH aqueous FeS complexes do not dissociate (Luther *et al.*, 1996). Assuming that solid phase FeS is not a major constituent of the natural sediment experiments, the determination of sulfide present as aqueous FeS during the experiments allows an estimation of the total amount of Fe(II) that has been solubilised during the reaction (i.e. Fe(II) as aqueous FeS plus dissolved $\text{Fe}^{2+}_{(\text{aq})}$). Thus, from these experiments, both the total rate of Fe reduction and the total rate of Fe(II) dissolution can be calculated.

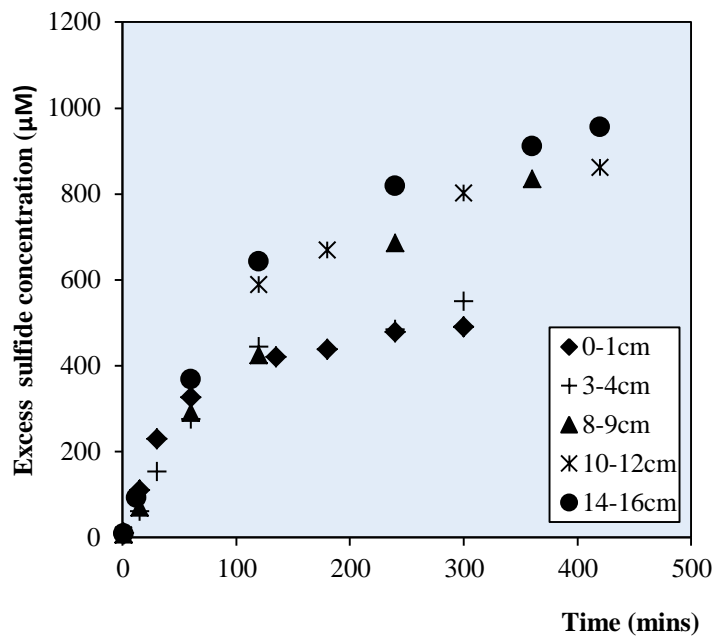


Figure 4.14: Additional sulfide measured above the average starting sulfide concentration for sulfidation experiments with Umpqua River sediment ($>1000\mu\text{M}$)

4.6.3. Determination of Fe mineral reactivity

4.6.3.1 The Rate Equation

In order to examine the rate of iron sulfidation, and hence dissolution of Fe oxide minerals occurring within natural systems, a rate equation is required which will characterise the influence of both dissolved sulfide and Fe(III) concentrations, whilst

reflecting the variable crystalline and mineralogical properties of an assemblage of Fe(III) oxides. Thus, for this study the reactive continuum approach of Postma (1993, Equation 4.3) is adopted (rather than initial rate theory described by Poulton, 2003) to ultimately characterise the rates at which Fe(III) reduction and Fe(II) dissolution occur for natural assemblages of Fe oxides, repeated below for reference.

$$J/M_0 = k' (m/M_0)^\gamma \quad \text{(Eq. 4.3)}$$

Where J defines the overall rate of dissolution (moles s⁻¹), M₀ is the initial mass of Fe(III) oxide, m/M₀ is the fraction of Fe(II) in solution in relation to initial mass of the undissolved mineral, k' is the rate constant (s⁻¹) and γ is the rate order related to changes in the crystalline structure and mineralogy over time, within a heterogeneous system.

Equation 4.3, however, relates to a reducing agent which exerts the same influence on the reaction regardless of concentration (i.e. for a reductant which is in excess; Postma, 1993). From the derivation of the empirical rate formula reported by Poulton (2003: Equation 4.2), it is clear that sulfidation reaction rates are highly dependent on the concentration of the reductant dissolved sulfide, which has been extensively determined as exerting a fractional (0.5) order influence on reaction rates (Pyzik & Sommer, 1981; Canfield & Berner, 1987; Poulton, 2003). To confirm this for the present experiments, the initial rates of Fe(II) dissolution (FeS plus dissolved Fe²⁺_(aq)) were determined for the three experiments performed with ferrihydrite. This gives Fe²⁺_(aq) dissolution rates of 1.2, 3.7 and 4.1 μM min⁻¹ for experiments with 0.13, 0.45 and 0.7 g of ferrihydrite, respectively (Table 4.9). However, the initial starting concentration of a particular Fe oxide is well known to exert a first order effect on reaction rates (Pyzik & Sommer,

1981; Dos Santos Afonso *et al.*, 1992; Peiffer *et al.*, 1992; Yao & Millero, 1996; Poulton, 2003; Poulton *et al.*, 2004), and so these reaction rates were normalized to a starting concentration of 0.7 g ferrihydrite, assuming a first order dependency on ferrihydrite concentration (Table 4.10). The logs of these normalized reaction rates are then plotted against a function of the logs of the initial sulfide concentrations in Figure 4.15. The slope of the regression through these data points confirm a 0.5 reaction order with respect to dissolved sulfide concentration, and although only three data points are presented, Figure 4.15 conforms to previously predicted models of fractional reaction orders described by Pyzik & Sommer (1981); Canfield & Berner (1987) and Poulton, (2003).

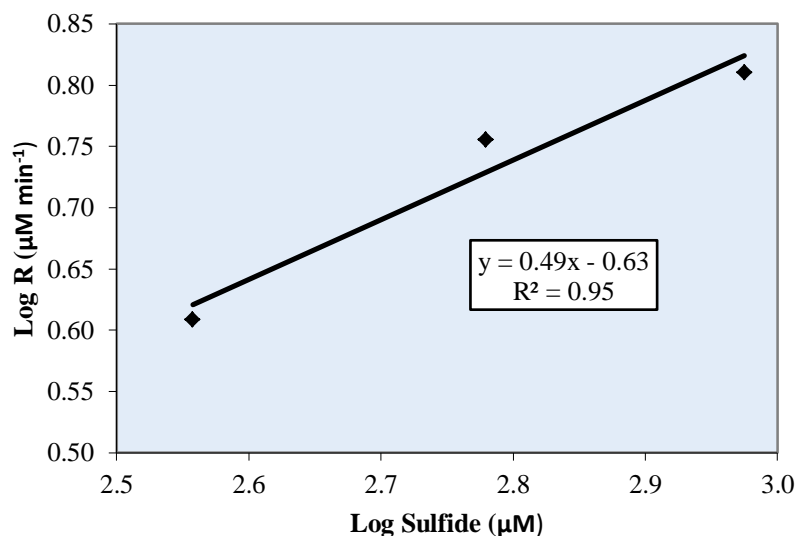


Figure 4.15: Determination of a fractional order (0.5) with respect to the initial sulfide concentration required for reductive dissolution

Therefore, in order to utilize Equation 4.3 for determining reaction kinetics, all subsequent rate determinations are corrected for dissolved sulfide concentration, relative to a 0.5 order dependency on dissolved sulfide. For this purpose, normalization of all

data was performed to calculate rates that would occur with a dissolved sulfide concentration of 1000 μM . This is a somewhat arbitrary figure, but was chosen as it is a typical porewater concentration during anoxic diagenesis of organic-rich sediments, and is also in the middle of the range over which the experiments were performed, and hence potential errors in calculated reaction rates introduced through this normalization procedure are kept to a minimum (e.g. Canfield *et al.*, 1992).

Table 4.9: Parameters derived for reaction order determination (with respect to initial sulfide concentration)

Ferrihydrite Sample	Rate Fe(II) diss	Rate corrected for initial Fe(III)	Log R	Initial S^{2-} (μM)	Log S^{2-}
Ferri 0.13	1.20	6.46	0.81	944	2.97
Ferri 0.45	3.66	5.69	0.76	602	2.78
Ferri 0.7	4.06	4.06	0.61	361	2.56

As well as investigating the influence of initial reductant concentration on the rate of Fe(III) reductive dissolution, the mineral properties of individual Fe(III) oxides must be examined with respect to surface area available for interaction with dissolved sulfide and structural constraints which effect the reactivity of minerals. Figure 4.16a and Figure 4.16b show plots of Fe(II)/FeHR which overlap when the data are normalized to an initial sulfide concentration of 1000 μM , irrespective of the initial amount of ferrihydrite added to the reaction vessel (0.13-0.7g), confirming a first order dependency on Fe(III) concentration (and hence surface area) for individual minerals. These plots also show that within this system, the rate of Fe(III) reduction occurs almost twice as fast as Fe(II) dissolution from the mineral surface, over the initial period of sulfidation, highlighting that release of reduced Fe(II) from the oxide surface (i.e. dissolution) is a slow process relative to reduction (see also Pyzik & Sommer, 1981;

Poulton, 2003; Poulton *et al.*, 2004). Figure 4.17 shows profiles of Fe(II)/FeHR for ferrihydrite, goethite and magnetite, which are known to react at different rates in the presence of dissolved sulfide. As described in Poulton *et al.*, 2004; ferrihydrite reacts significantly faster than goethite and magnetite.

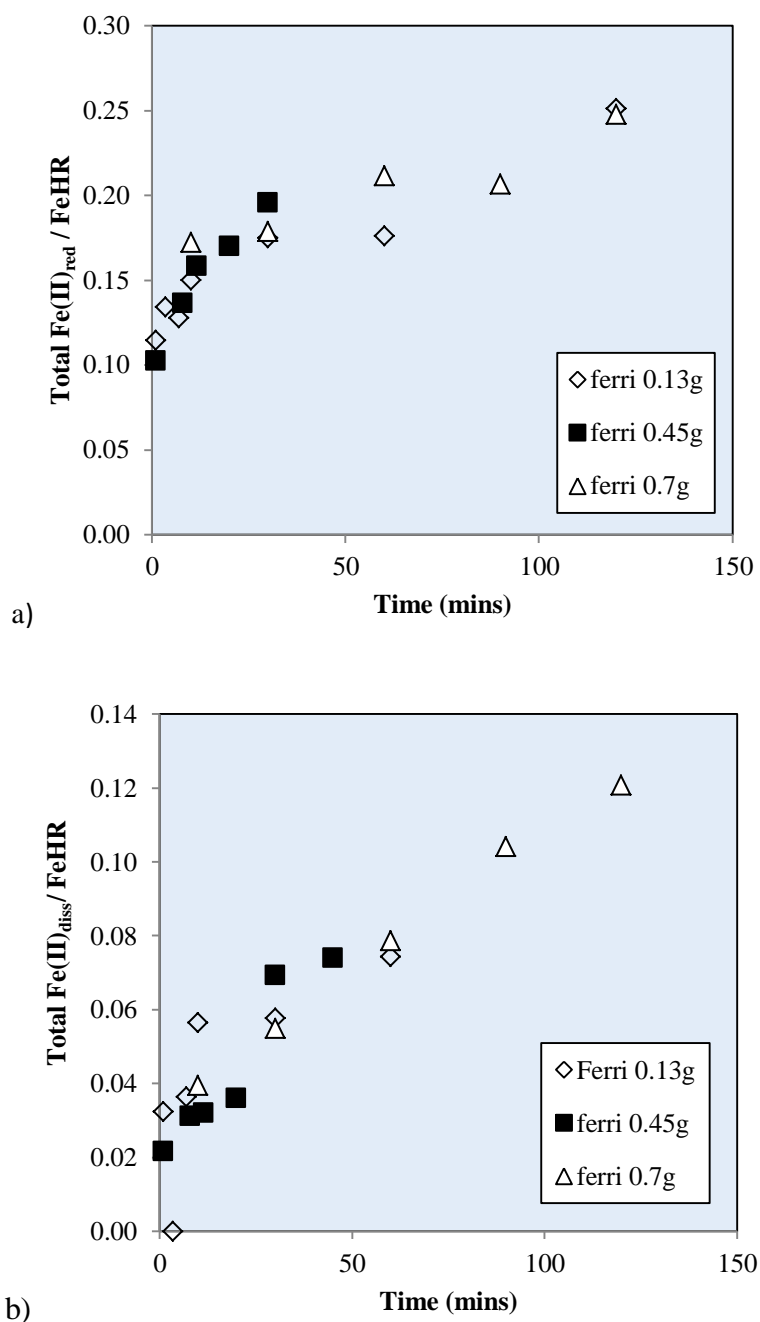
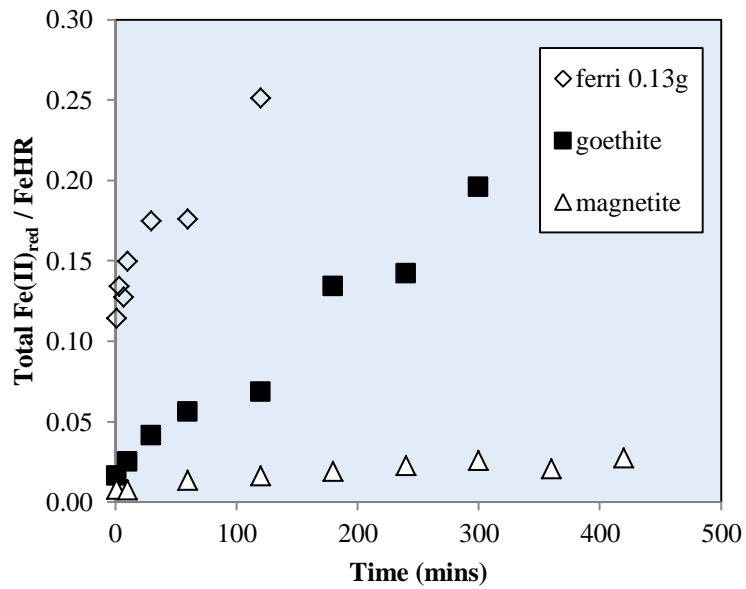
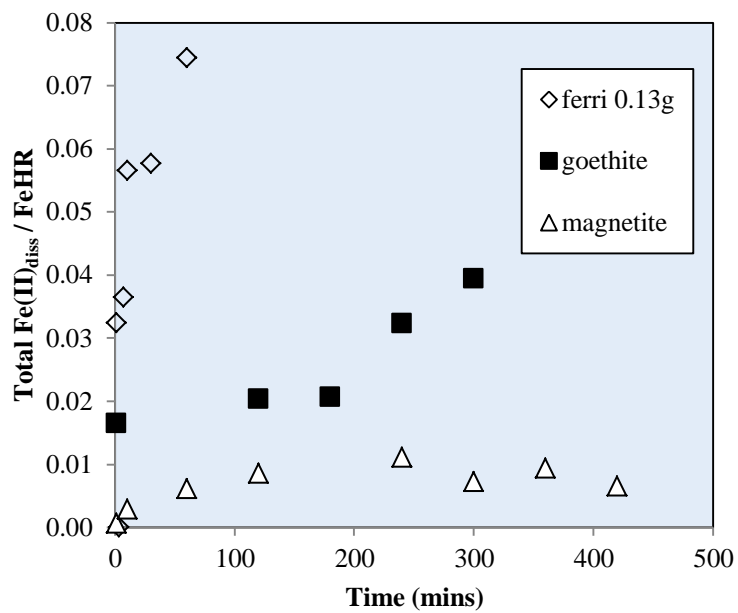


Figure 4.16 Profile of Fe a) reduction of Fe(III) to Fe(II) and b) subsequent dissolution of Fe(II)_{aq} for three synthetic ferrihydrite samples of different initial concentrations.



a)



b)

Figure 4.17: Profile of Fe(III) oxide a) reduction of Fe(III) to Fe(II) and b) subsequent dissolution of Fe(II)_{aq} of three synthetic Fe(III) oxide minerals varying in sulfide reactivity.

4.6.3.2 Determination of rate constant, K' and γ

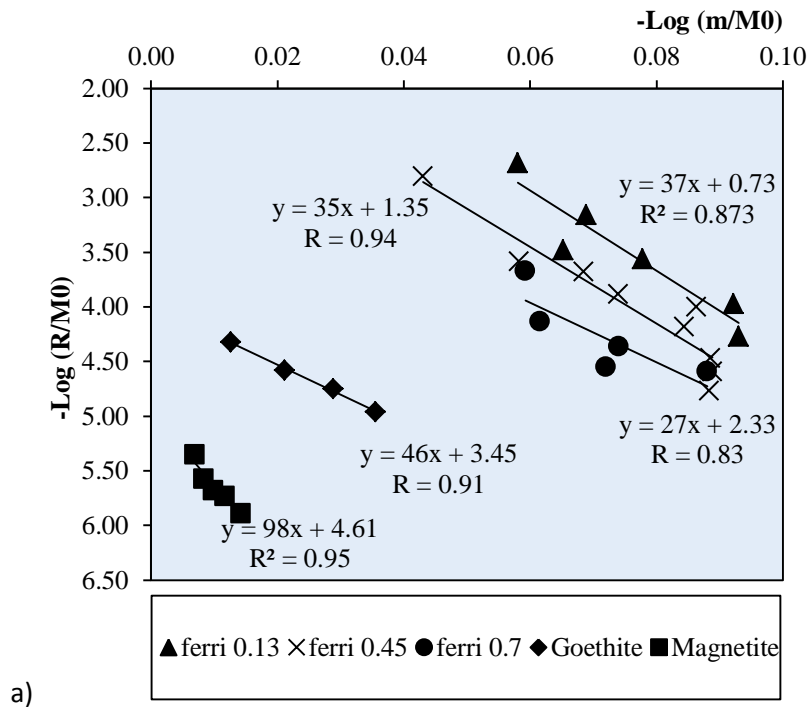
A comparable model in which the rate of sulfide mediated reductive dissolution between pure synthetic minerals and natural Fe(III) oxides within sediment assemblages, is by the evaluation of the rate constant (k') for each individual mineral. A evaluation of rate constants for synthetic minerals is compared with natural mineral assemblages to determine whether current reactivity schemes for synthetic minerals are in any way relevant in terms of the reactivity on natural mineral assemblages during diagenesis. The rate constant derived by Postma (1993) for Fe(III) oxide mineral reactivity within a sediment assemblage is related to an exponent (gamma, γ ; Equation 4.3) derived from measuring the rate of Fe reduction or dissolution of a mineral normalized to the initial Fe(III) concentration over the experimental timescale ($-\text{Log } m/M_0$; Postma, 1993) After correcting for differences in sulfide concentration within solution (to 1000 μM), the ratio of Fe(II) reduced or dissolved in relation to the initial concentration of iron in solution was plotted as $-\text{Log } R/M_0$ (an example of which is shown in Figure 4.18), allowing the determination of rate constant K' to be calculated from the negative log value of the slope of the regression line.

Synthetic Fe(III) oxide minerals

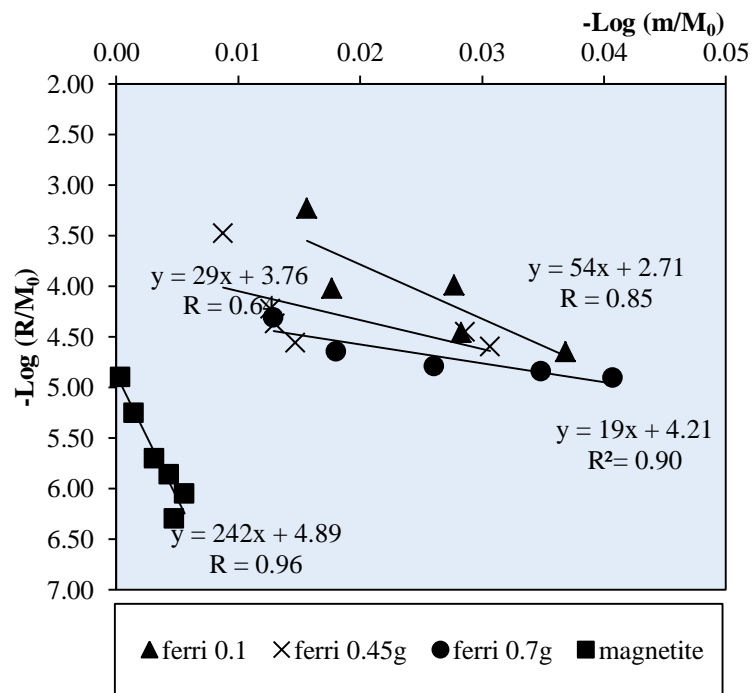
Table 4.10 details the rate equation parameters determined for sulfidation experiments with synthetic Fe(III) oxides. Data considered for goethite dissolution is not included in Table 4.10 as values were not considered robust under the current scheme of reactivity. In comparison with data reported by Postma (1993), Larsen & Postma, (2001) and Larsen *et al.*, (2006), the values of gamma (γ) determined in Figures 4.18a and 4.18b are significantly higher than those previously reported. In determining the reactivity of Fe(III) oxides with ascorbic acid, gamma values reported by Postma *et al.* range between 1 and 2.5 for pure for synthetic minerals, and < 5 for Fe oxides observed

within natural sediment assemblages (also see Table 4.3). Table 4.10 derives gamma values during Fe-sulfidation experiments of between 27 and 98 during reduction; and remarkably, 19 to 242 during dissolution. These values increase with decreasing reactivity for both reductive and dissolution processes, only decreasing when surface area availability increases. The marked difference in gamma values during the reaction of synthetic Fe(III) oxides with sulfide, and those reported in reaction with ascorbate, is in large due to the mechanism and surface processes which occur after the reduction of Fe(III) oxides with dissolved sulfide. Reactive Fe(III) surface sites are inhibited by the slow detachment of Fe(II) during dissolution at near-neutral pH values (Poulton, 2003); and also by the precipitation of FeS species on the mineral surface. Determination of the rate constant K' (observed in Figure 4.18a and 4.18b) indicates that in the reduction of Fe(III) to Fe(II) on a reactive mineral surface, k' values for ferrihydrite decrease with increasing Fe(III) concentration, and also with decreasing reactivity. K' values for the reduction of Fe(III) in pure synthetic experiments decrease 4 orders of magnitude, from 2×10^{-1} to 2.3×10^{-5} (s^{-1}), with decreasing reactivity, in the order ferrihydrite > goethite > magnetite. The rate constant k' associated with the dissolution of Fe(II) from the reactive surface of synthetic Fe(III) minerals indicates that values determined for ferrihydrite are similar for all concentrations (and hence, there is little influence on dissolution) with K values decreasing by two orders of magnitude with reactivity, between 2.1×10^{-3} to 1.2×10^{-5} k' . As expected, comparing reduction reactions with the process of Fe(II) dissolution shows rate constant k' values for dissolution are at least two orders of magnitude lower than for reduction, with respect to the fastest reacting minerals (Table 4.10) which describes a faster process occurring on the mineral surface as Fe sites adsorb sulfide, inducing a change in redox state (Fe(III)-Fe(II)).

Using Minitab 15 to analyse the significance of a correlation (or fit) of 2 variables, thought to incur a linear relationship, Table 4.11 predicts for synthetic experiments a good linear correlation between $-\text{Log}(R/M_0)$ vs. $-\text{Log}(m/M_0)$ will be observed; and during reduction processes, all data produced from ferrihydrite, goethite and magnetite experiments is considered significant (at 95% confidence level), and a good fit of linearity using both Levenes Test of correlation and simplified F testing of 2 variables. During dissolution processes however, statistically the data produced for ferrihydrite at higher surface areas (ferrihydrite 0.45g and 0.7g) are less likely to produce a statistically significant correlation as P values calculated with Levenes test are below the accepted level of confidence. This may be because when iron is released into solution from the mineral surface after reduction, it becomes readily available for further reactions (i.e. incorporation into FeS or oxidised) and therefore affects the concentrations of iron freely available in solution, especially from minerals with larger surface areas for reaction.



a)



b)

Figure 4.18: Derivation of rate constant K and gamma distribution (Postma, 1993) for synthetic Fe(III) minerals under experimental sulfidation during a) reductive processes
b) dissolution

Table 4.10: Derivation of rate constant K for individual synthetic Fe(III) oxides

Sample	Reduction		Dissolution	
	K' (s ⁻¹)	γ	K'(s ⁻¹)	γ
Ferrihydrite 0.13g	2x10 ⁻¹	37	2.1x10 ⁻³	54
Ferrihydrite 0.45g	6x10 ⁻²	35	2.7 x10 ⁻⁴	29
Ferrihydrite 0.7g	2x10 ⁻²	27	1.4x10 ⁻⁴	19
Goethite	3.3x10 ⁻⁴	46	nd	nd
Magnetite	2.3x10 ⁻⁵	98	1.2x10 ⁻⁵	242

Table 4.11: Collation of statistical data for synthetic mineral experiments: Comparison of linearity correlation F Test Vs Levenes Test

Figure	Name	Slope	R ² Excel	R ² Minitab	Calculated P value (F test)	Levenes Test of Correlation (P value)	Confidence (%)	Accept/Reject Null Hypothesis
4.18a	Ferri 0.13g	y= 37x + 0.73	0.87	0.92	0.000	0.016	98.4	A
	Ferri 0.45g	y= 35x + 1.35	0.88	0.88	0.000	0.030	97	A
	Ferri 0.7g	y=27x + 2.33	0.69	0.56	0.000	0.052	94.8	A
	Goethite	y=46x + 3.45	0.83	0.83	0.000	0.030	97	A
	Magnetite	y=98x + 4.61	0.95	0.92	0.000	0.046	95.4	A
4.18b	Ferri 0.13g	y= 54x + 2.71	0.72	0.64	0.000	0.047	95.3	A
	Ferri 0.45g	y= 29x + 3.76	0.41	0.21	0.000	0.099	90.1	R
	Ferri 0.7g	y = 19x + 4.21	0.90	0.81	0.000	0.112	88.8	R
	Magnetite	y = 242x+ 4.89	0.92	0.91	0.000	0.012	98.8	A

Aarhus Bay

Table 4.12 describes the values of K' and gamma derived from the iron sulfidation of two Aarhus Bay sediment sections. Figure 4.19a and 4.19b show γ values much closer to that reported by Postma *et al*, with values observed during reduction between 1-10, and 6-10 during dissolution.

The rate constants calculated in the reduction of Fe(III) decrease down core by three orders of magnitude (1.2×10^{-1} to $2.3 \times 10^{-4} \text{ s}^{-1}$ between 0-1 cm and 17–19 cm respectively). This decrease is reflective of the changing Fe-mineralogy already characterised within Figure 4.5a, which describes a change in Fe oxide predominance in each sample, from FeOx₁, highly reactive minerals within the uppermost core section to a consistent concentration of FeOx₁ and FeOx₂ sediments, heterogeneously mixed within the lower core section. This observation is reflected in the derived rate constant values of pure synthetic Fe(III) reactivity, which also propose ferrihydrite (an FeOx₁ mineral) to a significant contributor to the upper core section (comparing 1.2×10^{-1} 0-1 cm Aarhus Bay rate constant to ferrihydrite, 2×10^{-1}). Within the lower core section, a comparison of the rate constant associated with Fe(III) reduction agree that a value of 2.3×10^{-4} observed in Aarhus Bay sediments correlates to a value similar to highly crystalline, stable FeOx₂ goethite ($K'_{\text{red}} = 3.3 \times 10^{-4}$), which was also characterised during solid phase speciation of the initial sediment sample (Figure 4.5a). The derived rate constant associated with dissolution processes in Aarhus Bay sediments reflect a two order of magnitude change in rate with depth (1.1×10^{-3} to 3.6×10^{-5} ; Table 4.12). In comparison with the rate constants of synthetic mineral Fe(II) dissolution, these values support the suggestion that ferrihydrite dominates the upper core as an FeOx₁ mineral, with a slower reacting FeOx₂ phase constraining reaction kinetics within the lower core section.

Umpqua River

Table 4.12 also shows the calculated values of rate constant K' and gamma, associated with Fe(III) mineral reactivity in Umpqua River sediments. With respect to gamma values derived in Figures 4.20a and 4.20b, a value of 30 is reported for the uppermost sediment section (0-1 cm) before a sharp decline immediately with depth to give similar values of between 12-16 (ranging between 3-16cm depth). Gamma values reflecting dissolution processes in Umpqua River shelf sediments are consistent throughout the entire core section, between 7-10. The majority of these values are considered close to those which represent the reactivity of synthetic Fe(III) oxide kinetics, with very little influence from surface processes such as precipitated FeS.

Rate constant values associated with sediment from Umpqua River shelf (Table 4.12) observe a sharp decrease in K value with depth during Fe(III) reduction (3.1×10^{-1} to 1.8×10^{-4} between 0 - 16 cm respectively), becoming relatively constant in the lower section of the core (8-16 cm; Figure 4.20). The minimal decrease of k' values at depth indicate only a slight change in mineralogy down core (characterised in Figure 4.8a), characterised predominately by the slower reacting FeOx_2 minerals. These values are associated with decreasing rate constant values of ferrihydrite > goethite > magnetite measured in Figure 4.18. Rate constant values associated with dissolution slow marginally, between 1.6×10^{-4} and $4.1 \times 10^{-5} \text{ s}^{-1}$ over the entire core section. Values of this magnitude are associated with the dissolution of slower reacting minerals (goethite) (Table 4.12). The higher rate observed within the uppermost section (0-1 cm) may be due to the removal of highly abundant surface bound Fe(II) (measured in Figure 4.8b) which detaches from the mineral surface upon sulfidation.

Using Levenes Test to measure the significance of linear correlation of data in Figure 4.19 and Figure 4.20, it is clear that unlike for synthetic experiments (Table 4.11) which

generally expressed a good linear relationship between $-\text{Log}(R/M_0)$ Vs. $-\text{Log}(m/M_0)$ (at 95% confidence level), correlation of P values from these factors for natural sediments are less likely to be significant (Table 4.13). Whilst P values from F-test calculations appear to be highly significant in terms of correlating the difference in 2 variances, this would give a false result when recalculated using Levenes Test for correlation (Minitab15). Furthermore, the data associated with the Aarhus Bay sample set only contains $n=3$ samples over the depth 0-1cm. With caution this data must be interpreted, as this number of samples is too low to obtain a significant result with respect to determining linearity.

There are a number of possibilities why synthetic model experiments produce better correlations in terms of kinetic rate determinations. There are less likely to be influenced by competing surface reactions which would affect mineral assemblages in sediments greatly, i.e. the affect of organic acids and thiols on reduction rates. Further experimental work is required to increase the significance of natural sediment data to produce great correlations in linear relationships, by removing the processes which overwhelm reductive dissolution in sediments.

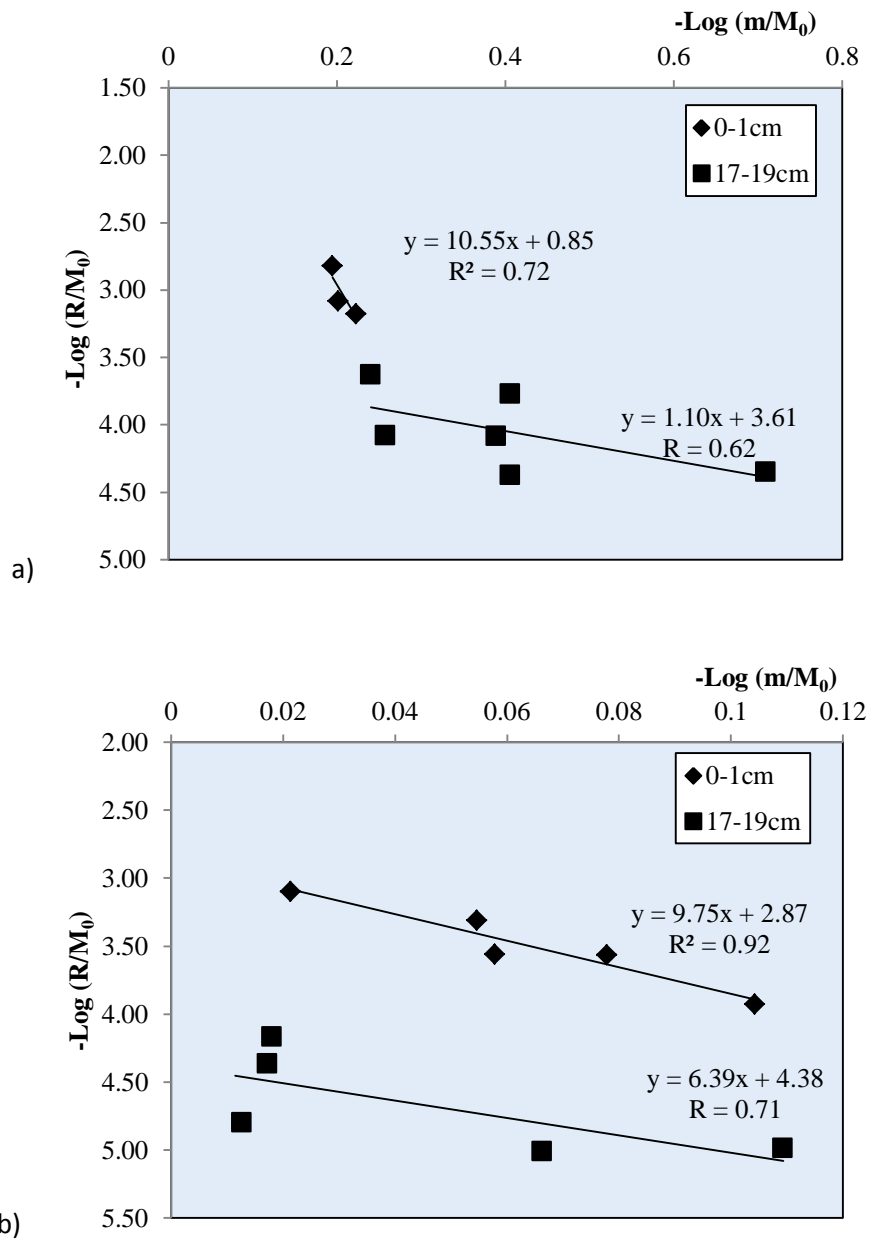
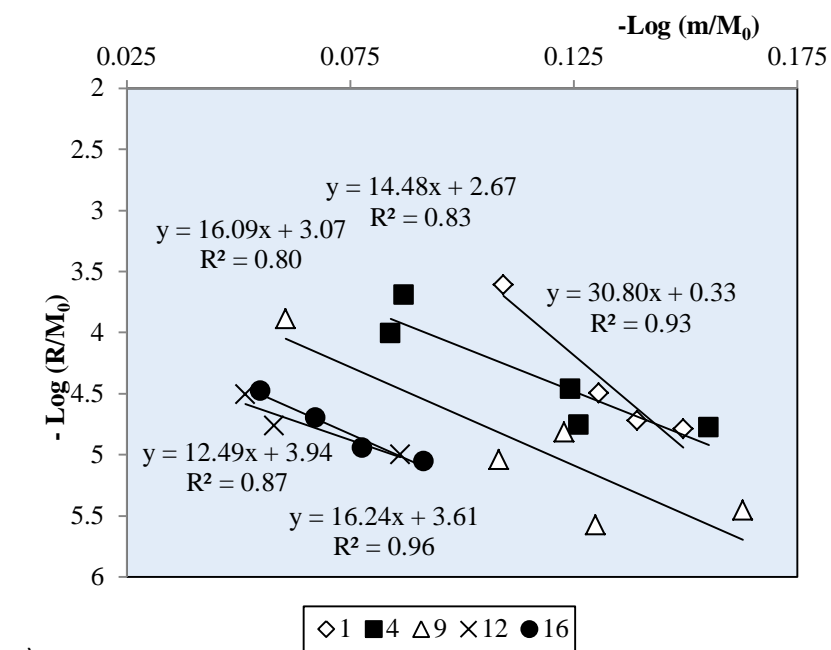
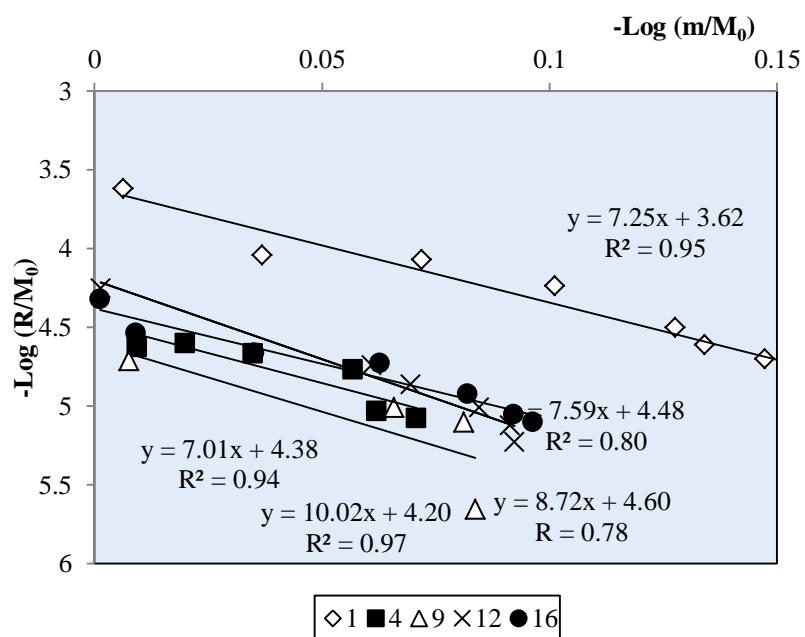


Figure 4.19: Derivation of rate constant K and gamma distribution (derived from Postma, 1993) for Aarhus Bay sediments under experimental sulfidation during a) reductive processes b) dissolution



a)



b)

Figure 4.20: Derivation of rate constant K and gamma distribution (Postma, 1993) for Umpqua River sediments under experimental sulfidation during a) reductive processes
b) dissolution

Table 4.12: Derivation of rate constant K for natural Fe sediment assemblages: Aarhus Bay (AB) and Umpqua River (UR) Shelf sediments

Sample	Reduction		Dissolution	
	K' (s ⁻¹)	γ	K'(s ⁻¹)	γ
AB 0-1 cm	1.2x10 ⁻¹	10.55	1.1x10 ⁻³	9.75
AB 17-19 cm	2.3x10 ⁻⁴	1.1	3.6x10 ⁻⁵	6.39
UR 0-1cm	3.1x10 ⁻¹	30.78	1.6x10 ⁻⁴	7.25
UR 3-4 cm	1.4x10 ⁻³	14.81	2.4x10 ⁻⁵	7.59
UR 8-9 cm	5.6x10 ⁻⁴	16.09	1.7x10 ⁻⁵	8.72
UR 10-12 cm	6.6x10 ⁻⁵	12.49	4.1x10 ⁻⁵	10.02
UR 14-16 cm	1.8x10 ⁻⁴	16.24	3.1x10 ⁻⁵	7.01

Table 4.13: Collation of statistical data for natural sediment experiments: Comparison of linearity correlation F Test Vs Levenes Test

Figure	Name	Slope	R ² Excel	R ² Minitab	Calculated P value (F test)	Levenes Test of Correlation (P value)	Confidence (%)	Accept/Reject Null Hypothesis
4.19a	0-1cm	y=10.55 + 0.85	0.72	0.71	0.000	0.232	76.8	R
	17-19cm	y=1.10x + 3.61	0.38	0.38	0.227	0.225	77.5	R
4.19b	0-1cm	y= 9.75x + 2.87	0.92	0.92	0.001	0.071	92.9	A
	17-19cm	y =4.56x+ 4.55	0.50	0.50	0.003	0.105	89.5	R
4.20a	0-1cm	y = 30.8 + 0.33	0.93	0.93	0.000	0.167	83.3	R
	3-4cm	y = 14.48+ 2.67	0.83	0.83	0.000	0.025	97.5	A
	8-9cm	y =16.09x + 3.07	0.80	0.81	0.000	0.054	94.6	A
	10-12cm	y= 12.49+ 3.94	0.87	0.87	0.011	0.138	86.2	R
	14-16cm	y = 16.24+ 3.61	0.96	0.96	0.001	0.011	98.9	A
4.20b	0-1cm	y= 7.25+ 3.62	0.95	0.95	0.000	0.001	99.9	A
	2-4cm	y= 7.59x+4.48	0.80	0.80	0.000	0.030	97	A
	8-9cm	y=8.72x+4.6	0.62	0.62	0.002	0.129	87.1	R
	10-12cm	y=10.02x+4.20	0.97	0.97	0.000	0.035	96.5	A
	14-16cm	y=7.01x+4.38	0.95	0.95	0.000	0.007	99.3	A

The approach taken within this study to derive rate constants for iron mineral sulfidation reactions appears to be valid, with respect to comparing rate constants derived from pure mineral sulfidation for a range of different reacting minerals, with sediment assemblages characterised for their highly reactive Fe content. In comparison to previously reported data of Postma *et al*, referred to in Table 4.3, these values are also of similar magnitudes with respect to the rate of Fe mineral reactivity by a reducing agent, especially when referring to slower reacting minerals such as goethite and magnetite. An important difference to these systems is the formation of metal sulfide species during iron-sulfur reactivity, which does not occur in the ascorbate reducing process, and imparts a significant influence on the dissolution of $\text{Fe}^{2+}_{(\text{aq})}$ from the mineral surface. The rate constant associated with ferrihydrite sulfidation is also 3 orders of magnitude faster than that occurring by ascorbate reaction, attributed to the rapid mechanism by which sulfide reacts on the highly reactive mineral surface.

Figures 4.21 and 4.22 summarize the initial K value of both pure mineral reactivity and that of natural sediments undergoing sulfidation, by comparing the logarithm of unreacted Fe ($-\log \text{ m/Mo}$) with the logarithmic value of initial rate, R, normalized to initial FeHR concentration.

Where the slope intercepts the y-axis, values of initial rate K are represented, with the slope of the line describing the exponential gamma of individual reactions, in relation to Equation 4.3. These plots show a good correlation between the initial rate constant of highly reactive minerals (ferrihydrite, goethite and magnetite) during both reduction and dissolution processes, with individual sediment cores which have been characterised during sequential extraction of highly reactive Fe phases, as a correlation between the the presence of similarly reacting minerals within each assemblage. Thus, one can be confident that the approach taken initially by Postma (1993) in describing the changing

reactivity within a Fe-rich sediment core (mediating ascorbic acid reactions) is akin to a reactive continuum process; and therefore can be used to describe similar processes of Fe morphology changes in sediments undergoing reductive dissolution mediated by dissolved sulfide.

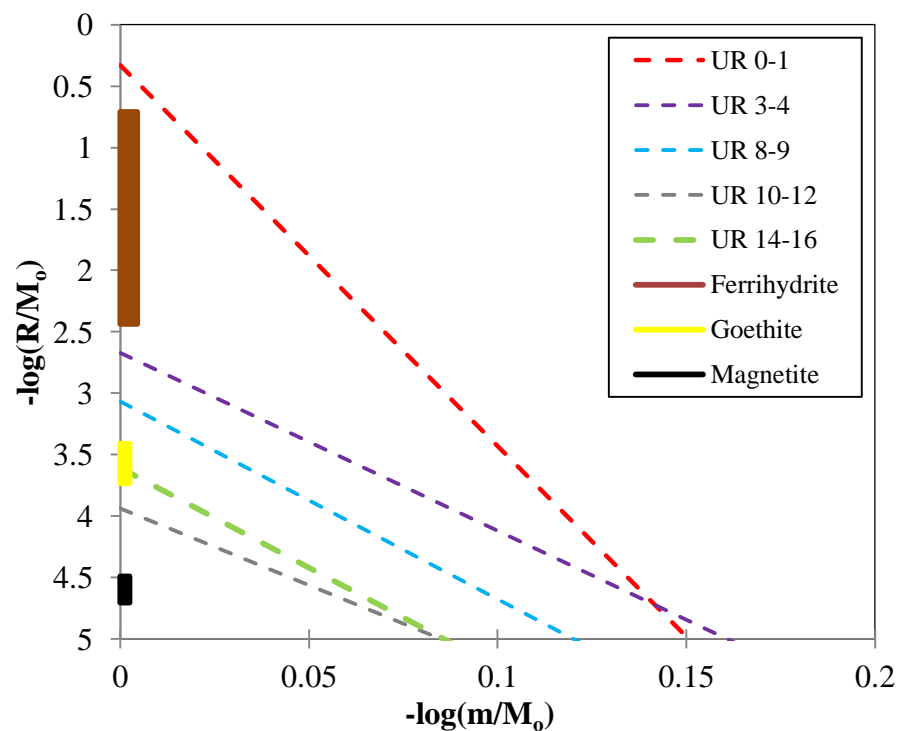
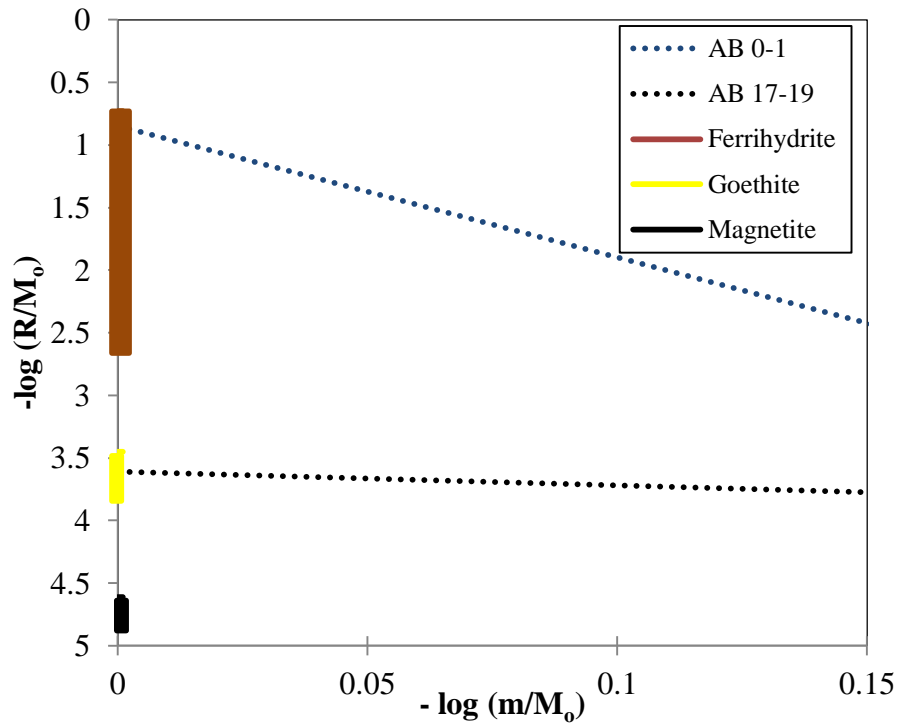


Figure 4.21 Comparison of synthetic Fe(III) oxide reduction rates with the reactivity of natural sediments from a) Aarhus Bay b) Umpqua River. Block colours on the y-axis represent initial K values of Ferrihydrite, Goethite and Magnetite, whilst coloured dashed lines indicate gamma distribution of natural sediments falling between synthetic K values. Here, values are presentative of containing predominantly ferrihydrite and goethite minerals, as $FeOx_1$ and $FeOx_2$ classes for both Aarhus Bay and Umpqua River sediments (during reduction of $FeIII$ to $FeII$).

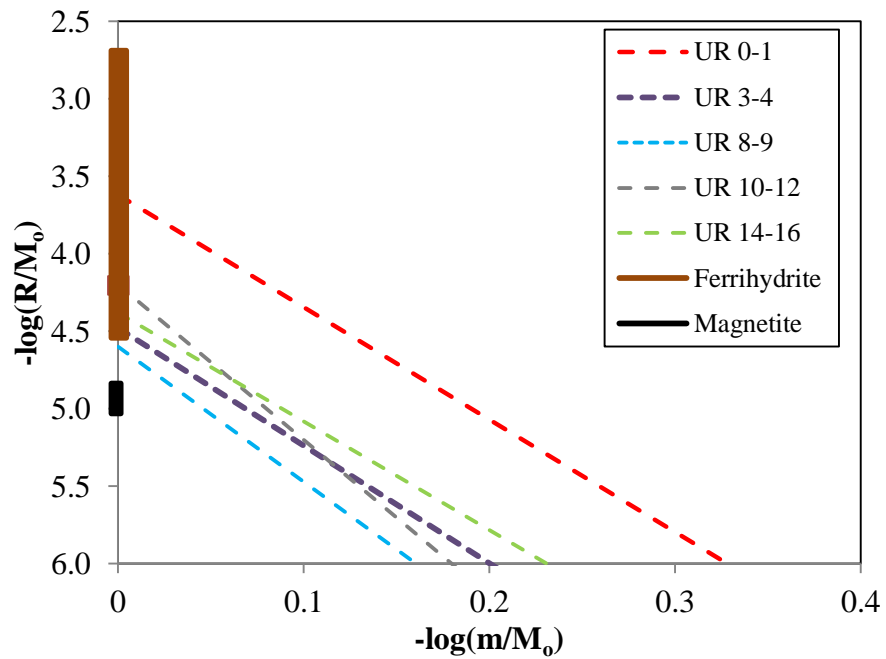
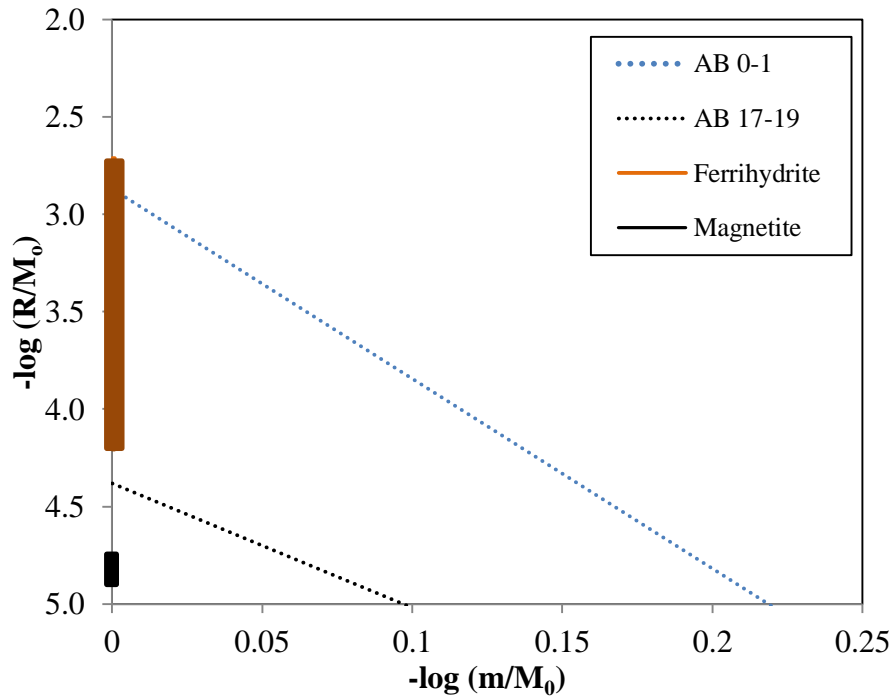


Figure 4.22 Comparison of synthetic Fe(III) oxide dissolution rates with the reactivity of natural sediments from a) Aarhus Bay b) Umpqua River. Block colours on the y-axis represent initial K values of synthetic ferrihydrite and magnetite, whilst coloured dashed lines indicate gamma distribution of natural sediments within the range of ferrihydrite as $FeOx_1$ for both Aarhus Bay and Umpqua River sediments (during dissolution of Fe(II) from the reactive mineral surface).

4.7 SUMMARY

- An experimental sulfidation approach was considered to determine the kinetics of Fe(III) mineral reductive dissolution within a sediment assemblage, and also provide a description of highly reactive Fe(III) minerals compared to that defined by a recognised sequential extraction procedure.
- A suite of synthetic Fe(III) minerals including ferrihydrite, goethite and magnetite; and two Fe-rich marine sediments (Umpqua River shelf and Aarhus Bay), were chosen to assess the rate at which sulfide mediated reductive dissolution occurs within pure synthetic minerals compared to heterogeneous sediment samples where the composition has been characterised in terms of highly reactive minerals classes (FeOx_1 , FeOx_2 , Fe_{mag}).
- Umpqua River Shelf sediments are defined as FeOx_2 (goethite/hematite) rich throughout the entire core, with little change in Fe mineralogy downcore. Aarhus Bay sediments in comparison change dramatically over the 20cm core section, from being dominated by poorly crystalline FeOx_1 phases (HFO, ferrihydrite, lepidocrocite) within the first 0-1 cm of the core (at surface), becoming highly ordered with depth, to observed abundant FeOx_2 -type minerals.
- Experimentally derived rates of Fe(III) reduction are at least two orders of magnitude faster than of $\text{Fe(II)}_{\text{aq}}$ dissolution during detachment from an Fe(III) mineral surface.
- Individual rate constant values derived from synthetic mineral experiments agree well with characterised sediment samples known to contain either predominantly FeOx_1 or FeOx_2 Fe mineral phases.
- Values of K inferred by Fe(III) reduction range between 2×10^{-1} and $2.3 \times 10^{-5} \text{ (s}^{-1}\text{)}$ for minerals decreasing in reactivity (ferrihydrite > goethite > magnetite), whilst

Fe(II)_{aq} dissolution occurs between 2.1×10^{-3} and 1.2×10^{-5} (s⁻¹). In comparison the range of K values expressed from the kinetics of sediment assemblage sulfidation covers a range between 1.2×10^{-1} and 6.6×10^{-5} (s⁻¹) during reductive processes, alongside rate constants of 1×10^{-3} and 4×10^{-5} (s⁻¹) during dissolution.

- Statistically, synthetic mineral experiments are of a good fit to a linear relationship (at 95% confidence level; Levenes test of correlation) with regards to determining constant and gamma values during both reductive and dissolution processes. However, experiments containing the sulfidation of Fe mineral assemblages often are rejected on the basis of significance of fit with linearity. This may be due to a number of natural interferences which affect the reductive dissolution process mentioned above, i.e. influence of organic acids and thiol species, the formation of aqueous FeS during reaction.
- Rates of iron reductive dissolution by sulfidation processes are similar to those determined using an ascorbic acid reductant, reported in Postma (1993) and Larsen *et al.*, (2006), validating this method of kinetic application, which may be used to infer the rate and composition of Fe (III) oxide minerals within natural sediments found within different depositional environments.

5. THE EXPERIMENTAL DISSOLUTION OF IRON CARBONATE MINERALS WITHIN SULFIDIC ENVIRONMENTS

5.1 INTRODUCTION

5.1.1. *Fe(II) carbonate minerals*

Whilst the sulfide mediated reductive dissolution of Fe(III) oxide minerals within sedimentary environments is the main focus overall within this thesis (due to the high abundance and reactivity of assemblages in near surface sediments; Pyzik & Sommer, 1981; Dos Santos Afonso & Stumm, 1992; Peiffer *et al.*, 1992; Poulton *et al.*, 2004), it is important to understand the reactivity of other Fe bearing minerals which commonly occur in diagenetic systems, and the role they play in contributing to the biogeochemical cycling of Fe under changing redox conditions. Carbonates such as siderite ($\text{Fe}^{\text{II}}\text{CO}_3$) are fine grained, authigenic minerals found within fresh water, lake and marine sedimentary systems, with their presence indicative of reduced aquatic conditions (Berner, 1971; Mozely & Wersin, 1992). Investigations of recent Fe carbonate formations (Pye, 1981; Postma, 1982; Pye, 1984; Pye *et al.*, 1990), have reported that siderite concretions commonly occur within Fe(II)-rich freshwater, lacustrine and brackish systems, with little evidence of extensive formation in modern marine settings (Pye, 1981).

The conditions under which siderite forms are well characterised from previous investigations, which indicate that iron carbonates require specific conditions for precipitation within an anoxic water column or in near surface sediments close to the sediment-water interface (Berner, 1971; Pye, 1981; Postma, 1982). At these boundaries, the rate of iron reduction is significantly higher compared to rate of bacterial sulfate

reduction, and organic matter is abundantly available (Froelich, 1979; Berner, 1981). From studies of siderite formation in modern environments, FeCO_3 occurs as a product of bacterial iron oxide reduction during organic matter respiration (Pye *et al.*, 1990; Mortimer & Coleman, 1997; Mortimer *et al.*, 1997). Where low rates of sulfate reduction dominate, iron mono-sulfides (FeS) may co-exist with Fe carbonate minerals (Pye *et al.*, 1990), however where sulfide concentrations are elevated due to an increase in the production of bacterially produced sulfide, pyrite is usually the dominant final stable reduced Fe mineral formed (Pye, 1981; Postma, 1982). During diagenesis of modern sediments, the formation of siderite will therefore occur either within reducing environments above the zone of sulfate reduction, or beneath the zone of BSR where high organic carbon contents persist (Curtis *et al.*, 1986; Pye *et al.*, 1990; Mozley & Wersin, 1992).

The geochemistry and structural composition of siderite concretions may also be indicative of the aqueous system from which they were formed (Raiswell & Fisher; 2000). For example, the composition of siderite in freshwater basins differs vastly from that in sediments from marine environments (Mozley, 1989). Cation substitutions occur readily at the mineral surface where Fe may be easily exchanged with Ca and Mg in oxygenated seawater to create an Fe-poor carbonate mineral (pure $\text{FeCO}_3 < 90\%$ Fe; Curtis *et al.*, 1986; Mozley, 1989; Pye, 1984; Mortimer & Coleman, 1997). This typical marine composition contrasts with commonly characterised freshwater siderite formed under reducing conditions (Mozley, 1989), where little cation substitution occurs, and Fe/Mn are the main substituted components of the outer layer lattice. Hence, the purity of siderite mineral composition acts as an indicator of the aquatic environment within which it was deposited.

5.1.2. The formation of siderite in ancient environments

As discussed, only small quantities of siderite are assumed to precipitate within modern, oceanic settings due to the present oxygenated state of marine systems (with the exception of discrete concretions which may be formed at depth, beneath the zone of sulfate reduction; Pye *et al.*, 1990). Instead siderite will form in environments where high concentrations of Fe(II) accumulate within low sulfate lakes or localised marsh-like or brackish waters. However, these settings contrast with many ancient anoxic marine environments.

Within the early rock record, banded iron formations (BIFs) were deposited during intermittent periods of the Archean and early Proterozoic eras (Holland, 1984; Klein & Beukes, 1989; Beukes *et al.*, 1990), with high concentrations of siderite commonly observed. These BIFs were precipitated under deep ocean conditions which were anoxic, and consequently Fe(II)-rich (*ferruginous*; Canfield & Thamdrup (2009)). The average measured oxidation state of these iron formations is Fe^{2.4+} (Klein & Beukes, 1992), but macro, meso and micro banding (on a scale of m, cm, and mm thickness) of iron carbonates, oxides and silicates are common (Veizer *et al.*, 1989; Kaufman *et al.*, 1990) corresponding to varying redox conditions. These ancient BIFs are observed in many parts of the modern world, including Western Australia (e.g. *Brockman Iron Formation, Hammersely*; Kaufman *et al.*, 1990), South Africa (e.g. *Kuruman Iron formation, Transvaal Supergroup*; Klein & Beukes, 1989; Veizer *et al.*, 1989; Beukes *et al.*, 1990; Johnson *et al.*, 2003), Northern America and Canada (e.g. *Gunflint and Biwabik Iron Formations; Superior Group*; Morey & Southwick, 1995; McSwiggen & Morey, 2008; Poulton *et al.*, 2010), suggesting widespread deposition over a substantial timescale from the early Archean up until about 1.8 billion years ago.

Siderite formation reactions¹

- a. $\text{Fe}^{2+} + \text{CO}_3^{2-} \rightarrow \text{FeCO}_3$
- b. $\text{Fe}^{2+} + \text{HCO}_3^- \rightarrow \text{FeCO}_3 + \text{H}^+$
- c. $\text{Fe}^{2+} + \text{OH}^- + \text{HCO}_3^- \rightarrow \text{FeCO}_3 + \text{H}_2\text{O}$
- d. $\text{Fe}^{2+} + \text{CO}_2 + \text{H}_2\text{O} \rightarrow \text{FeCO}_3 + 2\text{H}^+$

Respiration of organic carbon and iron reduction involved in siderite formation²:

- e. $4\text{FeOOH} + \text{CH}_2\text{O} + 3\text{H}_2\text{CO}_3 \rightarrow 4\text{FeCO}_3 + 6\text{H}_2\text{O}$
- f. $8\text{Fe}(\text{OH})_3 + \text{CH}_3\text{COO}^- \rightarrow 8\text{Fe}^{2+} + 2\text{HCO}_3^- + 15\text{OH}^- + 5\text{H}_2\text{O}$
- g. $2\text{Fe}_2\text{O}_3 + \text{CH}_2\text{O} + 3\text{H}_2\text{O} \rightarrow 4\text{Fe}^{2+} + \text{HCO}_3^- + 7\text{OH}^-$

Diagenetic reactions of siderite³:

- h. $\text{FeCO}_3 + \text{H}_2\text{O} \rightarrow \text{Fe}_3\text{O}_4 + 3\text{CO}_2 + \text{H}_2$
- i. $\text{FeCO}_3 + \text{Fe}_2\text{O}_3 \rightarrow \text{Fe}_3\text{O}_4 + \text{CO}_2$

Figure 5.1: Equations of siderite formation and reaction (Equations derived from :¹Curtis et al., (1986); Braun, (1991); Duckworth & Martin, (2004):²Johnson et al., (2003; 2008):³Curtis et al., (1986); Postma, (1982); Johnson et al., (2008))

From previous studies of these formations, it is hypothesised that within ancient marine environments, iron carbonates may have formed from either biological or abiological sources. Previously investigated pathways of siderite formation are compared in Figure 5.1. Primary siderite precipitation may have occurred following $\text{Fe}(\text{II})_{\text{aq}}$ release from hydrothermal sources (MOR's, seafloor weathering of basaltic formations derived from underwater volcanoes; Bekker *et al.*, 2009) into anoxic deep waters, allowing $\text{Fe}(\text{II})_{\text{aq}}$ concentrations to accumulate to sufficient saturation to promote precipitation of siderite via reaction with bacterially respired CO_2 ; in particular, following upwelling of deep water $\text{Fe}(\text{II})$ onto continental slopes beneath reasonably productive surface waters (Figure 5.2; Klein & Beukes, 1989; Beukes *et al.*, 1990).

After the evolution of oxygenic photosynthesis, at least 2.7 billion years ago (Ga) (Canfield, 2005), atmospheric oxygen was available within shallow surface waters (at the photic zone as eutrophic). At this time, oceanic Fe cycling was controlled by the upwelling of anoxic, ferruginous deep waters into oxic surface waters, where $\text{Fe(II)}_{\text{aq}}$ could be oxidised to form $\text{Fe(III)}_{\text{aq}}$ and precipitated to a variety of Fe(III) containing minerals (Figure 5.2; Klein & Beukes, 1989) including ferrihydrite, hematite and magnetite. These minerals could then be further reduced, during diagenesis at the redox boundary, via the mechanisms outlined in Figure 5.1 to produce Fe(II) that was subsequently available for siderite formation.

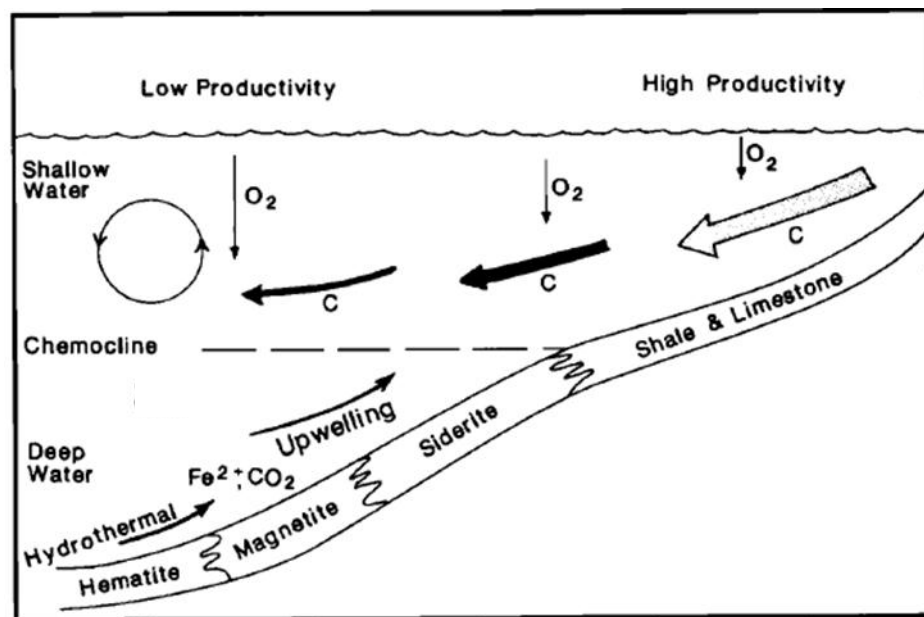


Figure 5.2: Model of iron formation deposition within a stratified ocean (Klein & Beukes, 1989).

Until recently, BIFs were considered the predominant rock type for significant concentrations of siderite to accumulate. With the development of new extraction

techniques which specifically evaluate siderite concentrations in ancient anoxic shales (Poulton & Canfield, 2005), it has become increasingly apparent that siderite formed an important component of fine-grained marine rocks throughout the Precambrian, from the Archean (Reinhard *et al.*, 2009; Kendall *et al.*, 2010), through the Paleoproterozoic (Poulton *et al.*, 2004; 2010), to the late Neoproterozoic (Canfield *et al.*, 2008; Johnston *et al.*, 2010). High concentrations of siderite in marine shales during this period were promoted by low marine sulfate concentrations (Habicht *et al.*, 2002; Canfield, 2005), which created conditions favourable for freshly precipitated Fe (oxyhydr)oxide reduction compared to sulfate reduction during diagenesis. It remains to be seen whether Phanerozoic anoxic events also produced significant concentrations of siderite, with recent data (Maerz *et al.*, 2008) suggesting that this may have been the case, caused by rapid redox cycling between euxinic and ferruginous conditions.

5.2 RESEARCH AIMS

The above discussion highlights siderite as an important component of marine sediments throughout significant periods of Earth history. Studies utilizing Fe speciation have assumed that Fe carbonates are highly reactive towards dissolved sulfide during diagenesis, and hence have classed this mineral as part of the highly reactive Fe pool. This has major implications for the reconstruction of paleodepositional redox conditions, but to date, no study has evaluated the kinetics of this reaction to determine the reactivity of siderite. Thus the purpose of this chapter is to investigate the rate and mechanism of Fe(II) carbonate dissolution within sulfidic environments via iron sulfidation experiments using synthetic FeCO₃ minerals, similar to those performed for Fe(III) oxide reductive dissolution.

The main objectives of this chapter are to:

- 1) Define a reaction mechanism for Fe(II) carbonate dissolution mediated by dissolved sulfide.
- 2) Determine the rate of Fe(II) dissolution during the sulfidation of siderite.
- 3) Compare the effects of pH on Fe(II) carbonate reactivity.
- 4) Discuss the incorporation of Fe carbonate reactivity into the Fe reaction scheme of Poulton *et al.* (2004).

5.3 METHODS

5.3.1 Materials

In order to synthesise fully reduced siderite minerals, strictly anoxic experimental conditions were required to avoid surface oxidation of iron (II) carbonate species. Several measures were taken to ensure oxygen was fully evacuated from the reaction vessel within which mineral precipitation occurred. The air-tight 1L vessel was sealed with vacuum grease and filled to capacity to minimise headspace within which oxygen could be trapped or leaked. The vessel, which contained 0.5 M $\text{FeCl}_2 \cdot 4\text{H}_2\text{O}$ in 1.5L DIW was purged for a minimum of two hours with ultrapure- $\text{N}_2(\text{g})$; with reagent solutions (0.5M Na_2HCO_3) deoxygenated for approximately one hour prior to being added dropwise into the vessel; synthesised according to the method of Poulton & Canfield (2005).

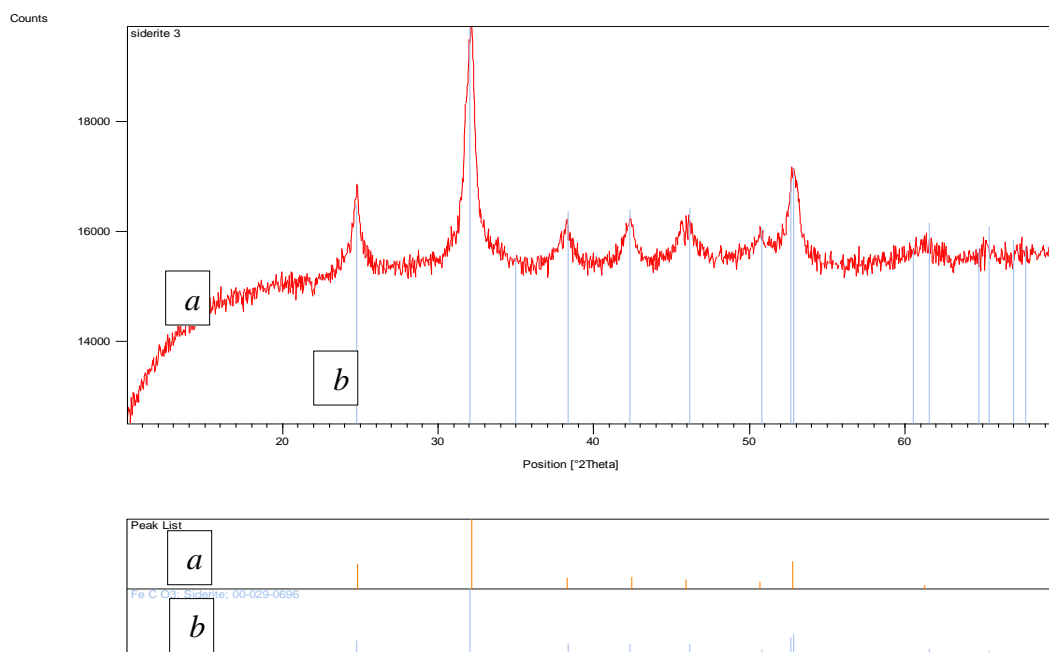


Figure 5.3: XRD pattern for (a) synthetic crystalline siderite comparing peak positioning and abundance with (b) internal library minerals

A light green precipitate was formed, which is consistent with pure iron carbonate synthesised during previous investigations (Jensen *et al.*, 2002). In order to avoid oxidation, samples were freeze-dried under vacuum, purged with N_{2(g)} and then immediately stored at -80°C. Precipitation of crystalline siderite occurred over approximately 8 hours during which time all reagents were subjected to continuous deoxygenation. X-ray diffraction analysis (XRD) was used to characterise the siderite minerals, in reference to an internal library standard, with the observed plots shown in Figure 5.3. The XRD traces did not show any evidence of oxidation to other minerals, impurities within the crystalline structure or the formation of Fe(III)/Fe(II) mineral structures such as green rust. The surface area of crystalline synthetic samples was measured for 1g of siderite by multi-point BET surface analysis as 11.60 m²/g (See Methodology Chapter 3.1). During sulfidation experiments, due to the highly unstable nature of siderite under oxic conditions, any oxidised material on the reactive surface layer of the mineral would be instantaneously reduced to Fe(II) on the addition of dissolved sulfide within the vessel. In order to avoid this occurrence, siderite experiments were always conducted under a constant flow of UPN₂.

5.3.2 Natural crystalline siderite

In addition to the experimental sulfidation of synthetic Fe carbonates, a sample of siderite from the 1.88 Ga Biwabik Iron Formation (Animikie Group, Minnesota, USA) was subjected to sulfidation under similar conditions. The sample was obtained by drilling a siderite-rich layer of the BIF and has previously been used to evaluate chemical extraction techniques for crystalline siderite (Poulton & Canfield, 2005). It is noted that this sample likely contains an oxidised surface mineral layer due to the sample being stored under normal oxygenated conditions.

5.3.3 Experimental Parameters

Initial conditions for the iron sulfidation experiments described in this chapter are referred to in Table 5.1.

Table 5.1 Initial conditions for iron sulfidation experiments

Experiment	Mineral	Surface	Initial	
	Concentration (g L ⁻¹)	Area (m ² L ⁻¹)	S ²⁻ (μM)	pH
1	0.098	1.113	839	7.44
2	0.101	1.172	401	7.35
3	0.099	1.148	165	7.38
4	0.100	1.160	637	7.45
5	0.100	1.160	69	7.30
6	0.100	1.160	268	7.40
7	0.100	1.160	431	7.31
8	0.100	1.160	575	7.48
9	0.100	1.160	251	7.43
10	0.195	2.262	401	7.40
11	0.250	2.900	399	7.40
12	0.050	0.580	346	7.31
13	0.200	2.320	388	7.30
14	0.350	4.060	397	7.25
15	0.150	1.740	390	7.44
16	0.075	0.870	455	7.50
17	0.225	2.610	311	7.48
18	0.100	1.160	451	6.50
19	0.100	1.160	498	8.50
20	0.100	-	1236	7.50

* Experiments 18 and 19 represent sulfidation of synthetic FeCO₃ under changing pH conditions; Experiment 20 indicates the use of a natural siderite sediment sample, total iron wt = 22.4% corrected for oxidised Fe via dithionite extraction (Poulton & Canfield, 2005)

In order to determine the influence of surface area associated with the initial concentration of mineral Fe(II), and also the initial concentration of dissolved sulfide in solution, a number of experiments were conducted which varied these conditions while maintaining other parameters constant, via the iron sulfidation procedure detailed in Methodology Chapter 3.3. As with Poulton (2003) and Poulton *et al.* (2004), the initial sulfide concentration was estimated via regression analysis of the initial linear phase of dissolved sulfide removal, to account for any oxidation of dissolved sulfide that may occur before and during addition of the siderite to the reaction vessel, and to account for any reaction of dissolved sulfide with minor amounts of oxidised surface Fe(III) potentially produced as the mineral was introduced to the reaction vessel. To maintain experimental pH either a borate buffer or known concentration of dilute NaOH was added to solution prior to sulfidation.

5.3.4 Siderite blanks - the effect of varying pH

To determine the magnitude of the synthetic siderite mineral dissolution under an aqueous, but non sulfidic system, an experiment was devised to measure $\text{Fe}^{2+}_{(\text{aq})}$ concentration over 60 minutes, with a known concentration of FeCO_3 under anoxic DIW conditions. The results observed from this reaction indicate that $< 15 \mu\text{M}$ of $\text{Fe}^{2+}_{(\text{aq})}$ are measured in solution over one hour, under neutral conditions (pH 7.5), as shown in Figure 5.4. From these measurements $\text{Fe}^{2+}_{(\text{aq})}$ is naturally released into an aquatic solution at $4 \mu\text{M}/\text{min}$, without the aid of a catalyst such as dissolved sulfide. Figure 5.4 also compares the dissolution of Fe(II) from carbonate surfaces under more acidic (pH 6.5) and alkaline conditions (pH 8.5). Under neutral conditions, which the majority of experiments within this study were conducted, very little Fe(II) is naturally dissolved into anoxic, nonsulfidic solutions in comparison with both acidic and alkaline

aquatic environments. This interpretation reflects the results of previous studies which concentrated on the dissolution of carbonate species (including iron carbonates) within non sulfidic solutions (e.g. Bruno *et al.*, 1992; Duckworth & Martin, 2005), which investigate the speciation of carbonate species from the mineral surface under conditions of varying pH. These studies investigate both proton promoted and water promoted dissolution of Fe and carbonate species under oxic and anoxic conditions. The concentration of Fe(II) under alkaline conditions produces a surprising result and the reasons behind these findings are unclear. Measuring the dissolved carbonate content of anoxic solutions may begin to answer why, at pH 8.5, an increased concentration of Fe(II) is measured (in comparison to in neutral solutions.) However, from these findings, proton-promoted dissolution of the siderite does not appreciably affect the calculation of the much faster dissolution rates observed in the presence of dissolved sulfide (see below).

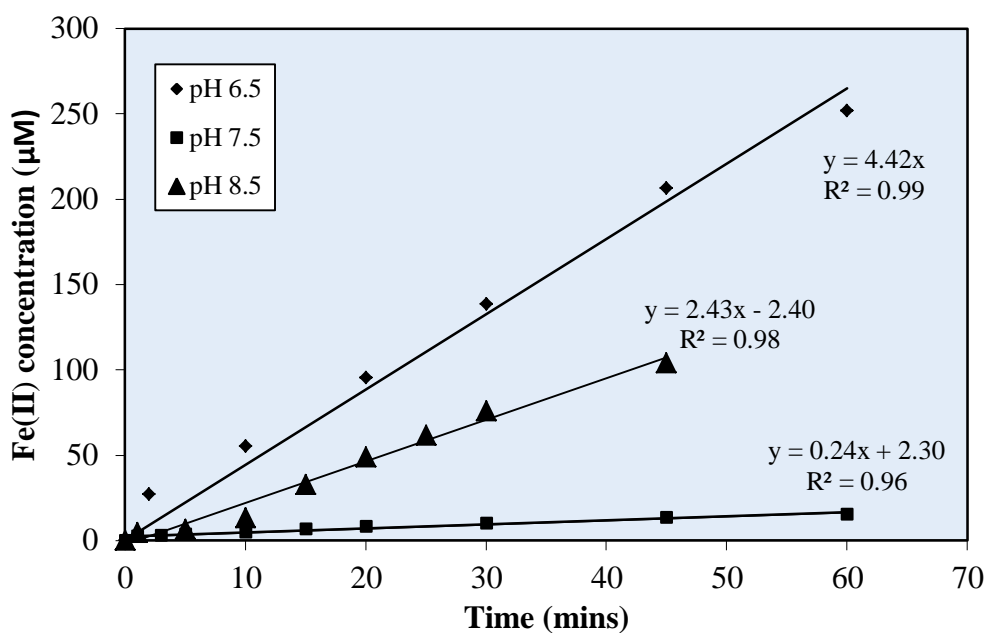


Figure 5.4: Dissolution of 0.1g siderite over pH range 6.5-8.5 in deionised water

5.4 RESULTS

5.4.1 Chemical Speciation

For the purposes of experimental analysis, total Fe(II) dissolution (Fe(II)_t) includes the measurement of Fe(II) associated with FeS, plus dissolved $\text{Fe}^{2+}_{(\text{aq})}$. Figure 5.5 displays a variety of typical speciation plots for the sulfide-promoted dissolution of siderite under varying initial experimental conditions (Table 5.1). At circumneutral pH, at which these experiments were conducted (\sim pH 7.3 - 7.5), very little $\text{Fe}^{2+}_{(\text{aq})}$ is observed in solution and the majority of Fe(II) released from the siderite mineral surface is present as FeS(s). During individual experiments ($n = 17$), total Fe(II) dissolution increases and FeS forms rapidly over the initial period of sulfidation, before slowing with time as dissolved sulfide is removed from solution. Plots for nine experiments with similar initial Fe(II) concentrations (~ 0.1 g) were performed, whilst varying initial sulfide added to the vessel (69-839 μM). Within the first ten minutes of sulfidation, FeS accounts for between 80-100% of the total Fe(II) in solution, indicating that FeS is forming directly in solution. The proportion of dissolved Fe(II) increases after this point in experiments where dissolved sulfide is at low concentrations, potentially due to the lack of dissolved sulphide left to produce solid phase FeS (see reaction mechanism and discussion below). A second batch of experiments ($n = 8$) were conducted to compare the effects of changing FeCO_3 surface area on the rate of Fe(II) dissolution, using an approximate initial dissolved sulfide concentration of 400 μM . In all cases, the amount of dissolved sulfide consumed during the reaction was close to the amount of FeS formed, but a slight overall loss of sulfide is observed, which may reflect oxidation of some of the dissolved sulfide during the reaction, potentially due to reaction with oxidised mineral surface (Fe(III)) produced during introduction of the siderite to the reaction vessel.

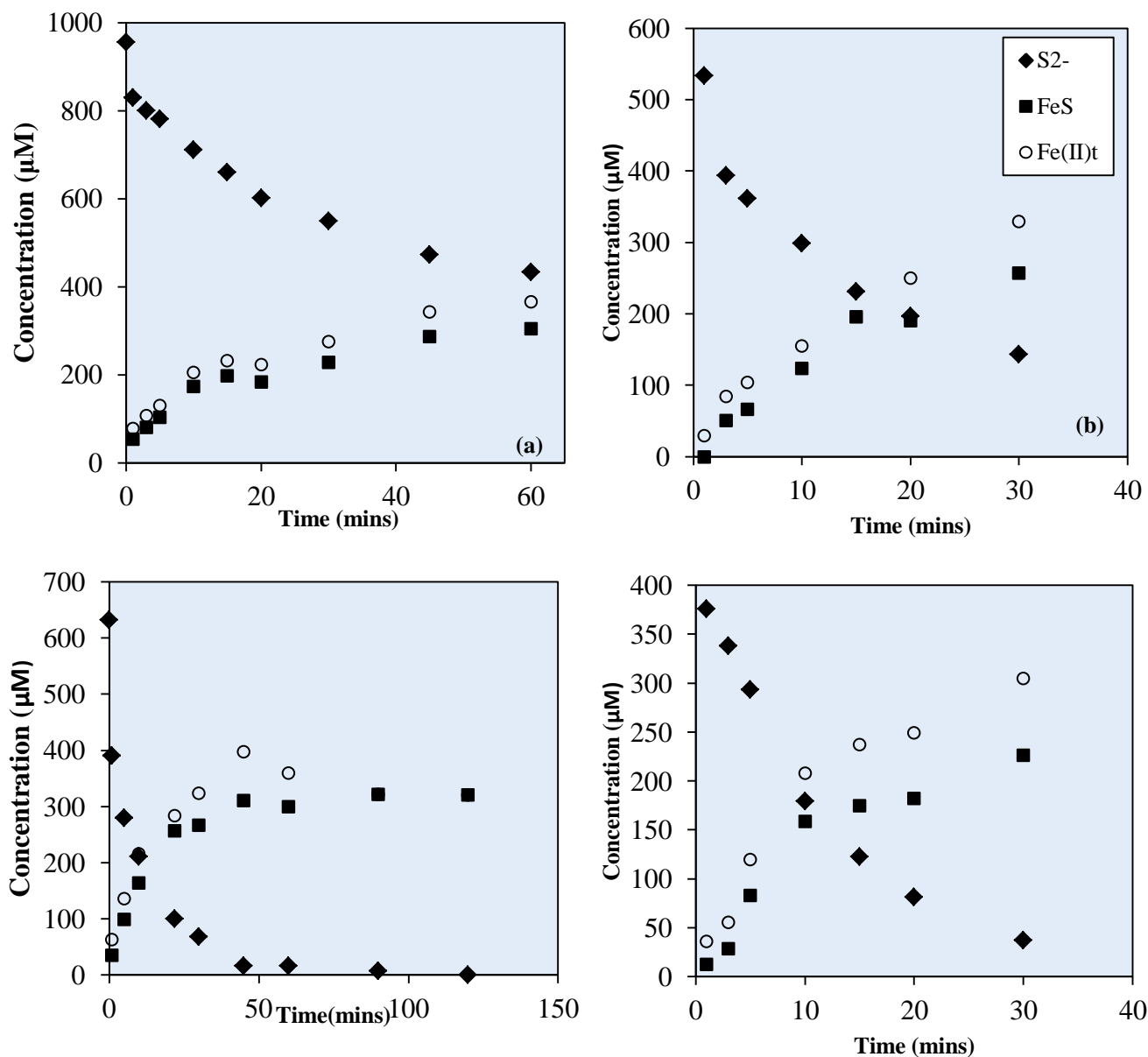


Figure 5.5: Dissolution of Fe(II) via iron sulfidation. Initial conditions a) 0.098g FeCO_3 , 839 μM S^{2-} , pH 7.44 b) 0.101g FeCO_3 , 401 μM S^{2-} , pH 7.35, c) 0.195g FeCO_3 , 401 μM S^{2-} , pH 7.4, d) 0.150g FeCO_3 , 390 μM S^{2-} , pH 7.4

Alternatively, this may be a consequence of the difficulty in accurately extracting solid particles from the reaction vessel, a problem which becomes larger as the reaction progresses and bigger particles are formed which sink to the bottom of the reaction vessel. Nevertheless, this slight mass balance discrepancy with regard to total S, the

differences are low and do not significantly affect quantification of the overall reaction rates from the total Fe(II) profiles (see Figures 5.6 and 5.7).

5.4.1.1 Fe(II) dissolution

In order to determine the initial rates of reaction, the Fe(II) dissolution data are only considered over the initial linear phase of dissolution (see Poulton, 2003; Poulton *et al.*, 2004). The measurement of total Fe(II) released from the siderite ($\text{Fe}^{2+}_{(\text{aq})} + \text{FeS}$) for 0.1g synthetic siderite material at pH 7.5 is shown in Figure 5.6, which compares experiments with varying initial concentrations of dissolved sulfide (mostly as HS^- under experimental pH). For 17 experiments conducted, dissolved Fe(II) accounted for only 10 - 20% of total Fe(II) released from the siderite, indicating the majority of Fe(II) is present as FeS(s). The general trend observed in Figure 5.6 describes an initial linear relationship between $\text{Fe}^{2+}_{(\text{aq})}$ dissolution and time, the rate of which increases with increasing initial sulfide concentration in solution. This indicates a heterogeneous reaction, following a zero order rate law over the initial period of reaction, and can be used to classify the rate at which Fe(II) dissolution occurs. An increase in Fe(II) dissolution rate is also observed with increasing surface area (Figure 5.7), suggesting a surface area control on rates of Fe(II) dissolution (as discussed within Poulton, 2003; Poulton *et al.*, 2004). Notably, a marked slowing of rate is observed with increasing concentrations of dissolved sulfide when concentrations appear to be in excess ($> 500 \mu\text{M}$), an important consideration within natural systems. Table 5.2 indicates that statistically, all data represented by Figures 5.6 and 5.7 provide a good linear correlation between Fe(II) concentration and time (hence, above 95% confidence level).

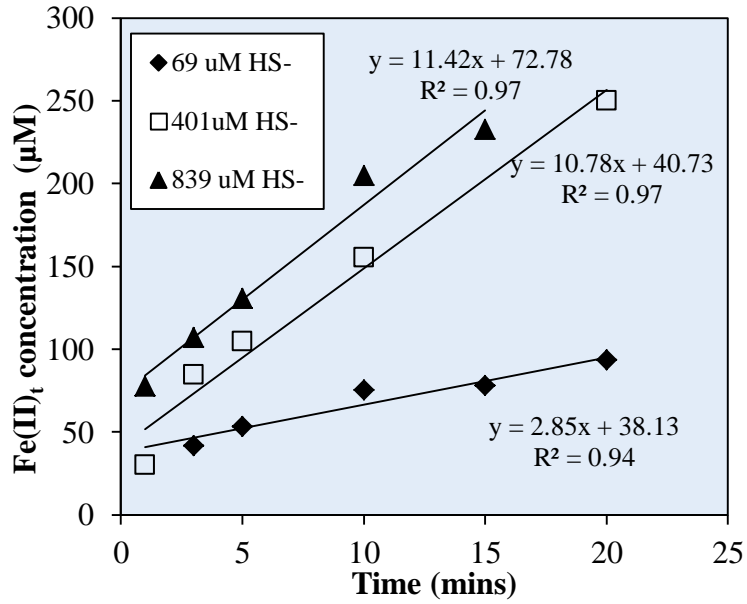


Figure 5.6: Total Fe(II) dissolution of siderite pH 7.5; for iron sulfidation experiments conducted at vary initial sulfide concentration (μM) (n.b. corrected for Fe carbonate dissolution under non-sulfidic conditions).

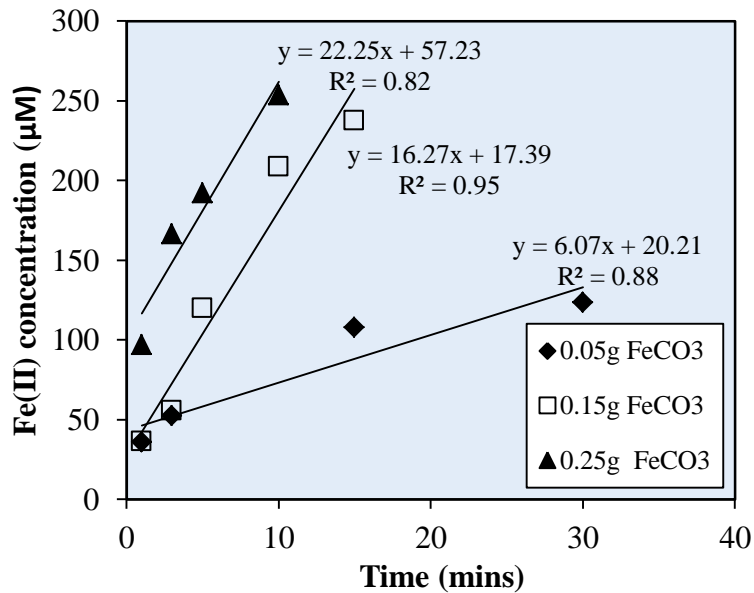


Figure 5.7: Total Fe(II) dissolution measured with varying initial FeCO₃ concentrations.

5.4.2 Dissolution of BIF stable siderite: Bilwārik Formation

In order to compare the experimental data collected for synthetic siderite dissolution with natural siderite, a sample of crystalline siderite from the Biwabik Iron Formation (N. America) was selected for iron sulfidation, the experimental conditions of which are described in Table 5.1 of this chapter. As with Chapter 4, a pronounced difficulty was observed in measuring FeS from natural samples, however, concentrations of total Fe(II) released from the mineral were measurable, allowing the rate of siderite dissolution to be determined (Figure 5.8). The rate of Fe(II) dissolution from the Biwabik iron carbonate samples is significantly lower than for synthetic minerals, at less than $1 \mu\text{M min}^{-1}$. Using Levenes Test of correlation (Table 5.2), the relationship between total Fe(II) and time for the sulfidation of Biwabik sediment sample can be determined highly significant, above 95% confidence level.

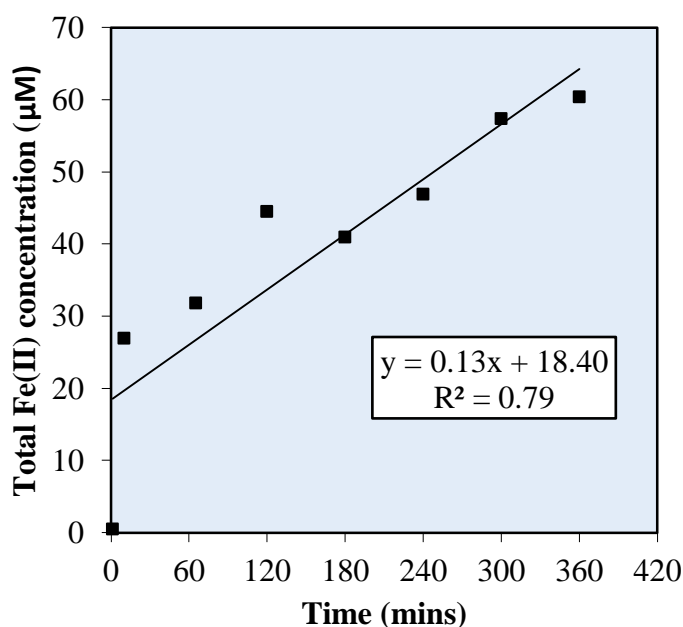


Figure 5.8: Speciation plot for the sulfidation of a natural siderite sample

Table 5.2: Collation of statistical data representing the dissolution rates of FeCO₃ during sulfidation: Experimental and Natural sediment studies.

Figure	Name	Slope	R ² Excel	R ² Minitab	Calculated P value (F test)	Levenes Test of Correlation (P value)	Confidence (%)	Accept/Reject Null Hypothesis
5.6	69	$y=2.85x+38.13$	0.94	0.97	0.000	0.049	95.1	A
	401	$y=10.78x +40.73$	0.97	0.97	0.000	0.049	95.1	A
	839	$y=11.42x+72.78$	0.97	0.97	0.000	0.033	96.7	A
5.7	0.05	$y=6.07X+20.21$	0.88	89	0.090	0.005	99.5	A
	0.15	$y=16.27X+17.39$	0.95	95	0.000	0.01	99	A
	0.25	$y=22.25X+57.23$	0.82	0.93	0.001	0.065	93.5	A
5.8	Biwabik sediment	$y=0.13x + 18.40$	0.79	0.79	0.000	0.001	99.9	A

5.5 DISCUSSION

5.5.1. Mechanism of siderite dissolution

The exact reaction mechanism for the sulfidation of siderite can not be characterised experimentally, however, reduced sulfur species in solution are hypothesised to undergo a direct substitution reaction with carbonate at the mineral surface to form FeS(s). It is proposed that the surface controlled reaction may proceed via two steps:



Equations 5.1 - 5.2 reveal the bond between the reduced Fe atom and the carbonate is broken as substitution of FeS occurs, freeing a bicarbonate species into solution. The resulting product is energetically unstable with regards to the mineral surface, and allows detachment of Fe(II) from the outer electron surface. FeS(s) formation then occurs (as described in Equation 5.2; Poulton 2003) as the dominant product of iron carbonate dissolution, providing dissolved sulfide remains available.

5.5.2 Determination of the Rate Equation

The reactivity of siderite, defined by Fe(II) dissolution kinetics (i.e. FeS plus dissolved Fe²⁺), is dependent upon surface-controlled processes (as with the reductive dissolution of Fe(III) oxide minerals), the rate of which is influenced by pH, dissolved sulfide concentration and the mineral surface area available for reactivity. Within this study it is suggested that the rate of dissolution can be determined by applying initial rate kinetics, previously applied to other Fe minerals (e.g. Pyzik & Sommer, 1981; Poulton *et al.*, 2002, Poulton, 2003; Yao & Millero, 1996) via the rate equation:

$$\mathbf{R}_{\text{Fediss}} = \mathbf{k}_{\text{Fediss}} (\mathbf{H}_2\mathbf{S}_{t=0})^a \mathbf{A}^b \quad (\text{Eq. 5.3})$$

where R represents the rate of Fe(II) dissolution ($d(\text{Fe(II)}_{\text{diss}}/dt)$; in M min^{-1}), ($\text{H}_2\text{S}_{t=0}$) is the initial concentration of dissolved sulfide (M L^{-1}) which is dependent on a reaction order (a); and A reflects the surface area of initial Fe(II) mineral in reaction ($\text{m}^2 \text{g}^{-1}$). $\mathbf{K}_{\text{Fediss}}$ defines the rate constant for siderite at pH 7.5.

The rate equation (Equation 5.3) is based on experimental kinetic studies of reductive dissolution for a range of synthetic iron oxide minerals with dissolved sulfide (Pyzik & Sommer, 1981; Dos Santos Afonso & Stumm (1992); Poulton (2003); See Chapter 4). It is important to note that within these previous studies, there is some disagreement over the influence that the initial concentration of dissolved sulfide has on the rate of Fe(II) dissolution, corresponding to the reaction order *a*, in Equation 5.3 (i.e. Dos Santos Afonso & Stumm, 1992; Peiffer *et al.*, 1992 and Yao & Millero 1996 maintain a 1st order relationship Vs. Pyzik & Sommer, 1981; Canfield & Berner, 1987; Poulton, 2003 who describe a fractional order). Previous to this investigation, there have also been no experimental studies relating to the rate of FeCO₃ mineral dissolution catalysed by

dissolved sulfide, and therefore the reaction co-efficients associated with a and b in Equation 5.4 are required to be determined experimentally.

Reaction orders are measured for Fe carbonate minerals by calculating the logarithmic values associated with initial reaction rates determined at various initial sulfide and surface area concentrations. Table 5.3 shows the influence of varying initial sulfide concentrations on measured rates of Fe(II) dissolution. Figure 5.9 indicates a fractional order of 0.5 for coefficient a , with regard to the influence of dissolved sulfide concentration on siderite dissolution, for data obtained with constant initial siderite concentrations (approximately 0.1g).

With reference to varying initial siderite concentrations (and therefore surface area measurements), coefficient b was determined via the regression on a logarithmic plot of data from experiments with varying initial surface areas (Table 5.4; initial sulfide average = 386 μM). Figure 5.10 indicates that a reaction order of 1 can be determined from the logarithmic plots of Fe(II) dissolution rate vs. surface area. After the determination of coefficients a and b (which for siderite are identical to those determined for the major Fe (oxyhydr)oxide minerals; Poulton, 2003; Poulton *et al.*, 2004), the value of rate constant K_{Fediss} can then be calculated for individual experiments (Table 5.4), with an average value of $k_{\text{Fe diss}} = 3.6 \times 10^{-4} \pm 4.6 \times 10^{-5}$ (in $\text{mol}^{0.5} \text{l}^{0.5} \text{m}^2 \text{min}^{-1}$). These values are consistent with values obtained for the sulfidation of Fe(III) oxides and are therefore valid for Fe(II) dissolution of FeCO_3 .

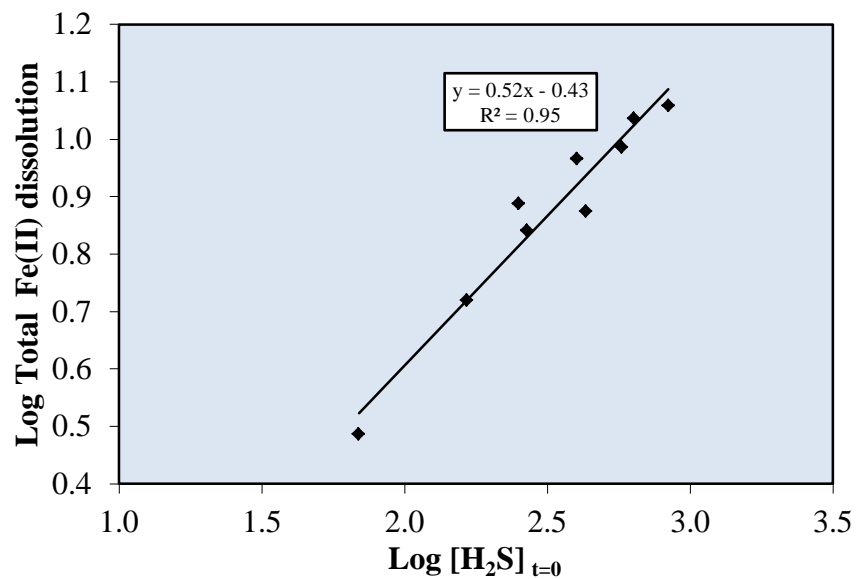


Figure 5.9: Determination of a 0.5 reaction order from logarithmic plots of total dissolution rate and initial sulfide concentration.

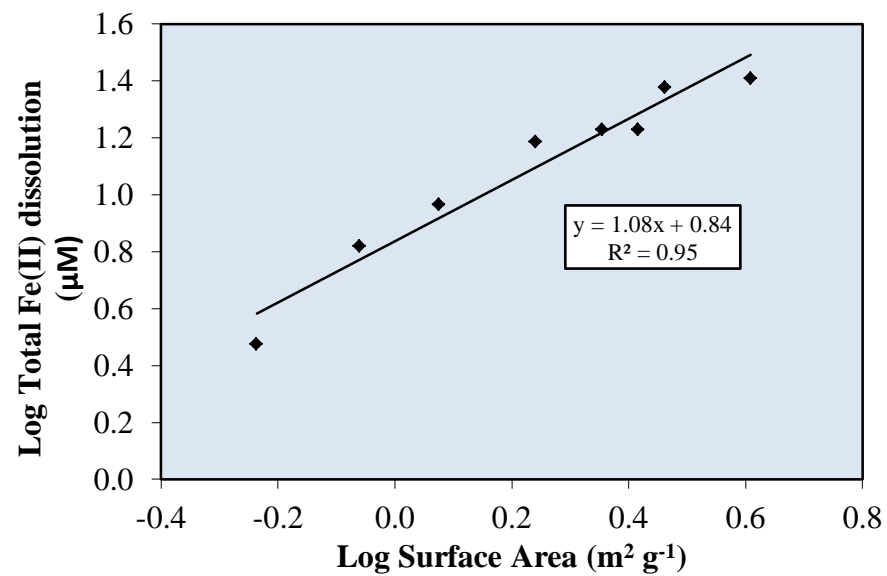


Figure 5.10: Logarithmic plot of total Fe(II) dissolution and surface area, observing a reaction order of 1 dependency on surface area.

Table 5.3: Values of logarithmic Fe(II) dissolution rate with varying initial dissolved sulfide and Fe(II) surface area (pH 7.3-7.5)

Experiment	Initial H₂S (μM)	Rate of Fe (II)		
		dissolution (μM/min)	Log initial H₂S	Log Fe(II) dissolution
1	839	11.43	2.924	1.058
2	401	9.24	2.603	0.966
3	165	5.24	2.217	0.719
4	637	10.87	2.804	1.036
5	69	3.07	1.839	0.487
6	268	6.94	2.428	0.841
7	431	7.50	2.634	0.875
8	575	9.68	2.760	0.986
9	251	7.72	2.400	0.888

Experiment	Initial Surf. A (m²/g)	Rate of Fe		
		dissolution (μM/min)	Log Surf A.	Log Fe(II) dissolution
10	1.189	9.24	0.075	0.966
11	2.262	16.99	0.354	1.230
12	2.900	23.80	0.462	1.377
13	0.580	2.99	-0.237	0.476
14	4.060	25.62	0.609	1.409
15	1.740	15.35	0.241	1.186
16	0.870	6.59	-0.060	0.819
17	2.610	16.97	0.417	1.230

Table 5.4: Determination of rate constant k Fe diss for individual experiments, associated with initial reactant parameters and rate of Fe(II) dissolution

Experiment	Initial H2S (μM)	Initial Surf.A (m² g⁻¹)	Rate Fe(II) dissolution (Mol min⁻¹)	K_{Fediss} Surf A (Mol^{0.5} L^{0.5} m⁻² min⁻¹)	K_{Fediss} Fe(II) (Mol^{0.5} L^{0.5} min⁻¹)
1	839	1.131	11.43	0.000349	0.932
2	401	1.189	9.24	0.000388	1.058
3	165	1.143	5.24	0.000357	0.954
4	637	1.160	10.87	0.000371	0.997
5	69	1.160	3.07	0.000319	0.856
6	268	1.160	6.94	0.000365	0.981
7	431	1.160	7.50	0.000311	0.836
8	575	1.160	9.68	0.000348	0.934
9	251	1.160	7.72	0.000420	1.128
10	401	2.260	9.24	0.000375	1.007
11	399	2.900	16.99	0.000411	1.103
12	346	0.580	23.80	0.000277	0.743
13	388	2.320	2.99	0.000373	1.003
14	397	4.060	25.62	0.000317	0.850
15	390	1.740	15.35	0.000447	1.200
16	455	0.870	6.59	0.000355	0.954
17	311	2.610	16.97	0.000285	0.764

5.5.3 Effect of pH

The rate of siderite dissolution is also dependent on pH. Figure 5.11 shows that the rate of $\text{Fe}^{2+}_{(\text{aq})}$ dissolution varies substantially with changing pH, due to the reaction of carbonate species under weakly acidic, neutral and alkaline conditions. Plots in Figure 5.11 have been corrected for the effect of dissolution of Fe^{2+} as pH varies under non sulfidic conditions. It is important to note that the rate of reaction is calculated from $t=1$ mins, as with sulfidic experiments. This will allow the pre-equilibrium reaction described by Poulton (2003) to be accounted for, meaning surface bound reactions not associated with the reductive dissolution process (and which are difficult to measure) can be excluded for the determination of rate. Under weakly acidic conditions (pH 6.5) the rate of dissolution of Fe(II) is fastest (Figure 5.11), due to the availability of H^+ ions to protonate the mineral surface, weakening Fe-C-O bonds, and rapidly allowing the detachment of FeS from the outer surface into solution. Table 5.6 describes the confidence level at which the linear relationship of Fe(II) concentration Vs. time operates. Only dissolution at pH 7.5 is accepted in terms of linearity above the 95% confidence interval and would describe the fit of the linear line as significant. At pH 6, only three points of data are included in the statistical calculation, a sample number too low to accurately predict the significance of the linear fit. At pH 8.5 the assumption that a linear relationship is observed is rejected as the observed P value corresponds to only 11% correlation to the linear line.

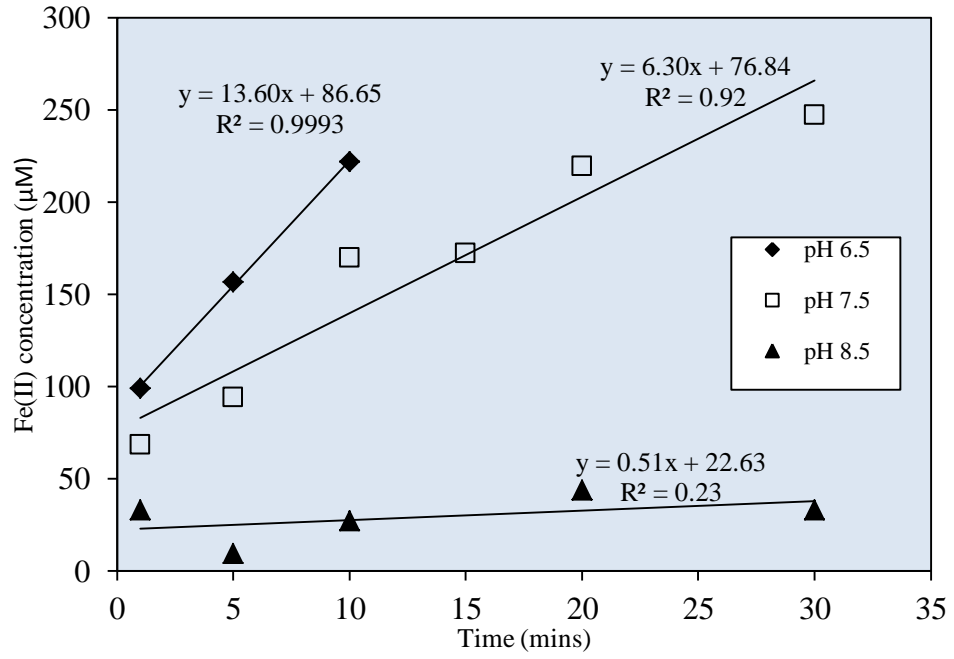


Figure 5.11: Fe(II) dissolution; 0.1g, 500µM initial sulfide, values corrected for Fe(II) dissolution under non sulfidic conditions (see Figure 5.4)

Table 5.5: Determination of rate constant k' for siderite dissolution experiments over pH range 6.5-8.5 (in terms of both surface area and Fe mineral concentration)

Experimental pH	Initial H ₂ S (μM)	Initial Surf A. ($\text{m}^2 \text{g}^{-1}$)	Rate of Fe dissolution (M min^{-1})	$K_{\text{Fediss Surf A}}$ ($\text{Mol}^{0.5} \text{L}^{0.5} \text{m}^{-2} \text{min}^{-1}$)	$K_{\text{Fediss Fe(II)}}$ ($\text{Mol}^{0.5} \text{L}^{0.5} \text{min}^{-1}$)
6.5	336.52	1.189	11.24	0.000525	1.418
7.5	431.00	1.189	7.52	0.000311	0.836
8.5	498.10	1.189	0.87	0.000033	0.090

Table 5.6: Collated statistical data of pH influencing Fe(II) dissolution experiments: F Test Vs Levenes Test

Figure	Name	Slope	R ² Excel	R ² Minitab	Calculated P value (F test)	Levenes Test of Correlation (P value)	Confidence (%)	Accept/Reject Null Hypothesis
5.11	pH 6.5	y=13.60x+86.65	0.9993	0.999	0.011	0.14	86	R
	pH 7.5	y=6.3x+76.84	0.92	0.92	0.001	0.033	96.7	A
	pH 8.5	y=0.51x+22.63	0.23	0.23	0.908	0.886	11.4	R

5.5.4. The Reactivity of Iron Minerals

The reaction rates with which Fe(III) oxide minerals react with dissolved sulfide in solution have been characterised experimentally in a variety of studies (Canfield *et al.*, 1992; Postma, 1993; Raiswell *et al.*, 1994; Poulton *et al.*, 2004; Pedersen *et al.*, 2006). Extrapolating the linear rate at which dissolution occurs between pH 6.5 to 8.5, the rate constant K_{Fediss} for each experiment can be determined (Table 5.5), and are found to increase with decreasing pH over similar experimental conditions (0.1g siderite, initial sulfide = 500 μM). Thus pH has a significant effect on the reactivity of siderite towards dissolved sulfide.

Table 5.7: Comparison of rate constant K_{Fediss} values: Iron Carbonates and Oxides

Mineral	K_{Fediss} (Initial solid phase Fe; μM)	K_{Fediss} (SA; m^2g^{-1})
<i>Siderite</i>	9.6×10^{-1}	3.6×10^{-4}
HFO	4.4	$4.3\text{-}8.6 \times 10^{-6}$
Lepidocrocite	3.4×10^{-2}	6.1×10^{-6}
Goethite	2.4×10^{-4}	7.3×10^{-8}
Magnetite	3.2×10^{-4}	1.0×10^{-6}
Hematite	8.9×10^{-5}	4.2×10^{-7}

These investigations are of good agreement with respect to the order of reactivity, from poorly crystalline minerals with unstable structures and large surface areas allowing

rapid reaction with dissolved sulfide (HFO, ferrihydrite, lepidocrocite), to highly crystalline, stable minerals such as goethite, magnetite and hematite with smaller surface areas for reaction. To compare the reactivity of Fe(II) carbonates with commonly observed Fe(III) oxide minerals, the rate constant K_{Fe} defined by the surface area of Fe mineral in solution was also converted to a rate constant K_{Fe} derived as a function of initial concentration of Fe(II) in the reaction (Table 5.7).

The reactivity of siderite falls between hydrous ferric oxide and lepidocrocite, but due to the low surface area of siderite, it is actually the most reactive mineral when considered in terms of this parameter. It is also useful to determine the half lives of the Fe minerals towards dissolved sulfide (Equation 5.4):

$$\text{Half life (t}_{1/2}\text{)} : \ln (2) / k \quad \text{(Eq. 5.4)}$$

Using Equation 5.4, the values reported in Table 5.8 reveal that the half life of pure synthetic crystalline siderite is 22 minutes (where K_{Fediss} is determined using initial Fe(II) concentration values) which places the reactivity of iron carbonate between amorphous HFO and 2-line ferrihydrite in the reactivity scheme of Poulton *et al.* (2004). This order reflects iron carbonate minerals inclusion as a mineral of high reactivity with regard to dissolved sulfide. It is important to note the difference in mineral structure, surface area and dissolution reaction compared to other iron oxides when placing siderite alongside HFO and ferrihydrite. Poulton *et al.*, 2004 refer to HFO as a poorly crystalline or amorphous iron oxide mineral with a significantly larger surface area

(~300-600 m²g⁻¹) than siderite (11.6 m²g⁻¹), which is closer in terms of available surface area, to more highly crystalline, slower reacting Fe(III) minerals.

Table 5.8: Reactivity of iron bearing minerals catalysed by 1000µM dissolved sulfide pH 7.5

<i>Mineral</i>	<i>t</i> <i>_{1/2}</i>
Freshly precipitated HFO	5.0 mins
<i>CRYSTALLINE SIDERITE</i>	<i>22.0 mins</i>
2-line ferrihydrite	12.3 h
Lepidocrocite	10.9 h
Goethite	63 days
Magnetite	72 days
Hematite	182 days
Reactive silicates	10 ⁵ -10 ⁶ yr

5.5.5. Application to natural environments: Rate of sulfide-mediated dissolution of siderite from the Biwabik Iron Formation

In order to infer the rate of dissolution of Fe(II)_{aq} from siderite minerals within ancient anoxic environments, a sample of naturally precipitated FeCO₃ from the Biwabik Iron Formation was subjected to dissolution mediated by sulfidation under the same conditions with which pure synthetic iron carbonate minerals were determined (with experimental parameters described in Table 5.1). A rate of dissolution of 0.14 µM min⁻¹

was determined (Figure 5.8), which equates to a rate constant of $K_{\text{Fediss}} = 0.018 \text{ (mol}^{0.5} \text{ l}^{0.5} \text{ min}^{-1}\text{)}$ and a half life ($\tau_{1/2}$) value of ~20 hours. Thus, this natural crystalline siderite is much less reactive than synthetic siderite, suggesting that in the environment the reactivity of siderite will vary greatly, dependent on ageing, impurities and surface area. Nevertheless, this ancient siderite still falls amongst the most reactive of the major Fe minerals occurring in the environment, supporting the inclusion of siderite as part of the ‘highly reactive’ pool of Fe minerals (Poulton *et al.*, 2004; 2010, Canfield *et al.*, 2007; 2008).

5.6 SUMMARY

- In modern aquatic environments, Fe carbonate minerals precipitate in low sulfide environments. Recent studies of Fe-rich iron formations <1.8 Ga observe intermittent periods of euxinia coinciding with well characterised anoxic intervals. Currently, no experimental study has been proposed to define the mechanism and kinetics of Fe(II) carbonate dissolution in ancient marine sediments.
- Sulfidation experiments were devised to calculate the rate of Fe(II) carbonate dissolution using pure synthetic minerals and a natural sediment sample from the Bawabik iron formation (N. Minnesota).
- The proposed mechanism of Fe(II) dissolution suggests the substitution of dissolved sulfide onto the carbonate mineral surface, and hence the direct formation of FeS in solution, followed by the release of Fe(II) and HS⁻ into a reduced environment.
- The rate constant of Fe(II) carbonate dissolution under near neutral conditions ranges from $K = 5.3 \times 10^{-4}$ to $3 \times 10^{-5} \text{ Mol}^{0.5} \text{ L}^{0.5} \text{ m}^{-2} \text{ min}^{-1}$ over pH range 6.5-8.5, indicating dissolution slows with increasing pH.
- The reactivity of siderite at pH 7.5 as defined by rate constant K, is two orders of magnitude larger than the fastest reacting Fe(III) minerals (HFO, $K = 4.3\text{-}8.6 \times 10^{-6} \text{ Mol}^{0.5} \text{ L}^{0.5} \text{ m}^{-2} \text{ min}^{-1}$). Hence, Fe(II) carbonate dissolution is significantly faster than Fe(III) bearing minerals. This difference relates to the difference in dissolution mechanisms, i.e. FeS substitution compared to multistep reductive dissolution processes.
- The half life of synthetic siderite minerals is approximately 22 minutes, compared to 20 hours for a sample from Bawabik natural (oxidised) siderite. Although the sediment sample is not representative of the reduced environment from which it was precipitated, the value derived is still indicative of a highly reactive Fe mineral.

CHAPTER 6: IRON ISOTOPE FRACTIONATION DURING SULFIDE PROMOTED REDUCTIVE DISSOLUTION OF IRON (OXYHYDROXIDE) MINERALS

6.1 INTRODUCTION

6.1.1. Iron isotope fractionation during reductive dissolution

Experimental investigations into the fractionation of iron isotopes in sedimentary and marine systems have provided an increasingly powerful tool for examining Fe cycling in modern and ancient environments. The biogeochemical processes associated with controlling the magnitude of Fe isotope fractionation in natural settings are debatable, however, with uncertainty surrounding the roles of an extensive number of biological and abiological reactions during early sediment diagenesis (Anbar, 2004; Czaja *et al.*, 2010; Heimann *et al.*, 2010; reviewed within Johnson *et al.*, 2004; Dauphas & Rouxel, 2006; Johnson & Beard, 2006; Anbar & Rouxel, 2007).

The largest Fe isotope fractionations (measured in regard to Fe cycling in natural settings), occur in association with changes in redox state and bonding environment (Beard *et al.* 1999; Johnson *et al.*, 2004; 2008), where the speciation and solubility of Fe (III) species effect the mobility and transformation of Fe within aqueous and sedimentary systems. Laboratory based studies of biogeochemical reactions are required when comparing the magnitude of fractionations observed during a variety of biological and abiological reaction pathways occurring within near surface sedimentary environments.

Experimental studies of both biological and abiotic mineral dissolution imply that larger fractionations between Fe isotopes are associated with dissimilatory iron reduction (DIR), with $\delta^{56}\text{Fe}$ fractionations between -0.5 to -2.5‰ indicate that the dissolved Fe(II) species is isotopically lighter than the initial Fe oxyhydroxide mineral (Beard *et al.*,

1999; 2003; Icopini *et al.*, 2004; Johnson *et al.*, 2005; Crosby *et al.*, 2007). A large proportion of studies examining the fractionation associated with both experimental and studies of DIR in natural settings (Beard *et al.*, 1999; 2003; Crosby *et al.*, 2005; 2007; Johnson *et al.*, 2005; Weiderhold *et al.*, 2006) suggest that dissolved $\text{Fe}^{2+}_{(\text{aq})}$ is significantly lighter than that produced by corresponding inorganic methods of mineral reductive dissolution (for which experimental data is so far limited). Hence, there may be a significant overlap of fractionation values observed during biological and abiological mineral dissolution within diagenetic environments. Nevertheless, previous studies observe that isotope fractionations associated with experimental DIR processes are significantly depleted in $\delta^{56}\text{Fe}$ values of dissolved $\text{Fe(II)}_{\text{aq}}$ (Johnson *et al.*, 2008); and have subsequently been applied to a number of studies examining the accumulation of Fe in porewaters and sediment assemblages from modern marine settings (Severmann *et al.*, 2006; Staubwasser *et al.*, 2006, Severmann *et al.*, 2008; Homoky *et al.*, 2009) and in the Fe isotope signatures in ancient marine rocks (Yamaguchi *et al.*, 2005; Archer & Vance 2006; Duan *et al.*, 2010).

Studies which have investigated experiments mediating dissolution with the addition of organic acids (e.g. oxalate: Wiederhold *et al.*, 2006) are more suited to terrestrial weathering processes in soil and sediment environments than within marine settings. Inorganic experiments detailing processes of mineral dissolution have not presently focused on processes of mineral reductive dissolution applicable to marine sedimentary environments, with only tentative suggestions that BSR associated sulfide may also induce an isotopic fractionation during iron redox mineral processes (Archer & Vance, 2006; Staubwasser *et al.*, 2006). This important reaction utilises the generation of dissolved sulfide from bacterial sulfate reduction in the mechanism described by Dos Santos Afonso & Stumm (1992; Chapter 4). Sulfide mediated reductive dissolution

plays an important role in the formation of FeS and FeS₂ with iron rich sediments (Berner, 1984; Rickard & Morse, 2005) and although there is little information regarding the isotopic fractionation associated with pyrite formation; experimental studies of FeS formation from Fe²⁺_(aq) and dissolved S²⁻ (Butler *et al.*, 2005) report a fractionation of $\delta^{56}\text{Fe} = 0.85 \pm 0.3\%$.

Currently, the fractionation factor associated with Fe isotope fractionation during sulfide mediated reductive dissolution is unknown, although the reaction is acknowledged as being an important process affecting modern and ancient marine systems (Poulton, 2003), with Canfield (1989) concluding that this process may be significant in terms of dominance over DIR during diagenesis of many organic-rich continental margin sediments.

6.1.2 Hypothesised mechanism of isotopic fractionation

The mechanism of reductive dissolution reported by Dos Santos Afonso & Stumm (1992) proposes two significant steps where isotopic fractionation may occur. The first is an observed change in oxidation state during the exchangeable electron transfer between Fe(III)-Fe(II) after HS⁻ surface complexation formation on the reactive outer electron shell of the Fe oxide surface (*the reduction step*).

I) *Surface complex formation*



II) *Electron transfer*

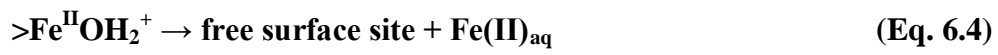


The second traces the detachment of the reduced Fe(II) complex during hydrolysis from the oxide surface (*the dissolution step*).

III) *Release of oxidised product:*



IV) *Detachment of Fe(II)*



6.2 RESEARCH AIMS

This chapter aims to ascertain the significance of a kinetic Fe isotope fractionation associated with sulfide mediated reductive dissolution for a number of synthetic Fe(III) oxide minerals via a series of batch sulfidation experiments. These experiments will trace the changing isotopic Fe fractionation as a two-step process: 1) the reductive step and 2) the dissolution step; the extent of which is dependent on mineral crystallinity, pH, initial sulfide and Fe(III) concentration. By assigning an isotopic fractionation value to individual Fe(III) oxide minerals (which differ in their rates of reaction with dissolved sulfide), a model of isotopic fractionation associated with an abiotic reductive dissolution mechanism is built upon, allowing a comparison to values well characterised for Dissimilatory Iron Reduction in both modern sedimentary systems and the ancient rock record. **The main objectives of this chapter:**

- 1) Design a series of closed system batch iron sulfidation experiments and derive a protocol for the sampling of different Fe isotope pools
- 2) Compare the Fe isotope signatures measured for individual Fe(III) oxides undergoing sulfide mediated reductive dissolution, which react with dissolved sulfide over a range of timescales.
- 3) To investigate the mechanism by which Fe fractionation occurs by measuring individual Fe isotope pools with regard to Fe(III) reduction from the original Fe(III) oxide, and the dissolution of $\text{Fe(II)}_{\text{aq}}$ from the surface reduced Fe(II) species.
- 4) To compare the measurement of Fe isotopic fractionation derived from abiotic processes with that of signatures associated with biological iron reduction reactions, which are regarded as the predominant diagenetic mechanism regulating the redox cycling of Fe in marine sediments.

6.3 METHODOLOGICAL CONSIDERATIONS

Fe(III) oxide minerals (2-line ferrihydrite, goethite, hematite and lepidocrocite) were synthesised via the methods of Schwertmann & Cornell (1991), and characterised via XRD and BET surface analysis, with surface areas described in Chapter 3. Anoxic batch experiments using a stock solution of $\text{Na}_2\text{S}\cdot 9\text{H}_2\text{O}$ as a sulfidation reagent were conducted as described in Methodology Chapter 3.3.2. Experiments were performed with a known volume of stock solution in 1L of deoxygenated D.I.W. with samples to measure the concentrations of dissolved sulfide, FeS, and $\text{Fe(II)}_{\text{aq}}$ taken periodically after the introduction of individual oxide into the closed reaction vessel. Elemental sulfur was calculated as the difference between initial and total sulfide concentrations over time (where total S is the sum of solid phase plus dissolved S). Values of surface reduced Fe(II) were derived via mass balance calculation, as the amount of Fe(III) reduced to Fe(II) is double the concentration of elemental sulfur in solution at any point during the reaction (minus the concentrations of $\text{Fe(II)}_{\text{aq}}$ and FeS; Poulton, 2003). In order to minimise the isotopic influence of FeS formation on iron isotope fractionation produced by pure reductive dissolution, experimental conditions were manipulated to minimise FeS precipitation, although a transient amount was still measured from within the system. Table 6.1 represents the initial conditions set for the individual sulfidation experiments.

10mL samples in an airtight syringe were taken for the isotopic analysis of dissolved Fe(II), surface reduced Fe(II) (which includes an FeS(s) phase) and unreacted Fe(III) as detailed in Methodology section 3.5). The isotopic composition of precipitated FeS could not be separated from the surface reduced Fe(II) phase as both species were dissolved in dilute acid (10% v/v).

Table 6.1: Experimental conditions for iron mineral sulfidation

Experiment	Synthetic Fe mineral	pH	Initial [S ²⁻] (μM)	Sample mass (g/L)
1	2-line ferrihydrite	4	212	1.00
2	2-line ferrihydrite	9.1	863	0.70
3	lepidocrocite	4	872	0.25
4	hematite	4	1092	0.50
5	goethite	4	885	0.50
6	lepidocrocite	8.5	963	0.30
7	2-line ferrihydrite	8.5	219	0.50

Isotopic analyses were performed at University of California, Santa Cruz and at the Woods Hole Oceanographic Institution by Dr Silke Severmann, using a Thermo Scientific Neptune Isoprobe MC-ICP-MS, relative to the original starting composition of the Fe(III) oxides. Data is reported using standard δ notation, per mil (‰), for ⁵⁶Fe/⁵⁴Fe ratios:

$$\delta^{56}\text{Fe} = \left(\frac{{}^{56}\text{Fe}/{}^{54}\text{Fe}_{\text{sample}}}{{}^{56}\text{Fe}/{}^{54}\text{Fe}_{\text{start.mat.}}} - 1 \right) \times 10^3 \quad (\text{Eq. 6.5})$$

Samples were introduced into the mass spectrometer as < 0.5 ppm Fe/Cu solutions, with bracketed standard of IRMM-14 internal isotopic standard, or a digest of the initial Fe (oxyhydr)oxide sample. Both black shale and basalt external standard reference materials were run alongside analyses, measuring an average analytical precision of $\delta^{56}\text{Fe}$ (2-SD) 0.13‰ and 0.10‰ respectively.

In order to evaluate the validity of the iron sulfidation experiments as a means of iron isotope fractionation, the mass balance of Fe throughout reduction, dissolution and un-

reacted Fe(III) phases was calculated (Equation 6.6) for a selection of samples, the results of which are reported in Table 6.2. The average mass balance (0‰) indicates that the sampling rational devised to measure all fractions of Fe in reaction is quantitative.

$$\delta^{56}\text{Fe}_{\text{MB}} = (\delta^{56}\text{Fe}_{\text{diss}} \times [\text{Fe}_{\text{diss}}/\text{FeT}]) + (\delta^{56}\text{Fe}_{\text{sur}} \times [\text{Fe}_{\text{sur}}/\text{FeT}]) + (\delta^{56}\text{Fe}^{\text{III}} \times [\text{Fe}^{\text{III}}/\text{FeT}])$$

(Eq. 6.6)

6.4. RESULTS

6.4.1. Chemical Speciation

All measured chemical and isotopic data are reported in Tables 6.2 and 6.3. As with similar closed system studies of iron (III) mineral sulfidation (Poulton, 2003; Poulton *et al.*, 2004), an initial increase in surface reduced Fe(II) is observed whilst dissolved sulfide is removed from solution either by oxidation to elemental S (Eq. 6.3); or the formation of FeS, which was transient only under acidic conditions. Faster reacting minerals such as ferrihydrite, lepidocrocite and goethite undergo rapid dissolution at the reduced oxide surface at pH 4, increasing the pool of Fe(II)_{aq} observed as the dominant Fe(II) phase over the timescale of each experiment. These minerals are characterised as highly reactive with respect to dissolved sulfide (Poulton *et al.*, 2004) whereas hematite, which is of low reactivity and dissolution rate, is dominated by surface reduced Fe(II), even at low pH (Figure 6.1).

Under circum-neutral to alkaline pH conditions (Figure 6.2), the rate of mineral dissolution significantly reduces as protonation of the nearest attached hydroxide ion is required to promote dissolution (Zinder *et al.*, 1986). Hence, experiments performed at

higher pH values observe the majority of reduced Fe(II) is still associated with the reactive oxide surface, with very little Fe(II) released into solution, and consequently little FeS is formed.

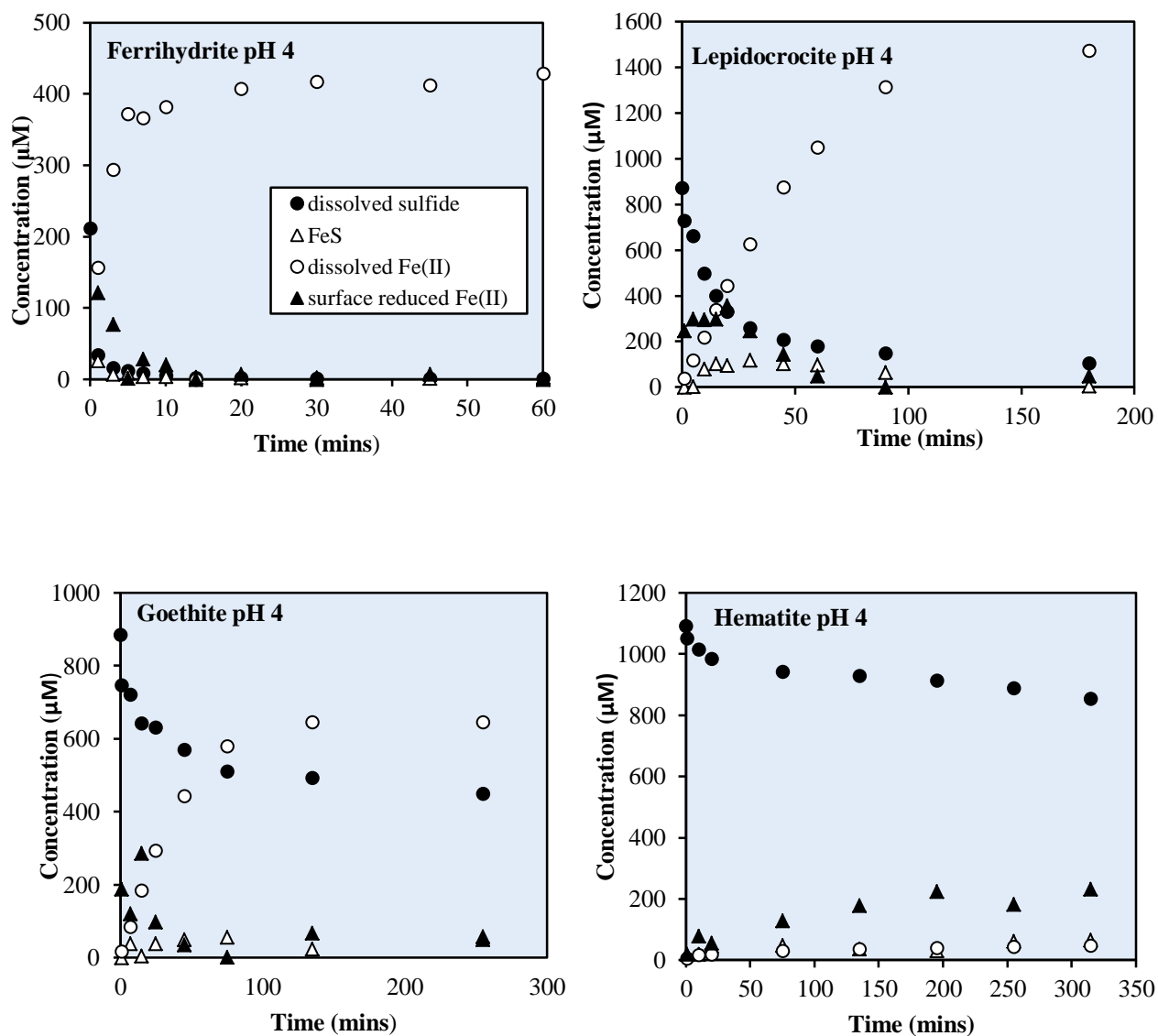


Figure 6.1: Chemical Speciation data for sulfidation experiment, pH 4. Data for surface-reduced Fe calculated from total Fe(II) mass balance

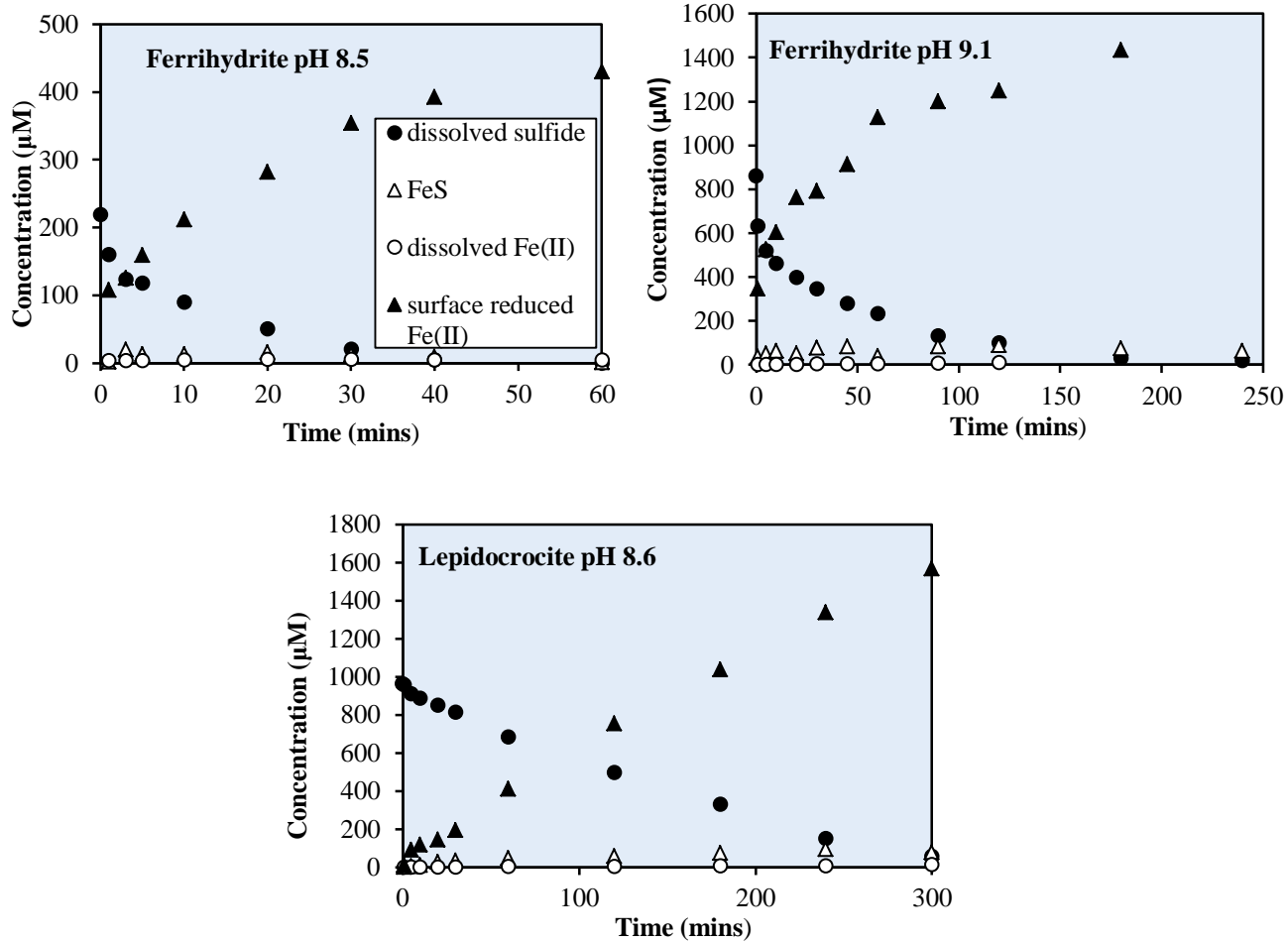


Figure 6.2: Chemical Speciation data for sulfidation experiments, circum-neutral to alkaline pH. Data for surface-reduced Fe calculated from total Fe(II) mass balance

Table 6.2: Initial experimental results: Chemical and raw isotope data (pH 4)

Chemical data							Isotopic Composition						
Sample	Time	S ²⁻ (aq)	FeS	Fe ²⁺ (aq)	Fe ²⁺ (surf)	Total Fe(II)	Dissolved Fe(II) $\delta^{56}\text{Fe}$ (‰)	error (‰)	Surface Fe(II) $\delta^{56}\text{Fe}$ (‰)	error (‰)	Unreacted Fe(III) $\delta^{56}\text{Fe}$ (‰)	error (‰)	Mass Balance (‰)
	(mins)	($\mu\text{M/L}$)		($\mu\text{M/L}$)	($\mu\text{M/L}$)	($\mu\text{M/L}$)	(‰)	±	(‰)	±	(‰)	±	(‰)
Ferrihydrite 1.0g/L; pH 4	0	212											
	1	34	26	157	112	304	-0.14	0.03	-0.20	0.03			
	3	16	7	294	77	378	-0.23	0.05	-0.06	0.02			
	5	12	9	372	1	382	-0.18	0.10	0.16	0.05			
	7	9	4	366	28	398	-0.16	0.06	0.20	0.00			
	10	5	4	382	20	406	-0.10	0.04	0.31	0.02			
	14	2	3	ND	ND	414	-0.08	0.10	0.30	0.01			
	20	2	2	407	7	416	-0.13	0.05	0.28	0.07			
	30	1	2	417	0	418	-0.16	0.03	0.25	0.07			
	45	1	1	412	7	420	-0.10	0.04	0.31	0.02			
60	1	3	429	0	416	-0.12	0.08	0.26	0.04				
Lepidocrocite 0.25g/L; pH 4	0	872											
	1	730	ND	38	246	284	0.34	0.02	0.28	0.08	0.02	0.04	0.05
	5	663	1	117	198	416							
	10	497	79	218	295	592	0.24	0.02	0.16	0.01			
	15	401	102	339	297	738							
	20	330	95	443	356	894	0.18	0.03	0.03	0.08	-0.02	0.03	0.002
	30	258	118	627	247	992							
	45	208	103	876	43	1122	0.06	0.04	0.03	0.08			
	60	178	97	1050	47	1194							
90	149	63	ND	ND	1320	0.05	0.05	0.07	0.05				
180	105	4	1474	48	1526	0.11	0.03						
Goethite 0.5g/L; pH 4	0	885											
	1	747	ND	18	188	206	-0.05	0.03	0.16	0.05	-0.04	0.04	-0.03
	7	722	38	85	121	244							
	15	642	5	185	286	476	0.115	0.05	0.4	0.08			
	25	632	38	294	98	430							
	45	571	50	443	35	528	0.29	0.08	0.53	0.08	-0.02	0.03	0.01
	75	510	56	580	2	638							
	135	493	24	645	67	736	0.25	0.05	0.58	0.01			
255	450	58	646	50	754	0.21	0	0.32	0.09	0.01	0.1	0.04	
Hematite 0.5g/L; pH 4	0	1092											
	1	1051	19	6	19	44	-0.33	0.03	0.27	0.05	0.03	0.01	0.03
	10	10115	19	18	79	116							
	20	985	46	20	56	122	-0.51	0.03	0.20	0.05	0.00	0.07	0.00
	75	942	47	31	128	206	-0.49	0.05	0.29	0.05			
	135	929	37	37	178	252							
	195	913	31	41	224	296	-0.49	0.11	0.36	0.05			
	255	888	61	44	181	286							
315	854	66	47	231	344	-0.51	0.10						

Table 6.3: Initial experimental results: Chemical and raw isotope data (alkaline pH)

Chemical data							Isotopic Composition						
Sample	Time	S ²⁻ (aq)	FeS	Fe ²⁺ (aq)	Fe ²⁺ (surf)	Total Fe(II)	Dissolved Fe(II) $\delta^{56}\text{Fe}$ (‰)	error (‰)	Surface Fe(II) $\delta^{56}\text{Fe}$ (‰)	error (‰)	Unreacted Fe(III) $\delta^{56}\text{Fe}$ (‰)	error (‰)	Mass Balance (‰)
		($\mu\text{M/L}$)		($\mu\text{M/L}$)	($\mu\text{M/L}$)	($\mu\text{M/L}$)		\pm		\pm		\pm	
Ferrihydrite 0.5g/L pH 8.5	0	291											
	1	160	2	4	108	114	-0.55	0.05	-0.63	ND			
	3	124	20	3.9	126	150	-0.61	0.05	-0.52	0.01			
	5	118	13	4.4	159	176	-0.69	0.13	-0.6	0.12			
	10	91	13	4.6	212	230			-0.58	0.16			
	20	51	16	5.8	282	304	-0.59	0.05	-0.64	0.13			
	30	21	12	5.9	354	372	-0.69	0.03	-0.63	0.05			
	40	5	10	5.1	393	408							
60	0	1	4.9	430	436								
Ferrihydrite 0.7g/L; pH 9.1	0	863											
	1	632	38	1.8	346	386	-0.73	0.05	-0.43	0.09	0.05	0.10	0.03
	5	520	53	2.3	525	580							
	10	463	64	2.8	605	672	-0.67	0.04	-0.36	0.12			
	20	400	53	3	764	820							
	30	346	79	4.9	792	876			-0.24	0.07	0.07	0.05	
	45	279	83	6	913	1002							
	60	235	41	5.8	1127	1174	-0.59	0.04	-0.23	0.12			
	90	133	84	8	1200	1292							
	120	102	88	10	1248	1346	-0.68	0.04	-0.15	0.00			
180	30	74	9	1435	1518								
240	19	64	ND	ND	1560	-0.77	0.01	-0.26	0.02	0.05	0.02		
Lepidocrocite 0.3g/L; pH 8.6	0	963											
	1	957	0	0.4	12	12			0.12	0	-0.01	0.05	
	5	911	5	0.1	89	94							
	10	888	11	0.4	117	128			0.14	0.07			
	20	852	26	0.7	143	170	-0.37	0.09					
	30	814	34	1.5	194	230	-0.14	0.02	0.16	0.05	-0.02	0.07	-0.02
	60	685	47	2.7	412	462	-0.09	0.02	0.21	0.09			
	120	496	58	5	755	818							
	180	330	74	7.4	1037	1118	0.02	0.02	0.17	0.06			
	240	150	93	8	1339	1440							
300	56	77	14	1569	1660	0.05	0.02	0.2	0.07	-0.02	0.07	0.08	

6.4.2. Reaction Kinetics

In order to consider assigning different Fe isotope fractionations to Fe (III) oxides with different mineralogy; both the general orders of Fe mineral reactivity and absolute reaction rates of Fe sulfidation were determined with respect to reaction with dissolved sulfide. Poulton (2003) and Poulton *et al.*, (2004) define a rate equation as:

$$R_{\text{Fe}} = k_{\text{Fe}} (\text{H}_2\text{S})_{t=0}^{0.5} (\text{Fe}^{3+})_{t=0} \quad (\text{Eq. 6.7})$$

Where R_{Fe} represents the rate of Fe(II) dissolution ($\text{mol L}^{-1} \text{min}^{-1}$), k_{Fe} is the rate constant ($\text{mol}^{-0.5} \text{L}^{0.5} \text{min}^{-1}$), $(\text{H}_2\text{S})_{t=0}$ is the initial sulfide concentration (mol L^{-1}) and $(\text{Fe}^{3+})_{t=0}$ is the initial concentration of solid phase ferric Fe (mol L^{-1}).

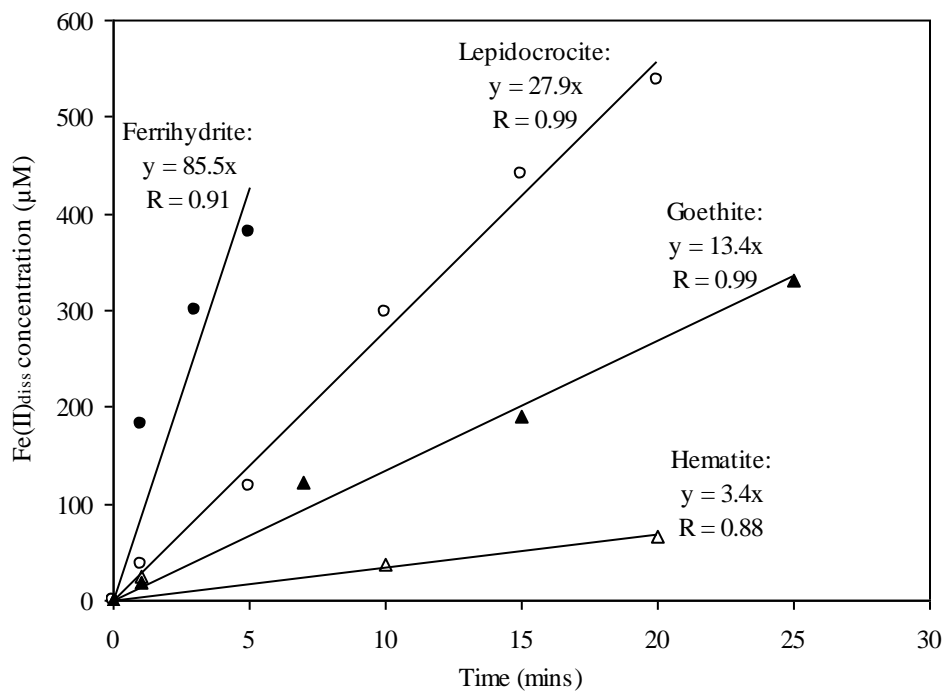


Figure 6.3: Initial linear rates of Fe(II) dissolution for Fe (oxyhydr)oxide minerals (pH 4)

The initial phase of total Fe(II) dissolution (dissolved $\text{Fe}^{2+}_{(\text{aq})} + \text{FeS}$) is shown in Figure 6.3 as linear, and hence the rate of dissolution was determined via simple linear regression. At pH 4, a comparison of calculated rate constants k_{Fe} (Table 6.4) using Eq. 6.7 demonstrates that reactivity increases in the order hematite < goethite < lepidocrocite < ferrihydrite as previously reported in a reactivity scheme devised by Poulton *et al.*, (2004) for experiments at pH 7.5, which also reports that ferrihydrite and lepidocrocite have an increased reactivity compared to the more highly crystalline minerals goethite and hematite, as also shown in Figures 6.1 - 6.3.

Table 6.4. Comparison for rate constant K_{Fe} for Fe(III) oxide mineral reactivity

Fe(III) oxide	Rate, R ($\times 10^{-6}$, $\text{mol L}^{-1} \text{min}^{-1}$)	$(\text{H}_2\text{S})_{t=0}$ ($\times 10^{-6}$, mol L^{-1})	$(\text{Fe}^{3+})_{t=0}$ ($\times 10^{-6}$, mol L^{-1})	K_{Fe} ($\times 10^{-2}$, $\text{mol}^{-0.5} \text{L}^{0.5} \text{min}^{-1}$)
Ferrihydrite	85.5	212	10386	56.5
Lepidocrocite	27.9	872	2811	33.6
Goethite	13.4	885	5622	8
Hematite	3.4	1092	6267	1.6

6.4.3 FeS Formation

The formation of FeS during reductive dissolution is shown in Equation 6.8. After Fe(II) is detached from the reduced surface Fe-oxide, excess $\text{Fe(II)}_{\text{aq}}$ in solution rapidly reacts with free dissolved sulfide in solution to form solid phase FeS:



As also observed in Figure 6.1, FeS formation is transient in solution at pH 4. This is shown further in Figure 6.4 for the individual Fe minerals, where FeS(s) is being formed at different rates due to the differing starting conditions and Fe mineralogy. Peaks in concentration occur between 1-10 mins, followed by a gradual decrease in concentration as the low pH promotes FeS dissolution (at pH 4).

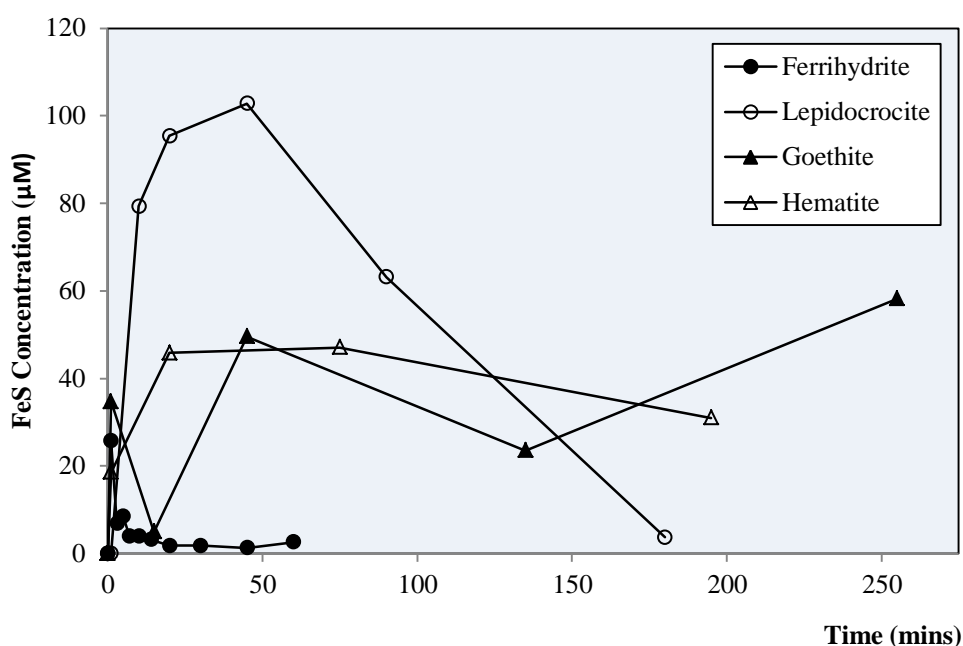


Figure 6.4: FeS formation via iron sulfidation experiments for Fe(III) oxide minerals, pH 4

6.4.4 Fe Isotope data

Iron isotope compositions were determined for dissolved Fe(II), surface reduced Fe(II) (which from here forward includes FeS(s)) and unreacted Fe(III), as reported in Table 6.2 and 6.3. The isotopic mass balance returns an average value close to zero ($0.02 \pm 0.03\%$; Eq. 6.6) for experiments which measured all three Fe pools, validating the experimental approach.

Isotopic data for dissolved Fe(II) and surface-reduced Fe(II) are shown for experiments performed at pH 4 in Figure 6.5. In most cases the dissolved Fe(II) pool is lighter than the solid phase Fe(II) pool, with the exception of the early stages of the reactions with lepidocrocite and ferrihydrite at low pH. The dissolved phase is also lighter than the starting material ($\delta^{56}\text{Fe} = 0$) for ferrihydrite and hematite, whilst for lepidocrocite and goethite the dissolved phases are isotopically heavier than the starting material (0‰), which is also the case at higher pH experiments (Figure 6.6).

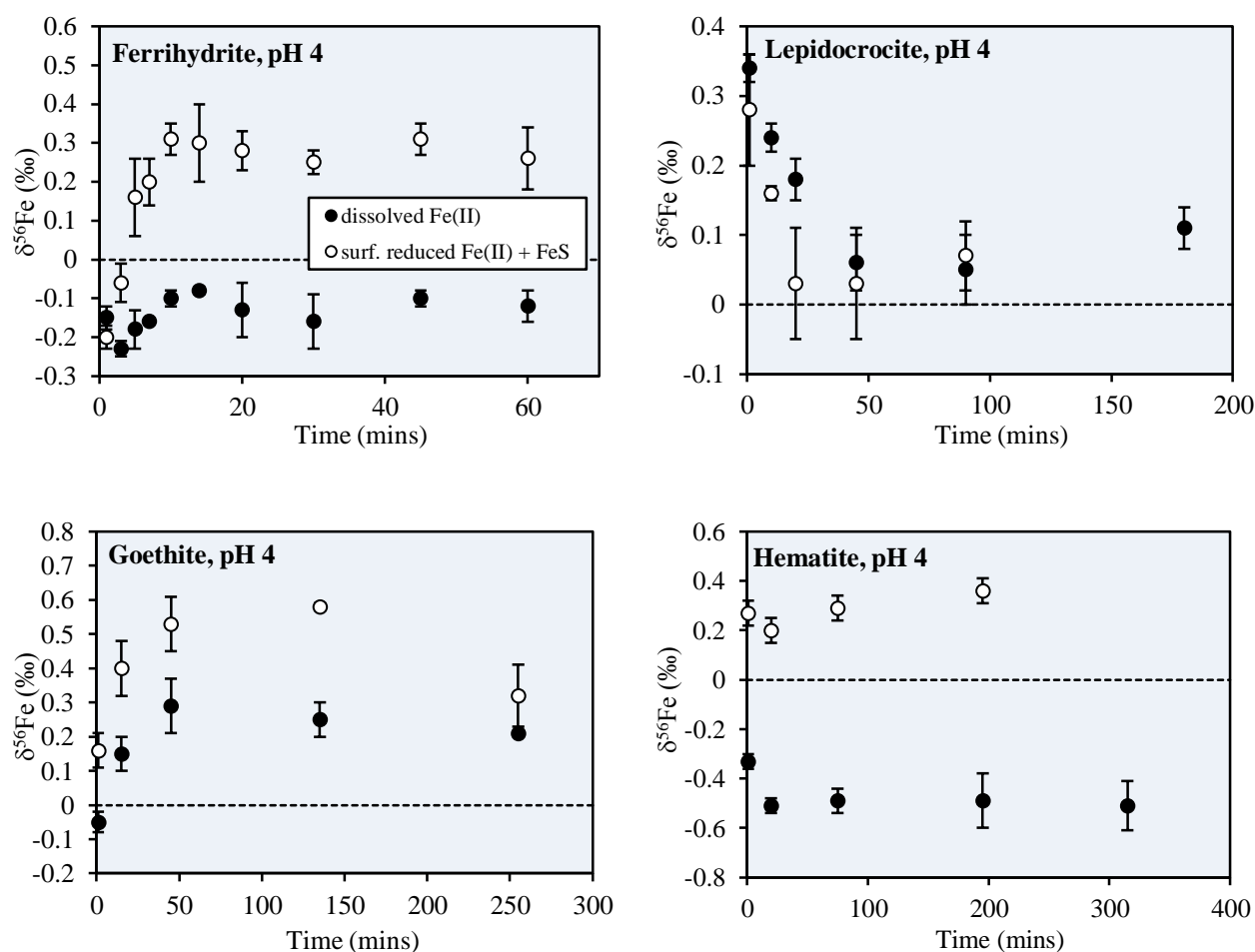


Figure 6.5: Raw data for dissolved $\delta^{56}\text{Fe}$ and surface reduced $\delta^{56}\text{Fe}$ isotopic composition calculated from experimental iron sulfidation

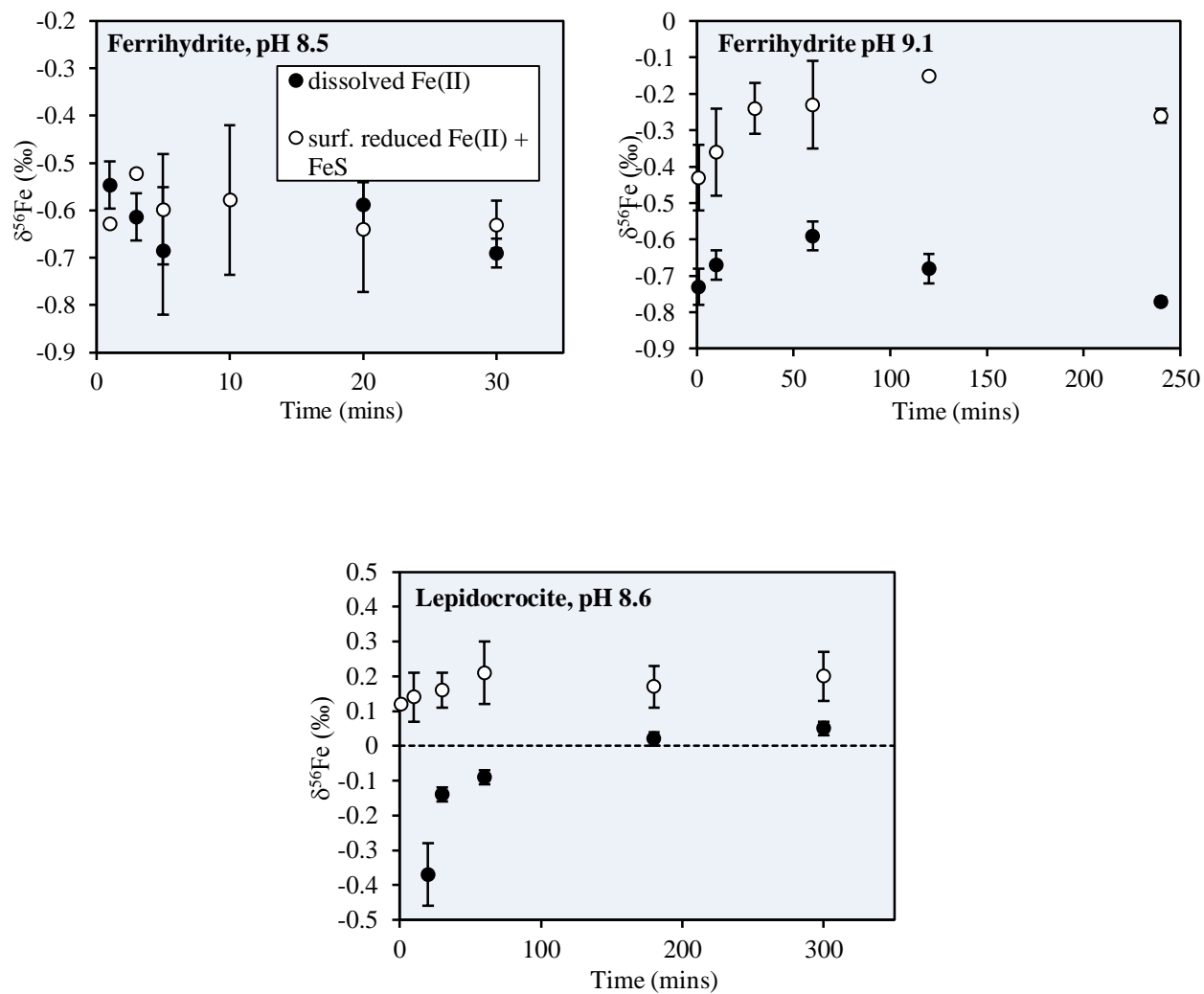


Figure 6.6: Raw data for dissolved $\delta^{56}\text{Fe}$ and surface reduced $\delta^{56}\text{Fe}$ isotopic composition calculated from experimental iron sulfidation

6.5. DISCUSSION

Figures 6.5 and 6.6 suggest that the sulfide promoted reductive dissolution of Fe(III) oxide minerals results in a discernable unidirectional kinetic isotope fractionation, defined by the observation that experiments are still in progress with dissolved sulfide still in solution after the last sample has been taken from the vessel (with the exception of ferrihydrite, pH 4). It is important to consider specific experimental influences which may control the isotopic fractionation measured, and also to evaluate individual steps of the reaction mechanism for their influence on the overall fractionation determined.

6.5.1. Mechanistic Controls on Isotopic Fractionation (I)

6.5.1.1. Reduction Step

The reduction of Fe(III) on the reactive oxide mineral surface to surface bound Fe(II) is the first step of the reaction presented by Dos Santos Afonso & Stumm (1992), and is likely to initiate a significant isotopic fractionation. During the electron transfer process occurring during the reduction of Fe(III) to Fe(II), an isotopic fractionation will occur. As all Fe(II) measured within the system (either as dissolved, surface or via FeS formation) has undergone an electron transfer between Fe(III)-Fe(II), taking place on the oxide surface, mass balance calculations have been derived to evaluate whether an individual step produces a significant isotopic fractionation (Equation 6.9)

$$\delta^{56}\text{Fe}_{\text{reductive-step}} (\text{‰}) = \left(\frac{\text{Fe(II)}_{\text{diss}}}{\text{Fe(II)}_{\text{total}}} \times \delta^{56}\text{Fe}_{\text{diss}} \right) + \left(\frac{\text{Fe(II)}_{\text{solid-phase}}}{\text{Fe(II)}_{\text{total}}} \times \delta^{56}\text{Fe}_{\text{solid-phase}} \right)$$

(Eq. 6.9)

Where Fe_{diss} represents dissolved Fe(II) and $\text{Fe}_{\text{solid-phase}}$ represents surface-reduced Fe(II) plus $\text{FeS}_{(s)}$. During the reduction of poorly crystalline ferrihydrite, the composition of surface bound Fe(II) is isotopically light, whereas with more crystalline minerals (lepidocrocite, goethite, hematite) the fractionation processes produce $\delta^{56}\text{Fe}$ values which are isotopically heavier than non crystalline species and the starting material. This observation is surprising as previous studies of both biological and abiological reductive dissolution of Fe oxide minerals (Icopini *et al.*, 2004; Crosby *et al.*, 2005; 2007; Johnson *et al.*, 2005; Wiederhold *et al.*, 2006) suggest that lighter isotopes preferentially undergo Fe dissolution.

It is likely that the preferential reduction of Fe(III) in forming heavier Fe isotopes relates to isotopic inhomogeneity of the more crystalline oxide minerals, compared to that of poorly crystalline ferrihydrite. Previous studies of partial dissolution of Fe oxides using HCl have tended to show that most Fe oxides are isotopically homogenous (Bullen *et al.*, 2001; Brantly *et al.*, 2004). However, it is unclear how sulfide behaves in terms of evenly reducing the outer most reactive mineral layers, and thus a comparison with reducing species other than sulfide (Skulan *et al.*, 2002; Wiederhold *et al.*, 2006; Crosby *et al.*, 2007) is not appropriate. Therefore, with sulfide present as a reductant, it is possible that reduction Fe(III) to obtained heavy isotopes on the mineral surface occurs initially during this reaction.

In contrast to lepidocrocite, goethite and hematite, the behaviour of ferrihydrite is consistent with the isotopically light Fe isotopes being favoured during the reductive step. Figure 6.7 shows the average $\delta^{56}\text{Fe}$ fractionations during the reductive step for ferrihydrite as a function of the initial reduction rate. For these experiments at different pH values, there is no consistent trend in the extent of fractionation as each reaction

progresses. Hence it is not simply the extent of reduction of surface layers that controls the magnitude of the reductive step fractionations. If this were the case, then for all experiments, the $\delta^{56}\text{Fe}$ value of surface bound isotopes would rapidly approach zero at an early stage of the reaction. An increase in magnitude of the reductive step fractionation is only observed for the experiment at pH 9.1, where a significant proportion of the mineral is reduced with only minor release of Fe(II) to solution. Therefore, it is clear that the lighter isotope is initially favoured during reduction but the retarded dissolution of the surface-reduced Fe(II) at high pH means that there are progressively fewer surface sites containing the lighter isotope available for reaction; hence, reduction of the heavier isotope becomes more significant with time.

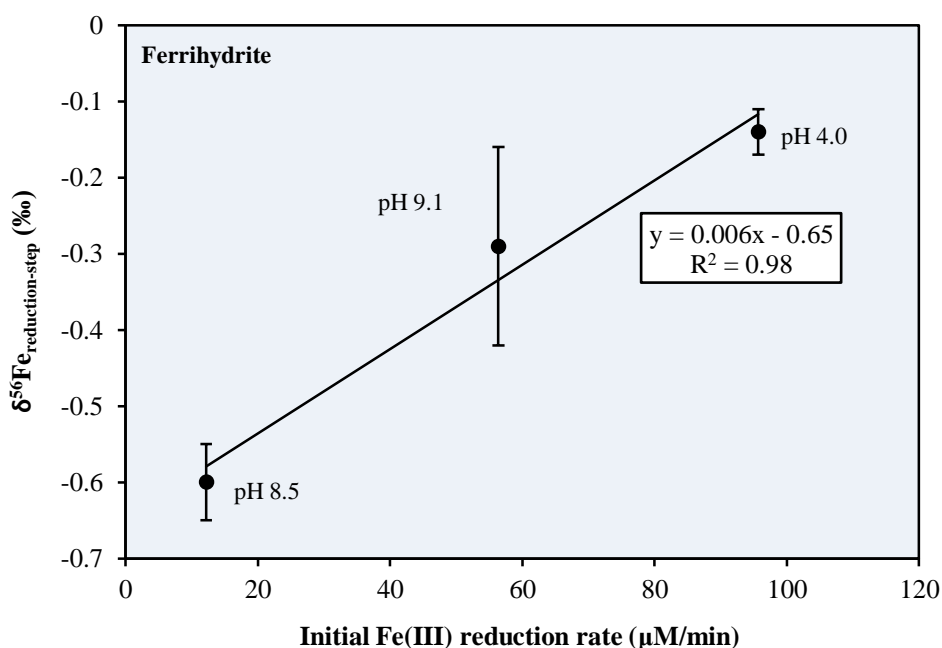


Figure 6.7: Surface reduced $\delta^{56}\text{Fe}$ fractionation as a function of initial reduction rate

Given these considerations, the relationship we observe in Figure 6.7, where the value of isotopic fractionations for the reductive step are plotted as a function of the initial

reduction rate for ferrihydrite, suggests that it is the *rate* at which the oxide surface is reduced that initially controls the extent of fractionation during the reductive step, with slower rates favouring larger fractionations. The magnitude of fractionation will thus be a function of the parameters that control reaction rates, including mineral surface area and concentration, sulfide concentration, and pH (Pyzik & Sommer, 1981; Dos Santos Afonso & Stumm, 1992; Peiffer, 1992; Yao & Millero, 1996; Poulton, 2003; Poulton *et al.*, 2004).

Previously, it has been assumed that only the dissolution step will become isotopically lighter than the surface reduced Fe(II) (and indeed, the starting material) during abiotic reductive dissolution of Fe (III) oxides (Wiederhold *et al.*, 2006). It is possible that extensive dissolution of the light $\delta^{56}\text{Fe}$ isotope (in preference to the heavier isotope) would give an overall isotopically light composition, due to continual dissolution of the lighter isotope from the oxide surface (if this process preferentially exposes the lighter isotope for subsequent reaction at the mineral surface). However, we observe significant enrichment of the lighter isotope during the reductive step, even for experiments where the dissolved Fe(II) pool (Fe_{diss} plus FeS) represents a very minor proportion of the total Fe(II) pool (e.g. ferrihydrite at pH 8.5; Table 6.3). The overwhelming influence of the surface-reduced Fe(II) pool suggests that the reductive step favours the lighter isotope. These observations provide support for the suggestion that larger fractionations, producing heavier isotopes calculated for lepidocrocite, goethite and hematite are a likely consequence of isotopic inhomogeneity. The precise process responsible for the preferential reduction of the lighter isotope is currently unclear, but may relate to an increased propensity for electron transfer to occur between the lighter isotope and adsorbed sulfide (Equation 6.2), or to an increased prevalence for the lighter Fe isotope to occupy sulfide adsorption sites (Equation 6.1).

6.5.2 Dissolution and Effect of Adsorption

When calculating isotopic fractionations during the dissolution step, it is important to consider co-occurring significant chemical processes which may influence dissolved and solid phase isotopic fractionations, for example the role of possible adsorption of dissolved Fe(II) at the oxide surface. This process has been suggested to result in $\delta^{56}\text{Fe(II)}_{\text{aq}} = < -2.6 \text{ ‰}$ in comparison to the starting oxide substrate in a natural circumneutral groundwater, attributable to preferential adsorption of isotopically heavier Fe(II) (Teutsch *et al.*, 2005) to mineral surfaces. Experiments evaluating isotopic fractionations during adsorption of dissolved Fe(II) onto goethite support this observation and suggest that rapid isotopic exchange occurs between dissolved and adsorbed Fe(II), resulting in an isotopic fractionation whereby adsorbed Fe(II) is enriched by $\sim 2.7\text{-}3.7\text{‰}$ relative to dissolved Fe(II) at equilibrium (Icopini *et al.*, 2004).

However, adsorption of Fe(II) on to Fe (oxyhydr)oxide surfaces at pH 4 is negligible (Zhang *et al.*, 1992; Silvester *et al.*, 2005) and unlikely to exert an influence on our experiments at low pH. At higher pH, Poulton (2003) demonstrates that adsorption of Fe(II) would also not be significant, providing sulfide is still present in solution at time of sampling. For experiments undertaken within this study at alkaline pH, isotopic measurements were only made for samples taken while sulfide was still present in solution, as presented in Table 6.2. The occurrence of adsorption is minimised as under these conditions, FeS forms almost instantaneously (Rickard, 1995) and any dissolved Fe(II) that has detached from the outer sphere of the oxide surface is unlikely to be re-adsorbed. The prevalence for surface-reduced Fe to remain associated with the oxide surface for considerable periods of time at alkaline pH (Poulton, 2003), itself prevents extensive re-adsorption of Fe(II) by blocking reactive Fe(III) adsorption sites. These observations find support in direct measurements of adsorbed Fe(II) during sulfidation reactions with ferrihydrite at alkaline pH (using CaCl_2 as an extractant for adsorbed

Fe(II)), whereby even at the end of experiments when dissolved sulfide was completely reacted from solution, adsorbed Fe(II) accounted for <2% of the total Fe(II) pool (Poulton, 2003). After all dissolved sulfide has reacted from solution, Fe(II) associated with the oxide surface continues to decrease (due to the slow dissolution of surface-reduced Fe(II)), rather than increase due to adsorption of dissolved Fe(II)). Therefore re-adsorption of dissolved Fe(II) may be discounted as a significant factor in all of our experiments.

6.5.3 FeS formation

A further consideration includes the formation of solid phase FeS from experimental reagents. Although experiments were conducted with the aim of minimizing formation of FeS_(s), this phase was present in all experiments, and in some cases represented a significant proportion of the total Fe(II) pool (Table 6.2/Table 6.3; Figure 6.4). Formation of FeS from dissolved Fe(II) (Equation 6.8) is associated with a large isotopic fractionation, with freshly precipitated FeS $< 0.85 \pm 0.30\%$ lighter than the dissolved Fe(II) from which it was formed (Butler *et al.*, 2005). Therefore, FeS formation has the potential to significantly overwhelm both dissolved Fe(II) and surface-reduced isotopic compositions.

In order to assess fractionations associated with the dissolution of the Fe (oxyhydr)oxides, rather than introducing secondary fractionations associated with FeS formation, dissolved Fe(II) data for FeS formation (Table 6.3) has been corrected using the formulae derived in Equations 6.10 and 6.11, assuming an isotopic fractionation of $\delta^{56}\text{Fe} = -0.85 \%$ for freshly precipitated FeS (Butler *et al.*, 2005).

FeS-Fe(II)_{diss} correction

$$\delta^{56}\text{Fe}_{\text{diss-corr}} = \left(\frac{\text{Fe}^{2+\text{diss}}}{\text{FeS} + \text{Fe}^{2+\text{diss}}} \times \delta^{56}\text{Fe}_{\text{diss}} \right) - \left(\frac{\text{FeS}}{\text{FeS} + \text{Fe}^{2+\text{diss}}} \times 0.85 \right)$$

(Eq. 6.10)

FeS-Fe(II)_{surf} correction

$$\delta^{56}\text{Fe}_{\text{surf-corr}} = \left(\frac{\text{Fe}_{\text{surf}}}{\text{FeS} + \text{Fe}_{\text{surf}}} \times \delta^{56}\text{Fe}_{\text{surf}} \right) - \left(\frac{\text{FeS}}{\text{FeS} + \text{Fe}_{\text{surf}}} \times 0.85 \right)$$

(Eq. 6.11)

Due to the low concentrations of FeS present, correcting data had little significant impact on dissolved Fe(II) fractionations, with the exception of lepidocrocite at pH 8.6 (Figure 6.4). For lepidocrocite, high concentrations of FeS relative to dissolved Fe(II) resulted in the corrected data being $\delta^{56}\text{Fe} \approx -0.7\text{--}0.8\text{‰}$ lighter than the measured Fe(II) compositions in Tables 6.2 and 6.3. Thus, for the majority of experiments, minor variations in the isotopic composition of the precipitated FeS will not significantly alter either our calculations of absolute fractionations or our conclusions

6.5.4 Mechanistic Controls on Isotopic Fractionation (II)

From our corrected dissolved Fe(II) data (Table 6.5), fractionations associated with the dissolution step of the reaction can be calculated, by subtracting fractionations resulting from the initial reductive step:

$$\Delta^{56}\text{Fe(II)}_{\text{diss-step}} = \delta^{56}\text{Fe(II)}_{\text{diss}} - \delta^{56}\text{Fe(II)}_{\text{reduction-step}}$$

(Eq. 6.12)

The resulting overall dissolution-step fractionations are reported in Table 6.5. In general, the magnitude of fractionations remain relatively constant during the course of each reaction, and in all cases the dissolution step results in the release of Fe which is isotopically-lighter than that produced during the reduction step.

This is consistent with evidence suggesting that reductive dissolution releases isotopically-light Fe(II) to solution, in comparison to surface reduced Fe(II), regardless of the precise reductive mechanism (Beard *et al.*, 1999; 2003; Brantley *et al.*, 2004; Icopini *et al.*, 2004; Crosby *et al.*, 2005; Johnson *et al.*, 2005; Wiederhold *et al.*, 2006; Crosby *et al.*, 2007). By also quantifying isotopic fractionations associated with the initial reductive step, the magnitude of fractionations attributable to the dissolution step alone are rigorously determined. In understanding the controls on isotopic fractionations during this step, it is important to consider the influence of reaction rates. Figure 6.8 demonstrated that for experiments performed at pH 4, the concentration of Fe(II) which had entered solution (i.e. dissolved Fe(II) plus FeS) produced a linear relationship with regard to the total reduced Fe(II) pool, allowing rates of dissolution of the reduced Fe(II) to be estimated by simple linear regression. Whilst the linear plots are not considered statistically significant (mostly below 95% confidence interval), the data points towards a general covariance between total Fe(II) and FeS+ Fe(II). When the resulting rates are considered in terms of isotopic fractionations determined for the dissolution step (Table 6.5), a general relationship is observed (Figure 6.9), although not statistically correlating (Table 6.6), possibly suggesting that dissolution-step fractionations are controlled by dissolution rates, regardless of the precise mineralogy of the (oxyhydr)oxide.

Dissolution rates are also strongly controlled by pH, with rates being faster at low pH (Pyzik & Sommer, 1981; Peiffer &., 1992; Yao & Millero, 1996; Poulton, 2003) due to increased surface protonation, which causes a polarization and weakening of the metal-oxygen bonds (Zinder *et al.*, 1986; Suter *et al.*, 1991). Experiments for individual minerals at different pH values show that average fractionations for the dissolution step increase at higher pH for both ferrihydrite and lepidocrocite (Table 6.5), thus providing support for the dissolution rate control on isotopic fractionations proposed above.

Table 6.5: Corrected isotopic composition for reduction and dissolution during iron sulfidation

Sample	Time (mins)	Reduced fraction (%)	Fe(II)diss $\delta^{56}\text{Fe}$ (‰)	Reduction step $\delta^{56}\text{Fe}$ (‰)	Dissolution step $\delta^{56}\text{Fe}$ (‰)	$\Delta\text{Fe(diss)-Fe(solid)}$ (‰)
Ferrihydrite 1.0g/L; pH 4	1	2.9	-0.25	-0.17	-0.08	-0.26
	3	3.6	-0.24	-0.19	-0.05	-0.25
	5	3.7	-0.2	-0.17	-0.03	-0.21
	7	3.8	-0.17	-0.13	-0.04	-0.18
	10	3.9	-0.11	-0.08	-0.03	-0.11
	20	4	-0.13	-0.12	-0.01	-0.14
	30	4	-0.16	-0.16	0	-0.17
	45	4	-0.1	-0.09	-0.01	-0.1
	60	4	-0.13	-0.12	-0.01	-0.14
Lepidocrocite 0.25g/L; pH 4	10	21	-0.05	0.29	-0.24	-0.06
	20	32	0	0.19	-0.1	0
	45	40	-0.04	0.1	-0.09	-0.06
	180	54	0.11	0.05	ND	0.23
Goethite 0.5g/L; pH 4	1	3.7	ND	0.14	ND	ND
	15	8.5	0.12	0.3	-0.18	0.12
	45	9.4	0.17	0.33	-0.16	0.19
	135	13	0.21	0.29	-0.08	0.24
	255	13	0.12	0.23	-0.11	0.14
Hematite 0.5g/L; pH 4	1	0.7	-0.72	0.19	-0.91	-0.72
	20	2	-0.75	0.08	-0.83	-0.76
	75	3.3	-0.71	0.17	-0.88	-0.72
	195	4.7	-0.61	0.24	-0.85	-0.62
Ferrihydrite 0.5g/L pH 8.5	1	2.2	-0.65	-0.59	-0.06	-0.65
	3	2.9	-0.81	-0.52	-0.29	-0.81
	5	3.4	-0.81	-0.6	-0.21	-0.81
	20	5.8	-0.78	-0.64	-0.14	-0.78
	30	7.2	-0.8	-0.63	-0.17	-0.8
Ferrihydrite 0.7g/L; pH 9.1	1	5.3	-0.84	-0.43	-0.41	-0.85
	10	9.2	-0.84	-0.36	-0.48	-0.85
	60	16	-0.82	-0.23	-0.59	-0.83
	120	19	-0.83	-0.15	-0.69	-0.84
Lepidocrocite 0.3g/L; pH 8.6	30	6.8	-0.81	0.16	-0.97	-0.82
	6	15	-0.8	0.21	-1.01	-0.81
	180	33	-0.77	0.17	-0.94	-0.79
	300	49	-0.71	0.2	-0.91	-0.73

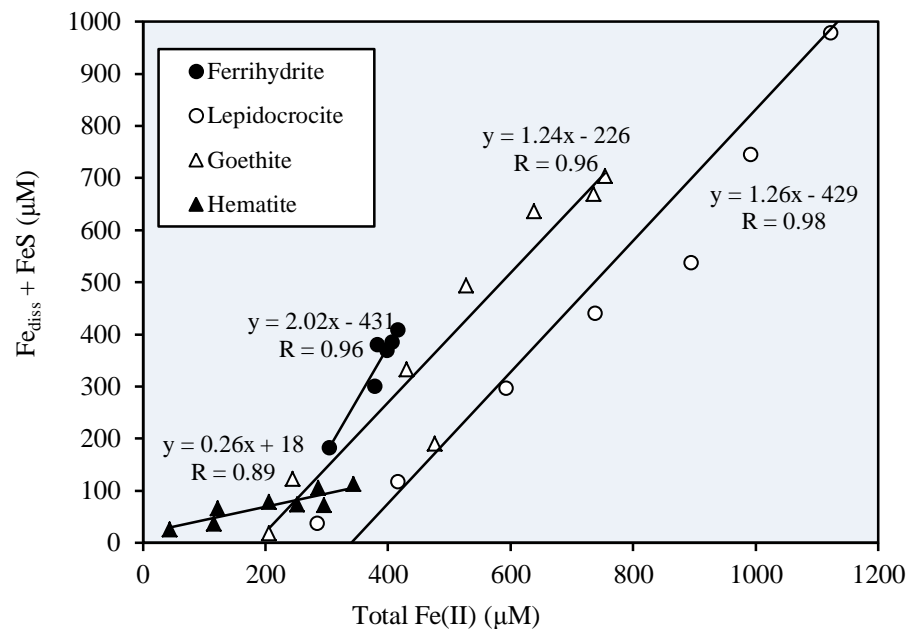


Figure 6.8: Rate of Fe(II) dissolution (pH 4)

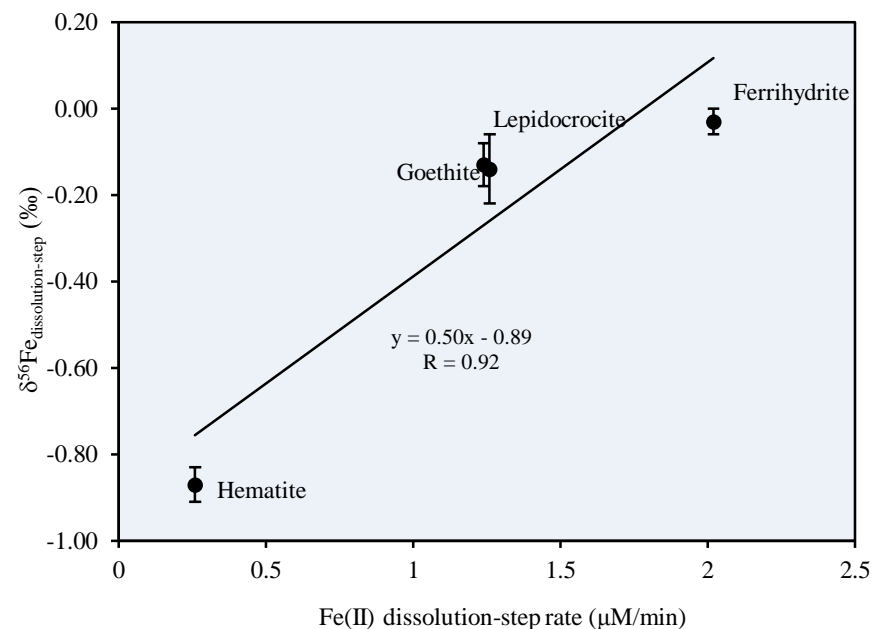


Figure 6.9: Linear relationship of dissolution- $\delta^{56}\text{Fe}$ isotopic fractionation as a function of Fe(II) dissolution rate (pH 4)

Table 6.6: Collated statistical data representing correlation of linearity of synthetic mineral experiments: F Test Vs Levenes Test

Figure	Name	Slope	R^2		Calculated P value (F test)	Levenes Test of Correlation (P value)	Confidence (%)	Accept/Reject Null Hypothesis
			Excel	R^2 Minitab				
6.8	Ferri	$y=2.02x - 431$	0.9216	0.93	0.085	0.357	64.3	R
	Lepi	$y= 1.26x - 429$	0.9604	0.97	0.472	0.376	62.4	R
	Goethite	$y= 1.24x - 226$	0.9216	0.98	0.622	0.585	41.5	R
	Hematite	$y= 0.26x + 18$	0.7921	0.8	0.004	0.007	99.3	A

6.5.5 Applications to Natural Environments

From this experimental work, it is important to evaluate the data reported in terms of applications to both modern sedimentary environments, and the ancient rock record. Firstly, the reaction of dissolved sulfide with Fe (oxyhydr)oxide minerals during marine sediment diagenesis may result in porewater dissolved Fe(II) isotopic compositions as light as $\delta^{56}\text{Fe}_{(\text{II})\text{aq}} = -0.8 \text{ ‰}$ (Table 6.5). Fractionations of this magnitude would be most likely to occur in the upper parts of organic-rich marine sediments, where despite sulfide production via sulfate reduction, concentrations of free sulfide are buffered by reaction with the most reactive Fe (oxyhydr)oxides (e.g. ferrihydrite; Canfield *et al.*, 1992; Poulton *et al.*, 2004). In this ferruginous zone (Canfield & Thamdrup, 2009), the lack of dissolved sulfide in porewaters may prevent extensive FeS formation, which would not reflect the light isotopic compositions of the dissolved Fe(II) pool (Butler *et al.*, 2005). Furthermore, our experiments at different pH values suggest that fractionations for individual minerals increase as pH increases (Table 6.5). Thus, with regard to the less reactive minerals such as hematite, the fractionations of around -0.7 ‰ observed at pH 4.0 (Table 6.5) may translate to significantly larger fractionations at the higher pH values characteristic of marine sediment porewaters.

Considering that the isotopic compositions of Fe (oxyhydr)oxide minerals supplied to marine sediments are not well constrained, it is also helpful to evaluate fractionations between dissolved Fe(II) and solid phase Fe (which includes unreacted Fe and surface-reduced Fe(II)), since these parameters are commonly measured or modelled in studies of modern marine sediments (Severmann *et al.*, 2006; Staubwasser *et al.*, 2006).

Fractionations between dissolved Fe(II) and solid phase Fe are presented as $\Delta^{56}\text{Fe}_{\text{Fe(diss)} - \text{Fe(solid)}}$:

$$\Delta^{56}\text{Fe}_{\text{Fe(diss)} - \text{Fe(solid)}} = \delta^{56}\text{Fe(II)}_{\text{diss}} - \delta^{56}\text{Fe}_{\text{solid}} \quad (\text{Eq. 6.13})$$

where $\delta^{56}\text{Fe(II)}_{\text{diss}}$ is the dissolved Fe(II) isotopic composition corrected for FeS precipitation (Table 6.7) and $\delta^{56}\text{Fe}_{\text{solid}}$ is the solid phase Fe isotopic composition calculated by mass balance.

Table 6.7: Fe isotope fractionation associated with sulfide mediate reductive dissolution

Sample	Reduction step $\delta^{56}\text{Fe}$ (‰)	error ±	Dissolution step $\delta^{56}\text{Fe}$ (‰)	error ±	$\Delta\text{Fe(diss)-Fe(solid)}$ (‰)	error ±
Ferri pH 4	-0.14	0.04	-0.03	0.03	-0.17	0.06
Lepi pH 4	0.16	0.11	-0.14	0.08	0.04	0.17
Goe pH 4	0.26	0.08	-0.13	0.05	0.17	0.05
Hem pH 4	0.17	0.07	-0.87	0.04	-0.71	0.06
Ferri pH 8.5	-0.60	0.05	-0.17	0.09	-0.77	0.07
Ferri pH 9.1	-0.29	0.13	-0.54	0.12	-0.84	0.01
Lepi pH 8.6	0.19	0.02	-0.96	0.04	-0.79	0.04

The resulting fractionations are reported in Table 6.7. However, since for the majority of experiments where a significant fractionation was evident, only a relatively minor proportion of the mineral was dissolved, the calculated $\delta_{\text{Fe(diss)} - \text{Fe(solid)}}$ fractionations do not differ greatly from the dissolved Fe(II) compositions (Table 6.7). Thus, maximum $\Delta^{56}\text{Fe}_{\text{Fe(diss)} - \text{Fe(solid)}}$ fractionations of around -0.85‰ might be expected in marine sediments as a consequence of sulfide-promoted reductive dissolution of Fe(III) oxides.

6.6 SUMMARY

- Tracing the isotopic fractionation of $\delta^{56}\text{Fe}$ isotopes during sulfide promoted reductive dissolution would offer a novel abiotic mechanism of $\text{Fe}^{2+}_{(\text{aq})}$ formation in sedimentary pore waters and ferruginous water columns; significant to both modern marine near surface sedimentary systems and within the ancient rock record.
- The experimental sulfidation of synthetic ferrihydrite, lepidocrocite, goethite and hematite minerals under anoxic conditions produces an isotopic fractionation $\delta^{56}\text{Fe} < -0.8\text{‰}$.
- The individual processes of Fe(III)-Fe(II) reduction on Fe(III) oxide surfaces; and the dissolution of $\text{Fe}(\text{OH})_2^+$ as $\text{Fe}(\text{II})_{\text{aq}}$, create significant isotopic fractionations associated with changing redox state and bonding environment .
- Factors likely to influence the magnitude of isotopic fractionation have been dismissed; primarily the isotopic effects of $\text{Fe}(\text{II})_{\text{aq}}$ re-adsorption to the oxide mineral surface, discouraged by omnipresence of HS^- in solution, allowing continual Fe(III) reduction and dissolution on the reactive surface site of the mineral; and the precipitation of FeS in solution, measured as solid phase Fe(II), the presence of which has been determined to be isotopically insignificant to the magnitude of fractionation occurring during sulfide mediated reductive dissolution.
- In comparison to the isotopic fractionation associated with well characterised, microbially derived $\text{Fe}^{2+}_{(\text{aq})}$, (DIR; $\delta^{56}\text{Fe} = -1.3\text{‰}$), the measured fractionation associated with the abiotic dissolution of $\text{Fe}^{2+}_{\text{aq}}$ from Fe(III) oxide minerals must be considered upon evaluating the redox cycling of Fe species in sedimentary systems upon early diagenesis.

7. CONCLUSIONS and FUTURE WORK

7.1 OVERALL SUMMARY

Previous laboratory based studies regarding sulfide mediated reductive dissolution have strived to represent a model Fe-bearing mineral reactivity within the natural environment, following either redox cycling within anoxic near-surface marine sediments, or in describing euxinic water columns. By defining the mechanisms with which individual Fe carbonate, oxide and silicate minerals react to reduce and dissolve in marine environments, it has been hoped that a simplistic view of continual iron recycling may be presented by the changing morphology of iron minerals within natural sediment assemblages. In order to do this, the rates at which iron within natural assemblages undergoes reductive dissolution with BSR produced dissolved sulfide occurs during periods of early sediment diagenesis were derived. The most widely recognised schemes of iron mineral reactivity (developed from Canfield, 1989; Canfield *et al.*, 1992; Poulton *et al.*, 2004) evaluate the rates of sulfidation for a variety of Fe(III) oxide and silicate minerals, classifying minerals based on their ability to react with dissolved sulfide present in porewaters or within an adjacent water column. However, early investigations of Fe(III) reductive dissolution within natural sedimentary assemblages (Postma, 1993; Larsen *et al.*, 2006) was based on evaluating the reaction mediated by an organic ligand (ascorbate) which is not significantly observed within marine environments.

Therefore, the main objective of this body of work was to contribute to the understanding of Fe redox cycles within marine environments by reproducing well validated sulfidation experiments using both individual synthetic Fe-bearing minerals and naturally Fe-rich sediments. The results obtained describe a variety of mechanisms

relating to the reductive dissolution of both pure synthetic Fe-bearing minerals, and naturally Fe- abundant marine sediments from a variety of marine settings including: modern sediment cores from *Aarhus Bay*, Denmark and the *Umpqua River continental shelf*, N. Pacific; and ancient iron carbonate samples from Biwabik Iron Formation, N. America (~1.8Ga); and also give further insight into mechanisms of FeS formation under sulfidation conditions.

i) Experimental sulfidation of Fe-rich sediment cores

The kinetic results of batch sulfidation reactions were compared between a variety of individual synthetic, pure Fe(III) oxides (ferrihydrite, goethite, magnetite) known to react over different times scale with respect to dissolved sulfide reactivity (mins-hours-days); with two sediment cores, the Fe-abundant content of which was characterised to define the class of Fe species as characterised within Poulton & Canfield, (2005). Using the rate equation defined by Postma (1993), rate constant values (K, s^{-1}) were assigned for individual Fe(III) minerals during both the reductive and dissolution stages of the reaction mechanism. The values obtain experimentally describe the decrease (or slowing) of rate constants alongside decreasing Fe(III) mineral reactivity with dissolved sulfide down core; and are reflected in the reactivity of specific characterised sediment assemblages, with respect to both $FeOx_1$ phases (ferrihydrite) and $FeOx_2$ phases (goethite). Hence, a record of mineralogy throughout a near surface sediment core can be determined via sulfidation with respect to the rate of reactivity with dissolved sulfide, as seen in comparing to 1) a sediment with little change in morphology, and hence reactivity over time 2) a sediment core which changes significantly over time.

The results reported in Chapter 4 provide a robust data set in which (for the first time) rates of iron reductive dissolution within natural sediment assemblages can be measured using well constrained laboratory procedures. Sediments can also be partially characterised by identical experiments sulfidizing individual synthetic Fe(III) oxide minerals, the rate of which occurs over similar orders of magnitude and has not previously been achieved experimentally. On a larger scale, where these reactions occur within the marine environment, a greater understanding of the geochemical cycling of Fe and S (and their subsequent reaction to form pyrite) is obtained by identifying the rates at which these reactions occur, which in turn controls the the flux of highly reactive Fe(II) into adjacent bottom waters and porefluids, and further influencing the precipitation and abundance of FeS species at the sediment-water boundary.

ii) Experimental dissolution of iron carbonate minerals within sulfidic environments

The experimental data reported within this novel study of siderite dissolution (Chapter 5) suggests that under sulfidic conditions, Fe carbonate species may significantly contribute to the availability of Fe(II)_{aq} in natural aquatic settings, also forming FeS reduced waters which contain siderite. This reaction likely occurs due to a direct substitution of sulfide for carbonate in the siderite structure, with the rate of reactivity of both synthetic and naturally occurring siderite with dissolved sulfide rapid (half life = 22 minutes and ~ 20 hours respectively) compared to the reactivity of the majority of commonly occurring Fe(III) oxide minerals. Hence, within ancient environments of transient euxinia, reaction with iron formations containing a high abundance of siderite would have enhanced Fe(II) cycling in ferruginous/euxinic waters. By utilising the same

sulfidation experimentation and rate equation associated with the reductive dissolution of Fe(III) oxides, a direct comparison between Fe carbonate and Fe oxide reactivity can be made, with regard to the reactivity scheme derived by Poulton *et al.* (2004), indicating that Fe carbonates dissolve at a faster rate than most crystalline Fe(III) oxide minerals, over a timescale of minutes. This indicates that Fe carbonates are suitable to be classed as ‘highly reactive’, and this premise holds even for ancient, highly crystalline siderite.

iii) Iron isotope fractionation during sulfide promoted reductive dissolution

The experimental tracing of Fe isotopes associated with solid phase iron minerals, and Fe(II) dissolved from the mineral surface during the sulfide-promoted reductive dissolution of Fe (oxyhydr)oxide minerals, provides new detail on the mechanisms driving the abiotic isotopic fractionation of iron species. Significant fractionations are evident during both the reductive step and the dissolution step of the reaction, with the magnitude of fractionation dependent on the nature of the Fe mineral and the geochemical processes controlling reaction rates. During dissimilatory Fe reduction, isotopic measurements of Fe(II)_{aq} tend to be -0.5 to -2.5‰ lighter than the starting Fe (oxyhydr)oxide mineral, but with the sum of all fractionation factors approximating -1.3‰ (Beard *et al.*, 1999; 2003; Icopini *et al.*, 2004; Crosby *et al.*, 2005; 2007; Johnson *et al.*, 2005). The isotopic data presented in Chapter 6 implies that $\Delta^{56}\text{Fe}$ values $> -0.8\text{‰}$ between the surface reduced Fe mineral and Fe(II) dissociated from the surface into solution may be achieved through abiotic reductive dissolution mechanisms during marine sediment diagenesis. This implies that biological isotopic fractionations of around -1‰ are required to provide an upper limit for the robust identification of active dissimilatory Fe reduction in modern and ancient settings.

It is not only in comparison to biologically mediated fractionations that the data presented in Chapter 6 is relevant. New experimental studies of the isotopic fractionation associated with pyrite formation (precipitated from synthetic FeS; Guillbaud *et al.*, 2010) require additional isotopic information of preceding iron-sulfur interactions, as described within this study; along with do studies of FeS and pyrite formation observed within natural environments.

7.2 FUTURE WORK

A number of improvements to experimental design, and subsequent suggestions which utilise the iron sulfidation procedure of sediments to different environmental studies are noted within this section. Building upon the reported findings of the mineral reactivity compared in two sediment assemblages (Chapter 4: Umpqua River and Aarhus Bay), a further comparison between these normal marine sediments should be made with those taken from different environments (euxinic, lake, deep sea). This would provide an inclusive inventory of Fe mineral abundances under different depositional settings, taking into account rates of mineral sulfidation (and hence classification) not previously detailed in studies aiming to characterise sedimentary core and porewater profiles, which use lengthy extraction processes to determine Fe content of sediments. In order to enhance this primary study, a method of extracting either solid phase or dissolved FeS from natural sediment assemblages must be developed in order to assess the true mass balance of Fe and S species cycling throughout the reductive dissolution processes. Further investigation is required to understand the organic acid and/or organic sulfur content of these sediments, which may be an important factor in controlling the unusual reactivity of these iron monosulfide species within these sediments.

It would also be useful to investigate if kinetic data obtained in Chapter 4, can be manipulated to constrain the reactivity of natural sediment assemblages via previously reported sulfidation kinetic equations (reported in Poulton (2003) and Poulton *et al.*, (2004)), which only rely upon parameters of initial sulfide concentration and either mineral surface area or concentration of initial reactive iron minerals to determine the rate constants associated with synthetic Fe(III) minerals. However, comparing these methods of rate determination may require additional components to incorporate the changing physical parameters associated with reactive, sediment assemblages (i.e. changing crystallinity, mineralogical structure and surface area); but are important to subsequent experimental studies of Fe rich minerals. To complete the natural sulfidation work of Chapter 4, an isotopic study tracing the reductive dissolution of characterised Fe(III) oxide minerals within natural sediment assemblages (during sulfide mediated reductive dissolution) would allow further information to be collected with respect to early diagenetic processes effecting the cycling of Fe in near surface environments, which are known to significantly change with depth and oxygen content. This would allow a comprehensive comparison to the well characterised isotopic fractionation values associated with biologically iron reduction and Fe(II) dissolution. Isotopic measurements regarding the precipitation of FeS within this system would also provide the first experimental signatures of FeS formation during the sulfidation of natural sediments, in compliment to the study of synthetically precipitated FeS reported by Butler *et al.*, (2005).

In order to compare the reactivity of naturally occurring siderite in its reduced state (Chapter 5) with a synthesised pure Fe(II) carbonate mineral experimentally; a freshly obtained sample from a well characterised ancient iron formation (which has not been

subjected to weathering or oxidative processes) may provide a more accurate account of iron reactivity within a transitional ferruginous-euxinic ancient ocean, currently reported by Poulton *et al.*, (2010), Kendall *et al.*,(2010) etc. In addition to the basic reactions which describe Fe(II) dissolution from iron carbonate minerals under sulfidic conditions, it is important to properly constrain the full reaction mechanism by which Fe(II) dissolution and FeS formation occurs, with further investigation required to obtain a solubility constant for siderite within sulfidic solutions, allowing the determination of prominent surface species observed upon the mineral surface.

With the emergence of euxinic conditions sporadically formed throughout periods of ocean anoxia between 2.4-1.8 Ga, it would be interesting and beneficial to trace the $\delta^{56}\text{Fe}$ isotope record associated with the formation and dissolution of siderite in analogous experiments, also measuring the formation of FeS within this reduced system. Although compared to the sulfide mediated reductive dissolution associated with iron oxides, there is no change in oxidation state to catalyse an isotopic fractionation, it would be interesting to observe a carbonate dissolution reaction in terms of kinetics with respect to FeS formation, in comparison to the previous study of Butler *et al.*, 2005, those of Fe carbonate formations (Wehrli *et al.*, 2003; Johnson *et al.*, 2004; 2005) and studies which hypothesis Fe reactivity (as DIR) within sulfidic environments (Archer & Vance, 2006).

Finally, to constrain and validate the experimental methods used to obtain dissolved and solid phase iron samples for Fe isotope analysis (Chapter 6), a number of changes should be made towards experimental design. Additional effort should be made to limit FeS formation by increasing the concentration of the initial Fe mineral in reaction, therefore avoiding the need to correct raw data for the possible influence, and hence uncertainty in results, of isotopic fractionations measured during reduction and

dissolution processes. Additional samples for unreacted Fe(III) should be collected for all experiments to assess isotopic mass balance associated with Fe(II) surface and dissolved phases measured, and each experiment should be allowed to run to completion (via the removal of all sulfide from solution) to allow the determination of isotopic fractionation over the initial period of reactivity (which is kinetically faster than the bulk dissolution of Fe oxide minerals). A further examination of the effects of mineral surface inhomogeneity is also required, as it is believed that in following the acid catalysed dissolution of several of the synthetic minerals over time shows similar heavy isotope effects as measured during dissolution, and an adjustment would be required in order to correct for these results. As mentioned in relation to Chapter 4, an isotopic study of Fe mineral reactivity within a characterised sediment core would be an ideal next step in firstly correlating the isotopic fractionation observed during Fe(III) mineral abiotic reductive dissolution to a natural system; and also providing a novel study of sulfide mediated reductive dissolution within diagenetic sediments, in comparison to reactions which have already been widely characterised in terms of bacterially mediated isotopic systems.

8. REFERENCES

- ALBAREDE, F., BEARD, B.L., (2004). Analytical methods for non-traditional isotopes. *Reviews in Mineralogy and Geochemistry*, **55**, 113-152.
- ANBAR, A.D., (2004). Iron stable isotopes: beyond biosignatures. *Earth and Planetary Science Letters*, **217**, 223-236.
- ANBAR, A.D., ROUXEL, O. (2007). Metal stable isotopes in paleoceanography. *Annual Reviews in Earth and Planetary Sciences*, **35**, 717-746.
- ANBAR, A. D., ROE, J. E., BARLING, J., NEALSON, K. H. (2000) Nonbiological fractionation of iron isotopes. *Science*, **288**, 126–128.
- APPELO, C.A.J., POSTMA, D., (2005). *Geochemistry, groundwater and pollution*. AA BALKEMA PUB., The Netherlands, 2nd edition.
- ARCHER, C., VANCE, D. (2006). Coupled Fe and S isotope evidence for Archean microbial Fe(III) and sulfate reduction. *Geology* **34**, 153-156.
- ARNOLD, G.L., ANBAR, A.D., WEYER, S., (2004). Fe isotope variations in natural materials measured using high mass resolution multiple collector ICPMS. *Analytical Chemistry*, **76**, 322-327.
- BALCI, N., BULLEN, T.D., WITTE-LIEN, K., SHANKS, W.C., MOTELICA, M., MANDERNACK, K.W., (2006). Iron isotope fractionation during microbially stimulated Fe(II) oxidation and Fe(III) precipitation. *Geochimica et Cosmochimica Acta*, **70**, 622-639.
- BANWART, S., DAVIES, S., STUMM, W., (1989). The role of oxalate in accelerating the reductive dissolution of hematite (α -Fe₂O₃) by ascorbate. *Colloids and Surfaces*, **39**, 303-309.
- BEARD, B.L., JOHNSON, C.M., (2004). Fe isotope variations in modern and ancient earth and other planetary bodies. *Reviews in Mineralogy and Geochemistry*, **55**, 319-357.
- BEARD, B.L., JOHNSON, C.M., COX, L., SUN, H., NEALSON, K.H., AGUILAR, C., (1999). Iron isotope biosignatures. *Science* **285**, 1889-1892.

- BEARD, B.L., JOHNSON, C.M., SKULAN, J.L., NEALSON, K.H., COX, L., SUN, H., (2003). Application of Fe isotopes to tracing the geochemical biological cycling of Fe. *Chemical Geology* **195**, 87-117.
- BEKKER, A., BARLEY, M.E., FIORENTINI, M.L., ROUXEL, O.J., RUMBLE, D., BERESFORD, S.W., (2009). Atmospheric sulfur in Archean komatite hosted nickel deposits. *Science*, **326**, 1086-1089.
- BENNING, L.G., WILKIN, R.T., BARNES, H.L., (2000). Reaction pathways in the Fe-S system below 100°C. *Chemical Geology*, **167**, 25-51.
- BERNER, R.A.,(1964). Distribution and diagenesis of sulfur in some sediments from the Gulf of California. *Marine Geology*, **1**, 117-140.
- BERNER, R.A., (1969). Migration of iron and sulfur within anaerobic sediments during early diagenesis. *American Journal of Science*, **267**, 19-42.
- BERNER, R.A., (1970). Sedimentary pyrite formation. *American Journal of Science*, **268**, 1-23.
- BERNER, R.A.,(1971). *Principles of sedimentology*, McGraw-Hill, New York, 1st edition.
- BERNER, R.A., (1980). *Early diagenesis: A theoretical approach*. Princeton University Press, Princeton, NJ. 1st edition.
- BERNER, R.A., (1981). A new geochemical classification of sedimentary environments. *Journal of sedimentary Petrology*, **51**, 359-365.
- BERNER, R.A.,(1984). Sedimentary pyrite formation: An update. *Geochimica et Cosmochimica Acta*, **48**, 605-615.
- BERNER, R.A., (1985). Sulphate reduction, organic matter decomposition and pyrite formation. *Philosophical Transactions of the Royal Society of London A*, **315**, 25-38.
- BERNER, R.A., (1991). Sulfate reduction in deep sea sediments. *American Journal of Science*, **291**, 177-188.
- BERQUIST, B.A., BOYLE, E.A., (2006). Iron isotopes in the Amazon River system: Weathering and transport signatures. *Earth and Planetary Science Letters*, **248**, 54-68.

- BEUKES, N.J., KLEIN, C., (1990). Geochemistry and sedimentology of a facies transition from microbanded to granular iron-formation in the early Proterozoic Transvaal Supergroup, South Africa. *Precambrian Research*, **47**, 99–139.
- BEUKES, N.J., KLEIN, C., KAUFMANN, A.J., HAYES, J.M., (1990). Carbonate petrography, kerogen distribution, and carbon and oxygen isotopic variations in an Early Proterozoic transition from limestone to iron-formation deposition, Transvaal Supergroup, South Africa. *Economic Geology*, **85**, 663–690.
- BONNEVILLE, S., BEHRENDTS, T., VAN CAPELLEN, P., HYACINTHE, C., ROLING, W.F.M., (2006). Reduction of Fe(III) colloids by *Schewanella putrefaciens*: A kinetic model. *Geochimica et Cosmochimica Acta*, **70**, 5842-5854.
- BORER, P.M., SULZBERGER, B., REICHARD, P., KRAEMER, S.M., (2005). Effect of siderophores on the light-induced dissolution of colloidal iron (III) (hydr)oxides. *Marine Chemistry*, **93**, 179-193.
- BOUDREAU, B.P., CANFIELD, D.E., (1988). A provisional diagenetic model for pH in anoxic porewaters: Application to the FOAM site. *Journal of Marine Research*, **46**, 429-455.
- BOUDREAU, B.P., RUDDICK, B.R., (1991). On a reactive continuum representation of organic matter diagenesis. *American Journal of Science*, **291**, 507-538.
- BRANTLEY, S. L., LIERMANN, L., BULLEN, T. D. (2001). Fractionation of Fe isotopes by soil microbes and organic acids. *Geology*, **29**, 535–538.
- BRANTLEY, S.L., LIERMANN, L.J., GUYNN, R.L., ANBAR, A., ICOPINI, G.A., BARLING, J., (2004). Fe isotopic fractionation during mineral dissolution with and without bacteria. *Geochimica et Cosmochimica Acta*, **68**, 3189-3204.
- BRATERMAN, P.S., CARINS-SMITH, A.G., SLOPER, R.W., (1983). Photooxidation of hydrated Fe(II)-significance for banded iron formations.
- BRAUN, R.D., (1991). Solubility of iron (II) carbonate at temperatures between 30-80°. *Talanta*, **38**, 205-211.

- BRUNO, J., WERSIN, P., STUMM, W., (1992). On the influence of carbonate in mineral dissolution: II. The solubility of $\text{FeCO}_3(\text{s})$ at 25 °C and 1 atm total pressure, *Geochimica et Cosmochimica Acta*, **56**, 1149–1155.
- BULLEN T. D., WHITE, A. F., CHILDS, C. W., VIVIT, D. V., SCHULTZ, M. S., (2001). Demonstration of significant iron isotope fractionation in nature. *Geology*, **29**, 699–702.
- BUTLER, I.B., RICKARD, D., (2000). Framboidal pyrite formation via the oxidation of iron (II) monosulfide by hydrogen sulfide. *Geochimica et Cosmochimica Acta*, **64**, 2665-2672.
- BUTLER, I.B., ARCHER, C., VANCE, D., OLDROYD, A., RICKARD, D., (2005). Fe isotope fractionation on FeS formation in ambient aqueous solution. *Earth and Planetary Science Letters*, **236**, 430-442.
- CALVERT, S.E., PEDERSEN, T.F., (1993). Geochemistry of recent oxic and anoxic marine sediments: Implications for the geological record. *Marine Geology*, **113**, 67-88.
- CANFIELD, D.E., (1989). Reactive iron in marine sediments. *Geochimica et Cosmochimica Acta*, **53**, 619-632.
- CANFIELD, D.E., (1991). Sulfate reduction in deep sea sediments. *American Journal of Science*, **291**, 177-188.
- CANFIELD, D.E., (1997). The geochemistry of river particulates from the continental USA: Major elements. *Geochimica et Cosmochimica Acta*, **61**, 3349-3365.
- CANFIELD, D. E., (2005). The early history of atmospheric oxygen: homage to Robert A.Garrels. *Annual Reviews in Earth and Planetary Sciences*, **33**, 1–36.
- CANFIELD, D.E., BERNER, R.A., (1987). Dissolution and pyritization of magnetite in anoxic marine sediments. *Geochimica et Cosmochimica Acta*, **51**, 645-659.
- CANFIELD, D.E, LYONS, T.W., RAISWELL, R., (1996). A model for iron deposition to euxinic Black Sea sediments. *American Journal of Science*, **296**, 818-834.
- CANFIELD, D.E., POULTON, S.W., NARBONNE, G.M., (2007). Late Neoproterozoic deep ocean oxygenation and the rise of animal life. *Science*, **315**, 92-95.

- CANFIELD, D.E., POULTON, S.W., KNOLL, A.H., NARBONNE, G.M., ROSS, G., GOLDBERG, T., STRAUSS, H., (2008). Ferruginous conditions dominated later neoproterozoic deep water chemistry. *Science*, **321**, 949-952.
- CANFIELD, D.E., RAISWELL, R., BOTTRELL, S., (1992). The reactivity of sedimentary iron minerals towards sulfide. *American Journal of Science*, **292**, 659-683.
- CANFIELD, D.E., RAISWELL, R., WESTRICH, J.T., REAVES, C.M., BERNER, R.A., (1986). The use of chromium reduction in the analysis of reduced inorganic sulfur in sediments and shales. *Chemical Geology*, **54**, 149-155.
- CANFIELD, D.E., ROSING, M.T., BJERRUM, C., (2006). Early anaerobic metabolisms. *Philosophical Transactions of the Royal Society*, **361**, 1819-1836.
- CANFIELD, D.E., THAMDRUP, B., (2009). Towards a consistent classification scheme for geochemical environments, or, why we wish the term 'suboxic' would go away. *Geobiology* **7**, 385-392.
- CANFIELD, D.E., THAMDRUP, B., HANSEN, J.W., (1993). The anaerobic degradation of organic matter in Danish coastal marine sediments: Iron reduction, manganese reduction and sulfate reduction. *Geochimica et Cosmochimica Acta*, **57**, 3867-3883.
- CANFIELD, D.E., THAMDRUP, B., (1996). Fate of elemental sulfur in an intertidal sediment. *FEMS Microbiology Ecology*, **19**, 95-103.
- CLINE, J.D.,(1969). Spectrophotometric determination of hydrogen sulphide in natural waters. *Limnology and Oceanography*, **14**, 454-458.
- CORNELL, R.M., SCHWERTMANN, U., (2003). *The iron oxides: Structure, properties, reactions, occurrences and uses*. WILEY-VCH Verlag GmbH & Co., 2nd edition.
- CROAL, L.R., JOHNSON, C.M., BEARD, B.L., NEWMAN, D.K., (2004a). Iron isotope fractionation by Fe(II)-oxidising photoautotrophic bacteria. *Geochimica et Cosmochimica Acta*, **68**, 1227-1242.
- CROAL, L.R., GRALNICK, J.A., MALASARN, D., NEWMAN, D.K., (2004b). The genetics of geochemistry. *Annual Reviews in Genetics*, **38**, 175-202.

- CROSBY, S.A., GIASSON, D.R., CUTTLER, A.H., BUTLER, I., TURNER, D.R., WHITFIELD, M., MILLWARD, G.E., (1983). Surface Areas and Porosities of Fe(III)-and Fe(II)-Derived Oxyhydroxides. *Environmental Science and Technology*, **17**, 709-713.
- CROSBY, H.A., JOHNSON, C.M., RODEN, E.E., BEARD, B.L., (2005). Coupled Fe(II)-Fe(III) electron and atom exchange as a mechanism for Fe isotope fractionation during dissimilatory iron oxide reduction. *Environmental Science and Technology*, **39**, 6698-6704.
- CROSBY, H.A., RODEN, E.E., JOHNSON, C.M., BEARD, B.B., (2007). The mechanisms of iron isotope fractionations produced during dissimilatory Fe(III) reduction by *Shewanella putrefaciens* and *Geobacter sulfurreducens*. *Geobiology*, **5**, 169-189.
- CROWE, S.A., KATSEV, S., LESLIE, K., STURM, A., MAGEN, C., NOMOSATRYO, S., PACK, M.A., KESSLER, J.D., REEBURGH, W.S., ROBERTS, J.A., GONZALEZ, L., DOUGLAS HAFFNER, G., MUCCI, A., SUNBY, B., FOWLE, D.A., (2011). The methane cycle in ferruginous Lake Matano. *Geobiology*, **9**, 61-78.
- CURTIS, C.D., COLEMAN, M.L., LOVE, L.G., (1986). Pore water evolution during sediment burial from isotopic and mineral chemistry of calcite, dolomite and siderite concretions. *Geochimica et Cosmochimica Acta*, **50**, 2321-2334.
- CZAJA, A.D., JOHNSON, C.J., BEARD, B.L., EIGENBRODE, J., FREEMAN, K.H., YAMAGUCHI, K.E., (2010). Iron and carbon isotope evidence for ecosystem and environmental diversity in the ~ 2.7 to 2.5Ga Hamersley Province, Western Australia. *Earth and Planetary Science Letters*, **292**, 170-180.
- DAUPHAS, N., ROUXEL, O., (2006). Mass spectrometry and natural variations of iron isotopes. *Mass Spectrometry Reviews*, **25**, 515-550.
- DAVISON, W., PHILLIPS, N., TABNER, B.J., (1999). Soluble iron sulfide species in natural waters: Reappraisal of their stoichiometry and stability constants. *Aquatic Sciences*, **61**, 23-43.

- DEMAISON, G.J., MOORE, G.T., (1980). Anoxic environments and oil source bed genesis. *The American Association of Petroleum Geologists Bulletin*, **64**, 1179-1209.
- DENG, Y., (1997). Effect of pH on the reductive dissolution rates of iron (III) hydroxide by ascorbate. *Langmuir*, **13**, 1835-1839.
- DOS SANTOS AFONSO, M., STUMM, W., (1992). Reductive dissolution of Iron (III) (hydr)oxides by hydrogen sulfide. *Langmuir*, **8**, 1671-1675.
- DOS SANTOS AFONSO, M., MORANDO, P.J., BLESÁ, M.A., BANWART, S., STUMM, W., (1990). The reductive dissolution of iron oxides by ascorbate: The role of carboxylate anions in accelerating reductive dissolution. *Journal of Colloid and Interface Science*, **138**, 74-82.
- DUCKWORTH, O.W., MARTIN, S.T., (2004). Role of molecular oxygen in the dissolution of siderite and rhodochrosite. *Geochimica et Cosmochimica Acta*, **68**, 607-621.
- DREVER, J.I., STILLINGS, L.L., (1997). The role of organic acids in mineral weathering. *Colloids and Surfaces A: Physicochemical Engineering*, **120**, 167-181.
- DUAN, Y., SEVERMANN, S., ANBAR, A.D., LYONS, T.W., GORDON, G.W., SAGEMAN, B.B., (2010). Isotopic evidence for Fe cycling and repartitioning in ancient oxygen-deficient settings: Examples from black shales of mid-to-late Devonian Appalachian basin. *Earth and Planetary Science Letters*, **290**, 244-253.
- ELDERFIELD, H., SCHULTZ, A., (1996). Mid-cocean ridge hydrothermal fluxes and the chemical composition of the ocean. *Annual Reviews in Earth and Planetary Science*, **24**, 191-224.
- ELROD, V.A., BERELSON, W.M, COALE, K.H., JOHNSON, K.S, (2004). The flux of iron from continental shelf sediments: a missing source for global budgets. *Geophysical Research Letters*, **31**, L12307.
- FANTLE, M.S., DePAOLO, D.J., (2004). Iron isotopic fractionation during continental weathering. *Earth and Planetary Science Letters*, **288**, 547-562.

- FOGO, J.K., POPOWSKY, M., (1949). Spectrophotometric determination of hydrogen sulfide: Methylene Blue Method. *Analytical Chemistry*, **21**, 732-734.
- FOSSING, H., JORGENSEN, B.B., (1989). Measurement of bacterial sulfate reduction in sediments: Evaluation of a single step chromium reduction method. *Biogeochemistry*, **8**, 205-222.
- FRENCH, B.M., (1971). Stability relations of siderite (FeCO₃) in the sytem Fe-C-O. *American Journal of Science*, **271**, 37-78.
- FROELICH, P.N., KLINKHAMMER, G.P., BENDER, M.L., LUEDTKE, N.A., HEATH, G.R., CULLEN, D., DAUPHIN, P., (1979). Early oxidation of organic matter in pelagic sediments of the eastern equatorial Atlantic: suboxic diagenesis. *Geochimica et Cosmochimica Acta*, **43**, 1075-1090.
- GOLDHABER, M.B., KAPLAN, I.R., (1980). Mechanisms of sulfur incorporation and isotope fractionation during early diagenesis in sediments of the Gulf of California. *Marine Chemistry*, **9**, 97-146.
- HABICHT, K.S., GADE, K., THAMDRUP, B., BERG, P., CANFIELD, D.E., (2002). Calibration of sulfate level in the Archean ocean. *Science*, **298**, 2372-2374.
- HAESE, R.R (2006). The Reactivity of Iron Oxides. In: SCHULZ, H.D., ZABEL, M (Eds), *Marine Geochemistry*. SPRINGER Verlag, Berlin, 2nd edition.
- HEIMANN, A., JOHNSON, C.M., BEARD, C.M., VALLEY, J.W., RODEN, E.E., SPICUZZA, M.J., BEUKES, N.J., (2010). Fe, C,O isotope compositions of banded iron formation carbonates demonstrate a major role for dissimilatory iron reduction in ~2.5 Ga marine environments. *Earth and Planetary Science Letters*, **294**, 8-18.
- HERING, J.G., STUMM, W (1990). Oxidative and reductive dissolution of minerals. In: HOCELLA JR, M.F., WHITE, A.F. (eds), *Mineral-water interface geochemistry: Reviews in Mineralogy*, Volume 23. Mineralogical Society of America, Washington DC, 1st edition.
- HERSMAN, L., LLOYD, T., SPOSITO, G., (1995). Siderophore-promoted dissolution of hematite. *Geochimica et Cosmochimica Acta*, **59**, 3327-3330.

- HILL, P.S., SCHAUBLE, E.A., (2008). Modeling the effects of bond environment on equilibrium iron isotope fractionation in ferric aquo-chloro complexes. *Geochimica et Cosmochimica Acta*, **72**, 1939-1958.
- HOLLAND, H. D., (1984). *The Chemical Evolution of the Atmosphere and Oceans*. Princeton University Press, Princeton, NJ., 1st edition.
- HOLLAND, H.D., (2006). The oxygenation of the atmosphere and oceans. *Philosophical Transactions of the Royal Society*, **B 361**, 903-915.
- HOMOKY, W.B., SEVERMANN, S., MILLS, R.A., STATHAM, P.J., FONES, G.R., (2009). Pore-fluid Fe isotopes reflect the extent of benthic Fe redox recycling: Evidence from continental shelf and deep-sea sediments. *Geology*, **37**, 751-754.
- HUNGER, S., BENNING, L.G., (2007). Greigite: a true intermediate on the polysulfide pathway to pyrite. *Geochemical Transactions*, **8**, doi:10.1186/1467-4866-8-1.
- HYACHINTHE, C., BONNEVILLE, S., VAN CAPELLEN, P., (2006). Reactive iron (III) in sediments: Chemical versus microbial extractions. *Geochimica et Cosmochimica Acta*, **70**, 4166-4180.
- ICOPINI, G.A., ANBAR, A.D., RUEBUSH, S.S., TIEN, M., Brantley S.L., (2004). Iron isotope fractionation during microbial reduction of iron: The importance of adsorption. *Geology*, **32**, 205-208.
- JENSEN, D.L., BODDUM, J.K., TJELL, J.C., CHRISTENSEN, T.H., (2002). The solubility of rhodocrosite (MnCO₃) and siderite (FeCO₃) in anaerobic aquatic environments. *Applied Geochemistry*, **17**, 503-511.
- JEON, B.H., DEMPSEY, B.A., BURGOS, W.D., (2003). Kinetics and mechanisms of Fe(II) with iron(III) oxides. *Environmental Science and Technology*, **37**, 3309-3315.
- JOHNSON, C.M., BEARD, B.L., (2005). Biogeochemical cycling of iron isotopes. *Science*, **309**, 1025-1027.

- JOHNSON, C.M., BEARD, B.L., (2006). Fe isotopes: An emerging technique for understanding modern and ancient biogeochemical cycles. *GSA Today* **16**, 4-10.
- JOHNSON, C.M., BEARD, B.L., RODEN, E.E., NEWMAN, D.K., NEALSON, K.H., (2004). Isotope constraints on biogeochemical cycling of Fe. *Reviews in Mineralogy and Geochemistry*, **55**, 359-408.
- JOHNSON, C.M., BEARD, B.L., BEUKES, N.J., KLEIN, C., O'LEARY, J.M., (2003). Ancient geochemical cycling in the Earth as inferred from Fe isotope studies of banded iron formations from Transvaal Craton. *Contributions to Mineralogy and Petrology*, **144**, 523-547.
- JOHNSON, C.M., BEARD, B.L., RODEN, E.E., (2008a). The iron isotope fingerprints of redox and biogeochemical cycling in modern and ancient earth. *Annual Reviews in Earth Planetary Science*, **36**, 457-493.
- JOHNSON, C.M., BEARD, B.L., KLEIN, C., BEUKES, N.J., RODEN, E.E., (2008b). Iron isotopes constrain biological and abiological processes in banded iron formation genesis. *Geochimica et Cosmochimica Acta*, **72**, 151-169.
- JOHNSON, C.M., RODEN, E.E., WELCH, S.A., BEARD, B.L., (2005). Experimental constraints on Fe isotope fractionation during magnetite and Fe carbonate formation coupled to dissimilatory hydrous ferric oxide reduction. *Geochimica et Cosmochimica Acta*, **69**, 963-993.
- JOHNSTON, D.T., POULTON, S.W., DEHLER, C., PORTER, S., HUSSON, J., CANFIELD, D.E., KNOLL, A.H., (2010). An emerging picture of Neoproterozoic ocean chemistry: insights from the Chuar Group, Grand Canyon. *Earth and Planetary Science Letters*, **290**, 64-73.
- JORGENSEN, B.B., (1977). The sulfur cycle of a coastal marine sediment (Limfjorden, Denmark). *Limnology and Oceanography*, **22**, 814-832.
- JORGENSEN, B.B., KASTEN, S., (2006). Sulfur cycling and methane oxidation. In: SCHULZ, H.D., ZABEL, M (Eds), *Marine Geochemistry*. SPRINGER Verlag, Berlin, 2nd edition.

- KAPLAN, I.R., EMERY, K.O., RITTENBURG, S.C., (1963). The distribution and isotopic abundance of sulfur in recent marine sediment off Southern California. *Geochimica et Cosmochimica Acta*, **27**, 297-331.
- KAPPLER, A., NEWMAN, D.K., (2004). Formation of Fe(III)-minerals by Fe(II)oxidising photoautotrophic bacteria. *Geochimica et Cosmochimica Acta*, **68**, 1217-1226.
- KAUFAMN, A.J., HAYES, J.M., KLEIN, C., (1990). Primary and diagenetic controls of isotopic compositions of iron-formation carbonates. *Geochimica et Cosmochimica Acta*, **54**, 3461-3473.
- KENDALL, B., REINHARD, C.T., LYONS, T.W., KAUFMAN, A.J., POULTON, S.W., ANBAR, A.D., (2010). Pervasive oxygenation along late Archean ocean margins. *Nature Geoscience*, **3**, 647-652.
- KLEIN, C., (2005). Some Precambrian banded iron formations (BIFs) from around the world: their age, geological setting, mineralogy, metamorphism, geochemistry, and origin. *American Mineralogy*, **90**, 1473-1499.
- KLEIN, C., BEUKES, N.J.,(1989). Geochemistry and sedimentology of a facies transition from limestone to iron-formation deposition in the Early Proterozoic Transvaal Supergroup, South Africa. *Economic Geology*, **84**, 1733–1774.
- KLEIN, C., BEUKES, N.J., (1992). *Time distribution, stratigraphy, sedimentological setting, and geochemistry of Precambrian iron-formations*. In: *The Proterozoic Biosphere: A multidisciplinary Study*, Cambridge University Press, 139-146.
- KRAEMER, S.M., (2004). Iron oxide dissolution and solubility in the presence of siderophores. *Aquatic Science*, **66**, 2-18.
- KRAUSKOPF, K.B., BIRD, D.K., (1995). *Introduction to Geochemistry*. McGRAW-HILL, Singapore, 3rd edition.
- KROM, M.D., MORTIMER, R.J.G., POULTON, S.W., HAYES, P., DAVIES, I.M., DAVISON, W., ZHANG, H., (2002). In-situ determination of dissolved iron production in recent marine sediments. *Aquatic Sciences*, **64**, 282-291.
- KUKKADAPU, R.K., ZACHARA, J.M., FREDRICKSEN, J.K., SMITH, S.C., DOHNALKOVA, A.C., RUSSEL, C.K., (2003). Transformation of 2-line

- ferrihydrite to 6-line ferrihydrite under oxic and anoxic conditions. *American Mineralogist*, **88**, 1903-1914.
- LANGMUIR, D., (1969). The Gibbs free energy of substances in the system Fe-O₂-H₂O-CO₂ at 25C. *US Geological Survey Professional Paper*, **650B**, 180-184.
- LARSEN, O., POSTMA, D., (2001). Kinetics of reductive dissolution of lepidocrocite, ferrihydrite, and goethite. *Geochimica et Cosmochimica Acta*, **65**, 1367-1379.
- LARSEN, O., POSTMA, D., JAKOBSEN, R., (2006). The reactivity of iron oxides towards reductive dissolution with ascorbic acid in a shallow sandy aquifer (Romo, Denmark). *Geochimica et Cosmochimica Acta*, **70**, 4827-4835.
- LIU, H., LI, P., ZHU, M., WEI, Y., SUN, Y., (2007). Fe(II)-induced transformation of ferrihydrite to lepidocrocite and goethite. *Journal of Solid State Chemistry*, **180**, 2121-2128.
- LOVELY, D.R., (1991). Dissimilatory Fe(III) and Mn(IV) reduction. *Microbiological Reviews*, **55**, 259-287.
- LOVELY, D.R., (1993), Dissimilatory metal reduction. *Annual Review in Microbiology*, **47**, 263-290.
- LOVELY, D.R., PHILLIPS, E.J.P., (1986). Organic matter mineralization with reduction of ferric iron in anaerobic sediments. *Applied and Environmental Microbiology*, **51**, 683-689.
- LUTHER III, G.W., RICKARD, D.T., THEBERGE, S.M., OLDROYD, A., (1996). Determination of metal (bi)sulfide stability constants of Mn²⁺, Fe²⁺, Co²⁺, Ni²⁺, Cu²⁺ and Zn²⁺ by voltammetric methods. *Environmental Science and Technology*, **30**, 671-679.
- LYONS, T.W., BERNER, R.A., (1992). Carbon-sulfur-iron systematics of the uppermost deep-water sediments of the Black Sea. *Chemical Geology*, **99**, 1-17.

- LYONS, T.W., SEVERMANN, S., (2006). A critical look at iron paleoredox proxies: New insights from modern euxinic marine basins. *Geochimica et Cosmochimica Acta*, **70**, 5698-5722.
- LYONS, T.W., ANBAR, A.D., SEVERMANN, S., SCOTT, C., GILL, B.C., (2009). Tracking euxinia in an ancient ocean: A multiproxy perspective and Proterozoic case study. *Annual Reviews in Earth and Planetary Sciences*, **37**, 507-534.
- MAERZ, C., POULTON, S.W., BECKMANN, B., KUSTER, K. WAGNER, T., S. KASTEN, S., (2008). Redox sensitivity of P cycling during marine black shale formation - dynamics of sulfidic and anoxic, non-sulfidic bottom waters. *Geochimica et Cosmochimica Acta*, **72**, 3703-3717.
- MCSWIGGEN, P.L., MOREY, G.B., (2008). Overview of the mineralogy of Biwabik Iron Formation, Mesabi Iron range, Northern Minnesota. *Regulatory Toxicology and Pharmacology*, **52**, S11-25.
- MILLERO, F.J., HUBINGER, S., FERNANDEZ, M., GARNETT, S., (1987). Oxidation of H₂S in seawater as a function of temperature, pH and ionic strength. *Environmental Science and Technology*, **21**, 439-443.
- MOREY, G.B., SOUTHWICK, D.L., (1995). Allostratigraphic Relationships of Early Proterozoic Iron-Formations in the Lake Superior Region. *Economic Geology*, **90**, 1983-1993.
- MORSE, J.W., WANG, Q., (1997). Pyrite formation under conditions approximating those in anoxic sediments: II. Influence of precursor iron minerals and organic matter. *Marine Chemistry*, **57**, 187-193.
- MORTIMER, R.J.G., COLEMAN, M.L., (1997). Microbial influence on the oxygen isotopic composition of diagenetic siderite. *Geochimica et Cosmochimica Acta*, **61**, 1705-1711.
- MORTIMER, R.J.G., COLEMAN, M.L., RAE J.E., (1997). Effect of bacteria on the elemental composition of early diagenetic siderite: implications for paleoenvironmental interpretations. *Sedimentology*, **44**, 759-765.
- MOZELY, P.S., (1989). Relation between depositional environment and the elemental composition of early diagenetic siderite. *Geology*, **17**, 704-706.

- MOZELY, P.S., WERSIN, P., (1992). Isotopic composition of siderite as an indicator of depositional environment. *Geology*, **20**, 817-820.
- PEDERSEN, H.D., (2006). *The transformation of Fe(III) oxides catalysed by Fe²⁺ and the fate of arsenate during transformation and reduction of Fe(II) oxides*. PhD Thesis. Institute of Environment & Resources, Technical University of Denmark.
- PEDERSEN, H.D., POSTMA, D., JAKOBSEN, R., LARSEN, O., (2005). Fast transformation of iron oxyhydroxides by the catalytic action of aqueous Fe(II). *Geochimica et Cosmochimica*, **69**, 3967-3977.
- PEDERSEN, T.F., CALVERT, S.E., (1990). Anoxia vs. productivity: What controls the formation of organic-carbon-rich sediments and sedimentary rocks? *The American Association of Petroleum Geologists Bulletin*, **74**, 454-466.
- PEIFFER, S., DOS SANTOS AFONSO, M., WEHRLI, B., GACHTER, R., (1992) Kinetics and mechanisms of the reaction of H₂S with lepidocrocite. *Environmental Science and Technology*, **26**, 2408-2413.
- PEIFFER, S., GADE, W., (2007). Reactivity of Ferric oxides towards H₂S at low pH. *Environmental Science and Technology*, **41**, 3159-3164.
- PHILLIPS, E.J.P., LOVELY, D.R., RODEN, E.E., (1993). Composition of non-microbially reducible Fe(III) in aquatic sediments. *Applied and Environmental Microbiology*, **59**, 2727-2729.
- POLYAKOV, V.B., MINEEV, S.D., (2000). The use of Mossbauer spectroscopy in stable isotope geochemistry. *Geochimica et Cosmochimica Acta*, **64**, 849-865.
- POSTMA, D., (1982). Pyrite and siderite formation in brackish and freshwater swamp sediments. *American Journal of Science*, **282**, 1151-1183.
- POSTMA, D., (1993). The reactivity of iron oxides in sediments: A kinetic approach. *Geochimica et Cosmochimica*, **57**, 5027-5034.
- POULTON, S.W., (2003). Sulfide oxidation and iron dissolution kinetics during the reaction of dissolved sulfide with ferrihydrite. *Chemical Geology*, **202**, 79-94.

- POULTON, S.W., CANFIELD, D.E. (2005). Development of a sequential extraction procedure for iron: implications of iron partitioning in continentally derived particulates. *Chemical Geology*, **214**, 209-221.
- POULTON, S.W., FRALICK, P.W., CANFIELD, D.E., (2004a). The transition to a sulphidic ocean ~1.84 billion years ago. *Nature*, **431**, 173-177.
- POULTON, S.W., FRALICK, P.W., CANFIELD, D.E., (2010). Spatial variability in oceanic redox structure 1.8 billion years ago. *Nature Geoscience Letters*, **3**, 486-491.
- POULTON, S.W., KROM, M.D., RAISWELL, R., (2004b). A revised scheme for the reactivity of iron (oxyhydr)oxide minerals towards dissolved sulfide. *Geochimica et Cosmochimica Acta*, **68**, 3703-3715.
- POULTON, S.W., RAISWELL, R., (2000). Solid phase associations, oceanic fluxes and the anthropogenic perturbations of transition metals in world river particulates. *Marine Chemistry*, **72**, 17-31.
- POULTON, S.W., RAISWELL, R., (2002). The low temperature geochemical cycle of iron: From continental fluxes to marine sediment deposition. *American Journal of Science*, **302**, 774-805.
- POULTON, S.W., RAISWELL, R., (2005). Chemical and physical characteristics of iron oxides in riverine and glacial melt water sediments. *Chemical Geology*, **218**, 203-221
- PYE, K., (1981). Marshrock formed by iron sulphide and siderite cementation in saltmarsh sediments. *Nature*, **294**, 650-652.
- PYE, K., (1984). SEM analysis of siderite cements in intertidal marsh sediment, North Norfolk, *Marine Geology*, **56**, 1-12.
- PYE, K., DICKSON, J.A.D., SCHIAVON, N., COLEMAN, M.L., COX, M., (1990). Formation of siderite-Mg-calcite –iron sulphide concretions in intertidal marsh and sandflat sediments, north Norfolk, England. *Sedimentology*, **37**, 325-343.
- PYZIK, A.J., SOMMER, S.E., (1981). Sedimentary iron monosulfides: Kinetics and mechanisms of formation. *Geochimica et Cosmochimic Acta*, **45**, 687-698.

- RAISWELL, R., (1982). Pyrite texture, isotopic composition and the availability of iron. *American Journal of Science*, **282**, 1244-1263.
- RAISWELL, R., (1993). Kinetic controls on depth variations in localised pyrite formation. *Chemical Geology*, **107**, 467-469.
- RAISWELL, R., (1997). A geochemical framework for the application of stable sulphur isotopes to fossil pyritization. *Journal of the Geological Society London*, **154**, 343-356.
- RAISWELL, R., (2006). Towards a global highly reactive iron cycle. *Journal of Geochemical Exploration*, **88**, 436-439.
- RAISWELL, R., BERNER, R.A., (1985). Pyrite formation in euxinic and semi-euxinic sediments. *American Journal of Science*, **285**, 710-724.
- RAISWELL, R., CANFIELD, D.E., (1996). Rates of reaction between silicate iron and dissolved sulfide in Peru Margin sediments. *Geochimica et Cosmochimica Acta*, **60**, 2777-2787.
- RAISWELL, R., CANFIELD, D.E., (1998). Sources of iron for pyrite formation in marine sediments. *American Journal of Science*, **298**, 219-245
- RAISWELL, R., CANFIELD, D.E., BERNER, R.A., (1994). A comparison of iron extraction methods for the determination of degree of pyritisation and the recognition of iron-limiting pyrite formation. *Chemical Geology*, **111**, 101-110.
- RAISWELL, R., FISHER, Q.J., (2000). Mudrock hosted carbonate concretions: a review of growth mechanisms and their influence on chemical and isotopic composition. *Journal of the Geological Society, London*, **157**, 239-251.
- RAISWELL, R., ANDERSON, T.F., (2005). Reactive iron enrichment in sediments deposited beneath euxinic bottom waters: constraints on supply by shelf recycling. *Geological Society, London, Special Publications*, **248**, 179-194.
- RAISWELL, R., BUCKLEY, F., BERNER, R.A., ANDERSON, T.F., (1988). Degree of pyritization of iron as a paleoenvironmental indicator of bottom water oxygenation. *Journal of Sedimentary Research*, **58**, 812-819.

- RAISWELL, R., TRANTER, M., BENNING, L.G., SIEGERT, M.J., HUYBRECHTS, P., (2006). Contributions from glacially derived sediment to the global iron (oxyhydr)oxide cycle: Implications for iron delivery to the oceans. *Geochimica et Cosmochimica Acta*, **70**, 2765-2780
- REDFIELD, A.C., (1958). The biological control of chemical factors in the environment. *American Journal of Science*, **46**, 206-226.
- REINHARD, C., RAISWELL, R., SCOTT, C., ANBAR, A.D., LYONS, T.W., (2009) A Late Archean sulfidic sea stimulated by early oxidative weathering of the continents. *Science*, **326**, 713-726.
- REVSBECH, N.P., LARSEN, H.H., GUNDERSEN, J., DALSGAARD, T., ULLOA, O., THAMDRUP, B., (2009). Determination of ultra-low oxygen concentrations in oxygen minimum zones by the STOX sensor. *Limnology and Oceanography: Methods*, **7**, 371-381.
- RICKARD, D. (1974). Kinetics and mechanisms of the sulfidation of goethite. *American Journal of Science*, **274**, 941-952.
- RICKARD, D., (1995). Kinetics of FeS precipitation: Part 1. Competing reaction mechanisms. *Geochimica et Cosmochimica Acta*, **59**, 4367-4379.
- RICKARD, D., (1997). Kinetics of pyrite formation by the H₂S oxidation of iron (II) monosulfide in aqueous solutions between 25 and 125°C: The rate equation. *Geochimica et Cosmochimica Acta*, **61**, 115-134.
- RICKARD, D., (2006). The solubility of FeS. *Geochimica et Cosmochimica Acta*, **70**, 5779-5789.
- RICKARD, D., MORSE, J.W., (2005). Acid volatile sulfide (AVS). *Marine Chemistry*, **97**, 141-197.
- RODEN, E.E., (2003). Fe(III) oxide reactivity toward biological versus chemical reduction. *Environmental Science and Technology*, **37**, 1319-1324.
- RODEN, E.E., (2004). Analysis of long term bacterial vs. chemical Fe(III) oxide reduction kinetics. *Geochimica et Cosmochimica Acta*, **68**, 3205-3216.

- RODEN, E.E., ZACHARA, J.M., (1996). Microbial reduction of crystalline (III) oxides: influence of oxide surface area and potential for cell growth. *Environmental Science and Technology*, **30**, 1618-1628.
- ROE, J.E., ANBAR, A.D., BARLING, J., (2003). Nonbiological fractionation of Fe isotopes: evidence of an equilibrium isotope effect. *Chemical Geology*, **195**, 69-85.
- ROUXEL, O.J., BEKKER, A., EDWARDS, K.J., (2005). Iron isotope constraints on Archean and Paleoproterozoic ocean redox state. *Science*, **307**, 1088-1091.
- SCHAUBLE E.A., ROSSMAN, G.R., TAYLOR, H.P., (2001). Theoretical estimates of equilibrium Fe –isotope fractionations from vibrational spectroscopy. *Geochimica et Cosmochimica Acta*, **65**, 2487-2497.
- SCHINDLER, P.W., STUMM, W., (1987). The surface chemistry of oxides, hydroxides, and oxide minerals. In: STUMM, W. (Ed), *Aquatic Surface Chemistry: Chemical processes at the particle-water interface*. J. Wiley & Sons, New York, 1st edition.
- SCHIPPERS, A., JORGENSEN, B.B., (2002). Biogeochemistry of pyrite and iron sulfide oxidation in marine sediments. *Geochimica et Cosmochimica Acta*, **66**, 85-92.
- SCHULZ, H.D., (2006). Quantification of Early Diagenesis; Dissolved Constituents in Marine Pore Water. In: SCHULZ, H.D., ZABEL, M (Eds), *Marine Geochemistry*. SPRINGER Verlag, Berlin, 2nd edition.
- SCHWERTMANN, U., TAYLOR, R.M., (1972). The influence of silicate on the transformation of lepidocrocite to goethite. *Clays and Clay Minerals*, **20**, 159-164.
- SCHWERTMANN, U., (1991). Solubility and dissolution of iron oxides. *Plant and Soil*, **130**, 1-25.
- SCHWERTMANN, U., CORNELL, R.M., (1991) *Iron Oxides in the Laboratory: Preparation and Characterization*. Weinheim, Cambridge.

- SEVERMANN, S., JOHNSON, C.M., BEARD, B.L., McMANUS J., (2006). The effect of early diagenesis on the Fe isotope compositions of porewaters and authigenic minerals in continental margin sediments. *Geochimica et Cosmochimica Acta*, **70**, 2006-2022.
- SEVERMANN, S., LYONS, T.W., ANBAR, A., McMANUS, J., GORDON, G. (2008) Modern iron isotope perspective on the benthic iron shuttle and the redox evolution of ancient ocean. *Geology*, **36**, 487-490.
- SILVESTER, E., CHARLET, L., TOURNASSAT, C., GEHIN, A., GRENECHE, J., LIGER, E., (2005). Redox potential measurements and Mossbauer spectrometry of Fe^{II} adsorbed onto Fe^{III}(oxyhydr)oxide. *Geochimica et Cosmochimica Acta*, **69**, 4801-4815.
- SKULAN, J.L., BEARD, B.L., JOHNSON, C.M., (2002). Kinetic and equilibrium Fe isotope fractionation between aqueous Fe(III) and hematite. *Geochimica et Cosmochimica. Acta*, **66**, 2995-3015.
- SONG, L., LIU, C.Q., WANG, Z.L., ZHU, Z., TENG, Y., LIANG, L., TANG, S., LI, J., (2011). Iron isotope fractionation during biogeochemical cycle: Information from suspended particulate matter (SPM) in Aha Lake and its tributaries, Guizhou, China. *Chemical Geology*, **280**, 170-179.
- SORENSEN J., JORGENSEN, B.B., REVSBECH, N.P., (1979). A comparison of oxygen, nitrate and sulfate reduction in coastal marine sediments. *Microbial Ecology*, **5**, 105-115.
- SORENSEN, J., (1982). Reduction of ferric iron in anaerobic, marine sediment and interaction with reduction of nitrate and sulfate. *Applied and Environmental Microbiology*, **43**, 319-324.
- STAUBWASSER, M., Von BLANKENBURG, F., SCHOENBERG, R., (2006). Iron isotopes in early marine diagenetic iron cycles. *Geology*, **34**, 629-632.
- STONE, A.T., MORGAN, J.J., (1987). Reductive dissolution of metal oxides. In: STUMM, W. (Ed), *Aquatic Surface Chemistry: Chemical processes at the particle-water interface*. J. Wiley & Sons, New York, 1st edition.

- STOOKEY, L.L., (1970). Ferrozine: A new spectrophotometric reagent for iron. *Analytical Chemistry*, **42**, 779-781.
- STUMM, W., SULZBERGER, B., (1992). The cycling of iron in natural environments: Considerations based on laboratory studies of heterogeneous redox processes. *Geochimica et Cosmochimica Acta*, **56**, 3233-3257.
- SULZBERGER, B., LAUBSCHER, H., (1995). Reactivity of various types of iron (III) (hydr)oxides towards light-induced dissolution. *Marine Chemistry*, **50**, 103-115.
- SUMOONDUR, A., SHAW, S., AHMED, I., BENNING, L.G., (2008). Green rust as a precursor for magnetite: an in situ synchrotron based study. *Mineralogical Magazine*, **72**, 201-204.
- SUTER, D., BANWART, S., STUMM, W., (1991) Dissolution of hydrous Fe(III) oxides by reductive mechanisms. *Langmuir* **7**, 809-813.
- SWEENEY, R.E., KAPLAN, I.R., (1980). Diagenetic sulfate reduction in marine sediments. *Marine Chemistry*, **9**, 165-174.
- TEUTSCH, N., VON GUTEN, U., PORCELLI, S., CIPKA, O.A., HALLIDAY, A.N., (2005). Adsorption as a cause for iron isotope fractionation in reduced groundwater. *Geochimica et Cosmochimica Acta* **69**, 4175-4185.
- TEUTSCH, N., SCHMID, M., MULLER, B., HALLIDAY, A.N., BURGMANN, H., WEHRLI, B., (2009). Large iron isotope fractionation at the oxic-anoxic boundary in Lake Nyos. *Earth and Planetary Science Letters*, **285**, 52-60.
- THAMDRUP, B., FINSTER, K., HANSEN, J.W., BAK, F., (1993). Bacterial disproportionation of elemental sulfur coupled to chemical reduction of iron or manganese. *Applied and Environmental Microbiology*, **59**, 101-108.
- THAMDRUP, B., FOSSING, H., JORGENSEN, B.B., (1994). Manganese, iron, and sulfur cycling in a coastal marine sediment, Aarhus Bay, Denmark. *Geochimica et Cosmochimica Acta*, **58**, 5115-5129.
- TYSON, R.V., PEARSON, T.H., (1991). Modern and ancient continental shelf anoxia: an overview. *Geological Society Special Publication*, **58**, 1-14.

- VAIRAVAMURTHY, A., MOPPER, K., (1987). Geochemical formation of organosulphur compounds (thiols) by addition of H₂S to sedimentary organic matter. *Nature*, **329**, 623-625.
- VAN CAPELLEN, P., WANG, Y., (1996). Cycling of iron and manganese in surface sediments: A general theory for the coupled transport and reaction of carbon, oxygen, nitrogen, sulfur, iron and manganese. *American Journal of Science*, **296**, 197-243.
- VAN DER WEIJDEN, C.H., (1992). Early diagenesis and marine pore water. In: WOLF, K.H., CHILINGARIAN, G.V. (eds), *Developments in Sedimentology 47: Diagenesis III*. ELSEVIER Science Publications, Amsterdam. 1st edition.
- VEIZER, J., HOEFS, J., RIDLER, R.H., JENSEN, L.S., LOWE, D.R., (1989). Geochemistry of Precambrian carbonates: 1. Archean hydrothermal systems. *Geochimica et Cosmochimica Acta*, **53**, 845-857.
- VOILLIER, E., INGLETT, P.W., HUNTER, K., ROYCHOUDHURY, A.N., VAN CAPELLEN, P., (2000). The ferrozine method revisited: Fe(II)/Fe(III) determination in natural waters. *Applied Geochemistry*, **15**, 785-790.
- WALSH, J.N., (1980). The simultaneous determination of the major, minor and trace metal constituents of silicate rocks using inductively coupled plasma spectrometry. *Spectrochimica Acta, Part B: Atomic Spectrometry*, **35**, 107-111.
- WANG, Q., MORSE, J.W., (1996). Pyrite formation under conditions approximating those in anoxic sediments; 1. Pathway and morphology. *Marine Chemistry*, **52**, 99-121.
- WEHRLI, B., SULZBERGER, B., STUMM, W., (1989). Redox processes catalysed by hydrous oxide surfaces. *Chemical Geology*, **78**, 167-179.
- WEILAND, E., WEHRLI, B., STUMM, W., (1988). The coordination chemistry of weathering: III. A generalization on the dissolution rates of minerals. *Geochimica et Cosmochimica Acta*, **52**, 1969-1981.
- WIELDERHOLD, J.G., KRAEMER, S.M., TEUTSCH, N., BORER, P.M., HALLIDAY, A.N., and KRETZSCHMAR, R., (2006). Iron isotope

- fractionation during proton promoted, ligand controlled, and reductive dissolution of goethite. *Environmental Science and Technology*, **40**, 3787-3793.
- WIESLI, R.A., BEARD, B.L., JOHNSON, C.M., (2004). Experimental determination of Fe isotope fractionation between aqueous Fe(II), siderite and “green rust” in abiotic systems. *Chemical Geology*, **211**, 343-362.
- WILKIN, R.T., BARNES, H.L., (1996). Pyrite formation by reactions of iron monosulfides with dissolved inorganic and organic sulfur species. *Geochimica et Cosmochimica Acta*, **60**, 4167-4179.
- WILKIN, R.T., BARNES, H.L., (1997). Formation processes of framboidal pyrite. *Geochimica et Cosmochimica Acta*, **61**, 323-339.
- WILLIAMS, A.G.B., SCHERER, M.M., (2004). Spectroscopic evidence for Fe(II)-Fe(III) electron transfer at the iron oxide-water interface. *Environmental Science and Technology*, **38**, 4782-4790.
- YAMAGUCHI, K.E., JOHNSON, C.M., BEARD, B.L., OHMOTO, H., (2005). Biogeochemical cycling of iron in the Archean- Paleoproterozoic Earth: Constraints from iron isotope variations in sedimentary rocks from the Kaapvaal and Pilbara Cratons. *Chemical Geology*, **218**, 135-169.
- YAO, W., MILLERO, F.J., (1996). Oxidation of hydrogen sulfide by hydrous Fe(III) oxides in seawater. *Marine Chemistry*, **52**, 1-16.
- ZHANG, Y., CHARLET, L., SCHINDLER, P.W., (1992). Adsorption of protons, Fe(II) and Al(III) on lepidocrocite (γ -FeOOH). *Colloids and Surfaces*. **63**, 259-268.
- ZHAO, J., HUGGINS, F.E., FENG, Z., HUFFMANN, G.P., (1994). Ferrihydrite: surface structure and its effects on phase transformation. *Clay and Clay Minerals*, **42**, 737-746.
- ZINDER, B., FURRER, G., STUMM, W., (1986). The coordination chemistry of weathering: II. Dissolution of Fe(III) oxides. *Geochimica et Cosmochimica Acta* **50**, 1861-1869.